Universidade de Aveiro Departamento de Ciências Médicas
2020

FÁBIO JORGE SOUSA TRINDADE

Estudo da remodelagem reversa miocárdica através da análise proteómica do miocárdio e do líquido pericárdico

Proteomic changes in incomplete reverse remodeling – a closer look at the heart through myocardial and pericardial fluid analysis

Universidade de Aveiro Departamento de Ciências Médicas
2020

FÁBIO JORGE SOUSA TRINDADE

Estudo da remodelagem reversa miocárdica através da análise proteómica do miocárdio e do líquido pericárdico

Proteomic changes in incomplete reverse remodeling – a closer look at the heart through myocardial and pericardial fluid analysis

Tese apresentada à Universidade de Aveiro para cumprimento dos requisitos necessários à obtenção do grau de Doutor em Biomedicina, realizada sob a orientação científica do Doutor Rui Miguel Pinheiro Vitorino, Investigador Principal do Departamento de Ciências Médicas da Universidade de Aveiro, do Doutor Joaquim Adelino Correia Ferreira Leite Moreira, Professor Catedrático do Departamento de Cirurgia e Fisiologia da Faculdade de Medicina da Universidade do Porto e da Doutora Inês Maria Falcão Sousa Pires Marques, Professora Auxiliar do Departamento de Cirurgia e Fisiologia da Faculdade de Medicina da Universidade do Porto

Este trabalho foi financiado através do Fundo Europeu de Desenvolvimento Regional (FEDER), Programa Operacional Factores de Competitividade (COMPETE) e por fundos nacionais através da Fundação para a Ciência e Tecnologia (FCT), com a bolsa individual SFRH/BD/111633/2015 e as bolsas do Instituto de Biomedicina (iBiMED), ID/BIM/04501/2013 e POCI-01-0145-FEDER-007628, e da Unidade de Investigação Cardiovascular (UnIC) UID/IC/00051/2013.

Dedico este trabalho à minha família.

o júri

presidente

Doutor Eduardo Anselmo Ferreira da Silva
professor catedrático da Universidade de Aveiro

vogais

Doutor Bruno José Fernandes Oliveira Manadas
investigador auxiliar da Universidade de Coimbra

Doutor José Alberto Ramos Duarte
professor catedrático da Faculdade de Desporto da Universidade do Porto

Doutor António de Sousa Barros
investigador auxiliar convidado da Faculdade de Medicina da Universidade do Porto

Doutora Cristina Maria Rodrigues Pinheiro Gavina
professor auxiliar convidada da Faculdade de Medicina da Universidade do Porto

Doutora Patrícia Isabel Gomes Alves
investigadora sénior do Instituto de Biologia Experimental Tecnológica

Doutora Rita Maria Pinho Ferreira
professora auxiliar da Universidade de Aveiro

Doutora Inês Maria Falcão Sousa Pires Marques
professora auxiliar da Faculdade de Medicina da Universidade do Porto

agradecimentos

Em primeiro lugar, agradeço à minha família o constante apoio e compreensão que demonstraram ao longo destes quatro anos.

Aos meus orientadores, o professor Rui Vitorino, a professora Inês Falcão Pires e o professor Adelino Leite Moreira, agradeço a absoluta disponibilidade, abertura científica e a motivação contínua, sem as quais esta jornada teria sido mais difícil e seguramente menos profícua.

À professora Rita Ferreira e à professora Margarida Fardilha tenho a agradecer o constante apoio e disponibilidade e pronta ajuda em várias fases desta jornada.

Aos colegas da UnIC agradeço o espírito de acolhimento, a boa disposição e a amizade desenvolvidas nestes quatro anos.

Ao pessoal do iBiMED agradeço os excelentes momentos de descompressão e de convívio, as gargalhadas e as novas amizades para a vida.

À professora Homa Tajsharghi, ao Simon e aos restantes colegas da divisão de Biomedicina da Universidade de Skövde agradeço por terem proporcionado uma experiência de internacionalização incrível assim como a simpatia com que me acolheram.

Aos de sempre, Filipa, Daniela, Francisca, Tiago, Ana, Dinis e Nica, por estarem sempre lá.

palavras-chave

estenose aórtica, remodelagem reversa incompleta, miocárdio, líquido pericárdico, proteoma, fosfoproteoma.

resumo

A substituição da válvula aórtica continua a ser a opção terapêutica de referência para doentes com estenose aórtica e visa a eliminação da sobrecarga de pressão, desencadeando a remodelagem reversa miocárdica. Contudo, apesar do benefício hemodinâmico imediato, nem todos os pacientes apresentam regressão completa da hipertrofia do miocárdio, ficando com maior risco de eventos adversos, como a insuficiência cardíaca. Atualmente, os mecanismos biológicos subjacentes a uma remodelagem reversa incompleta ainda não são claros. Além disso, não dispomos de ferramentas de prognóstico definitivos nem de terapias auxiliares para melhorar a condição dos pacientes indicados para substituição da válvula. Para ajudar a resolver estas lacunas, uma abordagem combinada de (fosfo)proteómica e proteómica para a caracterização, respetivamente, do miocárdio e do líquido pericárdico foi seguida, tomando partido de biópsias e líquidos pericárdicos recolhidos em ambiente cirúrgico.

Das mais de 1800 e 750 proteínas identificadas, respetivamente, no miocárdio e no líquido pericárdico dos pacientes com estenose aórtica, um total de 90 proteínas desreguladas foram detetadas. As análises de anotação de genes, de enriquecimento de vias celulares e discriminativa corroboram um cenário de aumento da expressão de genes pro-hipertróficos e de síntese proteica, um sistema ubiquitina-proteassoma ineficiente, uma tendência para morte celular (potencialmente acelerada pela atividade do complemento e por outros fatores extrínsecos que ativam *death receptors*), com ativação da resposta de fase aguda e do sistema imune, assim como da fibrose.

A validação de alguns alvos específicos através de *immunoblot* e correlação com dados clínicos apontou para a cadeia β do complemento C3, a *Muscle Ring Finger protein 1* (MuRF1) e a *dual-specificity Tyr-phosphoylation regulated kinase 1A* (DYRK1A) como potenciais marcadores de uma resposta incompleta. Por outro lado, a predição de cinases a partir do fosfoproteoma, sugere que a modulação da caseína cinase 2, a família de cinases do IκB, a glicogénio sintase cinase 3 e da DYRK1A pode ajudar a melhorar a condição dos pacientes indicados para intervenção. Em particular, a avaliação funcional de cardiomiócitos DYRK1A$^{+/-}$ mostraram que esta cinase pode ser um alvo importante para tratar a disfunção cardíaca, uma vez que os miócitos mutantes responderam de forma diferente ao estiramento e mostraram uma menor capacidade para desenvolver força (tensão ativa).

Este estudo levanta várias hipóteses na investigação da remodelagem reversa. No futuro, estudos de ganho e/ou perda de função realizados em cardiomiócitos isolados ou em modelos animais de *banding-debanding* da aorta ajudarão a testar a eficácia de modular os potenciais alvos terapêuticos encontrados. Além disso, estudos clínicos em coortes de maior dimensão trarão conclusões definitivas quanto ao valor de prognóstico do complemento C3, MuRF1 e DYRK1A.

keywords

aortic stenosis, incomplete reverse remodeling, myocardium, pericardial fluid, proteome, phosphoproteome.

abstract

Valve replacement remains as the standard therapeutic option for aortic stenosis patients, aiming at abolishing pressure overload and triggering myocardial reverse remodeling. However, despite the instant hemodynamic benefit, not all patients show complete regression of myocardial hypertrophy, being at higher risk for adverse outcomes, such as heart failure. The current comprehension of the biological mechanisms underlying an incomplete reverse remodeling is far from complete. Furthermore, definitive prognostic tools and ancillary therapies to improve the outcome of the patients undergoing valve replacement are missing. To help abridge these gaps, a combined myocardial (phospho)proteomics and pericardial fluid proteomics approach was followed, taking advantage of human biopsies and pericardial fluid collected during surgery and whose origin anticipated a wealth of molecular information contained therein.

From over 1800 and 750 proteins identified, respectively, in the myocardium and in the pericardial fluid of aortic stenosis patients, a total of 90 dysregulated proteins were detected. Gene annotation and pathway enrichment analyses, together with discriminant analysis, are compatible with a scenario of increased pro-hypertrophic gene expression and protein synthesis, defective ubiquitin-proteasome system activity, proclivity to cell death (potentially fed by complement activity and other extrinsic factors, such as death receptor activators), acute-phase response, immune system activation and fibrosis. Specific validation of some targets through immunoblot techniques and correlation with clinical data pointed to complement C3 β chain, Muscle Ring Finger protein 1 (MuRF1) and the dual-specificity Tyr-phosphorylation regulated kinase 1A (DYRK1A) as potential markers of an incomplete response. In addition, kinase prediction from phosphoproteome data suggests that the modulation of casein kinase 2, the family of IκB kinases, glycogen synthase kinase 3 and DYRK1A may help improve the outcome of patients undergoing valve replacement. Particularly, functional studies with DYRK1A$^{+/-}$ cardiomyocytes show that this kinase may be an important target to treat cardiac dysfunction, provided that mutant cells presented a different response to stretch and reduced ability to develop force (active tension).

This study opens many avenues in post-aortic valve replacement reverse remodeling research. In the future, gain-of-function and/or loss-of-function studies with isolated cardiomyocytes or with animal models of aortic banding-debanding will help disclose the efficacy of targeting the surrogate therapeutic targets. Besides, clinical studies in larger cohorts will bring definitive proof of complement C3, MuRF1 and DYRK1A prognostic value.

General Index

List of Figures

Chapter I

Chapter II

Chapter III

Chapter IV

Chapter V

Chapter VI

Chapter VII

List of Tables

Chapter I

Chapter II

Chapter III

Chapter IV

Chapter V

Chapter VI

List of Abbreviations

2W ANOVA RM	Two-way analysis of variance (repeated measures)
ACE	angiotensin-converting enzyme
ADA	adenosine deaminase
ADM	adrenomedullin
AGC	auto gain control
AHA	American Heart Association
ANP	A-type natriuretic peptide
AS	aortic stenosis
AT2R	angiotensin II receptor
AUC	area under the curve
AVA	aortic valve area
AVAi	aortic valve area, indexed
AVR	aortic valve replacement
BMI	body mass index
BNP	B-type natriuretic peptide
BSA	bovine serum albumin
CAD	coronary artery disease
CaM	calmodulin
CAMK2	calcium/calmodulin-dependent kinase type II
CaN	calcineurin
CASP	caspase
CEA	carcinoembryonic antigen
CK2	casein kinase 2
cMyBP-C	cardiac-specific myosin-binding protein C
DAG	diacylglycerol
DDA	data-dependent acquisition
DEP	differentially expressed protein
DIA	data-independent acquisition
DTT	dithiothreitol
DYRK	Dual specificity tyrosine-phosphorylation-regulated kinase
ECM	extracellular matrix

EDTA	N-(trimethoxysilylpropyl)ethylenediamine triacetic acid
EDTA-TMS	N-(trimethoxysilylpropyl)ethylenediamine triacetate trisodium salt
EGF	epidermal growth factor
EGFR	epidermal growth factor receptor
ESC	European Society of Cardiology
ESI	electrospray ionization
FA	formic acid
FDR	false discovery rate
FGF	fibroblast growth factor
FTIR	Fourier Transform Infrared
GO	gene ontology
GOEA	gene ontology enrichment analysis
GPLD1	phosphatidylinositol-glycan-specific phospholipase D
GPS	Group-based Prediction System
GSK	glycogen synthase kinase
HDAC	histone deacetylase
HPLC	high performance liquid chromatography
IAA	iodoacetamide
ID	internal diameter
IFN	interferon
IKK	IκB kinase
IMAC	immobilized metal affinity chromatography
IP_3	inositol triphosphate
IVST	interventricular septal thickness
KEGG	Kyoto Encyclopedia of Genes and Genomes
Ktr	rate of force redevelopment
LC	liquid chromatography
LDH	lactate dehydrogenase
LDL	low-density lipoprotein
LFQ	label-free quantification
LV	left ventricle
LVAD	left ventricular assist device
LVEDD	left ventricle end-diastolic dimension
LVEF	left ventricle ejection fraction
LVM	left ventricle mass

LVMi	left ventricle mass, indexed
MALDI	matrix-assisted laser desorption ionization
MAPK	mitogen activated protein kinase
MARS	Multiple Affinity Removal System
MB	myoglobin
MDM2	murine double minute 2
MES	2-(N-Morpholino)ethanesulfonic acid
MHC	myosin heavy chain
min	minute(s)
MLK	mixed lineage kinase
MMP	matrix metalloprotease
MOAC	metal oxide affinity chromatography
MS	mass spectrometry
MuRF	Muscle Ring Finger
NFAT	nuclear factor of activated T cells
NF-κB	nuclear factor kappa B
NLRX1	NLR family member X1
NMR	nuclear magnetic resonance
NOTCH	neurogenic locus notch homolog protein
NPs@EDTA	EDTA-functionalized magnetic nanoparticles
NYHA	New York Heart Association
OD	optical density
OPG	osteoprotegerin
PCR	polymerase chain reaction
Peak Ao	peak aortic valve velocity
PF	pericardial fluid
PGF2αR	prostaglandin F2-α receptor
PHK	phosphorylase kinase
PKA	protein kinase A
PKC	protein kinase C
PLC	phospholipase C
PLS-DA	partial least square discriminant analysis
PSMD1	26S proteasome non-ATPase regulatory subunit 1
PTM	post-translational modification
PWT	posterior wall thickness

qPCR	quantitiative PCR
RANK	receptor activator of nuclear factor κB
RANKL	RANK ligand
RhoA	Ras homolog family member A
ROC	receiver operator characteristic
ROS	reactive oxygen species
RR	reverse remodeling
RWT	relative wall thickness
SDS-PAGE	Sodium Dodecyl Sulfate-Polyacrylamide Gel Electrophoresis
SELDI	surface enhanced laser desorption/ionization
SERCA	sarco(endo)plastic reticulum Ca2+-ATPase
ssTnI	slow-twitch skeletal muscle isoform of troponin I
STKR	serine threonine receptor kinase
TAF1	transcription initiation factor TFIID subunit 1
TAVI	transcatheter aortic valve implantation
TEM	transmission electron microscopy
TGF-β	transforming growth factor-β
TIMP	tissue inhibitor of metalloproteinase
TKL	tyrosine kinase-like
TNF	tumor necrosis factor
TOF	time-of-flight
TRAIL	TNF-related apoptosis-inducing ligand
TUNEL	terminal deoxynucleotidyl transferase dUTP nick end labeling
UPS	ubiquitin-proteasome system
VEGF	vascular endothelial growth factor
VRK	vaccinia related kinase
WT	wild-type

Chapter I

Introduction

Contents

Ageing societies are facing new challenges in healthcare. The continuous rise in life expectancy carries the bitter taste of increased prevalence of noncommunicable diseases. Latest facts released by the World Health Organization (June 1st, 2018) show that silent conditions are the leading cause of death globally. Particularly, cardiovascular diseases kill close to 18 million people annually, twice as much as cancer, remaining the first cause of death today [1]. Despite the broad spectrum of cardiovascular diseases, a big slice of the economical and scientific investment has been applied to coronary artery disease (CAD) [2,3]. This is not surprising since its estimated prevalence is of 4.4% in Europe [4] and of 6.7% in the United States of America [5], being responsible for >40% of the cardiovascular deaths in both regions [4,5]. Nonetheless, the burden of other cardiovascular diseases such as valvular heart disease (VHD) has been keeping up with population ageing. The most recent Cardiovascular Disease Statistics report from the European Society of Cardiology (ESC) shows a prevalence of 2.2% for "Other Cardiovascular Diseases", where valvular disorders are included [4]. The American Heart Association, in turn, shows a prevalence of 2.5% for VHD alone in the American population [5,6]. While, at first glance, these may seem rather low numbers in comparison to coronary disease, an unceasing rise is expected with the ageing of developed countries. This is due to the observed exacerbation of the VHD prevalence with age. For instance, in an American study, it was found a prevalence of <2% in patients <65 years old to 8.5% in patients between 65 to 75 years of age and >13% in older patients (>75 years old) [7]. In turn, a Norwegian population study revealed a prevalence of 0.2% in patients between 50 and 59 years old, contrasting to 9.8% in patients between 80 and 89 years old [8]. The growing number of patients, conjugated with the asymptomatic nature of the onset and the halted progress in the treatment has turned VHD into a new cardiac epidemic [2,3], caressing further attention.

What is generically designated as VHD is, indeed, a group of etiologically distinct conditions affecting the left or the right side of the heart or even both sides. Left-sided valvular disorders encompass mitral and aortic stenosis (AS) and regurgitation, while right-sided disorders comprise tricuspid and pulmonary stenosis and regurgitation. Besides individual valve disease, multiple valve disorders, combined valve stenosis and regurgitation are also observed in the clinical practice [9]. However, left-sided valve diseases remain the most insidious, as a reflex of the higher pressures exerted on the heart's left side. For instance, on a nationwide Swedish study, AS, aortic regurgitation and mitral regurgitation collectively represented >89% of all diagnosed cases. Remarkably, AS contributed to most of the VHD diagnoses (47.2%), almost twice of mitral regurgitation (24.2%), the second most incident valve disease [10].

The expanding relevance of AS in cardiovascular medicine is demonstrated by the fact that this condition is the most common valve disease demanding surgery or catheter intervention in Europe and in North America [9,11]. In fact, despite the AS sharing some etiological features with atherosclerosis, randomized trials have shown that statin therapy has not been able to arrest AS progression [12,13]. Therefore, surgical and catheter-based interventions prevail as the only effective treatments for improving survival [14]. The complexity circumventing AS treatment is further amplified by the secondary repercussions on left ventricle (LV) structure and function. The chronic pressure overload imposed by a progressive narrowing of the aortic valve triggers a myocardial response known as myocardial remodeling. This is a complex phenomenon involving a series of morphological and structural changes, such as cardiomyocyte hypertrophy, collectively aiming at normalizing wall stress [15]. Unfortunately, the limited ability of the myocardium to cope with persistent pressure overload places AS patients in a higher risk of maladaptive remodeling and, consequently, of heart failure, myocardial infarction, stroke and death [15,16]. It is, thus, valve replacement presently the only available treatment to effectively treat AS. By removing the worn and torn valve and implanting a new prosthetic valve, physicians aim at triggering the opposite response, known as myocardial reverse remodeling (RR). This response is mainly characterized by regression of LV hypertrophy, restoration of chamber shape and concomitant improvement of LV function [17,18]. Although, whereas some patients end up attaining a complete structural and functional recovery, many fall on the wayside and demonstrate incomplete RR [19] or even adverse remodeling at follow-up [20]. This phenotypical divergence is associated with poor outcome of these frail patients. Hence, incomplete myocardial RR keeps on this millennium's priority list of cardiovascular medicine challenges.

Notwithstanding the invasiveness required to perform surgical aortic valve replacement (AVR), this is a great opportunity to access and obtain valuable biological samples such as myocardial biopsies and pericardial fluid. A large biobank of these samples collected from AS patients in Hospital São João ensured the viability of this thesis. Acknowledging the wealth of molecular information contained therein, substantial focus was placed on the use of proteomic approaches to extract new biological knowledge from such biological material. A high throughput approach, as provided by proteomics, is expected to provide substantial input with regard to the biological mechanisms underlying the divergent phenotypes, after AVR, as well as to pinpoint potential prognostic surrogate markers and, perhaps more importantly, to identify potential new therapeutic targets to improve the outcome of patients with incomplete RR. The work presented in this PhD thesis is, thus, a contribution to the

third goal for a Sustainable Development: *to ensure healthy lives and promote well-being for all at all ages* (United Nations). Specifically, the results herein reported are expected to pave the way to the improvement of the 'healthy leaving' period of the fragile population with AS.

1. From aortic valve stenosis to incomplete myocardial reverse remodeling: the complex pathological course

Understanding the phenomenon of incomplete myocardial RR requires a prior comprehension of the mechanisms underlying the pathogenesis of AS. Even AS, *per se*, should be perceived as the progression of another clinical entity, the aortic valve sclerosis, sharing some features with CAD. In this section, a brief introduction to AS pathogenesis is given, in addition to the mechanisms behind myocardial remodeling and post-AVR myocardial RR. Provided that the biological samples used in this thesis were collected in a surgical environment, healthy volunteers could not be enrolled. Hence, CAD was used as a control condition, whenever necessary. Consequently, the major similarities and differences between AS and CAD are also covered.

1.1. The pathophysiology of aortic stenosis: convergences and divergences from coronary artery disease

Aortic stenosis is generally regarded as the advanced stage of aortic valve sclerosis. During the sclerotic stage, a chronic and progressive thickening and calcification of the aortic valve occurs [16], being limited to morphological changes [21]. Overt AS is, thus, referred when, beyond morphological changes, functional abnormalities are appreciable, i.e. when there is considerable obstruction of the LV outflow tract [21]. Not surprisingly, similarly to AS, the prevalence of aortic valve sclerosis increases with age: from 26% in patients over 65 years old to 48% in those over 85 years old [7]. Annually, it is estimated that 1.8-1.9% of patients with sclerosis develop overt AS [16]. Aortic sclerosis/stenosis

shares a plethora of etiologies with the remaining VHDs, which can be of degenerative, rheumatic, congenital (e.g. bicuspid valve), inflammatory, infective (endocarditis) or ischemic origin [7]. AS may seldom be a consequence of familial hypercholesterolemia, hyperuricemia, hyperparathyroidism, Paget disease, ochronosis, Fabry disease, lupus erythematosus and of radiation and drug therapy [7,11]. Nevertheless, if some decades ago rheumatic heart disease prevailed as the major cause, today the 'degenerative' etiology represents the majority (>81%) of the cases in the developed countries [7]. Due to its epidemiological relevance, the pathogenesis of AS will be elucidated in light of the cellular and molecular mechanisms of degeneration.

The process of aortic valve sclerosis (and later stenosis) used to be referred to as a passive degenerative phenomenon. The current view, though, assumes that the sclerosing valves are a consequence of an active inflammatory and highly regulated process, sharing many of the features of atherosclerosis [21], the driving mechanism of CAD. **Figure 1** illustrates the main differences between the pathogenesis of AS and CAD. Despite the lack of strong evidence, it is generally agreed that in both pathologies an initial endothelial lesion takes place, as a result of increased mechanical stress and reduced shear stress. Then, lipid deposition (mainly low-density lipoprotein, LDL) and oxidation ensue, creating a very inflammatory and cytotoxic environment. Consequently, endothelial cells increase the expression of adhesion molecules leading to the infiltration of monocytes and T cells. Inside the stenotic valves/atheroma, monocytes differentiate into macrophages and T cells release several pro-inflammatory cytokines, such as tumor necrosis factor-α, transforming growth factor-β (TGF-β), interleukin (IL)-1-β and the profibrotic angiotensin II. The paracrine cues of such cells communicate with endothelial and smooth muscle cells, in CAD, and with fibroblast-like valve interstitial cells, in AS, which together are responsible for the secretion of matrix metalloproteases (MMPs) and tissue inhibitors of metalloproteases (TIMPs). Such molecules disorganize extracellular matrix (ECM) and, in combination with increased secretion of collagen by fibroblasts, are responsible for increased valve or artery stiffness, in AVS and CAD, respectively. ECM disarray is also sided with *in situ* angiogenesis [22–30].

Despite the aforementioned similarities, AS and CAD display also specific pathogenic features (**Figure 1**), starting in rheology. While the coronary artery is subjected to sustained laminar blood flow, the aortic valve is exposed to pulsatile shear stress on the ventricular side and low and reciprocating shear stress on the aortic side. This is thought to induce the

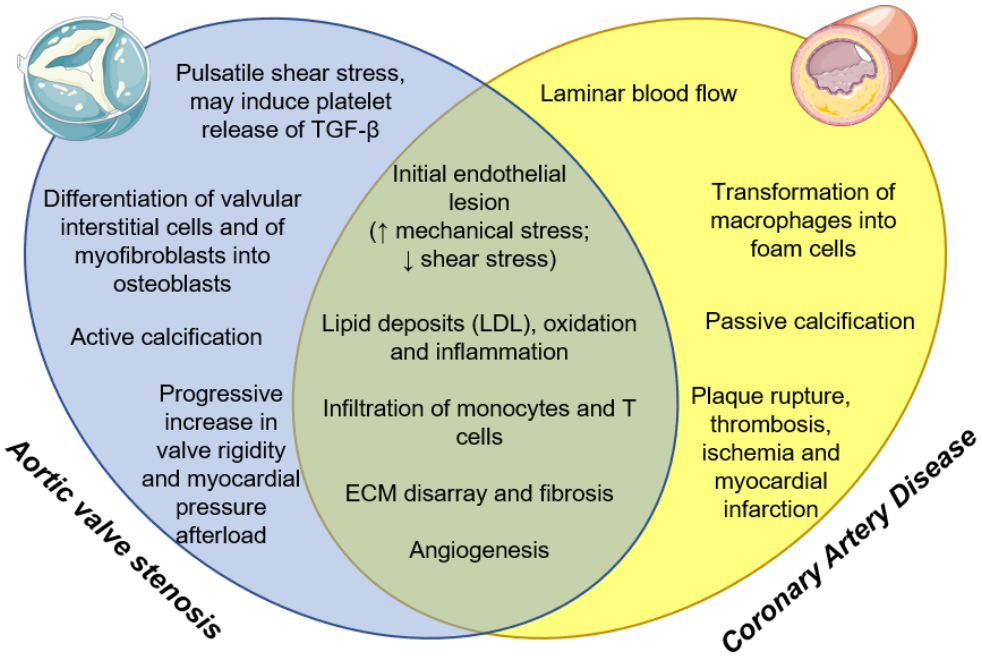

Figure 1. Major hallmarks of aortic valve stenosis and coronary artery disease pathogenesis. The common features are presented in the middle, while aortic stenosis and coronary disease specific features are presented on the left and on the right, respectively. Some graphical elements were adapted from Servier Medical Art. Abbreviations: ECM: extracellular matrix; LDL: low-density lipoprotein; TGF-β: transforming growth factor-β.

release of TGF-β1 from platelets and to activate it. TGF-β1 may, in turn, lead to valve narrowing and fibrosis, further increasing shear stress in a vicious cycle-manner [31]. Other differences reside in the cellular entities involved in the pathogenesis. For instance, foam cells are more characteristic of CAD and osteoblasts are more specific of AS (although they can be found in both cases). Foam cells result from the transformation of macrophages when they are no longer able to mobilize cholesterol from internalized oxidized LDL. Eventually, the phagocytic activity of these cells is hampered, and they undergo apoptosis leading to passive calcification [32]. Osteoblasts, in turn, are thought to result from myofibroblast-like valve interstitial cells differentiation due to the activation of several osteogenesis-related pathways, together leading to active calcification and bone formation [23]. The Neurogenic locus notch homolog protein (NOTCH), the Wnt3/LDL receptor-related protein 5 pathways and the osteoprotegerin (OPG)/receptor activator of nuclear factor κB (RANK)/RANK ligand (RANKL) axis are among such pro-osteogenic pathways. NOTCH signaling is activated by pro-inflammatory cues and stimulates immature osteoblast proliferation, while still inhibiting terminal osteoblast differentiation. The Wnt pathway, in turn, leads to the stabilization of β-catenin that promotes osteoblast differentiation and calcification, by enhancing the expression of Runt-related transcription factor 2. Finally, the

reduced levels of OPG and a higher RANKL/RANK ratio further promote osteoblastic transformation of valvular interstitial cells and active calcification, by inducing cell proliferation, MMP1 and MMP2 activation as well as osteocalcin and alkaline phosphatase expression [21,23]. Finally, AS and CAD remarkably differ in the impact on the myocardium and in secondary adverse events. The progressive coronary narrowing in CAD may lead to thrombosis due to plaque rupture or to ischemic insults (e.g. infarction) that may result in regional myocardial necrosis. In turn, in AS, the progressive valve rigidity increases pressure afterload and myocardial wall stress, leading to myocardial structural and functional adaptations (myocardial remodeling – next section) that may, ultimately, become maladaptive and prime heart failure [23,28,32].

*This section was adapted from the third section of the paper: **F. Trindade**, R. Ferreira, B. Magalhães, A. Leite-Moreira, I. Falcão-Pires, R. Vitorino. How to use and integrate bioinformatics tools to compare proteomic data from distinct conditions? A tutorial using the pathological similarities between Aortic Valve Stenosis and Coronary Artery Disease as a case-study. Journal of Proteomics. 171 (2018): 37-52. doi: 10.1016/j.jprot.2017.03.015.*

1.2. Myocardial remodeling

The myocardium is continuously experiencing and responding to rapid and transient changes in volume and pressure throughout the cardiac cycle. Whenever mechanical stress or neurohumoral load becomes persistent, a myocardial response is set in motion to preserve myocardial performance. This response spans from microscopic cellular and extracellular adaptations to global macroscopic geometric changes and is generically designated as myocardial remodeling [33]. In what regards AS, the continuous tightening of the aortic valve orifice is responsible for increased LV afterload pressure that heightens myocardial wall stress. It is, thus, a chronic pressure overload state the major driver of myocardial remodeling in AS patients (**Figure 2**) [15,21,23,34]. Since cardiomyocytes are terminally differentiated cells and display a very low turnover rate, these adapt to pressure overload through hypertrophy with reactivation of the fetal gene program [35]. The cellular

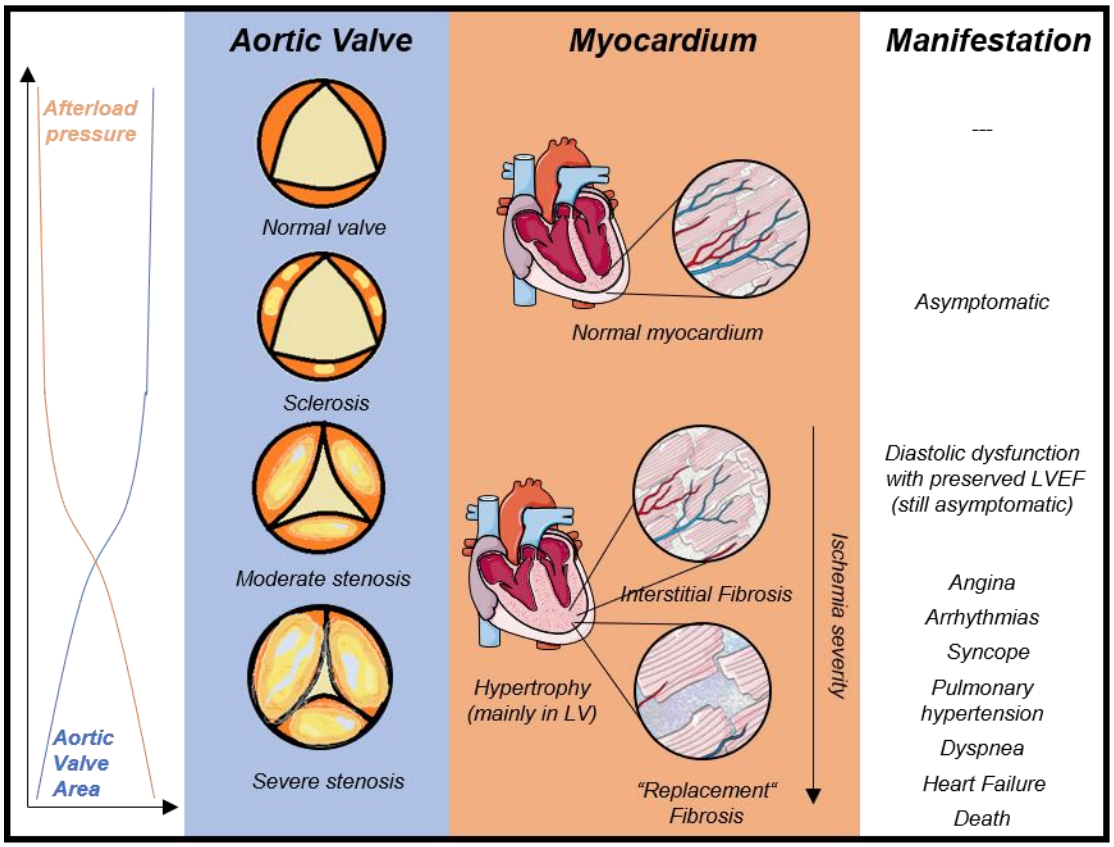

Figure 2. Aortic valve stenosis, myocardial remodeling and their clinical manifestation. Aortic stenosis is a silent, multi-stage disease (blue section). During the sclerotic phase there is lipid accumulation (yellow deposits) and activation of the inflammatory cascades in the valve leaflets. In this period, the orifice of the aortic valve is preserved (blue line on the left graph – aortic valve area) and, thus, the myocardium is not subjected to hemodynamic overload (orange line on the left graph – afterload pressure). At this point, the disease is asymptomatic. Once the aortic valve begins to narrow, due to lipid overload and active calcification (light blue blur), the LV outflow tract becomes progressively obstructed, and the LV pressure overload increases. In this stage (moderate stenosis), the myocardium starts to grow due to cardiomyocyte hypertrophy (orange section), and "reactive" interstitial fibrosis is triggered. At this point, the heart develops diastolic dysfunction, but LVEF is maintained. Therefore, unless by occasion of heart imaging or stress testing, AS patients remain undiagnosed, as symptoms are generally not evident. However, as stenosis worsens (low valve area) and the pressure overload escalates, the hypertrophic response is not enough to cope with the hemodynamic challenge, and the poor vascularization leads to myocyte apoptosis. The dead cardiomyocytes are, thus, replaced by fibrotic tissue, and the myocardial function is compromised. Hence, it is during the severe phase where most symptoms become clear, such as angina, syncope, arrhythmias. In the end stage of the disease, patients may develop secondary pulmonary hypertension, exertional dyspnea, heart failure, all increasing the risk of death. Some graphical elements were adapted from Servier Medical Art. Abbreviations: LV: left ventricle; LVEF: left ventricle ejection fraction.

growth is characterized by the parallel addition of myofilaments, leading to cellular widening. Macroscopically, this results in increased wall thickness and concentric remodeling, which normalizes wall stress, while preserving LV ejection fraction (LVEF). The continuous growth of cardiomyocytes demands ECM support and equally sustained growth of capillary and neuronal meshwork. In the early stage of the disease, the cardiac expression of the profibrotic angiotensin-converting enzyme (ACE) and of TGF-β are increased. Angiotensin II is generated by ACE activity and primes the phenotypical conversion of fibroblast into

myofibroblasts. These cells secrete and respond to TGF-β signaling by synthesizing collagen type I and III as well as fibronectin, to create new ECM. The newly formed matrix is deposited in a diffuse pattern and is responsible for the so-called interstitial fibrosis. This “reactive” process is essential to keep myocardial viability and is considered to be potentially reversible [15,21,35,36].

Even though the cardiomyocytes display remarkable plasticity to cope with pressure overload, myocardial hypertrophy has a huge potential to become maladaptive. Hence, the view that hypertrophy is a protective mechanism is frequently questioned. Indeed, if not timely managed AS-driven myocardial remodeling may result in myocardial ischemia, which may be manifested as angina episodes. Myocardial ischemia, in this setting, is explained by a slow neovascularization process that cannot keep up with the fast-growing myocytes, thus driving to an oxygen and nutrient demand-supply mismatch. Moreover, the increased LV transmural pressure favors coronary vascular resistance, altogether driving to a reduction in coronary flow reserve [23,34,35,37]. Defective myocardial perfusion is also associated with cardiomyocyte apoptosis and consequent development of “replacement” fibrosis, which is deemed irreversible. This type of fibrosis is generally observed in the subendocardial and mid-wall layers of the LV and is associated with poorer outcomes [15,23,35]. For instance, mid-wall fibrosis was associated with an 8-fold increase in mortality of AS patients [38]. Intricately associated with fibrosis is the impairment of LV relaxation and the resulting diastolic dysfunction. This kind of dysfunction occurs early on the onset, but it is aggravated as the stenosis and fibrosis worsen. In fact, LV fibrosis is regarded as the main vector from a compensated hypertrophic state to heart failure [35,37]. Fibrosis also predisposes to arrhythmias due to the impaired electrical conduction [23]. In the late stages of the disease, systolic dysfunction generally ensues (associated with a reduction in LVEF) that might be explained by the insufficient capacity of the myocardium to cope with increased afterload, although the exact mechanisms are yet to demonstrate [34]. In the end-stage of AS and myocardial decompensation, the rise of LV filling and left atrium pressures (and the subsequent development of secondary pulmonary hypertension) accentuates signs and symptoms, such as pulmonary congestion and dyspnea [34,35]. Therefore, if not timely treated, AS patients have low chances of survival. Indeed, one-year survival in AS patients without valve replacement is just 50% [37].

1.3. Diagnosis and therapeutic options in aortic stenosis

One of the challenges in the diagnosis of AS patients is the existence of a prolonged subclinical phase, without manifestation of symptoms [35,39]. Hence, clinicians need to be aware of the risk factors and closely monitor patients at higher risk. Congenital abnormalities, such as bicuspid valves, age, gender, smoking history, hyperuricemia, hypertension, hypercholesterolemia, high levels of LDL and/or lipoprotein(a), obesity, diabetes, metabolic syndrome, hypercalcemia, decreased bone mineral density, secondary hyperparathyroidism, hypercreatinemia and renal disease are all risk factors to consider on the AS setting [21,35,40]. The diagnosis is generally performed under echocardiography examination, following the appearance of symptoms such as systolic murmur, angina, syncope and dyspnea. Not surprisingly, the diagnosis of AS is sometimes an incident finding upon screening for other pathologies. Unfortunately, though, a considerable number of the patients (5-10%) is also diagnosed in the late phase of the disease, when heart failure is already patent [35]. Indeed, several recent studies have questioned the timing of intervention in AS (reviewed in [41,42]). **Table 1** summarizes the main tools and variables used for the diagnosis and assessment of AS severity. Beyond the use of echocardiography (under standard or stress conditions), cardiac magnetic resonance and computed tomography, it should be highlighted the use of serum biomarkers, such as the B-type natriuretic peptide (BNP). This peptide is released by the LV due to continuous mechanical stress and, for that reason, is a useful indicator of LV dysfunction, being correlated with LVEF. BNP is, thus, helpful in risk stratification and in defining the optimal time for intervention [9,11,35,43].

The use of bioimaging tools is important not only for the diagnosis of AS, but also for the screening of co-morbidities (e.g. CAD), risk stratification and for the therapy decision-making process [11,35]. For details on the guidelines for the choice of the most suitable therapies in AS patients, the reader is referred to the latest ESC report [9].

Currently, despite the disappointing attempt of statin therapy [12,13], there is no pharmacological therapy available to prevent or treat AS or, at least, delay the need for valve replacement [21,23,35,44]. Consequently, AS patients are carefully monitored and evaluated to decide if, when and which treatment they can benefit from. Valve replacement, unfortunately, is not an option for all patients. Indeed, patients with a life expectancy lower than one year, presenting severe co-morbidities or those to whom an intervention (either

surgical or non-surgical) would unlikely result in improved quality of life are generally not candidates for valve replacement. Instead, this subgroup of patients is enrolled in palliative care, often being treated with digoxin, diuretics, ACE inhibitors or angiotensin receptor blockers to mitigate heart failure [11]. Besides, some subjects may also be candidates for balloon aortic valvuloplasty, where an inflated balloon is used to apply pressure on the stenotic valve in order to widen the orifice of the aortic valve. In spite of providing short-term benefits (restenosis is soon triggered), this intervention can be used for palliation or as a preparation for definitive treatment [45]. Today, the only effective treatment for AS is, *de facto*, valve replacement. Depending on the surgery risks, the patients may be selected for percutaneous transcatheter aortic valve implantation (TAVI) or surgical AVR. In the case of high surgical risk, for instance, due to porcelain aorta, existing co-morbidities or general frailty, patients become surrogates for TAVI. This is a less invasive approach, through which a valve is implanted by transfemoral, transapical, transaortic or by subclavian routes. However, this approach is not devoid of risks and is associated with paravalvular aortic regurgitation, stroke, vascular complications and the need for new pacemaker [11,35,46]. In turn, if the patients fall in the low-to-intermediate risk category, they are good candidates for surgical AVR. Surgical AVR, henceforth referred to AVR, remains as the standard therapeutic choice due to the long-term record of safety, efficacy and durability [9,35].

Table 1. Main tools used for the diagnosis and assessment of aortic stenosis severity; the measured variables and current classification criteria [9,11,35,47].

Diagnostic and severity assessment tool	Variables/ Object of analysis	Definition (units)	ESC/AHA[a] classification criteria		
			Mild	Moderate	Severe
Doppler echocardiography	AVA	Aortic Valve Area – surface of the aortic valve orifice (cm^2)	>1.5	1.0-1.5	<1.0
	AVAi	indexed AVA – surface of the aortic valve orifice normalized to body surface area (cm^2/m^2)	>0.85	0.60-0.85	<0.60
	Peak Ao	Peak aortic jet velocity – maximal blood flow velocity across the aortic valve (m/s)	2.6-2.9[b]	3.0-4.0	>4.0
	Mean gradient	Mean transvalvular gradient – average of the pressure difference between LV and the aorta (mmHg)	<30 (<20†)	30-50 (20-40†)	>50 (>40†)
Stress test - Exercise - Low dose dobutamine test	Stress AVA Stress mean gradient	Aortic valve area (cm^2) and mean transvalvular pressure gradient (mmHg) measured under stress conditions (either induced by exercise or by dobutamine infusion)	Especially important for risk stratification in apparently asymptomatic patients		
	Coronary flow reserve/stroke volume	The ratio between the maximal and resting blood flow through coronary arteries. It can be indirectly assessed through calculation of stroke volume (amount of blood ejected by the heart, during systole)	Also important for risk stratification. An increase ≥20% in the stroke volume during dobutamine test is associated with a better outcome		
Cardiac Magnetic Resonance	Aorta geometry	Evaluation of the aortic root and ascending aorta dimensions and shape	Useful tools for the evaluation of AS severity and prognosis		
	Fibrosis	Assessment of the pattern/extent of the fibrotic areas			
	Calcification	Evaluation of the extent of calcified areas			
Multi-slice Computed tomography	Aorta geometry	Evaluation of the aortic root and ascending aorta dimensions and shape			
	AVCS[c]	Aortic Valve Calcification Score – a measure of the calcium deposits extent in aortic valve (Agatston units)	-	♂ ≥1200 ♀ ≥700	♂ ≥2000 ♀ ≥1200

a) American Heart Association (AHA) guidelines are marked with †; b) Aortic sclerosis is defined by peak Ao ≤2.5 m/s; c) It is only included in the European Society of Cardiology (ESC) guidelines, but not in AHA guidelines

1.4. Myocardial reverse remodeling

As soon as the valve is replaced, AS patients experience immediate relief of LV afterload, triggering a response in the opposite direction of the (pathological) remodeling and, thus, called myocardial reverse remodeling (RR). The concept of “reverse remodeling” was first introduced in 1995 by Kass and his colleagues, during a study of cardiomyoplasty. In such experiment, the *latissimus dorsi* muscle was wrapped around the heart of patients with dilated cardiomyopathy and chronically paced synchronously with ventricular systole. The term “reverse remodeling” was associated to the positive effects of cardiomyoplasty on systolic function and on heart chamber size (shrinking back to normal) [48]. Today, the definition of RR has broadened and refers to any normative change in chamber geometry and function in failing hearts that are prompted by any given therapy, either pharmacological (e.g. ACE inhibitors, β-blockers, mineralocorticoid receptor antagonists) or interventional (e.g. LV assist devices, LVAD, revascularization, resynchronization, valve surgery) [17,18,33,49].

Concerning AS, the post-AVR RR response is characterized by regression of LV hypertrophy, restoration of chamber shape and concomitant improvement of LV function [17,18]. Unlike the studies involving LAVDs, where studying molecular changes occurring during RR in human samples is possible [49]; in the case of AS, myocardial biopsies are only available during AVR. Therefore, most knowledge stems from animal models of aortic banding-debanding. In these models, usually the transverse (arch) or the ascending sections of the aorta are constricted (banding), restricting the blood flow from the LV and, consequently, inducing pressure overload as in AS. After reaching the plateau phase of hypertrophy, generally between 4 and 5 weeks of banding, the animals are submitted to a second intervention to remove the constricting suture/knot (debanding). In fact, aortic banding is enough to recapitulate the consequences of stenosis on LV structure and function. Animals surviving the procedure show myocardial remodeling, as corroborated by increased hypertrophy, interstitial fibrosis and diastolic dysfunction. In turn, aortic debanding, mimicking RR, is generally followed by hypertrophy regression, but less often by resolution of fibrosis and improvement of myocardial dysfunction towards sham levels [50–53]. In **Figure 3**, one can find a brief representation of the main cellular and molecular changes occurring during RR, illations taken from aortic banding-debanding studies.

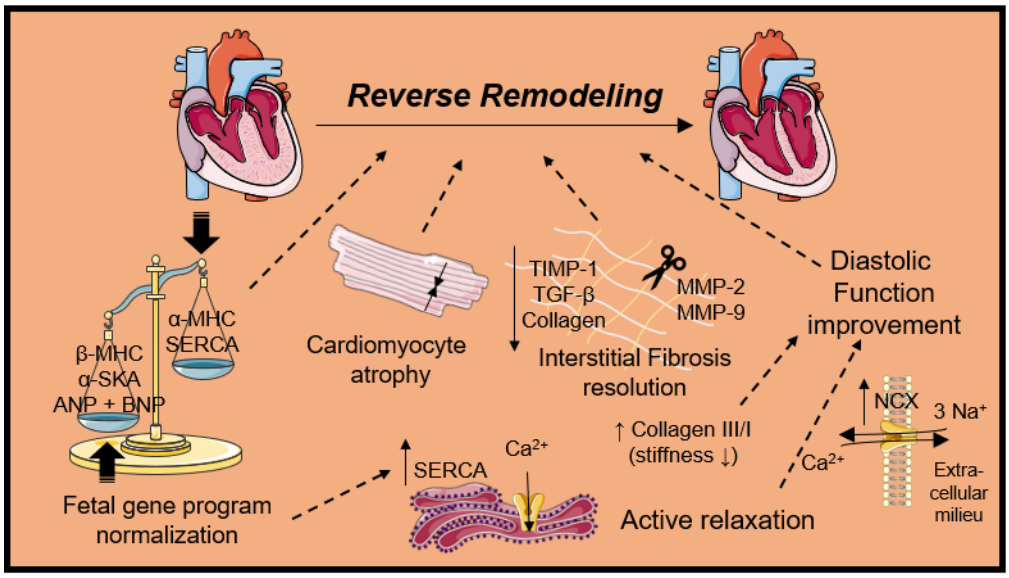

Figure 3. Representation of the main cellular, extracellular and molecular changes underlying myocardial reverse remodeling. During reverse remodeling, there is a normalization of the fetal gene program, with downregulation of the β-MHC, α-SKA and natriuretic peptides genes and upregulation of the α-MHC and SERCA genes. This is accompanied by a reduction in cardiomyocyte dimensions and volume (atrophy). In the extracellular milieu, the matrix remodels due to an increased activity of matrix metalloproteinases and reduced expression of pro-fibrotic TIMPs and TGF-β. Thus, the overall content of collagen drops, reducing interstitial fibrosis. The extracellular matrix remodeling is also characterized by a shift between the stiffer collagen I and the compliant collagen III, with a net reduction of myocardial stiffness. The increase in the expression of calcium extrusion channels, such as SERCA and the NCX, favors active relaxation which, together with reduced myocardial stiffness, underly the improvement of diastolic function. Some graphical elements were adapted from Servier Medical Art. Abbreviations: α-SKA: α-skeletal actin; ANP: A-type natriuretic peptide; BNP: B-type natriuretic peptide; MHC: myosin heavy chain; MMP: matrix metalloprotease; NCX: Na^+/Ca^{2+}-exchanger; SERCA: sarco(endo)plastic reticulum Ca^{2+}-ATPase; TGF-β: transforming growth factor-β; TIMP1: tissue inhibitor of metalloproteinase-1

One of the most striking observations taking place during RR is the regression of hypertrophy. Many studies on murine models demonstrate a reduction in LV dimensions as well as a decrease of heart or LV mass and of myocardial wall thickness after debanding. Histological assessment of cardiomyocyte size also emphasizes reduction of hypertrophy, showing significantly lower cardiomyocyte diameter or cross-sectional area [50–53]. At the same time, fetal genes expression is normalized, with reduction of the β-myosin heavy chain (MHC), α-skeletal actin and of the natriuretic peptides (A-type, ANP, and BNP), concomitant with the restoration of α-MHC and of sarco(endo)plastic reticulum Ca^{2+}-ATPase (SERCA) expression [50,52,54]. While hypertrophy is often reverted to the pre-morbid state, with no differences found between sham and debanded animals, as assessed by markers such as heart-to-body weight ratio or cardiomyocyte size [51,55], the same is frequently not the case for fibrosis [50,52,54–56]. For instance, Gao *et al*. [50] reported a 5-fold increase of the interstitial collagen (stained with Picrosirius Red) after banding, which remained 2.5-fold

higher after debanding compared to sham. During myocardial RR not only the content in collagen is tendentiously decreased, but also the balance between collagen isoforms is altered. An initial preponderance of the stiffer collagen isoform (type I) is observed, which is then shifted to the extensile isoforms, such as type III and VIII [54]. Beyond collagen, the amount of other ECM constituents, such as periostin, falls after debanding, but still being higher than in non-operated animals [56]. The process of ECM remodeling is orchestrated by a fine balance between MMPs and TIMPs [15]. For instance, an increase in MMP2 and TIMP1 expression was observed after banding, which were then reverted after debanding [54]. MMP9 and TIMP1, though, have not shown significant changes throughout the course of the protocol (4 weeks of banding). Still, in a study with an extended period of banding (12 weeks), MMP9 was found to increase significantly when compared to control animals and to decline upon debanding [53]. The relevance of ECM remodeling was confirmed by Bjørnstad *et al*. [54] after performing functional analysis of gene expression data derived from microarrays. These authors showed that the most strongly regulated biological process term after debanding was “ECM structural constituent”. Notably, the term “TGF-β receptor binding” was also found significantly dysregulated after debanding and the TGF-β2, in particular, was confirmed to be increased before banding and decreased upon debanding [54]. The TGF-β family is, similarly to angiotensin-II, responsible for myocardial fibrosis during myocardial remodeling [17].

A common observation in studies with animal models of aortic banding-debanding is the presence of diastolic dysfunction, even after the removal of the ligature causing pressure overload. Diastolic dysfunction is mainly the result of two factors: impaired active relaxation and myocardial stiffness. The former may result from the decreased expression of cytoplasmic calcium extrusion systems, such as SERCA and the Na^{+}/Ca^{2+}-exchanger (NCX), which are normalized after unloading [50,53]. The latter persists after debanding because the regression of fibrosis takes longer than the resolution of hypertrophy, impairing complete muscle relaxation [50,54]. Systolic dysfunction might also manifest in the course of myocardial remodeling, disappearing gradually during RR. For example, the systolic tissue velocity (decreased upon banding) stepped up from three to seven and fourteen days after debanding in a mice model of ascending aortic banding [52]. In turn, others reported normalization of LVEF, stroke volume and of LV systolic pressure in debanded rats, with the former two stabilizing at sham levels [53]. These animal studies also evidence that the timing of the intervention (debanding) is crucial to the extent of reverse remodeling.

1.5. The problem of incomplete myocardial reverse remodeling

In the human setting, even more than in animal models, not all patients show a complete recovery after AVR. In fact, the extent of RR is extremely variable, with many patients presenting an incomplete structural and functional recovery. For instance, Biederman *et al*. [19] reported that 85% of an AS population presented LV mass above normal 4 years past AVR. Others reported that 50% of patients with isolated AS or with combined AS and insufficiency still exhibit hypertrophy 5 years after AVR [57]. Recently, our group confirmed the existence of residual hypertrophy in 44% of the patients 5 years after AVR in a cohort of isolated AS with over 120 individuals [58]. Therefore, despite the instant hemodynamic relief conferred by AVR, many patients present with incomplete myocardial RR. So far, there is no categorical confirmation of the causes of such disparity in the post-AVR myocardial response. Albeit, many risk factors have been pointed to exert influence in the extent of RR.

One of the classical risk factors for incomplete RR is the co-existence of uncontrolled systemic hypertension. This is because, similarly to AS, systemic hypertension imposes a pressure overload state on the LV. Thus, notwithstanding the AVR surgery, if left unmanaged, co-existing hypertension may preclude myocardial RR. In fact, LV mass regression was shown to be lower in patients with hypertension, even after correcting for afterload, meaning that systemic and neurohumoral factors, other than load, contribute for this outcome [59–61]. One of the possible mechanisms explaining the preservation of LV mass in AS patients with concomitant hypertension is the increased expression of TIMP2, an inhibitor of MMPs, limiting collagen turnover, which favors ECM maintenance. Moreover, an increased collagen I/III ratio in patients with AS and hypertension may lead to diastolic dysfunction as a result of increased myocardial stiffness [59].

Other frequent co-morbidities, such as diabetes mellitus, obesity and CAD, have also been shown to influence RR. Pre-existing diabetes mellitus was found to be an independent predictor of inadequate LV mass regression one year after valve replacement [59,62]. Furthermore, it was associated with worse diastolic performance, as demonstrated by higher cardiomyocytes' passive force, sided with hypophosphorylation of the stiffer titin isoform (N2B). The same study evidenced an increase in interstitial fibrosis concomitant with advanced glycation end products deposition in patients with both conditions, together contributing to myocardial stiffness and, consequently, to the diastolic dysfunction status [63]. In turn, subjects with higher body mass index (BMI) were found to be at higher risk for

prevalent post-AVR LV hypertrophy, which may be induced by cardiac steatosis [64]. Notwithstanding, studies reporting the association between obesity and post-AVR survival have been conflicting, with some advocating that more obese patients display higher survival (the so-called “obesity paradox”) [65], others claiming that overweight, but not obese, patients are more protected [66] and others rebutting any sort of protection [67]. Concerning CAD, it was reported that non-revascularized patients with moderate coronary atherosclerosis present poorer RR 3 years after valve replacement, as shown by lower reduction of LV mass, LV diastolic dimension, posterior wall thickness and interventricular septum thickness [68]. Besides the slower regression of the LV mass, the mechanical performance of this subpopulation (AS + CAD), evaluated by magnetic resonance-tracked intramyocardial circumferential strain, is overall ~50% lower than that of subjects with AS alone [69].

The remarkable capacity of the myocardium to regulate mechanical force, through hypertrophy and atrophy, in response to changes in afterload is intimately dependent on the ECM integrity. The collagenous and non-collagenous framework of the ECM is crucial to preserve the alignment of the myofibrils as well as to connect the contractile elements of different cardiomyocytes, working in a synchronous syncytium [15]. During AS-induced myocardial remodeling, the deposition of collagen is required, but the transition from adaptive (interstitial) to adverse (replacement) fibrosis might also be viewed as a limbo between a favorable and a poor outcome [15,23,35]. In a study using late enhancement cardiac magnetic resonance to assess the levels of replacement fibrosis, it was reported that only patients without replacement fibrosis before AVR improved their New York Heart Association (NYHA) class during RR. Furthermore, it was demonstrated that the levels of late enhancement were unaltered nine months after AVR, further showing the irreversibility of this phenomenon and the associated myocardial function decline [70]. More recently, our group demonstrated that the histologically determined perioperative collagen volume fraction remained a predictor of residual LV hypertrophy even in multivariate analysis (odds ratio of 7.1 for collagen volume fraction ≥15.4%, with 95% confidence) [58].

The patient-prosthesis mismatch (PPM) is probably the most important patient-independent risk factor, and it refers to the case when the effective prosthetic valve area is lower than the initially required, in relation to the body surface area. Consequently, in spite of the normal prosthesis function, the transvalvular pressure gradient remains higher than desired, hence jeopardizing complete myocardial RR [15]. As with the case of obesity, available data is not consensual with regard to the patients’ outcome [15]. For example,

while Howel *et al.* [71] reported no association between PPM and post-AVR survival, others have shown that PPM impairs LV mass regression, induces congestive heart failure [72] and is an independent predictor of short- and long-term mortality [73].

Non-modifiable risk factors such as age and gender have also been scrutinized with respect to the extent of RR. Nevertheless, in any case, the association with worse regression and survival is controversial. For instance, while some proclaim a lack of association between age and LV mass [60,74], others show a relationship between the age of the patients at the time of AVR and increased mortality [61,75]. Concerning gender, some groups have shown that women have lower odds of displaying incomplete RR, probably due to the anti-fibrotic role of estrogens [15,76,77]. Others have shown that women are more likely to display worse regression [62] or even that gender, *per se*, does not influence mortality one year after surgery [78].

All the aforementioned studies point to the complexity of the biological processes underlying the process of RR and highlight our inability to forecast the subset of patients that will likely display an incomplete myocardial RR. Regardless of the risk-addictive or preventive nature of both the modifiable and non-modifiable factors, the bottom-line today is that AVR follow-up studies denunciate a high proportion of patients with poor regression [19,57,58]. In addition, patients with incomplete RR (with postoperative LV hypertrophy) are at higher risk for adverse cardiac and extracardiac events, hospitalization and all-cause death [58,79,80]. Therefore, the incomplete myocardial RR prevails as a major problem in the current paradigm of VHD management. Cardiologists, interventionalists and cardiothoracic surgeons urgently require new prognostic tools as well as adjuvant therapies to expand the proportion of patients with complete myocardial recovery with minimal or, at least, with similar risk of cardiovascular events or death to age-matched healthy individuals.

2. Myocardial (phospho)proteomics as a powerful tool to uncover the biological differences between complete and incomplete reverse remodeling

Despite being an invasive procedure, the AVR offers a great opportunity to collect myocardial biopsies and other less conventional biological samples, such as pericardial fluid (see ***section 3***), bestowing a wealth of biological information. Nowadays, this is yet not a routine in operating rooms since all the information required for the diagnosis, prognosis and disease management is gathered from clinical history, imaging and blood tests (e.g. BNP), as recommended by ESC guidelines [9]. Nonetheless, the molecular characterization of these biological samples may provide insight into the molecular mechanisms and biological processes underlying the complete and incomplete RR phenotypes. Moreover, a molecular survey through omics approaches is also a valid means to identify biomarkers, either for diagnosis or prognosis that concur or add to those already established [81]. Last, but not least, large-scale molecular analysis may also help by pinpointing new potential therapeutic targets to improve the outcome of AS patients.

In this era of fast-growing analytical technologies, such as sequencing, microarrays, mass spectrometry (MS) or nuclear magnetic resonance (NMR) spectroscopy, the use of any fundamental omics discipline (genomics, transcriptomics, proteomics and metabolomics) is expected to provide valuable molecular insight into post-AVR myocardial RR. When compared to the traditional wet lab techniques, omics approaches deliver data with high throughput, i.e. large amounts of data are obtained in smaller time frames, providing integrated molecular knowledge and being highly hypothesis-generating [82]. Each of the classic omics approaches has their own advantages and limitations. Genomics and transcriptomics identify dysregulated genes/transcripts and pathways in disease, but hardly allow the prediction of the phenotypical effect, due to epigenetic effects and to the regulation at the post-transcriptional and translational levels [82]. Proteomics and metabolomics, however, aim at profiling the dynamic by- or end-products of transcription and translation, i.e. proteins and metabolites, which are more directly related to the observed phenotype. The downside of the latter two is the need to use technologies with enough sensitivity and resolving power to analyze molecules in a high dynamic range of concentrations [82,83]. At first glance, it could be argued that metabolomics is

advantageous over proteomics, since it targets much less endogenous metabolites than proteomics target proteins, their isoforms and post-translationally modified counterparts. Although, metabolites are highly dynamic showing high temporal and spatial variability, and metabolomics is currently a less mature field than the remaining omics. In fact, only a combination of different analytical platforms (e.g. NMR and combinations of gas chromatography or liquid chromatography (LC) and MS) allows the coverage of the most metabolites possible [82,84]. In turn, proteomics relies primarily on different LC-MS modalities to uncover the largest number of proteins possible, thus easing data integration and interpretation. For all these reasons, but still acknowledging the complementarity of the different omics, a combined proteomics and phosphoproteomics approach was deemed the most suitable to sketch the molecular profile and to study the biological processes underlying incomplete myocardial RR. Particularly, myocardial phosphoproteomics was hypothesized to deliver potential therapeutic targets in this setting, because it is possible to predict dysregulated kinases that control cardiomyocyte response upon unloading.

In this section, a brief introduction to the field of proteomics and phosphoproteomics (hereafter collectively referred to as (phospho)proteomics for simplicity) is given, followed by an outline of the studies taken, so far, on human myocardium in the setting of myocardial remodeling/RR and the correspondent animal models of pressure overload.

2.1. The (phospho)proteomics workflow

Proteomics is a very broad and continuously expanding field of research, whose main goal is to identify and/or quantify all proteins present at a given time, in a given biological system, such as cells, tissues, organs, biofluids or organisms. Through proteomics, it is also possible to study protein localization, protein-protein interactions, protein activity, functional domains, isoforms and post-translational modifications (PTMs), with direct implications in an observed phenotype [83,85,86]. In the cardiovascular setting, its helpfulness has been shown in biomarker discovery for heart disease through plasma screening, identification of potential therapeutic targets as well as in tissue-based mechanistic research from preclinical to translational studies (reviewed in [85]).

MS remains as the gold standard technique for proteomics research, being particularly useful for the identification and quantification of proteins as well as for PTMs

characterization. It is often preceded by uni- or multidimensional separation steps, most commonly, gel-based (one- or two-dimensional gel electrophoresis) or gel-free methods, such as LC-based techniques (e.g. size exclusion, ion exchange, affinity or reverse phase chromatography) that improve the resolution of the separation as well as the chances to detect low-abundance species (sensitivity), sometimes masked by high-abundance ones [87]. There are three main approaches used in proteomics, namely discovery proteomics (shotgun approach), targeted proteomics and targeted discovery proteomics. The former follows a data-dependent acquisition (DDA) approach, which allows the coverage of a higher number of proteins. The main drawbacks of a DDA method are the lower throughput, sensitivity and quantification accuracy, essentially due to the stochastic nature of precursor ion selection. In turn, in the targeted approach, one monitors a lower number of analytes, but with increased sensitivity and specificity. Although, this method requires the development of specific methods (multiple reaction monitoring) and more demanding instrument programming. Lastly, the targeted discovery approach stands in the middle of both methods, and it is established by a commitment between coverage (number of proteins) and the throughput (number of samples). It uses a data-independent acquisition (DIA) method, such as the sequential window acquisition of all theoretical mass spectra (SWATH-MS) to collect the data. Nevertheless, DIA approaches require sophisticated tools and demand for large informatics resources. Thus, while targeted approaches are the preferred methods for the analysis of surrogate biomarker subsets, the shotgun is the best suited approach for initial unbiased fishing of surrogate biomarkers for the condition at scope and for mechanistic research as well [85,88,89]. This is the reason why shotgun proteomics was followed in this thesis to characterize the myocardial and pericardial fluid proteome.

A typical shotgun proteomics workflow comprises 4 major steps: sample preparation, protein separation, LC-MS/MS analysis and bioinformatics analysis (**Figure 4**). First, proteins are purified directly from biofluids or extracted from cells or tissues, usually with a combination of detergents, reducing agents, chaotropic agents and protease inhibitors. Then, proteins are separated using gel-free or gel-based approaches to reduce the complexity of the mixture. Following pre-fractionation and separation steps, proteins are

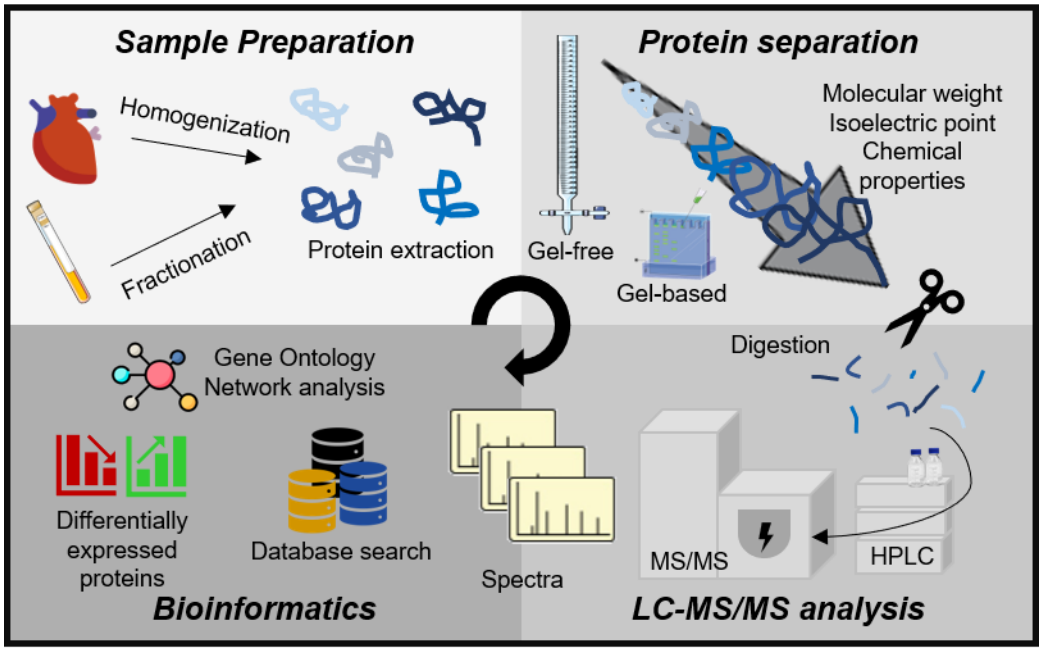

Figure 4. Simplified shotgun proteomics workflow. A typical workflow comprises four main steps. First, solid samples are homogenized, and proteins are extracted with a combination of detergents, reducing agents and inhibitors. Alternatively, proteins are purified or enriched from liquid biopsies. The result is a complex mixture of proteins with different sizes and chemical properties. Second, the proteins are separated by one or a combination of gel-based (e.g. isoelectric focusing and SDS-PAGE) and gel-free (e.g. size-exclusion, strong cation exchange or affinity-based chromatography) methods to reduce the complexity of the samples. Third, the protein fractions are digested with one or more enzymes sequentially (e.g. trypsin, LysC, ArgC, etc) into a mixture of peptides. The peptides are then separated by nanoHPLC, and the fractions are either directly (online) or indirectly (offline) submitted to MS analysis. In the spectrometer, peptides are ionized, fragmented (one or several times – tandem MS) and detected. Finally, the collected spectra are analyzed *de novo* (amino acid sequencing) or compared to existing databases for identification of the proteins by peptide fingerprinting. Proteins may also be quantified by label-based or label-free methods to determine the differentially expressed ones. Bioinformatics analysis also encompasses gene ontology enrichment analysis to identify potentially dysregulated biological processes and molecular functions as well as network analysis of protein-protein interactions in order to identify therapeutic targets and surrogate biomarkers for the disease at scope. Some graphical elements were adapted from Servier Medical Art. Abbreviations: HPLC: high-performance liquid chromatography; MS: mass spectrometry.

digested into peptides, using trypsin, Lys-C or other proteases. In the third step, samples are separated and analyzed through high-performance LC (HPLC) offline or online with MS. The mass spectrometer performs the separation of the molecules and measures the mass-to-charge ratio (*m/z*) of each species, after one or more rounds of fragmentation. The MS instrument is divided into three parts: the ionization source, the mass analyzer and the detector. The peptides (or proteins) to be analyzed are first ionized and transferred from a solid or liquid state to a gas phase. The most used ionization methods comprise matrix-assisted laser desorption ionization (MALDI), surface enhanced laser desorption/ionization (SELDI) and the electrospray ionization (ESI), this last frequently used to couple LC and MS. Next, ions are separated inside the mass analyzer, based on their *m/z,* through

variations of the electric or magnetic fields. There are several mass analyzers available, such as are the time-of-flight (TOF) or the Fourier transform ion cyclotron resonance, but the quadrupole, the linear ion trap and the Orbitrap are currently the most popular in proteomics. These can be used either alone or in tandem, to upgrade resolving power, sensitivity, mass accuracy and the coverable dynamic range. Finally, the ions are detected, the intensity of each *m/z* signal is recorded, and the mass spectra are generated [83,86,87]. Still, a proteomics workflow is only complete after performing bioinformatic analysis. Complex algorithms are required to compile, align and digest mass spectra. For instance, the integration of the area under the curve in a plot of *m/z* versus LC retention time is required for the quantification of the peptides. In turn, protein identification is possible by matching tandem mass spectra to those found in protein sequence databases or spectral libraries, such as Andromeda (MaxQuant), SEQUEST or MASCOT, with an associated probability score or false discovery rate. Finally, bioinformatics is required to attribute a biological meaning to the large proteome datasets. Briefly, bioinformatics tools are important to uncover differentially expressed proteins, to identify protein clusters explaining a given biological variable (e.g. phenotype, disease, response to treatment), through multivariate analysis and to decipher dysregulated biological processes, pathways and molecular reactions through gene ontology (GO) enrichment analysis (GOEA). Ultimately, bioinformatics help isolate surrogate markers for the condition at scope [86,87,90].

The majority, if not all, biological processes governing cell physiology, are regulated by protein PTMs. Particularly, phosphorylation and dephosphorylation by kinases and phosphatases, respectively, regulate protein function, enzymatic activity, interaction partners and localization, with major implications in cell metabolism, signal transduction, excitation-contraction coupling, cell growth, proliferation, survival and apoptosis. Therefore, protein phosphorylation has gained growing attention in cardiovascular research. In this context, researchers have been adapting existing proteomics approaches to characterize the complete set of phosphoproteins in a cell or tissue, giving rise to the field of phosphoproteomics [91,92]. The phosphoproteomics methodological approach is overall similar to the shotgun approach, with some adaptations. First, a higher amount of protein (mg vs µg) is required because phosphoproteins represent only a small proportion of a cell's proteome. Then, protein extraction needs to be carried at low temperatures, usually in the presence of urea and thiourea and compulsorily with phosphatase inhibitors. After digestion, phosphopeptides need to be enriched. There are essentially three enrichment methods: immunoaffinity chromatography, immobilized metal affinity chromatography (IMAC) and metal oxide affinity chromatography (MOAC). In the former, antibodies anti-phospho-

tyrosine or anti-phospho-serine/threonine are used to selectively capture phosphopeptides from the tryptic peptides' mixture, according to the presence of phospho-tyrosine- or phospho-serine/threonine-modified peptides. IMAC and MOAC, in turn, are able to non-selectively enrich phosphopeptides using multivalent metal cations (e.g. ferric (III), gallium (III), aluminum (III), zirconium (II), nickel (II) and titanium (IV)) or metal oxides (e.g. TiO_2, ZrO_2, Al_2O_3, $Al(OH)_3$, Nb_2O_5). These methods are not completely alternatives. IMAC is biased to multi-phosphorylated peptides, whilst MOAC shows preference to mono-phosphorylated peptides. Though, MOAC is compatible with most reagents that cannot be used in IMAC (e.g. chelating agents), shows higher selectivity and better recovery rates under more acidic conditions (required to minimize non-phosphorylated but still negatively charged peptides). Ultimately, the sequential use of both methods provides the highest coverage. Finally, in phosphoproteomics the use of specific bioinformatics assets is required to assign phosphosites localization and to survey kinase/phosphatase recognition motifs. *In silico* tools, such as the group-based phosphorylation scoring (GPS) method, are important to predict potentially active kinases that can be deemed potential therapeutic targets. Besides, pathway knowledge bases, such as Kyoto Encyclopedia of Genes and Genomes (KEGG), are useful to inquire the biological relevance of modified proteins in the various intracellular pathways [91–95].

2.2. The input of (phospho)proteomics to the comprehension of the mechanisms underpinning myocardial (reverse) remodeling

The present understanding of the molecular mechanisms underlying myocardial remodeling and the opposite process, RR, stems above all from established animal models of aortic banding or hypertension. Provided that in both models, a pressure overload state is achieved, leading to LV hypertrophy, it is generally accepted that both mimic the hemodynamics effects of chronic pressure overload (AS or systemic hypertension) on the LV. Thus, the characterization of the LV (phospho)proteome in these animals is a valid avenue to scrutinize dysregulated biological processes and molecular pathways in myocardial remodeling and RR. **Table 2** summarizes the contribution of (phospho)proteomics to this field till today.

Table 2. Main findings of proteomics and phosphoproteomics studies in the setting of myocardial remodeling and reverse remodeling.

Myocardial Remodeling			
Animal Model	**Setting**	**Main findings**	**Ref.**
C57/BL6 mice	TAC-induced pressure overload and LVH	– 123 dysregulated proteins under pressure overload – Most proteins were associated with metabolism (36%), cell structure and motility (21%), closely followed by those linked to transcription, translation and trafficking (18%) – ↑ Myosin light chain – ↓ 60 kDa Hsp, creatine kinase (mitochondrial), glyceraldehyde-3-phosphate dehydrogenase and elongation factor tu 3 – Post-TAC rise of SERCA2 and of peroxiredoxin V further confirmed by immunoblotting	[96]
Sprague-Dawley rats	TAC-induced pressure overload and LVH (mitochondria-targeted)	– ↑ glycolysis enzymes, 2 Krebs cycle members (aconitase 2 and succinate dehydrogenase complex, subunit A, flavoprotein) – ↓ fatty acid oxidation proteins – Clear dysregulation in the electron transport chain subunits, predominantly downwards. Specifically, 21 proteins were found downregulated and 10 upregulated throughout the 5 complexes: (10 vs. 1, I; 0 vs. 2, II; 3 vs. 0, III; 5 vs. 0, IV and 3 vs. 5, V)	[97]
C57bl6 mice	TAC-induced pressure overload and LVH	– 62 proteins differently expressed under pressure overload – Most upregulated proteins are found in the cytoskeleton or in the cytoplasm and most downregulated proteins in the mitochondria – ↑ organization of actin filaments (e.g. adenylyl cyclase-associated protein 1 and plastin-2), response to TGF-β/ECM organization (e.g. collagen alpha-1(I) chain and periostin) and proteostasis (e.g. Hsp β1 and β6) – ↓ electron transport chain activity (e.g. NADH dehydrogenase [ubiquinone] 1β subcomplex, subunit 3 (complex I), cytochrome c oxidase subunit VIb polypeptide 1 (complex IV)) and oxidative phosphorylation (e.g. ATP synthase, H+ transporting; mitochondrial F0 complex, subunit F (complex V))	[98]
Dahl-salt resistant rats; Spontaneously Hypertensive rats; Wistar rats	Hypertension- or TAC-induced pressure overload and LVH	– In the 3 models of hypertrophic remodeling: – ↑ enolase 3 (glycolysis), aconitate hydratase, mitochondrial (Krebs cycle), tropomyosin α-4 chain, troponin I (structural proteins), elongation factor 1-δ (transcription) and proteasome subunit α type-3, β type-7 (proteostasis)	[99]

(Dahl-salt resistant and Wistar-Kyoto rats used as controls)		– ↓ branched-chain ketoacid dehydrogenase E1 (amino acid metabolism), cardiac myosin regulatory light chain 2 (structural) and protein phosphatase 1 regulatory subunit 7 (signal transduction) – The dysregulation of enolase, tropomyosin α-4 chain, troponin I, the branched-chain ketoacid dehydrogenase and of myosin regulatory light chain was further perpetuated when Dahl-salt sensitive and spontaneously hypertensive rats were used as models of systolic failure	
C57BL/6 mice	TAC-induced pressure overload and LVH	– Most phosphoproteomics changes after banding took place in the contractile fibers. GOEA showed that most phosphorylated proteins 2 weeks after banding lie on the Z disc, cell-matrix junction, perinuclear region, cell surface and focal adhesions. Moreover, these proteins are involved in cell projection, actin filament organization, lymphocyte activation and in the regulation of protein complex disassembly – ↑ Hsps αB-crystallin (Ser59) and Hsp β1/Hsp27 (Ser86) phosphorylation may protect cardiomyocytes from apoptosis – ↓ α-tropomyosin phosphorylation (Thr282 and Ser283) may suppress sarcomere tension and ATPase activity in hypertrophied myocardium – Phosphorylation of the dynamin-related protein 1 (involved in mitochondrial fission) on Ser622 was found soon after banding (10 min). Its inhibition prevented hypertrophy and decreased significantly the expression of the fetal gene program, 2 weeks after banding	[100]
C57BL/6N mice	TAC-induced pressure overload and LVH	– 330 dysregulated proteins in the LV after TAC in a time series (4 to 56 days after surgery). – Pathway and biological processes analysis depicted a time-dependent pattern: – ↑ Early activation of the RhoA-mediated regulation of actin motility, PLC and PKA pathways – ↑ Early cell proliferation and transformation (probably reflecting myofibroblasts conversion) – ↑ Early enhancement of contractility – ↑ Later flux through the glycolytic, ketolytic and pentose phosphate metabolic pathways – ↑ Apoptosis, necrosis, inflammation (progressive) – Xin actin-binding proteins 1 and 2, ECM proteins periostin and biglycan are early indicators of heart failure. Hsp β6 and β7 remained elevated during myocardial remodeling	[101]
C57BL/6J mice	TAC-induced pressure overload and LVH vs. Exercise (swimming)-induced physiological LVH	– 53 differentially expressed proteins between pathological and physiological hypertrophy and 225 differentially expressed proteins exclusively found in the TAC model – Gene ontology and pathways analysis showed a time-dependent regulation: – ↑ Early actin filament organization, cytokinesis, translational elongation and nuclear transport – ↓ Early ubiquinone biosynthesis	[102]

		– ↓ Late fatty acid metabolism, Val, Leu and Ile degradation, oxidative phosphorylation and aminoacyl-tRNA biosynthesis – The proteins plastin 3 T-isoform, fibronectin 1, myosin heavy chain 9, nestin and destrin were confirmed to be increased 1 week after TAC by western blot	
Myocardial Reverse Remodeling			
Animal Model	**Setting**	**Main findings**	**Ref.**
Spontaneously Hypertensive rats (normotensive Wistar-Kyoto rats used as controls)	Hypertension-induced pressure overload and LVH vs. Long-term (11 months) anti-hypertensive therapy (ACE inhibitor, AT2R type I blocker and α1-adrenergic receptor blocker)	– Hypertensive rats showed dysregulation of myocardial sarcomeric/cytoskeletal proteins, metabolism- and stress-related proteins. Some proteins were normalized by one or more drugs, but 17 proteins could not be reverted by any treatment. Examples: – ↑ Tropomyosin isoforms, annexin III and desmin (all reverted by ≥1 anti-hypertensive agents) – ↓ Mitochondrial electron transport chain, such as cytochrome c oxidase polypeptide Va (reverted by therapy), the NADH ubiquinone oxidoreductase 13 kDa subunit B and the NADH dehydrogenase 1α subcomplex subunit 10 (both could not be rescued) – ↑ α-enolase 1, involved in glycolysis (not targeted by therapy) – ↑ Stress-related protein Hsp27 (normalized after administration of ≥1 drug) – ↓ Thiol-specific antioxidant and Cu/Zn superoxide dismutase (reverted by at least one drug) – Despite long-term therapy, LVH regression is associated with partial proteome normalization	[103]
Spontaneously Hypertensive rats (normotensive Wistar-Kyoto rats used as controls)	Hypertension-induced pressure overload and LVH vs. Medium-term (11 weeks) anti-hypertensive therapy (ACE inhibitor and AT2R type I blocker)	– The myocardial proteome of hypertensive rats demonstrated changes in glycolytic and lipolytic metabolism, in the mitochondrial electron transport chain as well as in antioxidant systems, when compared to the normotensive counterparts. Some of these adaptions could be reverted by pharmacotherapy. Examples: – ↑ glycolytic enzymes α-enolase and lactate dehydrogenase B (resistant to pharmacotherapy) – ↓ aldehyde reductase (lipid peroxides-derived aldehydes neutralizer, resistant to therapy) – ↓ fatty acid oxidation enzymes propionyl-CoA carboxylase and enoyl-CoA hydratase (rescued by anti-hypertensive agents); – ↑ NADH-ubiquinone oxidoreductase 30 kDa subunit (complex I) and ubiquinol-cytochrome C reductase core protein 1 (complex III) (attenuated by therapy)	[104]
Spontaneously Hypertensive rats (normotensive Wistar-Kyoto	Hypertension-induced pressure overload and LVH vs. Long-term (~8/9 months) anti-hypertensive	– Hypertension induced-pressure overload led to time-dependent proteomic changes in rats' myocardium, with implications on oxygen transport, mitochondrial respiratory chain, glycolysis, stress response and contractility: – ↑ cytochrome C oxidase polypeptide Vb (mitochondrial), ATP synthase subunit D and DJ-1 (exclusively early at 12 weeks)	[105]

rats used as controls)	therapy (ACE inhibitor and α1-adrenergic receptor blocker)	– ↓ myoglobin, pyruvate dehydrogenase (lipoamide β), Hsp β-6 and tropomyosin 1α chain (exclusively early at 12 weeks) – ↑ calsarcin-1 (up to 48 weeks), – ↓ ubiquinone biosynthesis protein COQ7 homolog (up to 48 weeks) – Calsarcin-1 and the ubiquinone biosynthesis protein could not be normalized upon treatment – The pro-hypertrophic NF-κB pathway, which may be indirectly activated by calsarcin-1, was only partially downregulated by pharmacotherapy	
Sprague-Dawley rats	Abdominal aorta constriction-induced pressure overload and LVH Medium-term (8 weeks) anti-hypertensive therapy (AT2R type I blocker)	– Pressure overload-induced LVH resulted in the dysregulation of 17 proteins, covering many biological functions: cell structure, metabolism, translation and stress response – ↑ 13 proteins (e.g. myosin light polypeptides, β-myosin heavy chain, myosin light chain-2 isoform, Jumonji domain containing 1A isoform), mitigated by drug administration – ↓ H^+-transporting ATP synthase, L-3-hydroxyacyl-Coenzyme A dehydrogenase and ATP synthase β subunit, less markedly with AT-1 receptor blocker administration – Only the treated rats displayed detectable expression of the heat shock factor 2	[106]
C57BL6 mice	TAC-induced pressure overload and LVH vs. Short-term (4 weeks) antioxidant therapy with mitochondria-targeted SS31 and SS20 peptides	– Over 300 and over 400 proteins were found confidently changed, respectively, between pressure-challenged and sham animals and between treated and untreated animals – SS31 and SS20 peptides remodeled, respectively, 84% and 63% of the mitochondrial proteins, in addition to 69% and 56% of the non-mitochondrial proteins – SS31 attenuated 52 out of 53 canonical pathways affected by TAC. SS20 performed weaker. Notably, SS31 attenuated pressure overload-induced changes in cytoskeleton pathways (e.g. actin and integrin/RhoA signaling upregulation), intermediate metabolism (e.g. fatty acid, pyruvate, β-alanine, lysine and branch-chain amino acid metabolism downregulation), glycolysis, gluconeogenesis, Krebs cycle and mitochondrial function (e.g. ubiquinone biosynthesis and oxidative phosphorylation downregulation)	[107]

The studies were gathered through a comprehensive screen of two large proteome datasets repositories (PRIDE and ProteomeXchange) as well as by a thorough PubMed query. The search query in both repositories included the keywords myocardi*; cardia*; heart; remodel*; pressure; TAC; transverse aortic constriction; aortic stenosis; hypertroph*. The PubMed's argument used was (myocardi* AND phosphoproteom*) OR (cardia* AND phosphoproteom*) OR (heart AND phosphoproteom*) OR (remodel* AND phosphoproteom*) OR (pressure AND phosphoproteom*) OR (TAC AND phosphoproteom*) OR (transverse aortic constriction AND phosphoproteom*) OR (hypertroph* AND phosphoproteom*). Alternatively, proteom* was used instead of phosphoproteom*. Words were truncated (*) to cover as much derived term as possible. Studies covering physiological hypertrophy (e.g. induced by exercise or insulin) alone or pathological hypertrophy induced by phenylephrine and isoproterenol were not included because these do not resemble the patterns of pressure overload-induced hypertrophy.

Abbreviations: ACE: angiotensin-converting enzyme; AT2R: angiotensin II receptor; ECM: extracellular matrix; GOEA: gene ontology enrichment analysis; Hsp: heat shock protein; LVH: left ventricle hypertrophy; NADH: nicotinamide adenine dinucleotide; NF-κB: nuclear factor kappa B; PKA: protein kinase A; PLC: phospholipase C; SERCA: sarco(endo)plastic reticulum Ca^{2+}-ATPase; TAC: transverse aortic constriction; TGF: transforming growth factor.

In the beginning of the proteomics era, most studies about myocardial remodeling and RR employed two-dimensional electrophoresis combined with MALDI-TOF/TOF MS to identify differentially expressed proteins (DEPs) upon pressure overload [96,103–105]. A limited number of proteins could be screened by this approach. However, the advancement of MS instrumentation (e.g. Linear Trap Quadrupoles and Orbitrap), providing increased resolution and sensitivity to the analysis, has boosted the output from tens to hundreds of DEPs (while identifying thousands of proteins) [101,102,107].

The comparison of the LV (phospho)proteome between aortic-banded and sham animals or between hypertensive and normotensive animals evidences a myriad of adaptations in the course of myocardial remodeling. These include intracellular and extracellular structural changes, activation of stress response pathways and metabolic, transcriptional and translational regulation. Cardiomyocyte hypertrophy, a major hallmark of the remodeling process, is reflected by pathway or gene enrichment analysis (e.g. KEGG's "Hypertrophic cardiomyopathy" [102] and Ingenuity's pathway term "Cardiac Hypertrophy signaling" [101]) and supported by an increase in sarcomere elements such as myosin light chain [96], troponin I, tropomyosin α-4 [99] and myosin heavy chain 9 [102]. Although the growth of the force-generating units, i.e. the sarcomeres, is a coping mechanism to increased workload, the benefit in contractility may not be propagated in time. For instance, Chang *et al*. [100] showed, through a quantitative phosphoproteomics approach, reduced phosphorylation of Thr282 and Ser283 in α-tropomyosin in mice (two weeks after banding) that has been associated with depression of the sarcomeric tension and ATPase activity.

Soon after established pressure overload, an upregulation of the protein kinase A (PKA), phospholipase C (PLC) and of the Ras homolog family member A (RhoA) pathways is observed [101]. This may reflect the integration of the mechanical stress exerted on ECM into intracellular signals. The PKA and PLC pathways may be triggered, among others, by the angiotensin II receptor (AT2R) type I, which can be activated through stress, without angiotensin II interaction [108]. The RhoA pathway, in turn, may be activated by integrins, certain G-protein coupled receptors and growth factor receptors [109,110]. The initial stimulation of the PKA and PLC pathways may explain the enhanced contractility after aorta constriction [101]. This is probably due to the higher sarcoplasmic reticulum release of calcium, respectively, from ryanodine receptors and inositol triphosphate-gated channels [109]. Nonetheless, a raise in SERCA expression is also found in mice after aortic constriction [96], probably to compensate calcium leakage and promote lusitropy. The

phosphatase RhoA, in turn, is a key regulator of the actin cytoskeleton, explaining, at least in part, the early upregulation of actin filament organization [101,102]. A recent study has shed some light on the role of RhoA in pressure overload-challenged cardiomyocytes, demonstrating that RhoA has simultaneously protective and deleterious effects. If, at the one hand, RhoA promotes non-dilating hypertrophy (probably through indirect PLC and, subsequent, extracellular-regulated kinase activation), in the other hand, RhoA signaling leads to fibrosis, due to the release of myocardin response transcription factor from G-actin (continuously assembled onto growing F-actin stress fibers), which together with myocardin and serum response factor induce the expression of pro-fibrotic genes [110]. The early fibrogenic process is further demonstrated by high rates of cell proliferation, cytokinesis and cell transformation [101,102], in line with the well-known fibroblast activation and conversion to myofibroblasts that occurs under chronic pressure overload [15]. The ECM buildup is corroborated by augmented protein levels of collagen α-1 (I) chain, periostin, fibronectin-1 and biglycan, among others [98,101,102].

Proteomics further evidences the metabolic shift associated to pathological hypertrophy. Overall, the studies in **Table 2** report a reduction in fatty acid oxidation (e.g. decreased acyl-coenzyme A dehydrogenase, for short-chain and very long-chain fatty acids [97]) and in amino acid metabolism, specifically related to Val, Leu and Ile degradation [102] (e.g. downregulation of branched-chain ketoacid dehydrogenase E1 [99]). This is compensated by increased flux through the glycolytic (e.g. increased enolase [99]), ketolytic and pentose phosphate metabolic routes [97,99,101,102]. The preference for lower energy, but less oxygen-demanding, substrates may be due to mitochondrial dysfunction, specifically due to the dysregulation of the electron transport chain and reduced oxidative phosphorylation capacity [97,98,102]. For example, Köcher and colleagues [98] reported a drop of over 1.5-fold in the protein components of the mitochondrial complexes I (e.g. NADH dehydrogenase [ubiquinone] 1β subcomplex, subunit 3), IV (cytochrome c oxidase subunit VIb polypeptide 1) and V (ATP synthase, H^+ transporting; mitochondrial F0 complex, subunit F). Moreover, increased myocardial fission may also add to the decline of mitochondrial activity and may favor cardiac hypertrophy with reactivation of the fetal gene program. In fact, the phosphorylation of the mitochondrial fission protein dynamin-related protein 1 on Ser622 was found ten minutes after aortic banding and its inhibition prevented the development of hypertrophy and significantly reduced fetal genes expression two weeks after constriction [100].

Finally, in the setting of myocardial remodeling, (phospho)proteomics studies elicit the activation of proteostasis defense mechanisms to promote cell survival. For example, an upregulation of the heat shock proteins β1, β6 and β7 as well as αB-crystallin, after induction of pressure overload, has been reported [98,100,101]. Besides, higher phosphorylation of αB-crystallin on Ser59 and of the heat shock protein β1 on Ser86 is observed soon after banding and again two weeks after, and this has been associated with protection against apoptosis [100]. However, this protection should be limited under chronic stress because a progressive increase in apoptosis, necrosis and inflammation is observed progressively up to seven weeks after aortic constriction [101].

So far, there are no studies addressing the (phospho)proteomics changes in animal models of pressure overload after aortic debanding. Most studies aim at exploring the effects of anti-hypertensive therapy on models of hypertension- [103–105] (using spontaneously hypertensive rats) or aorta constriction-induced [106] pressure overload. In general terms, the administration of anti-hypertensive drugs (e.g. ACE inhibitors, AT2R type I or α1-adrenergic receptor blockers) in hypertensive animals results in partial myocardial proteome RR, affecting many biological processes: cytoskeletal/sarcomeric dynamics, glycolytic and lipolytic metabolism, mitochondrial respiration, antioxidant defense and stress response (**Table 2**). For instance, the increase in myocardial tropomyosin and desmin in hypertensive rats could be reverted by one or more anti-hypertensive drugs [103]. With regard to metabolism, if the reduction in fatty acid oxidation enzymes could be rescued by therapy [104], the increase in glycolytic enzymes (α-enolase and lactate dehydrogenase, LDH) has shown resistance [103,104]. This may be explained by defective myocardial perfusion, decreasing local O_2 concentration in the hypertrophied myocardium [35]. The effects of anti-hypertensive therapy in the mitochondrial electron transport chain is more complex because the dysregulation of the complex subunits occurs in both directions. For instance, while the expression of cytochrome c oxidase polypeptide Va (complex IV) was normalized by therapy, some complex I subunits remained downregulated with the administration of any of three drugs [103]. The incompleteness of myocardial RR upon anti-hypertensive therapy is also shown at the level of antioxidant defenses, with the rescue of the thiol-specific antioxidant and of the Cu/Zn superoxide dismutase [103], but not of the aldehyde reductase [104]. Still, the rise in heat shock protein 27, involved in protection from oxidative stress-induced cell death, could be normalized by three different blood pressure-lowering drugs [103].

The use of an anti-hypertensive agent (AT2R type I blocker) in a rat model of aortic constriction-induced pressure overload, which is more rapidly translatable to the AS setting, was also attempted [106]. Curiously, the dysregulation of all 17 proteins upon induction of pressure overload (e.g. increased β-myosin heavy chain and decreased H^+-transporting ATP synthase), was attenuated (but not completely normalized) by therapy. A similar study was also conducted with mitochondria-targeted peptides, administrated right after surgery. Depending on the peptide used (SS20 and SS31), 63 to 84% of the mitochondrial proteome has been remodeled. SS31 performed better and notably attenuated almost all pathways targeted by aortic banding, including the upregulation of the RhoA pathway and of the glycolytic pathway as well as the downregulation of fatty acid and amino acid metabolism, ubiquinone metabolism and oxidative phosphorylation [107]. Yet, in these two studies, drug administration was initiated either straight [107] or one week after banding [106]. Thus, in any case, proteomics changes are better regarded as the effect of prevention rather than treatment of the remodeled myocardium.

In summary, the complete comprehension of the mechanisms underlying myocardial RR remains elusive. While hypertension models may provide a similar physiological picture of the pressure overload repercussions on the LV, one must acknowledge that hypertension and AS have different etiologies. In fact, systemic hypertension involves the activation of several neurohormonal pathways, which may influence the process of LV remodeling [111]. Therefore, the proteomics results in these animal models should be interpreted with caution. Preferably, mechanistic research on myocardial RR should be performed with animal models of aortic constriction that more closely resemble the consequences of AS on the LV. However, thus far, (phospho)proteomics studies in animal models have only addressed the effect of drug therapy on the overloaded myocardium, but not the direct benefit of myocardial unloading (debanding). To widen the gap in AS research, no study characterizing the myocardial (phospho)proteome in AS patients undergoing AVR is available at this point. In fact, it is unethical to collect myocardial biopsies postoperatively, and these are only available on rare occasions where patients undergo a second surgery (coronary artery bypass grafting - CABG, valve substitution due to mismatch or wearing out, implantation of LVADs – which are themselves confounding factors). This, of course, precludes the investigation of the proteomics dynamics during RR in humans. Nevertheless, direct proteomic characterization of the human myocardium, collected during AVR, eradicates any doubts that arise from the translation of preclinical models' findings and, thus, may provide important clues concerning the dysregulated biological phenomena and molecular pathways in the origin of incomplete RR (see ***Chapter II***).

3. Pericardial Fluid: an underrated molecular library of heart conditions and an important reservoir of paracrine factors

In the course of heart surgery, but also by means of pericardiocentesis, it is possible to collect another biological material with exquisite properties for molecular research: the pericardial fluid (PF). Despite its existence being early recognized by Hippocrates in Ancient Greece, who described PF as "*resembling urine*" [112], not long ago (more precisely in the end of the 20th century) researchers have paid attention to the potential diagnostic value of this biofluid for heart diseases and not only those directly affecting the pericardium with evident clinical manifestations. In fact, the remote but heart-encircling location grants this biofluid unique properties. This liquid concentrates many heart-derived factors, thus enclosing several surrogate markers for the diagnosis or prognosis of a large spectrum of diseases either pericardial or non-pericardial/heart diseases, such as CAD or AS. Advances in the molecular biology and omics sciences are expected to deliver unprecedented knowledge of the molecular features of this biofluid. However, large-scale screening of PF proteome [113] and miRNome [114] just started. Moreover, the recognition of the heart not solely as a muscle but also as an active endocrine/paracrine organ (reviewed by [115]) has emerged the hypothesis of the PF to be, itself, a reservoir of bioactive substances which may regulate heart function and, thus, a relevant material for clinical research [116]. That was, indeed, demonstrated by the trophic and paracrine effects on cultured cardiomyocytes [117,118]. Albeit, only recently have the pericardial exosomes been isolated and their therapeutic properties tested [119,120], showing that PF holds great promise in both clinical and biotechnology research fields.

In this section, the first thorough characterization of PF molecular features is presented, based on an in-depth literature search and mining, which is then translated into a network map of the diseases influencing PF composition. The suitability of PF for biomarker research could be demonstrated by evident molecular profiles between different conditions as well as by stronger correlations to cardiac structural and functional parameters, fainter or lacking in plasma/serum. This analysis provided the rationale for the utilization of PF to study the molecular differences between patients with complete and incomplete myocardial RR (***Chapter VI***).

3.1. Systematic review of pericardial fluid molecular features

Aiming to collect and analyze all molecular studies on PF, an exhaustive literature research was performed using the keywords “pericardial fluid”. Over 2800 abstracts were retrieved and revised and three levels of exclusion criteria were followed, achieving 88 valid reports for further analysis (the reader is referred to **Figure 5** for details on the literature research and data mining). The majority of the included studies were based on human samples, except for two cases, one where the fluid was collected from a rat model of primary hypertension and another where pericardial effusions were retrieved from dogs. Data from the reports were manually curated and organized to extract all molecular entities (e.g. proteins, peptides, enzymes, metabolites and glycans) that could be identified and whose variation has been assessed between two or more conditions. If the experimental design included more than two experimental groups, data was organized in pairs to unfold multiple comparisons. Furthermore, whenever the variation of a molecule between conditions was not reported in the main text, a graphical interpretation was translated numerically. To avoid misidentification, proteins, peptides and enzymes codes were gathered from UniProt knowledge base, while metabolites and glycans codes were collected from KEGG or from Human Metabolome Database, if no codes were found in the former. Furthermore, an effort was made to harmonize pathology terms and methodological approaches between different reports to ease interpretation. A network analysis was then conducted to elicit conditions that have been studied in more detail through PF analysis and, more importantly, to evaluate the biomarker potential of the screened molecular species. To that end, an interaction table was created to summarize the variation of those species between different conditions. Only studies reporting significant differences (p <0.05) between two conditions and reporting the direction or degree (fold-change) of the variation were considered. An undirected network was then generated with the Cytoscape [121] program (v.3.6.1), with the conditions defined as nodes and the molecules as edges. Further details are available at https://doi.org/10.1007/s00395-019-0716-3 and on ***section 3.3***.

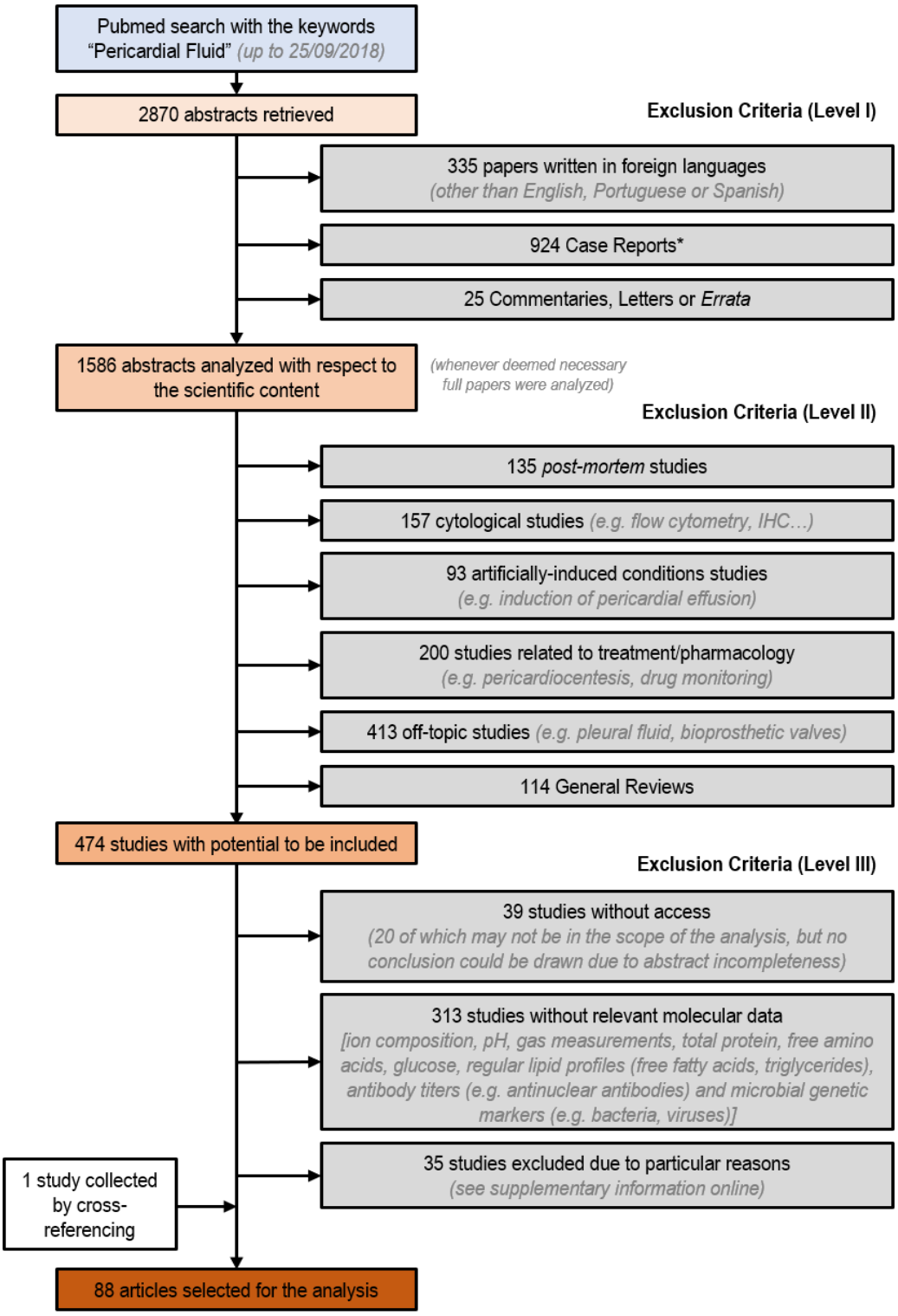

Figure 5. Search strategy flowchart. From the 2870 abstracts collected in PubMed, using the keywords "Pericardial Fluid", 88 reports were selected for review and 2782 were excluded, according to the 3 criteria levels depicted in the right. * Even though many case reports described molecular analysis, these were not considered due to the enrollment of one or few subjects and due to the lack of more than one experimental group. Abbreviations: IHC: immunohistochemistry.

3.2. The origin, functions and diagnostic properties of the pericardial fluid

The human heart and the roots of the great vessels diverging from and converging to this organ are surrounded by a protective structure called pericardium (**Figure 6A**). Pericardium is a double-walled sac composed of an external layer of connective tissue (fibrous pericardium) and of an internal layer of mesothelial cells (serous pericardium) that coats the inner surface of the fibrous pericardium (parietal layer) and also firmly adheres to the epicardium surface (visceral layer). Apart from the function of a biological barrier to prevent infection, the pericardium, albeit not essential for life, plays important mechanical, metabolic, immunologic and hemodynamic functions [122,123]. Enclosed in the pericardium lies a serous, clear and pale-yellow fluid, the PF. As compared to plasma, the PF presents similar levels of sodium, potassium and chloride, but lower levels of calcium and phosphorus [124] (**Figure 6B** summarizes major biochemistry characteristics of PF). Still, its protein concentration is about half of the plasmatic counterpart and albumin occupies a larger fraction (~70%) of the total protein [125,126]. In physiological conditions, PF volume is found in the milliliter range (15-60) [127,128]. In spite of the low volume, the existence of a fluid surrounding the heart is important to absorb shock, to prevent epicardial friction by providing lubrication and also to equalize transmural pressures during heartbeat [122,123]. In fact, rabbit pericardium was found to actively secrete hyaluronic acid, which contributes significantly to the resilience and compliance of the PF to the permanently experienced compressive and stretching forces [129,130].

The growing interest in PF is explained by its peculiar production and clearance dynamics. Initially, the PF was defined as a mere plasma ultrafiltrate. The first evidence was collected by Maurer *et al*. [131], who demonstrated that PF and serum followed Donnan's law for two fluids in equilibrium. This was later corroborated by Gibson and Segal through experiments with rabbits and greyhounds [132]. Indeed, they found that sodium, chloride, calcium and magnesium, but not potassium, ions behaved as expected from a passive plasma ultrafiltrate. However, following findings of Stewart *et al*. [133] showing that fluid flows from the epicardium to the pericardial sac, changed the perspective over PF origin. Using a hemispheric capsule firmly attached to the epicardium and filled with albumin in

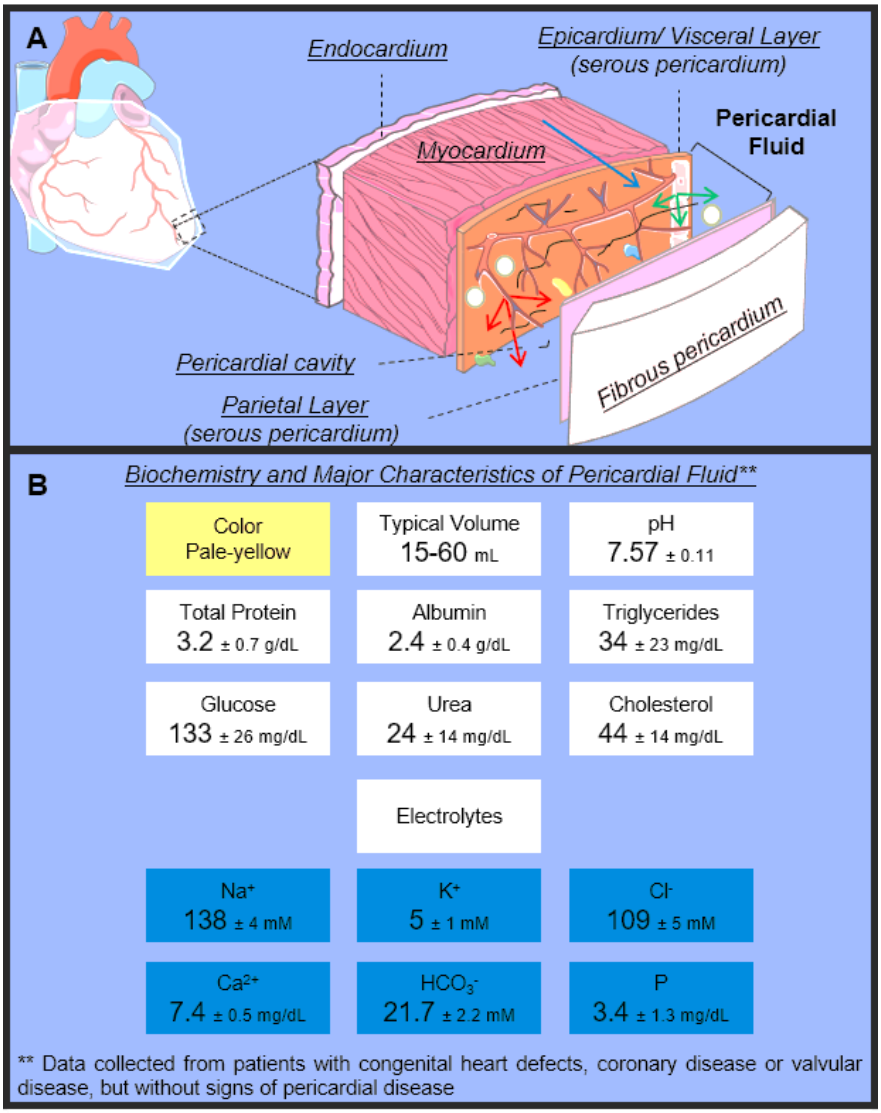

Figure 6. The Pericardial Fluid ID card. **A.** Anatomical representation of pericardium and currently accepted mechanisms of pericardial fluid formation. The pericardial fluid lies in the pericardial cavity and is considered to be the output of plasma ultrafiltration from the epicardial capillaries (red arrows), secretions from pericardial mesothelial cells (green arrows) and contributions of the myocardial interstitial space as a result of hydrostatic and osmotic pressures (blue arrow). **B.** Major biochemistry characteristics of the pericardial fluid (data derived from Ben-Horin S. *et al.* (2005) Am J Med and Hutchin P. *et al*. (1971) Arch Surg). Some graphical elements were adapted from Servier Medical Art.

physiological concentrations, followed by measurements of pericardial hydrostatic pressure and flow, the Starling equation was found to govern epicardium-to-pericardium flow. Currently, it is well established that despite higher epicardial osmotic pressure, the difference between the intrapericardial hydrostatic pressure (lower) and the intramyocardial pressure (higher) drives the flow from the myocardium and epicardium to the pericardial sac [122,134]. PF is, thus, currently better defined as the net result of plasma ultrafiltration from the epicardial capillary bed (red arrows in **Figure 6A**) and possibly from the pericardial

parietal layer, but also the product of secretions from the pericardial mesothelial cells (green arrows in **Figure 6A**) and contributions of the myocardial interstitial space (blue arrows in **Figure 6A**) [120,122,123]. Consequently, the pericardial cavity stocks many different bioactive substances [116] such as cardiac hormones [135–137], growth factors [138–140], prostaglandins [141] and cytokines [142–144], whose implications in heart function are still not entirely clear, but may include paracrine regulation of heart contractility, vasodilation and efferent cardiac sympathetic stimulation [141,145]. These functions are supported by the predominance of biological processes related to the response to stress, stimulus and to wounding, according to the GOEA of the PF proteins identified so far (analysis performed using STRING database version 10.5 on 29th November 2017; 1084/1328 recognized proteins; electronic supplementary information available at https://doi.org/10.1007/s00395-019-0716-3).

Radioactivity tracing studies following intrapericardial delivery of radiolabeled albumin had significantly added to the knowledge of PF clearance pathways [134,146,147]. A significant fall in radioactivity traces in blood upon blockage of the major lymphatic ducts (thoracic and right), defined lymphatics as the predominant clearance system [134,148]. Still, the disappearance pathways of PF constituents are somewhat heterogeneous. In a series of experiments, both the size and the chemical properties were found determinant for the clearance and systemic distribution of the materials introduced in the pericardial cavity [149–152]. For instance, Cho *et al*. [152] showed the inverse relationship between molecular weight and clearance rate (sodium > Cr-EDTA > inulin). In general terms, though, pericardial drainage is considered a slow process. Indeed, while human blood is filtrated at a rate of ~120 mL/min [153] (with plasma complete filtration of plasma in less than half-hour), complete drainage of sheep's PF (~8 mL) was estimated to take between 5.4 to 7.2 hours [148].

The balance of PF formation and clearance can be affected in certain pathological conditions and accumulation of fluid may ensue. For instance, concomitant pulmonary and systemic venous hypertension resulted in PF buildup in canine pericardia [154]. Epicardial transudation was also found to increase with coronary sinus hypertension in dogs [133]. In humans, up to liters of fluid may accumulate, upon inflammation of the pericardium (pericarditis) or physical injury, originating pericardial effusions [155]. Ultimately, this may give rise to life-threatening conditions such as cardiac tamponade, characterized by atrial and pericardial pressure elevation, *pulsus paradoxus* and arterial hypotension [123,145]. Siding with volume imbalance, molecular changes are also observed in PF and both are

considered a reflex of heart's pathophysiological status. Currently, though, routine analysis is often limited to biochemical, hematological and cytological/microbiological tests in cases of pericardial effusions. These are generally managed by means of pericardiocentesis and molecular testing is used to inspect the effusion etiology [128]. Determination of total protein and assessment of LDH are two of the most common biochemical tests applied, as these are required for the classification of transudates and exudates [126,127]. This classification is essential to uncover the underlying cause of the effusion. For instance, transudative effusions are usually associated with heart failure, hypoalbuminemia, radiotherapy, cirrhosis and renal insufficiency, while exudative effusions are mainly due to infective, auto-immune or malignant conditions [155,156]. Other presentations of PF include hemopericardium (presence of blood), chylopericardium (chylous appearance, with high levels of triglycerides and lymphocytes), pyopericardium (presence of pus) and pneumopericardium (presence of air) [156]. A culture of PF, bacteriological smears and Gram stains are generally ordered when there is suspicion of pericarditis and cytological examinations (such as histological studies and leucocyte counts) are performed when malignancy is imminent [127,156].

The ethical restraints of collecting PF from healthy individuals, requiring an invasive procedure, explain why this is better characterized in conditions manifested as pericardial effusions. However, PF can be easily and safely collected during open-heart surgery [116]. Moreover, the low turnover rate of PF makes this biofluid an appetizing source of biomarkers for heart conditions and the pericardium itself a luring reservoir for drug delivery aiming higher residence time and therapeutic efficacy. Thus, in the next section, the results of a systematic review of molecular markers analyzed in the PF with important diagnostic/prognostic implications for pericardial and non-pericardial diseases are presented.

3.3. A network view over the molecular signatures of different conditions in pericardial fluid

The networks illustrated in **Figure 7** and **8** summarize the current knowledge on PF molecular research. Pericardial (**Figure 7**) and non-pericardial (**Figure 8**) diseases and their phenotypic variations (nodes) are compared regarding the variation of molecular species

(edges). Despite the general lack of information in the literature regarding the sensitivity, specificity and positive/negative predictive values, these maps report molecular variations studied so far between different conditions with influence in PF composition. Therefore, whether alone or in multiplex, several molecules presented in such networks deserve further scrutiny to evaluate their potential as diagnostic/prognostic markers. The color of the edges represents the degree of variation of a molecule between a pair of conditions. For instance, the green edge of adrenomedullin (ADM) between CAD and atrial/mitral regurgitation represents a weaker elevation (2.1-fold) in the latter (in every case, the arrow indicates where the molecule was found in higher amounts). In turn, myoglobin (MB) has shown an intermediate elevation in acute coronary syndrome as compared to AS (10-fold higher); thus, this edge is found yellower (**Figure 8**). A final example is the stronger elevation (>1000-fold) of interferon (IFN) γ in tuberculous pericarditis versus malignant pericarditis, which is reflected in a redder edge (**Figure 7**). As one may see, PF molecular research was mainly devoted to conditions directly afflicting the pericardium (tuberculous and malignant pericarditis) or to prevalent heart diseases such as CAD, valvular disease, angina and myocardial infarction. The remaining network's node pairs related to less explored diseases or phenotypical variations of some conditions can be found at https://doi.org/10.1007/s00395-019-0716-3.

3.3.1. Pericardial diseases influencing the composition of pericardial fluid

Probably one of the first conditions to be studied through PF analysis was tuberculous pericarditis. Driven by the difficulty of establishing a definitive diagnosis of *Mycobacterium tuberculosis* infection in patients with strongly suspected tuberculosis and due to the long time required for the culture and identification of the bacilli, researchers have attempted to translate routine analysis of adenosine deaminase (ADA) in pleural fluid to the diagnosis of tuberculous pericarditis [157–159]. Indeed, ADA has been found elevated in the PF of patients with tuberculous pericarditis as compared to other conditions such as malignant [160–163], idiopathic [159,160,162,163] and radiotherapy-associated pericarditis [163] as well as heart disease [157]. Besides ADA, other molecules may be helpful in identifying tuberculous pericarditis, such as lysozyme [159,164], which presents bacteriolytic activity and IFN γ [165–168], a cytokine released during *M. tuberculosis* infection.

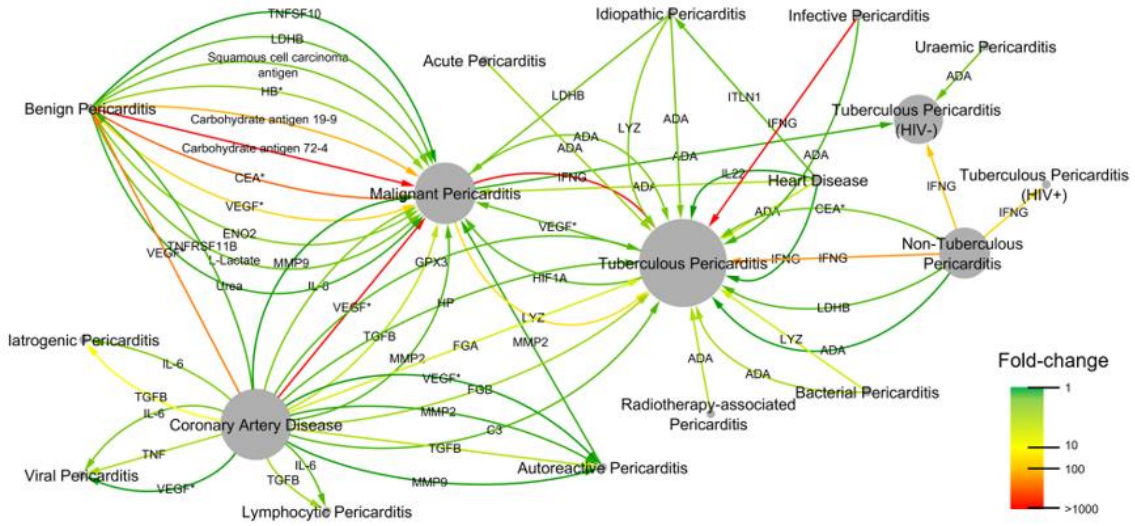

Figure 7. Current pericardial disease–pericardial disease molecular associations reported in pericardial fluid: a network built using Cytoscape v.3.6.1. Diseases were defined as nodes and the molecular comparisons were represented as edges. Node size represents betweenness centrality (empiric measure of the disease relevance through the number of shortest paths that go through disease to fulfill the entire network). Edge color translates the mean decimal logarithm of a molecule fold-change: green edges represent less intense variations (log_{10} closer to 0 ≈ fold-change 1) and red edges represent variations of higher magnitude (log_{10} closer to 3 ≈ fold-change 1000). Arrows indicate in each pair of diseases, where a given molecule is found in higher amounts. To be readily recognized, proteins are identified with their respective gene name and peptides, glycans and metabolites are given with the respective full name. Abbreviations: HIV: human immunodeficiency virus.

Similarly to the advances in tuberculous pericarditis research, the diagnosis of malignant pericarditis through the assessment of specific molecules, such as the carcinoembryonic antigen (CEA), has been inspired by observations in pleural and peritoneal fluids [157,161,169]. This is probably one of the best established PF markers of malignancy as it is generally found over 100 times elevated in subjects with malignant versus benign pericarditis [157,169,170], and because, in combination with cytological examinations, the assessment of this glycoprotein may achieve 100% of diagnostic sensitivity [169]. Besides CEA, the squamous cell carcinoma antigen and the carbohydrate antigens 19-9 and 72-4 have been compared between patients with malignant and benign pericarditis, but only the latter has shown enough discriminant power [170]. Moreover, MMP2 and MMP9 were reported as elevated in patients with malignant pericarditis, which may be explained by the inflammatory burden, but also due to tumor migration [171]. Probably due to the same reason, the pro-angiogenic vascular endothelial growth factor (VEGF) was found in higher amounts in PF collected from patients with malignant pericarditis as compared to those with tuberculous [172] autoreactive or viral pericarditis as well as with CAD [173]. Researchers have also attempted to distinguish malignant pericarditis by assessing some cytokines. Indeed, the tumor necrosis factor-related

apoptosis-inducing ligand (TNFSF10, commonly named TRAIL), was found elevated in malignant pericarditis when compared to benign pericarditis, but reduced when compared to CAD patients [174]. Despite the assessment of different cytokines and paracrine cues, these analyses require validation due to the limited number of reports available.

Unlike tuberculous and malignant pericarditis, much less research has been conducted for other pathologies manifesting as pericardial effusions, such as idiopathic, iatrogenic, autoreactive, viral and lymphocytic pericarditis. Still, there are several examples of proteins that were found to be particularly associated with etiologically distinct pericardial effusions. For instance, the level of the adipokine omentin-1 was found to be 2-fold elevated in idiopathic pericarditis as compared to heart disease, through PF proteomics [175]. TGF-β was also reported as elevated in iatrogenic, autoreactive and lymphocytic pericarditis when compared to CAD [143]. A final example is the downregulation of fibroblast growth factor (FGF) 2 in viral pericarditis, also when confronted with CAD [176], although further studies are required to validate such association.

3.3.2. Non-pericardial diseases influencing the composition of the pericardial fluid

Most of the conditions (pericarditis) discussed previously have in common the fact that they may manifest as effusions, which may threaten life through the development of cardiac tamponade [123,128]. Often, this medical emergency is resolved by means of pericardiocentesis, which is itself a window of opportunity for the direct exploration of the pericardial sac content. However, in symptomatic patients, pericardiocentesis can be performed for diagnostic purposes only, as there is the need to identify the etiology of the pericarditis in order to select appropriate treatment [128]. Still, it should be noted that PF can be safely and easily collected after pericardiotomy, during open-heart surgery [116], and, in some cases, postoperatively, through puncture of pericardial drainage tubes [177], which together increase the chance to look over potential diagnosis/prognosis markers of several heart diseases. As a matter of fact, several proteins and peptides present in PF correlate with structural and functional cardiac parameters, while the same markers assessed in plasma or serum do correlate poorly or do not even show significant correlation with the same (**Table 3**). Except the BNP, which associated slightly better to left atrial diameter in plasma (0.59) than in PF (0.55) [43], or its N-terminal peptide, which showed

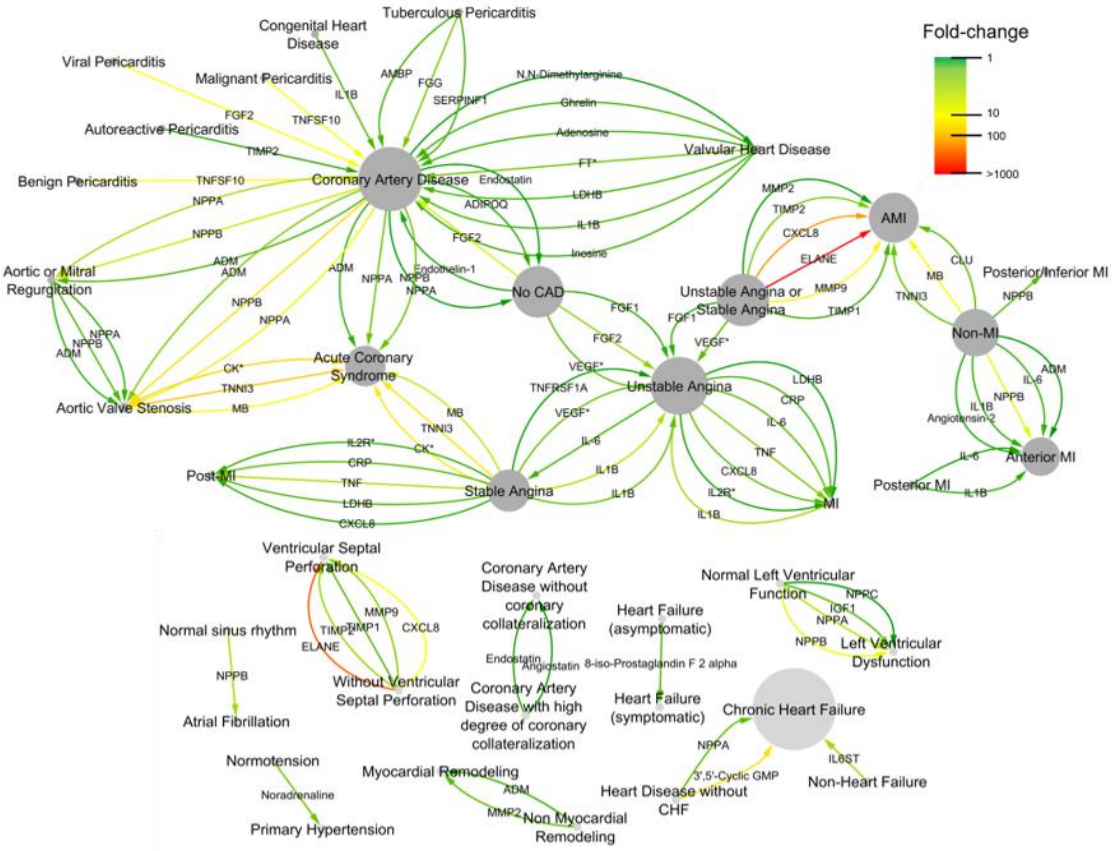

Figure 8. Current heart disease–heart disease molecular associations reported in pericardial fluid: a network built using Cytoscape v.3.6.1. Diseases were defined as nodes and the molecular comparisons were represented as edges. Node size represents betweenness centrality (empiric measure of the disease relevance through the number of shortest paths that go through disease to fulfill the entire network). Edge color translates the mean decimal logarithm of a molecule fold-change: green edges represent less intense variations (log_{10} closer to 0 ≈ fold-change 1) and red edges represent variations of higher magnitude (log_{10} closer to 3 ≈ fold-change 1000). Arrows indicate in each pair of diseases, where a given molecule is found in higher amounts. To be readily recognized, proteins are identified with their respective gene name and peptides, glycans and metabolites are given with the respective full name. Abbreviations: AMI: acute myocardial infarction; CHF: chronic heart failure; MI: myocardial infarction; CAD: coronary artery disease.

comparable correlations to left ventricle end-systolic volume and LVEF in both fluids [178], the remaining molecules displayed stronger correlations to all the parameters analyzed through PF analysis. For instance, the PF levels of the active (mature) and inactive (glycine-extended) forms of adrenomedullin (ADM, a vasodilator peptide) [137,179,180], the insulin-like growth factor-1 [181], the MMP2 [182], required for left ventricle remodeling, and the metabolite asymmetric dimethylarginine [183], an endothelial nitric oxide synthase blocker, showed robust negative correlations to LVEF, which is of tremendous prognosis value in clinical practice, while the respective plasmatic/serum levels exhibited either weaker or non-significant correlations. Despite the exception of BNP concerning left atrial diameter, more powerful correlations were discovered in PF versus plasma/serum in other relevant physiological parameters such as the left ventricle end-systolic or end-diastolic dimensions,

right ventricle end-diastolic diameter and the pulmonary artery systolic pressure [43]. In addition to the parameters found in **Table 3**, it is worth mentioning that there is an inverse relationship of NYHA's classification of heart failure to the concentration of endothelin-1 in PF, which is not found in plasma [184]. Furthermore, many of the differences reported between conditions affecting the heart have been exclusively detected in PF, while no significant differences were detected when analyzing plasma or sera from the same individuals [144,159,173,174,185–191] (**Table 4**). Interestingly almost all markers depicted in this table have a molecular weight below or very close to 40 kDa, which supports the hypothesis that PF may accumulate endocardium/myocardium-derived factors [117,118], migrating through epicardium into the pericardium sac [192].

Table 3. Comparison of the pericardial fluid with the plasma/serum molecular correlations to structural and functional cardiac parameters.

Marker / Parameter	Total ADM		Mature ADM		ADM-Gly		Total IGF-1		Free IGF-1		Total MMP2		Active MMP2		BNP		NT-proBNP		ADMA		Total Ghrelin		Acylated Ghrelin	
Biofluid	PF	P/S	PF	P/S	PF	P/S	PF	P/S	PF	P/S	PF	P/S	PF	P/S	PF	P/S	PF	P/S	PF	P/S	PF	P/S	PF	P/S
LVESV	**0.66** **0.41**	0.41 n.s.	**0.63** **0.28**	0.25 n.s.	- **0.44**	- n.s.					**0.69**	0.48	**0.64**	n.s.			0.54	**0.55**						
LVEDV	**0.60** **0.33** **0.40**	0.35 n.s. 0.33	**0.60** **0.28** n.s.	0.28 n.s. n.s.	- **0.29** **0.48**	- n.s. n.s.					**0.61**	0.53	**0.56**	n.s.			**0.58**	0.54						
LVEDD															**0.62**	0.56			**0.43**	n.s.				
LVESD															**0.50**	0.43			**0.49**	n.s.				
RVEDD															**0.64**	0.59								
LAD															0.55	**0.59**								
PASP															**0.75**	0.71								
LVDd															**0.63**	n.s.								
PWT																					**-0.35**	n.s.	**-0.31**	n.s.
LVSP	**0.63**	0.50	**0.60**	0.42	**0.56**	0.48																		
LVEDP	**0.44**	n.s.	**0.36**	n.s.	**0.44**	n.s.																		
LVMi	**0.47**	0.38	**0.47**	0.36																				
LVEF	**-0.59** **-0.55** **-0.44** **-0.32**	0.41 -0.31 -0.34 n.s.	**-0.54** **-0.36** **-0.39** n.s.	-0.19 -0.34 n.s. n.s.	- **-0.59** **-0.43** **-0.33**	- -0.31 -0.33 n.s.	**-0.45**	n.s.	**-0.37**	-	**-0.59**	n.s.	**-0.70**	n.s.	**-0.70**	-0.69	-0.55	-0.55	**-0.45**	n.s.				

Correlations evaluated in different works are given in different rows. For each study, the best correlation (PF vs. P/S) is marked in bold. Only studies published after 2000 were included.

Abbreviations: ADM: adrenomedullin; IGF-1: insulin-like growth factor 1; MMP2: matrix metalloproteinase-2; BNP: brain natriuretic peptide; ADMA: asymmetric dimethylarginine; LV: left ventricle; RV: right ventricle; LVESV: LV end-systolic volume; LVEDV: LV end-diastolic volume; LVEDD: LV end-diastolic diameter; LVESD: LV end-systolic diameter; RVEDD: RV end-diastolic diameter; LAD: left atrial diameter; PASP: pulmonary artery systolic pressure; LVDd: LV diastolic dimension; PWT: posterior wall thickness; LVSP: LV systolic pressure; LVEDP: LV end-diastolic pressure; LVMi: LV mass index; LVEF: LV ejection fraction; PF: pericardial fluid; P/S: plasma/serum.

Table 4. Markers with significant changes between two conditions in pericardial fluid but without significance in blood-derived fluids.

Molecule	MW (kDa)	Condition at scope	Compared Condition	Fold-change in PF	Ref.
Pericardial Diseases					
Adenosine Deaminase	40.8	Tuberculous Pericarditis	Idiopathic Pericarditis	5	[159]
			Malignant Pericarditis	18.7	
Lysozyme C	16.5	Tuberculous Pericarditis	Idiopathic Pericarditis	3.1	
Non-Pericardial Diseases					
Fibroblast Growth Factor 1	17.5	Class III Unstable Angina	Class I/II Unstable Angina	1.8	[190]
Adenosine	2.7	Coronary Artery Disease	Valvular Heart Disease	2.1	[191]
Inosine	2.7	Coronary Artery Disease	Valvular Heart Disease	1.9	
Ferritin	20+21.2	Coronary Artery Disease	Valvular Heart Disease	3	[189] [188]
Fibroblast Growth Factor 2	30.8	Coronary Artery Disease	Several (Valve Stenosis and/or Regurgitation; Myxoma)	7.4	
Fatty acid-binding protein, heart	14.9	Class III Unstable Angina	Class I/II Unstable Angina	1.7	[186]
Ghrelin	3.2	Coronary Artery Disease	Valvular Heart Disease	2	[185]
C-type natriuretic peptide	13.2	Left Ventricular Dysfunction (LVEF ≤45%)	Normal Left Ventricular Function (LVEF ≥50%)	1.2	[187]
Interleukin-1-beta	30.7	Anterior Myocardial Infarction	Posterior Myocardial Infarction	1.7	[144]
Interleukin-6	23.7	Anterior Myocardial Infarction	Posterior Myocardial Infarction	1.4	
Non-pericardial vs. Pericardial diseases					
TNF ligand superfamily member 10	32.5	Coronary Artery Disease	Malignant Pericarditis	10	[174]
Vascular Endothelial Growth Factor (VEGF165 isoform)	22.3	Coronary Artery Disease	Malignant Pericarditis	0.0004	[173]
Average MW	24.9				

Abbreviations: LVEF: left ventricle ejection fraction; MW: molecular weight: TNF: tumor necrosis factor.

Acknowledging all the aforementioned reasons, briefly, the easiness and safeness of collection during heart surgery, the concentration of heart-derived factors and their correlation to echocardiographic and hemodynamic parameters, PF should be regarded as a valid and sensitive tool for the diagnosis of heart diseases or even to predict the outcome of patients undergoing cardiac surgery. Indeed, several PF molecules could be mapped to many heart diseases, such as CAD, VHD and myocardial infarction (**Figure 8**). Of note is chronic heart failure that, despite being disconnected from the main network, was also associated with increased levels of ANP and the metabolite 3',5'-cyclic guanosine monophosphate [193].

CAD is, perhaps, the most studied heart condition through PF analysis. Patients with ischemic heart disease often undergo CABG, which is an excellent opportunity to collect and analyze PF. Many proteins have been found to distinguish this from other conditions. For instance, the level of the apoptosis-inducer cytokine TRAIL was found ten times higher in CAD than in malignant pericarditis [174]. Another cytokine, the interleukin-1-β, a major player in atherosclerosis, was reported to be at least two-fold more concentrated in CAD than in valvular and congenital heart diseases [194]. Growth factors have also been assessed due to their crucial role in coronary collateralization (angiogenesis). Indeed, these factors have proved capable of discriminating CAD from other well-defined pathologies. Such is the case of FGF2, which induces coronary collateralization by promoting DNA synthesis and mitosis of both vascular endothelial and smooth muscle cells [188]. Its levels were found to be 10-fold higher when compared to patients with viral pericarditis [176] and more than 7-fold higher when compared with patients with no signs of CAD but with VHD (aortic or mitral stenosis or regurgitation) [188]. Beyond the possibility to identify CAD, which is usually diagnosed before heart surgery, perhaps more interesting is the chance to predict the outcome of patients regarding the coronary collateralization by PF analysis. This hypothesis arises from the observation of increased levels of endostatin, a peptide with anti-angiogenic and pro-apoptotic activities, and of angiostatin, a peptide commonly associated with inhibition of tumor-derived angiogenesis and metastasis, in patients without coronary collateralization (Grade 0 in Rentrop scale) as opposed to those with high degree of collateralization (Grade 2-3 in Rentrop scale) [195,196]. Although, it should be noted that such associations require further validation as, for instance, when categorizing patients in Grades 0-1 versus 2-3, endostatin levels were shown to be similar across the groups [139].

Another example of the research conducted in the PF is in the context of angina and myocardial infarction. It has been demonstrated that assessment of myocardial injury

through PF analysis is feasible, which is important for the diagnosis of perioperative myocardial infarction. Despite that, not always the assessment of the classic markers in the PF was shown to be better than the assessment in plasma or serum. In fact, while cardiac troponin I performs better in serum to diagnose infarction [197], the determination of the pericardial/serum MB ratio right after admission in the intensive care unit allows its early diagnosis [198]. Curiously, the pericardial cytokine profile differs according to the site of infarction. Indeed, interleukin-6 and interleukin-1-β were found in higher levels in subjects with anterior as compared to those with posterior myocardial infarction [144]. Additionally, several proteins were shown to distinguish myocardial infarction patients from those with other pathologies. For instance, the C-reactive protein, MMP2 and MMP9, their tissue inhibitors (TIMP1 and TIMP2), the interleukin-8 and the neutrophil elastase were reported to be elevated in patients that have experienced infarction as compared to those with stable or unstable angina [199,200]. Also, unlike the subjects with aortic root aneurysm or valvular disease, the exosomal clusterin could be identified in the PF of patients that have had acute myocardial infarction [119]. Through PF analysis, it seems that it is also possible to discriminate between different angina classes (Braunwald's classification). For instance, the FGF1 (acidic) was found 1.8-fold elevated, while the VEGF was reported to be 3-fold increased between Class III and Class I/II patients [190,201]. Therefore, even though most patients with unstable angina or suffering an episode of myocardial infarction do not display a tappable pericardial effusion, on occasion of CABG it is possible to obtain PF and evaluate the performance of markers such as growth factors (e.g. FGF and VEGF) and MB. Their levels might be useful to predict the aggravation of the angina grade or the emergence/recurrence of myocardial infarction episodes.

Valve replacement surgery, likewise, bestows a good opportunity for the collection and study of PF. Comparisons made between patients with VHD and CAD elicited differences at the molecular level, such as the elevation of asymmetric dimethylarginine [183] and the reduction of adenosine, LDH, ferritin and ghrelin in those with valvopathies [185,189,202]. Particularly, AS can be distinguished from ischemic disease and aortic or mitral regurgitation by an increase in ANP and BNP, in addition to the anti-hypertrophic and anti-fibrotic ADM peptide [137]. In the same study, a correlation of the different forms of such peptide (mature, Gly-linked) to some hemodynamic indices (e.g. left ventricle systolic pressure and LVEF) was also verified, thus making it an attractive indicator of the severity of heart failure. Therefore, one can hypothesize, that routine analysis of PF upon cardiac surgery may help anticipate the outcome of the patients and, thus, adjust medication to prevent adverse outcomes after AVR.

3.4. The usefulness beyond diagnosis/prognosis: the pericardial fluid as a functional liquid

So far, the promise of the PF as a diagnostic or prognostic platform for numerous heart diseases has been demonstrated (**Figures 7** and **8**). Indeed, the PF's molecular analysis has often shown to perform better than plasma's or serum's (**Table 4**) and to correlate with relevant functional parameters (**Table 3**). Notwithstanding, exploration of PF is not solely helpful for biomarker discovery. In addition, the PF has been used for mechanistic research as well as to address the effects of bioactive compounds, drugs, gene therapy and stem cell therapy on specific pathological conditions (reviewed in [203]). **Figure 9** provides a snapshot of the PF properties uncovered from mechanistic research, which are herein briefly discussed.

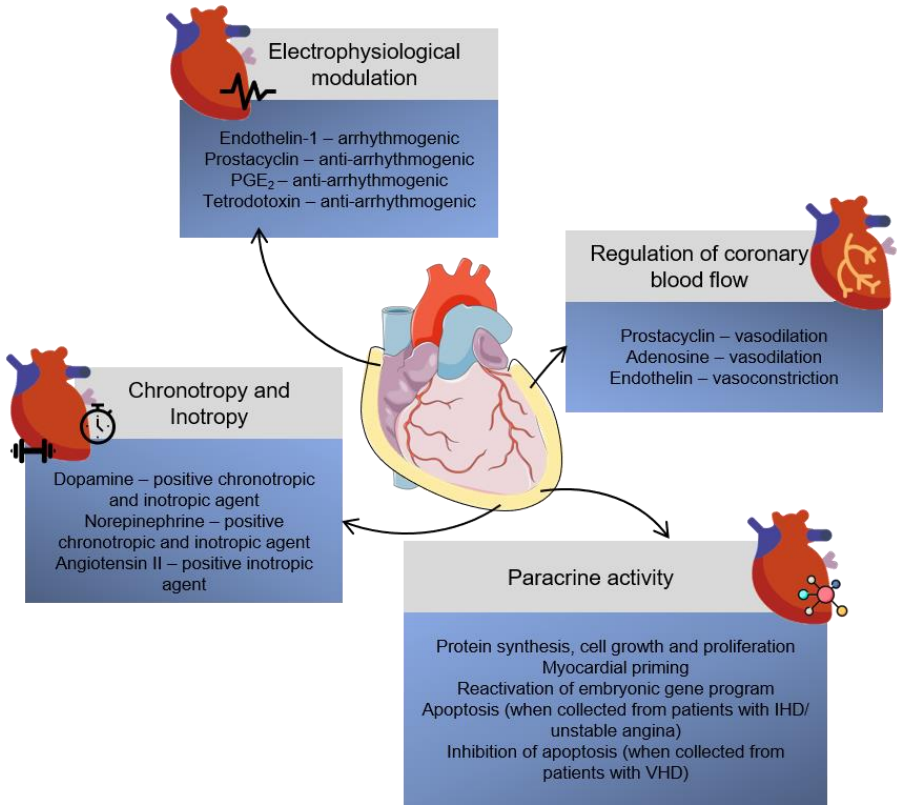

Figure 9. Summary of the pericardial fluid properties derived from mechanistic research (instillation or monitoring of biological or pharmacological compounds in pericardium with assessment of the biological effects and incubation of cells with pericardial fluid). Some graphical elements were adapted from Servier Medical Art. Abbreviations: IHD: ischemic heart disease; PGE_2: prostaglandin E_2; VHD: valvular heart disease.

3.4.1. Modulation of coronary blood flow, electrophysiological properties and cardiac inotropy and chronotropy by pericardial fluid

Coronary blood flow regulation has always been a hot topic of research because a tight adjustment of the oxygen and nutrient supply is needed to meet the demand of the cardiac workload. In this sense, the focus has been deposited in understanding if and how coronary blood flow is regulated by molecules present in the PF. By artificially increasing afterload (e.g. thoracic aortic constriction) or by β-adrenergic stimulation (e.g. with angiotensin II or isoproterenol), the release of prostacyclin in the canine pericardial cavity has been reported [204–206]. Soon the role of prostacyclin in the regulation of coronary blood flow was established. By incubating the different cardiac layers with arachidonic acid *in vitro*, the main source of this hormone was attributed to parietal pericardium in the dog, ox and rat [204]. Beyond prostacyclin, adenosine was also suggested to couple myocardial oxygen consumption with coronary blood flow. The evidence arises from the decrease of PF adenosine levels after vagal stimulation (decreasing both parameters) and the increase after atrial constriction, atrial pacing or intravenous delivery of calcium, norepinephrine or isoproterenol (all heightening oxygen demand and, thus, coronary blood flow) [207]. An opposite effect has been described for endothelin-1. Rat carotid arteries incubated with PF collected from ischemic heart disease patients exhibited vasoconstriction, and this was prevented by adding an endothelin receptor antagonist [208]. Interestingly, endothelin-1-induced ischemia is sided by increases in PF levels of the vasodilatory adenosine (and its metabolites - inosine and hypoxanthine) [209,210]. Vice-versa, adding adenosine and inosine to canine pericardial cavity led to an increase in endothelin-1 levels [211]. Therefore, vasomodulatory agents present in PF regulate coronary blood flow in response to different stimuli. Besides, unlike in plasma, adenosine metabolites can be easily monitored in the PF due to the relative lower clearance rate [211].

The electrophysiological properties of the cardiac tissue were early hypothesized to be modulated by substances naturally present or added to the PF. This was based on the premise that vagal and sympathetic efferent fibers lie at the epicardial surface. Indeed, intrapericardial instillation of tetrodotoxin, prostacyclin and prostaglandin E_2 could rescue the *ansae subclaviae* stimulation-induced shortening of effective refractory period (i.e. the period when an action potential cannot be initiated) [141,212]. In turn, administration of hexamethonium and tetrodotoxin could mitigate the vagal stimulation-induced lengthening

of effective refractory period [212]. Hence, intrapericardial drug delivery may help treat patients with peri- or postoperative arrhythmia. Of note, some PF proteins can be themselves arrhythmogenic. For instance, intrapericardial delivery of endothelin-1 induced a significant increase in ST segment, QT interval duration and prolonged the monophasic action potential in dogs. Besides, endothelin-1 caused episodes of ventricular extrasystoles, couplets and triples, tachycardia and fibrillation in a dose-dependent fashion [210,213–216].

Administration of inotropic and chronotropic agents to the heart can be life-saving in conditions requiring urgent correction of hemodynamic imbalances such as in cardiogenic shock [217]. In this regard, the intrapericardial route is effective. For instance, intrapericardial delivery of dopamine and norepinephrine in a canine model translated into increased chronotropy and inotropy as demonstrated by, respectively, increased heart rate and LV contractile force [218]. In turn, angiotensin II induced a rise in the vasoconstrictor endothelin-1 and increased the maximal rate of pressure development (d*P*/d*T*) in dogs [219].

3.4.2. Exploration of pericardial fluid's paracrine activity

Since the first assessment of growth factors, in 1996, the PF has been regarded not only as of diagnostic value but also as a liquid with important paracrine properties. In order to explore these features, mechanistic research has been conducted by incubating specific cardiac and vascular cells with PF collected from different animals and humans with different pathological conditions. For instance, Yoneda *et al*. [188] demonstrated that the incubation of human aortic smooth muscle cells with 10% of PF collected from patients with ischemic heart disease could accelerate their growth as compared to that retrieved from nonischemic patients. Such an effect was, in part, attributed to the higher content in FGF2 in ischemic patients. The same factor was also found responsible for the stimulation of protein synthesis in cultured adult rat cardiomyocytes after incubation with PF collected from patients with ischemic, valvular or congenital heart diseases [118]. PF from ischemic heart disease patients also induced beneficial effects in human umbilical vein endothelial cells and in mouse embryo stem cells. While the former presented higher ability of capillary-like tube formation and increased proliferative activity, the latter showed augmented expression of the cardiac marker Nkx2.5 [220]. Perhaps more importantly, the addition of the ischemia-

conditioned PF to the pericardial sac of immunodeficient mice boosted the reactivation of the epicardial cells' embryonic gene program [220].

Despite these apparent positive effects on cells, caution should be given to the biofluid source because its contents may induce disparate effects according to the species, the pathological background and the cell type tested. For instance, fluid collected from sheep pericardial sac was shown to decrease the amplitude of myocyte shortening and to increase the resting sarcomere length, through a calcium-independent effect [117]. Also, PF obtained from subjects with different conditions exhibited opposite effects in cultured endothelial cells: while fluid from patients with unstable angina promoted apoptosis [221], fluid (exosomes) collected from patients with valvular heart disease inhibited [120]. Finally, in primary mouse ventricular cardiomyocytes, fluid from ischemic heart disease subjects also induced apoptosis. In this case, an oxidative stress-sensitive p38 mitogen-activated protein kinase cascade was suggested to be the responsible for cell death activation [222].

3.5. What is settled and what is expected in pericardial fluid research?

If previously considered a bare plasma ultrafiltrate without readily palpable applications, today's perspective on PF has changed radically. Accumulating evidence shows that PF is a stable biofluid with low clearance rates and stocking heart-derived factors released from regions as deep as the myocardium. Hence, the exploration of its diagnostic, prognostic and therapeutic properties has gained popularity. However, the relative difficulty in the collection and the ethical limitations of using samples from healthy individuals has lagged the knowledge of PF features over other biofluids commonly used in clinical practice and in research, such as serum/plasma and urine. This explains why the behavior of PF and its molecular profile is better known for pericardial diseases, as these often require urgent pericardial drainage. It is pretty much settled that PF analysis is important to discern the etiology of pericarditis (e.g. total protein, LDH; PCR for tuberculous pericarditis, but also ADA, lysozyme and IFN γ; tumor markers such as CEA for suspected neoplasms and triglycerides for chylopericardium) as recently recommended by ESC guidelines on the diagnosis and management of pericardial diseases [223]. Nonetheless, the perioperative analysis of PF (easily and safely accessed during surgery) may be of great value in the

future to predict the outcome of the patients undergoing cardiac surgery, to design risk stratification algorithms and, ultimately, to tailor personalized adjuvant pharmacotherapies. Indeed, the systematic review on this topic elicited several potential markers deserving further research to validate their prognostic potential. For instance, in the AS setting, the assessment of ADM and of MMP2 may help to predict left ventricular RR on occasion of AVR.

Beyond the clinical applicability, the close contact between PF and the heart makes this biofluid a great vehicle for mechanistic studies. Reported effects of PF elements are diverse and comprise regulation of coronary blood flow, modulation of cardiac electrophysiological properties as well as tuning of heart chronotropy and inotropy. Notably, the PF has demonstrated potent paracrine activity with important therapeutic implications *ex vivo*.

The application of high-throughput omics approaches such as miRNomics and proteomics to the molecular characterization of PF will certainly help explain the biological properties of this liquid. In fact, Beltrami *et al*. [120] have already identified the miRNA let-7b-5p as a key PF pro-angiogenic player in a mouse model of unilateral limb ischemia. In turn, Foglio and colleagues showed that PF exosomal clusterin is an important adjuvant for myocardial recovery after an ischemic insult [119]. Thus, the continuous collection and screening of PF from patients undergoing heart surgery is strongly warranted. These approaches will certainly speed the pace towards personalized medicine by prompting effective prognostic tools as well as by pushing towards effective and targeted heart therapy.

This section was adapted from the paper: ***F. Trindade****, R. Vitorino, A. Leite-Moreira, I. Falcão-Pires. Pericardial fluid: an underrated molecular library of heart conditions and a potential vehicle for cardiac therapy. Basic Research in Cardiology. 114 (2019): 10. doi: 10.1007/s00395-019-0716-3.*

4. Motivation, aims and outline of the thesis

The growing prevalence of AS and the concomitant rise in valve replacement surgeries conveying to the unsolved problem of incomplete myocardial RR that increases the morbimortality of the patients, fed the primary motivation for this PhD thesis. The

mechanisms underlying the phenotypical divergence during myocardial RR remain elusive, not to mention the lack of reliable prognostic tools and of effective, non-palliative, adjuvant therapies in the present clinical scenario. Considering the high throughput nature and the comprehensiveness of the (phospho)proteomics approaches, the working hypothesis was that the (phospho)proteomic profiling of AS patients undergoing AVR would help to shed light into the mechanisms driving to an incomplete response and, simultaneously, to provide surrogate markers and therapeutic targets for incomplete RR. Beyond the myocardium, the primary site of heart's adaptation to increased afterload, it was hypothesized that the molecular content of the PF, in close contact to the heart, would complement the insights provided by myocardial (phospho)proteomics. Hence, the specific aims of the present thesis were to:

i) Characterize the myocardial proteome of AS patients with complete and incomplete RR in order to uncover new biological and molecular mechanisms underlying the phenotypical divergence in RR;
ii) Assess the phosphoproteome differences between AS patients with complete and incomplete RR and identify dysregulated pathways;
iii) Pinpoint new potential therapeutic targets through kinase prediction and *in vitro* functional assays with isolated cardiomyocytes;
iv) Validate a fractionation approach to the characterization of PF proteome;
v) Profile the PF proteome in complete and incomplete RR;
vi) Identify new surrogate prognostic markers and therapeutic targets of incomplete RR through myocardial and PF proteomics.

The connection between the aims of this thesis and the scope of each chapter is depicted in **Figure 10**. A general discussion and the final remarks of the thesis are provided in ***Chapter VII***. ***Chapter II*** covers the characterization of the myocardial proteome and phosphoproteome in AS patients with complete and incomplete RR. It also comprises the prediction of dysregulated kinases and the validation of some markers by western blot. In ***Chapter III***, the association between ubiquitin-proteasome system players and reverse remodeling was explored, following the clues provided by the previous chapter. Next, in ***Chapter IV***, the functional effects of the kinase deemed with the highest therapeutic potential were explored in single isolated cardiomyocytes. ***Chapter V*** and ***Chapter VI*** are centered on PF research. In the former, a fractionation approach is presented to bypass the problem of low proteome coverage due to the presence of high amounts of albumin in PF. In the latter, the PF proteome is profiled to identify surrogate prognostic markers for

incomplete RR and to complement the biological insights provided by myocardial proteomics into the pathophysiology of this condition.

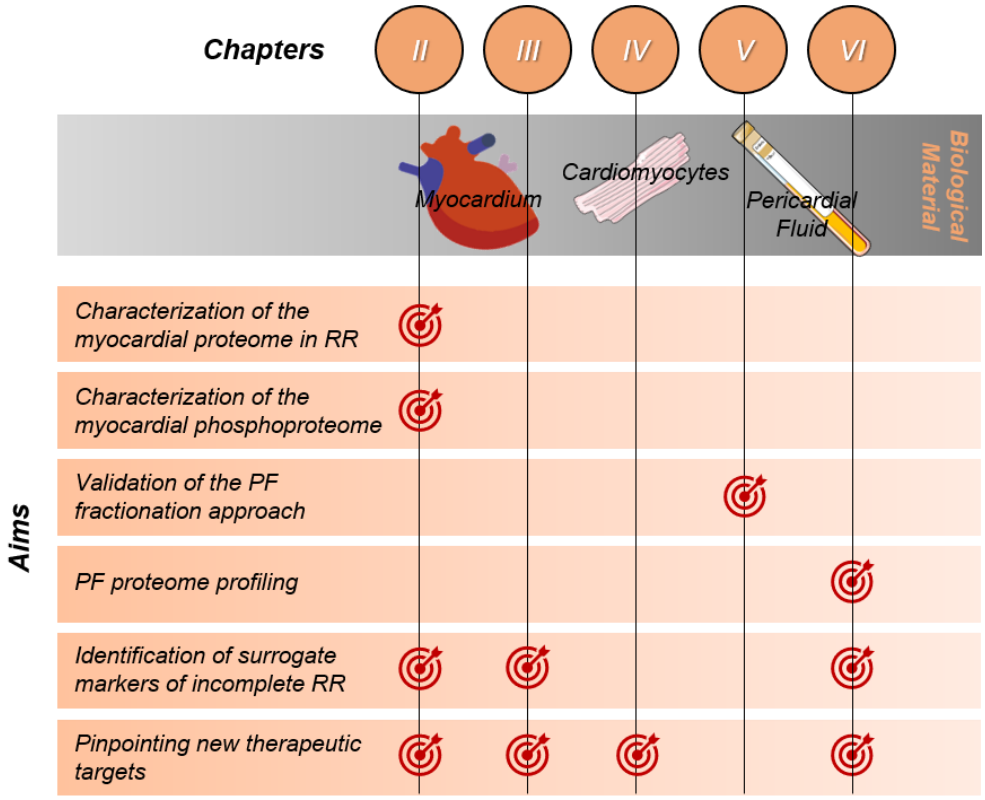

Figure 10. The structure of the thesis: connection between aims and the scope of each chapter. Also presented is the biological material used in each chapter. Abbreviations: PF: pericardial fluid; RR: reverse remodeling.

5. References

[1] World Health Organization - Noncommunicable diseases - Key facts, (n.d.). https://www.who.int/news-room/fact-sheets/detail/noncommunicable-diseases (accessed June 18, 2019).

[2] J.L. D'Arcy, B.D. Prendergast, J.B. Chambers, S.G. Ray, B. Bridgewater, Valvular heart disease: the next cardiac epidemic, Heart. 97 (2011) 91–93. doi:10.1136/hrt.2010.205096.

[3] S. Coffey, J.L. D'Arcy, M.A. Loudon, D. Mant, A.J. Farmer, B.D. Prendergast, The OxVALVE population cohort study (OxVALVE-PCS)—population screening for undiagnosed valvular heart disease in the elderly: study design and objectives, Open Hear. 1 (2014) 1–8. doi:10.1136/openhrt-2014-000043.

[4] A. Timmis, N. Townsend, C. Gale, R. Grobbee, N. Maniadakis, M. Flather, E. Wilkins, L. Wright, R. Vos, J. Bax, M. Blum, F. Pinto, P. Vardas, European Society of Cardiology: Cardiovascular Disease Statistics 2017, Eur. Heart J. 39 (2017) 508–579. doi:10.1093/eurheartj/ehx628.

[5] B.E. J., M. Paul, A. Alvaro, B.M. S., C.C. W., C.A. P., C.A. M., C.A. R., C. Susan, D.S. R., D.F. N., D. Luc, E.M. S.V., F.J. F., F. Myriam, J.L. Chaffin, K.S. S., K.B. M., K.K. L., K.T. W.,

L.D. T., L.T. T., L.J. H., L.C. T., L.M. Shane, L.P. L., M.S. S., M. Kunihiro, M.A. E., M.M. E., O. Martin, P. Ambarish, P.A. M., R.W. D., R.G. A., S.U. K.A., S.G. M., S.E. B., S.S. H., S.N. L., S. Andrew, T.D. L., T.C. W., T.M. P., V.L. B., W.J. T., W.S. S., V.S. S., null null, Heart Disease and Stroke Statistics—2019 Update: A Report From the American Heart Association, Circulation. 139 (2019) e56–e528. doi:10.1161/CIR.0000000000000659.

[6] V.T. Nkomo, J.M. Gardin, T.N. Skelton, J.S. Gottdiener, C.G. Scott, M. Enriquez-Sarano, Burden of valvular heart diseases: a population-based study, Lancet. 368 (2006) 1005–1011. doi:10.1016/S0140-6736(06)69208-8.

[7] B. Iung, A. Vahanian, Epidemiology of valvular heart disease in the adult, Nat. Rev. Cardiol. 8 (2011) 162. doi:10.1038/nrcardio.2010.202.

[8] G.W. Eveborn, H. Schirmer, G. Heggelund, P. Lunde, K. Rasmussen, The evolving epidemiology of valvular aortic stenosis. The Tromsø Study, Heart. 99 (2013) 396–400. doi:10.1136/heartjnl-2012-302265.

[9] V. Falk, H. Baumgartner, J.J. Bax, M. De Bonis, C. Hamm, P.J. Holm, B. Iung, P. Lancellotti, E. Lansac, D.R. Muñoz, R. Rosenhek, J. Sjögren, P. Tornos Mas, A. Vahanian, T. Walther, O. Wendler, S. Windecker, J.L. Zamorano, 2017 ESC/EACTS Guidelines for the management of valvular heart disease, Eur. J. Cardio-Thoracic Surg. 52 (2017) 616–664. doi:10.1093/ejcts/ezx324.

[10] P. Andell, X. Li, A. Martinsson, C. Andersson, M. Stagmo, B. Zöller, K. Sundquist, J.G. Smith, Epidemiology of valvular heart disease in a Swedish nationwide hospital-based register study, Heart. 103 (2017) 1696–1703. doi:10.1136/heartjnl-2016-310894.

[11] H. Baumgartner, T. Walther, Aortic stenosis, in: ESC Textb. Cardiovasc. Med., Oxford University Press, Oxford, UK, 2018: pp. 1–58. doi:10.1093/med/9780198784906.003.0766.

[12] C.K. Leung, T. Koon, D.J. G., N. Andy, T. James, Effect of Lipid Lowering With Rosuvastatin on Progression of Aortic Stenosis, Circulation. 121 (2010) 306–314. doi:10.1161/CIRCULATIONAHA.109.900027.

[13] A.B. Rossebø, T.R. Pedersen, K. Boman, P. Brudi, J.B. Chambers, K. Egstrup, E. Gerdts, C. Gohlke-Bärwolf, I. Holme, Y.A. Kesäniemi, W. Malbecq, C.A. Nienaber, S. Ray, T. Skjærpe, K. Wachtell, R. Willenheimer, Intensive Lipid Lowering with Simvastatin and Ezetimibe in Aortic Stenosis, N. Engl. J. Med. 359 (2008) 1343–1356. doi:10.1056/NEJMoa0804602.

[14] H. Baumgartner, B. Iung, P. Kappetein, Introduction and general comments, in: ESC Textb. Cardiovasc. Med., Oxford University Press, Oxford, UK, 2018: pp. 1–38. doi:10.1093/med/9780198784906.003.0764.

[15] C. Gavina, I. Falcão-Pires, F. Rocha-Goncalves, A. Leite-Moreira, Left Ventricular Hypertrophy in Isolated Aortic Stenosis: Primetime for the Ventricle, Curr. Pharm. Biotechnol. 13 (2012) 2503–2514. doi:10.2174/1389201011208062503.

[16] S. Coffey, B. Cox, M.J.A. Williams, The Prevalence, Incidence, Progression, and Risks of Aortic Valve Sclerosis: A Systematic Review and Meta-Analysis, J. Am. Coll. Cardiol. 63 (2014) 2852–2861. doi:10.1016/j.jacc.2014.04.018.

[17] P.G. Rodrigues, A.F. Leite-Moreira, I. Falcão-Pires, Myocardial reverse remodeling: how far can we rewind?, Am. J. Physiol. Circ. Physiol. 310 (2016) H1402–H1422. doi:10.1152/ajpheart.00696.2015.

[18] J.L. Hellawell, K.B. Margulies, Myocardial Reverse Remodeling, Cardiovasc. Ther. 30 (2012) 172–181. doi:10.1111/j.1755-5922.2010.00247.x.

[19] R.W.W. Biederman, J.A. Magovern, S.B. Grant, R.B. Williams, J.A. Yamrozik, D.A. Vido, V.K. Rathi, G. Rayarao, K. Caruppannan, M. Doyle, LV reverse remodeling imparted by aortic valve replacement for severe aortic stenosis; is it durable? A cardiovascular MRI study sponsored by the American Heart Association, J Cardiothorac Surg. 6 (2011) 1–8. doi:10.1186/1749-8090-6-53.

[20] M.A. Magalhaes, E. Koifman, R. Torguson, S. Minha, J. Gai, S. Kiramijyan, R.O. Escarcega, N.C. Baker, Z. Wang, S. Goldstein, F. Asch, L.F. Satler, A.D. Pichard, R. Waksman, Outcome of Left-Sided Cardiac Remodeling in Severe Aortic Stenosis Patients Undergoing Transcatheter Aortic Valve Implantation, Am. J. Cardiol. 116 (2015) 595–603. doi:10.1016/j.amjcard.2015.05.018.

[21] I. Falcão-Pires, C. Gavina, A.F. Leite-Moreira, Understanding the molecular and cellular changes behind aortic valve stenosis, Curr. Pharm. Biotechnol. 13 (2012) 2485–2496. doi:10.2174/138920112804583050.

[22] B.R. Hughes, G. Chahoud, J.L. Mehta, Aortic stenosis: Is it simply a degenerative process or

an active atherosclerotic process?, Clin. Cardiol. 28 (2005) 111–114. doi:10.1002/clc.4960280303.
[23] M.R. Dweck, N.A. Boon, D.E. Newby, Calcific Aortic Stenosis: A Disease of the Valve and the Myocardium, J. Am. Coll. Cardiol. 60 (2012) 1854–1863. doi:10.1016/j.jacc.2012.02.093.
[24] G. Christodoulidis, T.J. Vittorio, M. Fudim, S. Lerakis, C.E. Kosmas, Inflammation in coronary artery disease, Cardiol. Rev. 22 (2014) 279–288. doi:10.1097/CRD.0000000000000006.
[25] G.K. Hansson, Inflammation, Atherosclerosis, and Coronary Artery Disease, N. Engl. J. Med. 352 (2005) 1685–1695. doi:10.1056/NEJMra043430.
[26] I. Ikonomidis, C.A. Michalakeas, J. Parissis, I. Paraskevaidis, K. Ntai, I. Papadakis, M. Anastasiou-Nana, J. Lekakis, Inflammatory markers in coronary artery disease, BioFactors. 38 (2012) 320–328. doi:10.1002/biof.1024.
[27] E. Yetkin, J. Waltenberger, Molecular and cellular mechanisms of aortic stenosis, Int. J. Cardiol. 135 (2009) 4–13. doi:10.1016/j.ijcard.2009.03.108.
[28] P. Libby, P. Theroux, Pathophysiology of Coronary Artery Disease, Circulation. 111 (2005) 3481–3488. doi:10.1161/CIRCULATIONAHA.105.537878.
[29] T. Martín-Rojas, F. Gil-Dones, L.F. Lopez-Almodovar, L.R. Padial, F. Vivanco, M.G. Barderas, Proteomic Profile of Human Aortic Stenosis: Insights into the Degenerative Process, J. Proteome Res. 11 (2012) 1537–1550. doi:10.1021/pr2005692.
[30] A. Alexopoulos, A. Kaoukis, H. Papadaki, V. Pyrgakis, Pathophysiologic mechanisms of calcific aortic stenosis, Ther. Adv. Cardiovasc. Dis. 6 (2012) 71–80. doi:10.1177/1753944712439337.
[31] Y.Q. Tang, J. Yuan, G. Osapay, K. Osapay, D. Tran, C.J. Miller, a J. Ouellette, M.E. Selsted, A cyclic antimicrobial peptide produced in primate leukocytes by the ligation of two truncated alpha-defensins., Science. 286 (1999) 498–502. doi:10.1126/science.286.5439.498.
[32] F. Otsuka, S. Yasuda, T. Noguchi, H. Ishibashi-Ueda, Pathology of coronary atherosclerosis and thrombosis, Cardiovasc. Diagn. Ther. 6 (2016) 396–408. doi:10.21037/cdt.2016.06.01.
[33] G.H. Kim, N. Uriel, D. Burkhoff, Reverse remodelling and myocardial recovery in heart failure, Nat. Rev. Cardiol. 15 (2017) 83–96. doi:doi:10.1038/nrcardio.2017.139.
[34] G.L. Perrucci, M. Zanobini, P. Gripari, P. Songia, B. Alshaikh, E. Tremoli, P. Poggio, Pathophysiology of Aortic Stenosis and Mitral Regurgitation, Compr. Physiol. 7 (2017) 799–818. doi:doi:10.1002/cphy.c160020.
[35] B.R. Lindman, M.-A. Clavel, P. Mathieu, B. Iung, P. Lancellotti, C.M. Otto, P. Pibarot, Calcific aortic stenosis, Nat. Rev. Dis. Prim. 2 (2016) 16006. doi:10.1038/nrdp.2016.6.
[36] M. Dobaczewski, W. Chen, N.G. Frangogiannis, Transforming growth factor (TGF)-β signaling in cardiac remodeling, J. Mol. Cell. Cardiol. 51 (2011) 600–606. doi:10.1016/j.yjmcc.2010.10.033.
[37] A.N. Rassi, P. Pibarot, S. Elmariah, Left Ventricular Remodelling in Aortic Stenosis, Can. J. Cardiol. 30 (2014) 1004–1011. doi:10.1016/j.cjca.2014.04.026.
[38] M.R. Dweck, S. Joshi, T. Murigu, F. Alpendurada, A. Jabbour, G. Melina, W. Banya, A. Gulati, I. Roussin, S. Raza, N.A. Prasad, R. Wage, C. Quarto, E. Angeloni, S. Refice, M. Sheppard, S.A. Cook, P.J. Kilner, D.J. Pennell, D.E. Newby, R.H. Mohiaddin, J. Pepper, S.K. Prasad, Midwall Fibrosis Is an Independent Predictor of Mortality in Patients With Aortic Stenosis, J. Am. Coll. Cardiol. 58 (2011) 1271–1279. doi:10.1016/j.jacc.2011.03.064.
[39] J. Joseph, S.Y. Naqvi, J. Giri, S. Goldberg, Aortic Stenosis: Pathophysiology, Diagnosis, and Therapy, Am. J. Med. 130 (2017) 253–263. doi:10.1016/j.amjmed.2016.10.005.
[40] D.A. Lerman, S. Prasad, N. Alotti, Calcific Aortic Valve Disease: Molecular Mechanisms and Therapeutic Approaches, Eur. Cardiol. 10 (2015) 108–112. doi:10.15420/ecr.2015.10.2.108.
[41] R.J. Everett, M.-A. Clavel, P. Pibarot, M.R. Dweck, Timing of intervention in aortic stenosis: a review of current and future strategies, Heart. 104 (2018) 2067–2076. doi:10.1136/heartjnl-2017-312304.
[42] B.R. Lindman, M.R. Dweck, P. Lancellotti, P. Généreux, L.A. Piérard, P.T. O'Gara, R.O. Bonow, Management of Asymptomatic Severe Aortic Stenosis: Evolving Concepts in Timing of Valve Replacement, JACC Cardiovasc. Imaging. n/d (2019) 1–13. doi:10.1016/j.jcmg.2019.01.036.
[43] L.-P. Chen, T.-M. Wei, L.-X. Wang, Relationship between Pericardial Fluid B-type Natriuretic Peptide and Ventricular Structure and Function, Arch. Med. Res. 38 (2007) 326–329. doi:10.1016/j.arcmed.2006.12.006.
[44] Y.I. Zeng, R. Sun, X. Li, M. Liu, S. Chen, P. Zhang, Pathophysiology of valvular heart disease,

Exp. Ther. Med. 11 (2016) 1184–1188. doi:10.3892/etm.2016.3048.
[45] K. Sandhu, S. Krishnamoorthy, A. Afif, J. Nolan, M.G. Gunning, Balloon aortic valvuloplasty in contemporary practice, J. Interv. Cardiol. 30 (2017) 212–216. doi:10.1111/joic.12384.
[46] J.L.M. Tham, H. Adams, S. Paleri, C. Wright, J. Dimitriou, A. Newcomb, A.I. MacIsaac, R.J. Whitbourn, S.C. Palmer, Clinical outcomes of self-expandable vs. balloon-expandable TAVI for severe aortic stenosis, Acta Cardiol. (2019) 1–8. doi:10.1080/00015385.2019.1572959.
[47] H. Baumgartner, J. Hung, J. Bermejo, J.B. Chambers, A. Evangelista, B.P. Griffin, B. Iung, C.M. Otto, P.A. Pellikka, M. Quiñones, Echocardiographic Assessment of Valve Stenosis: EAE/ASE Recommendations for Clinical Practice, J. Am. Soc. Echocardiogr. 22 (2009) 1–23. doi:10.1016/j.echo.2008.11.029.
[48] D.A. Kass, K.L. Baughman, P.H. Pak, P.W. Cho, H.R. Levin, T.J. Gardner, H.R. Halperin, J.E. Tsitlik, M.A. Acker, Reverse Remodeling From Cardiomyoplasty in Human Heart Failure, Circulation. 91 (1995) 2314–2318. doi:10.1161/01.CIR.91.9.2314.
[49] N. Koitabashi, D.A. Kass, Reverse remodeling in heart failure—mechanisms and therapeutic opportunities, Nat. Rev. Cardiol. 9 (2011) 147–157. doi:10.1038/nrcardio.2011.172.
[50] X.-M. Gao, H. Kiriazis, X.-L. Moore, X.-H. Feng, K. Sheppard, A. Dart, X.-J. Du, Regression of pressure overload-induced left ventricular hypertrophy in mice., Am. J. Physiol. Heart Circ. Physiol. 288 (2005) H2702–H2707. doi:10.1152/ajpheart.00836.2004.
[51] W.E. Stansfield, M. Rojas, D. Corn, M. Willis, C. Patterson, S.S. Smyth, C.H. Selzman, Characterization of a model to independently study regression of ventricular hypertrophy, J. Surg. Res. 142 (2007) 387–393.
[52] J.L. Bjørnstad, B. Skrbic, I. Sjaastad, S. Bjørnstad, G. Christensen, T. Tønnessen, A mouse model of reverse cardiac remodelling following banding-debanding of the ascending aorta, Acta Physiol. 205 (2012) 92–102. doi:10.1111/j.1748-1716.2011.02369.x.
[53] M. Ruppert, S. Korkmaz-Icöz, S. Li, B.T. Németh, P. Hegedűs, P. Brlecic, C. Mátyás, M. Zorn, B. Merkely, M. Karck, T. Radovits, G. Szabó, Myocardial reverse remodeling after pressure unloading is associated with maintained cardiac mechanoenergetics in a rat model of left ventricular hypertrophy, Am. J. Physiol. - Hear. Circ. Physiol. 311 (2016) H592–H603. doi:10.1152/ajpheart.00085.2016.
[54] J.L. Bjørnstad, I. Sjaastad, S. Nygård, A. Hasic, M.S. Ahmed, H. Attramadal, A.V. Finsen, G. Christensen, T. Tønnessen, Collagen isoform shift during the early phase of reverse left ventricular remodelling after relief of pressure overload, Eur. Heart J. 32 (2010) 236–245. doi:10.1093/eurheartj/ehq166.
[55] J.S. Cho, E.J. Cho, J. Lee, H.-D. Choi, K.C. Park, K.-H. Lee, K.-J. Yang, M.-W. Park, G.-M. Park, S.-H. Her, C.J. Kim, Myocardial Mechanics in a Rat Model with Banding and Debanding of the Ascending Aorta, J Cardiovasc Ultrasound. 22 (2014) 189–195. doi:10.4250/jcu.2014.22.4.189.
[56] W.E. Stansfield, N.M. Andersen, R.-H. Tang, C.H. Selzman, Periostin Is a Novel Factor in Cardiac Remodeling After Experimental and Clinical Unloading of the Failing Heart, Ann. Thorac. Surg. 88 (2009) 1916–1921. doi:10.1016/j.athoracsur.2009.07.038.
[57] T. Waszyrowski, J.D. Kasprzak, M. Krzemińska-Pakuła, J. Drożˇ, A. Dziatkowiak, J. Zasłonka, Regression of left ventricular dilatation and hypertrophy after aortic valve replacement, Int. J. Cardiol. 57 (1996) 217–225. doi:10.1016/S0167-5273(96)02803-3.
[58] C. Gavina, I. Falcão-Pires, P. Pinho, M.-C. Manso, A. Gonçalves, F. Rocha-Gonçalves, A. Leite-Moreira, Relevance of residual left ventricular hypertrophy after surgery for isolated aortic stenosis, Eur. J. Cardio-Thoracic Surg. 49 (2015) 952–959. doi:10.1093/ejcts/ezv240.
[59] C. Gavina, I. Falcão-Pires, J. Rodrigues, B. Marinho, N. Gonçalves, R. Lopes, M.J. Amorim, J. Almeida, P. Pinho, A. Gonçalves, F. Rocha-Gonçalves, A. Leite-Moreira, Load independent impairment of reverse remodeling after valve replacement in hypertensive aortic stenosis patients, Int. J. Cardiol. 170 (2014) 324–330. doi:10.1016/j.ijcard.2013.11.006.
[60] O. Lund, K. Emmertsen, I. Dørup, F.T. Jensen, C. Flø, Regression of left ventricular hypertrophy during 10 years after valve replacement for aortic stenosis is related to the preoperative risk profile, Eur. Heart J. 24 (2003) 1437–1446. doi:10.1016/S0195-668X(03)00316-6.
[61] M. Gaudino, F. Alessandrini, F. Glieca, N. Luciani, C. Cellini, C. Pragliola, M. Morelli, C. Canosa, G. Nasso, G. Possati, Survival after aortic valve replacement for aortic stenosis: does left ventricular mass regression have a clinical correlate?, Eur Hear. J. 26 (2005) 51–57. doi:10.1093/eurheartj/ehi012.

[62] T. Nakamura, K. Toda, T. Kuratani, S. Miyagawa, Y. Yoshikawa, S. Fukushima, S. Saito, D. Yoshioka, N. Kashiyama, T. Daimon, Y. Sawa, Diabetes Mellitus Impairs Left Ventricular Mass Regression after Surgical or Transcatheter Aortic Valve Replacement for Severe Aortic Stenosis, Hear. Lung Circ. 25 (2016) 68–74. doi:10.1016/j.hlc.2015.05.019.
[63] I. Falcão-Pires, N. Hamdani, A. Borbély, C. Gavina, C.G. Schalkwijk, J. van der Velden, L. van Heerebeek, G.J.M. Stienen, H.W.M. Niessen, A.F. Leite-Moreira, W.J. Paulus, Diabetes Mellitus Worsens Diastolic Left Ventricular Dysfunction in Aortic Stenosis Through Altered Myocardial Structure and Cardiomyocyte Stiffness, Circ. . 124 (2011) 1151–1159. doi:10.1161/CIRCULATIONAHA.111.025270.
[64] E. Einarsen, S. Saeed, D. Cramariuc, J.B. Chambers, H. Midtbø, E. Gerdts, Impact of Obesity on Persistent Left Ventricular Hypertrophy After Aortic Valve Replacement for Aortic Stenosis, Am. J. Cardiol. 123 (2019) 942–947. doi:10.1016/j.amjcard.2018.12.012.
[65] M. Vaduganathan, R. Lee, A.J. Beckham, A.-C. Andrei, B. Lapin, N.J. Stone, E.C. McGee, S.C. Malaisrie, P. Kansal, R.A. Silverberg, D.M. Lloyd-Jones, P.M. McCarthy, Relation of Body Mass Index to Late Survival After Valvular Heart Surgery, Am. J. Cardiol. 110 (2012) 1667–1678. doi:10.1016/j.amjcard.2012.07.041.
[66] W.C. Roberts, C.C. Roberts, T.J. Vowels, J.M. Ko, G. Filardo, B.L. Hamman, G.J. Matter, A.C. Henry, R.F. Hebeler, Effect of Body Mass Index on Survival in Patients Having Aortic Valve Replacement for Aortic Stenosis With or Without Concomitant Coronary Artery Bypass Grafting, Am. J. Cardiol. 108 (2011) 1767–1771. doi:10.1016/j.amjcard.2011.09.010.
[67] V.D. Bruno, P. Chivasso, F. Rapetto, G. Guida, E. Di Tommaso, H.M. Chau, H. Vohra, Impact of Body Mass Index on Short- and Long-Term Outcomes After Isolated First-Time Surgical Aortic Valve Replacement for Aortic Stenosis, J. Cardiothorac. Vasc. Anesth. (2019). doi:10.1053/j.jvca.2019.02.015.
[68] J.A.L. Vicente, I.L. Blasco, P.P. Perez, B.S. Sanchez, M.R.O. Nadal, J.R.R. Arroyo, M.G. Carretero, A.D.R. Ligorit, Impact of moderate coronary atherosclerosis on long-term left ventricular remodeling after aortic valve replacement, Cardiol. J. 18 (2011) 277–281.
[69] B.R. W.W., D. Mark, Y. June, W.R. B., R.V. K., V. Diane, C. Ketheswaram, O. Nael, B. Valerie, R. Geetha, B.C. M., M. Sunil, M.J. A., R. Nathaniel, Physiologic Compensation Is Supranormal in Compensated Aortic Stenosis: Does it Return to Normal After Aortic Valve Replacement or Is it Blunted by Coexistent Coronary Artery Disease?, Circulation. 112 (2005) I-429-I–436. doi:10.1161/CIRCULATIONAHA.104.525501.
[70] W. Frank, H. Sebastian, S. Stefan, N. Markus, F. Stefan, L. Volkmar, B. Meinrad, G. Stefan, V. Wolfram, E. Georg, S.J. M., Impact of Myocardial Fibrosis in Patients With Symptomatic Severe Aortic Stenosis, Circulation. 120 (2009) 577–584. doi:10.1161/CIRCULATIONAHA.108.847772.
[71] N.J. Howell, B.E. Keogh, V. Barnet, R.S. Bonser, T.R. Graham, S.J. Rooney, I.C. Wilson, D. Pagano, Patient-prosthesis mismatch does not affect survival following aortic valve replacement, Eur. J. Cardio-Thoracic Surg. 30 (2006) 10–14. doi:10.1016/j.ejcts.2006.03.046.
[72] A. Kulik, I.G. Burwash, V. Kapila, T.G. Mesana, M. Ruel, Long-Term Outcomes After Valve Replacement for Low-Gradient Aortic Stenosis, Circulation. 114 (2006) I-553-I–558. doi:10.1161/CIRCULATIONAHA.105.001180.
[73] T. Walther, Patient prosthesis mismatch affects short- and long-term outcomes after aortic valve replacement, Eur. J. Cardio-Thoracic Surg. 30 (2006) 15–19. doi:10.1016/j.ejcts.2006.04.007.
[74] U.C. Sharma, P. Barenburg, S. Pokharel, W.R.M. Dassen, Y.M. Pinto, J.G. Maessen, Systematic review of the outcome of aortic valve replacement in patients with aortic stenosis, Ann Thorac Surg. 78 (2004) 90–95. doi:10.1016/j.athoracsur.2004.02.020.
[75] R.E. Zybach-Benz, B.C. Aeschbacher, M. Schwerzmann, Impact of left ventricular hypertrophy late after aortic valve replacement for aortic stenosis on cardiovascular morbidity and mortality, Int. J. Cardiol. 109 (2006) 41–47. doi:10.1016/j.ijcard.2005.05.050.
[76] G. Petrov, V. Regitz-Zagrosek, E. Lehmkuhl, T. Krabatsch, A. Dunkel, M. Dandel, E. Dworatzek, S. Mahmoodzadeh, C. Schubert, E. Becher, H. Hampl, R. Hetzer, Regression of Myocardial Hypertrophy After Aortic Valve Replacement - Faster in Women?, Circulation. 122 (2010) S23 LP-S28. doi:10.1161/CIRCULATIONAHA.109.927764.
[77] N. Hanayama, G.T. Christakis, H.R. Mallidi, V. Rao, G. Cohen, B.S. Goldman, S.E. Fremes, C.D. Morgan, C.D. Joyner, Determinants of Incomplete Left Ventricular Mass Regression

Following Aortic Valve Replacement for Aortic Stenosis, J. Card. Surg. 20 (2005) 307–313. doi:10.1111/j.1540-8191.2005.200485.x.
[78] S.C. Stamou, M. Robich, R.E. Wolf, A. Lovett, S.-L.T. Normand, F.W. Sellke, Effects of gender and ethnicity on outcomes after aortic valve replacement, J. Thorac. Cardiovasc. Surg. 144 (2012) 486–492. doi:10.1016/j.jtcvs.2011.11.023.
[79] J.M. Beach, T. Mihaljevic, J. Rajeswaran, T. Marwick, S.T. Edwards, E.R. Nowicki, J. Thomas, L.G. Svensson, B. Griffin, A.M. Gillinov, E.H. Blackstone, Ventricular hypertrophy and left atrial dilatation persist and are associated with reduced survival after valve replacement for aortic stenosis, J. Thorac. Cardiovasc. Surg. 147 (2014) 362–369. doi:10.1016/j.jtcvs.2012.12.016.
[80] T. Hatani, T. Kitai, R. Murai, K. Kim, N. Ehara, A. Kobori, M. Kinoshita, S. Kaji, T. Tani, Y. Sasaki, T. Yamane, T. Koyama, M. Nasu, Y. Okada, Y. Furukawa, Associations of residual left ventricular and left atrial remodeling with clinical outcomes in patients after aortic valve replacement for severe aortic stenosis, J. Cardiol. 68 (2016) 241–247. doi:10.1016/j.jjcc.2015.09.017.
[81] R. Huss, Biomarkers, in: Transl. Regen. Med., Elsevier, 2015: pp. 235–241. doi:10.1016/B978-0-12-410396-2.00019-0.
[82] B. Karahalil, Overview of systems biology and omics technologies, Curr. Med. Chem. 23 (2016) 4221–4230. doi:10.2174/0929867323666160926150617.
[83] L. Mourino-Alvarez, C.M. Laborde, M.G. Barderas, Proteomics and Metabolomics in Aortic Stenosis: Studying Healthy Valves for a Better Understanding of the Disease, in: C.M. Laborde (Ed.), Calcif. Aortic Valve Dis., IntechOpen, Rijeka, 2013: pp. 151–172. doi:10.5772/55589.
[84] M.S. Monteiro, M. Carvalho, M.L.B. and P.G. de Pinho, Metabolomics Analysis for Biomarker Discovery: Advances and Challenges, Curr. Med. Chem. 20 (2013) 257–271. doi:10.2174/092986731132002006.
[85] M.P.Y. Lam, P. Ping, E. Murphy, Proteomics Research in Cardiovascular Medicine and Biomarker Discovery, J. Am. Coll. Cardiol. 68 (2016) 2819–2830. doi:10.1016/j.jacc.2016.10.031.
[86] B. Aslam, M. Basit, M.A. Nisar, M. Khurshid, M.H. Rasool, Proteomics: Technologies and Their Applications, J. Chromatogr. Sci. 55 (2017) 182–196. doi:10.1093/chromsci/bmw167.
[87] Z. Zhang, S. Wu, D.L. Stenoien, L. Paša-Tolic, High-throughput proteomics, Annu. Rev. Anal. Chem. 7 (2014) 427–454. doi:10.1146/annurev-anchem-071213-020216.
[88] N. Pappireddi, L. Martin, M. Wühr, A Review on Quantitative Multiplexed Proteomics, ChemBioChem. 20 (2019) 1210–1224. doi:10.1002/cbic.201800650.
[89] C. Ludwig, L. Gillet, G. Rosenberger, S. Amon, B.C. Collins, R. Aebersold, Data-independent acquisition-based SWATH-MS for quantitative proteomics: a tutorial, Mol. Syst. Biol. 14 (2018) e8126–e8126. doi:10.15252/msb.20178126.
[90] A. Schmidt, I. Forne, A. Imhof, Bioinformatic analysis of proteomics data, BMC Syst. Biol. 8 (2014) S3. doi:10.1186/1752-0509-8-S2-S3.
[91] A.V.G. Edwards, S.J. Cordwell, M.Y. White, Phosphoproteomic Profiling of the Myocyte, Circ. Cardiovasc. Genet. 4 (2011) 575. doi:10.1161/CIRCGENETICS.110.957787.
[92] Z. Sun, K.L. Hamilton, K.F. Reardon, Phosphoproteomics and molecular cardiology: techniques, applications and challenges., J. Mol. Cell. Cardiol. 53 (2012) 354–368. doi:10.1016/j.yjmcc.2012.06.001.
[93] Y. Xue, F. Zhou, M. Zhu, K. Ahmed, G. Chen, X. Yao, GPS: a comprehensive www server for phosphorylation sites prediction, Nucleic Acids Res. 33 (2005) W184–W187. doi:10.1093/nar/gki393.
[94] L. Negroni, S. Claverol, J. Rosenbaum, E. Chevet, M. Bonneu, J.-M. Schmitter, Comparison of IMAC and MOAC for phosphopeptide enrichment by column chromatography, J. Chromatogr. B. 891–892 (2012) 109–112. doi:10.1016/j.jchromb.2012.02.028.
[95] H. Ogata, S. Goto, K. Sato, W. Fujibuchi, H. Bono, M. Kanehisa, KEGG: Kyoto Encyclopedia of Genes and Genomes, Nucleic Acids Res. 27 (1999) 29–34. doi:10.1093/nar/27.1.29.
[96] M.L. Lindsey, D.K. Goshorn, S. Comte-Walters, J.W. Hendrick, E. Hapke, M.R. Zile, K. Schey, A multidimensional proteomic approach to identify hypertrophy-associated proteins, Proteomics. 6 (2006) 2225–2235. doi:10.1002/pmic.200500013.
[97] H. Bugger, M. Schwarzer, D. Chen, A. Schrepper, P.A. Amorim, M. Schoepe, T.D. Nguyen, F.W. Mohr, O. Khalimonchuk, B.C. Weimer, T. Doenst, Proteomic remodelling of

mitochondrial oxidative pathways in pressure overload-induced heart failure, Cardiovasc. Res. 85 (2009) 376–384. doi:10.1093/cvr/cvp344.
[98] T. Köcher, P. Pichler, M. Schutzbier, C. Stingl, A. Kaul, N. Teucher, G. Hasenfuss, J.M. Penninger, K. Mechtler, High Precision Quantitative Proteomics Using iTRAQ on an LTQ Orbitrap: A New Mass Spectrometric Method Combining the Benefits of All, J. Proteome Res. 8 (2009) 4743–4752. doi:10.1021/pr900451u.
[99] K. Kotlo, K.R. Johnson, J.M. Grillon, D.L. Geenen, P. DeTombe, R.S. Danziger, Phosphoprotein abundance changes in hypertensive cardiac remodeling, J. Proteomics. 77 (2012) 1–13. doi:10.1016/j.jprot.2012.05.041.
[100] Y.-W. Chang, Y.-T. Chang, Q. Wang, J.J.-C. Lin, Y.-J. Chen, C.-C. Chen, Quantitative Phosphoproteomic Study of Pressure-Overloaded Mouse Heart Reveals Dynamin-Related Protein 1 as a Modulator of Cardiac Hypertrophy, Mol. &Amp; Cell. Proteomics. 12 (2013) 3094–3107. doi:10.1074/mcp.M113.027649.
[101] J. Rüdebusch, A. Benkner, A. Poesch, M. Dörr, U. Völker, K. Grube, E. Hammer, S.B. Felix, Dynamic adaptation of myocardial proteome during heart failure development, PLoS One. 12 (2017) e0185915. doi:10.1371/journal.pone.0185915.
[102] H.K. Kwon, H. Jeong, D. Hwang, Z.-Y. Park, Comparative proteomic analysis of mouse models of pathological and physiological cardiac hypertrophy, with selection of biomarkers of pathological hypertrophy by integrative proteogenomics, Biochim. Biophys. Acta - Proteins Proteomics. 1866 (2018) 1043–1054. doi:10.1016/j.bbapap.2018.07.006.
[103] J. Gallego-Delgado, A. Lazaro, J.I. Osende, M.G. Barderas, M.C. Duran, F. Vivanco, J. Egido, Comparison of the Protein Profile of Established and Regressed Hypertension-Induced Left Ventricular Hypertrophy, J. Proteome Res. 5 (2006) 404–413. doi:10.1021/pr0503275.
[104] X. Jin, L. Xia, L.-S. Wang, J.-Z. Shi, Y. Zheng, W.-L. Chen, L. Zhang, Z.-G. Liu, G.-Q. Chen, N.-Y. Fang, Differential protein expression in hypertrophic heart with and without hypertension in spontaneously hypertensive rats, Proteomics. 6 (2006) 1948–1956. doi:10.1002/pmic.200500337.
[105] J. Gallego-Delgado, A. Lazaro, J.I. Osende, V. Esteban, M.G. Barderas, C. Gomez-Guerrero, R. Vega, F. Vivanco, J. Egido, Proteomic Analysis of Early Left Ventricular Hypertrophy Secondary to Hypertension: Modulation by Antihypertensive Therapies, J. Am. Soc. Nephrol. 17 (2006) S159–S164. doi:10.1681/ASN.2006080937.
[106] L. Liu, W. Wang, X. Meng, J. Gao, H. Wu, P. Wang, W. Wu, L. Wang, L. Ma, W. Zhang, Left ventricular hypertrophy induced by abdominal aortic banding and its prevention by angiotensin receptor blocker telmisartan—a proteomic analysis, J. Physiol. Biochem. 66 (2010) 329–338. doi:10.1007/s13105-010-0039-1.
[107] D. Dao-Fu, H.E. J., C. Tony, M.L. G., B.N. B., T. Lauren, B.R. P., C.D. A., S.N. J., S.H. H., T. Rong, M.M. J., R.P. S., Global Proteomics and Pathway Analysis of Pressure-Overload–Induced Heart Failure and Its Attenuation by Mitochondrial-Targeted Peptides, Circ. Hear. Fail. 6 (2013) 1067–1076. doi:10.1161/CIRCHEARTFAILURE.113.000406.
[108] S.J. Forrester, G.W. Booz, C.D. Sigmund, T.M. Coffman, T. Kawai, V. Rizzo, R. Scalia, S. Eguchi, Angiotensin II Signal Transduction: An Update on Mechanisms of Physiology and Pathophysiology, Physiol. Rev. 98 (2018) 1627–1738. doi:10.1152/physrev.00038.2017.
[109] Z.K. Haque, D.-Z. Wang, How cardiomyocytes sense pathophysiological stresses for cardiac remodeling, Cell. Mol. Life Sci. 74 (2017) 983–1000. doi:10.1007/s00018-016-2373-0.
[110] J. Lauriol, K. Keith, F. Jaffré, A. Couvillon, A. Saci, S.A. Goonasekera, J.R. McCarthy, C.W. Kessinger, J. Wang, Q. Ke, P.M. Kang, J.D. Molkentin, C. Carpenter, M.I. Kontaridis, RhoA signaling in cardiomyocytes protects against stress-induced heart failure but facilitates cardiac fibrosis, Sci. Signal. 7 (2014) ra100. doi:10.1126/scisignal.2005262.
[111] A. Rassa, F. Zahr, Hypertension and Aortic Stenosis: A Review, Curr. Hypertens. Rev. 14 (2018) 6–14. doi:10.2174/1573402114666180416161326.
[112] D.H. Spodick, Medical history of the pericardium: The hairy hearts of hoary heroes, Am. J. Cardiol. 26 (1970) 447–454. doi:10.1016/0002-9149(70)90701-0.
[113] F. Xiang, X. Guo, W. Chen, J. Wang, T. Zhou, F. Huang, C. Cao, X. Chen, Proteomics analysis of human pericardial fluid, Proteomics. 13 (2013) 2692–2695. doi:10.1002/pmic.201200317.
[114] S.M. Kuosmanen, J. Hartikainen, M. Hippeläinen, H. Kokki, A.-L. Levonen, P. Tavi, MicroRNA Profiling of Pericardial Fluid Samples from Patients with Heart Failure, PLoS One. 10 (2015) e0119646. doi:10.1371/journal.pone.0119646.

[115] W.-G. Forssmann, K. Nokihara, M. Gagelmann, D. Hock, S. Feller, P. Schulz-Knappe, F. Herbst, The Heart is the Center of a New Endocrine, Paracrine, and Neuroendocrine System, Arch. Histol. Cytol. 52 (1989) 293–315. doi:10.1679/aohc.52.Suppl_293.
[116] M. Fujita, M. Komeda, K. Hasegawa, Y. Kihara, R. Nohara, S. Sasayama, Pericardial fluid as a new material for clinical heart research, Int. J. Cardiol. 77 (2016) 113–118. doi:10.1016/S0167-5273(00)00462-9.
[117] A. Mebazaa, R.C. Wetzel, J.M. Dodd-o, E.M. Redmond, A.M. Shah, K. Maeda, G. Maistre, E.G. Lakatta, J.L. Robotham, Potential paracrine role of the pericardium in the regulation of cardiac function, Cardiovasc. Res. 40 (1998) 332–342. doi:10.1016/S0008-6363(98)00134-5.
[118] S. Corda, A. Mebazaa, M.-P. Gandolfini, C. Fitting, F. Marotte, J. Peynet, D. Charlemagne, J.-M. Cavaillon, D. Payen, L. Rappaport, J.-L. Samuel, Trophic Effect of Human Pericardial Fluid on Adult Cardiac Myocytes, Circ. Res. 81 (1997) 679–687. doi:10.1161/01.RES.81.5.679.
[119] E. Foglio, G. Puddighinu, P. Fasanaro, D. D'Arcangelo, G.A. Perrone, D. Mocini, C. Campanella, L. Coppola, M. Logozzi, T. Azzarito, F. Marzoli, S. Fais, L. Pieroni, V. Marzano, A. Germani, M.C. Capogrossi, M.A. Russo, F. Limana, Exosomal clusterin, identified in the pericardial fluid, improves myocardial performance following MI through epicardial activation, enhanced arteriogenesis and reduced apoptosis, Int. J. Cardiol. 197 (2015) 333–347. doi:10.1016/j.ijcard.2015.06.008.
[120] C. Beltrami, M. Besnier, S. Shantikumar, A.I.U. Shearn, C. Rajakaruna, A. Laftah, F. Sessa, G. Spinetti, E. Petretto, G.D. Angelini, C. Emanueli, Human Pericardial Fluid Contains Exosomes Enriched with Cardiovascular-Expressed MicroRNAs and Promotes Therapeutic Angiogenesis, Mol. Ther. 25 (2017) 679–693. doi:10.1016/j.ymthe.2016.12.022.
[121] P. Shannon, A. Markiel, O. Ozier, N.S. Baliga, J.T. Wang, D. Ramage, N. Amin, B. Schwikowski, T. Ideker, Cytoscape: A Software Environment for Integrated Models of Biomolecular Interaction Networks, Genome Res. . 13 (2003) 2498–2504. doi:10.1101/gr.1239303.
[122] K. Vogiatzidis, S.G. Zarogiannis, I. Aidonidis, E.I. Solenov, P.-A. Molyvdas, K.I. Gourgoulianis, C. Hatzoglou, Physiology of pericardial fluid production and drainage, Front. Physiol. 6 (2015) 1–6. doi:10.3389/fphys.2015.00062.
[123] B.D. Hoit, Pathophysiology of the Pericardium, Prog. Cardiovasc. Dis. 59 (2017) 341–348. doi:10.1016/j.pcad.2016.11.001.
[124] P. Hutchin, N. HV, R. Suberman, Electrolyte and acid-base composition of pericardial fluid in man, Arch. Surg. 102 (1971) 28–30. doi:10.1001/archsurg.1971.01350010030007.
[125] W. Geinitz, H. Hobitz, Proteins of the pericardial fluid in man, Clin. Chim. Acta. 3 (1958) 84–88. doi:10.1016/0009-8981(58)90061-5.
[126] S. Ben-Horin, A. Shinfeld, E. Kachel, A. Chetrit, A. Livneh, The composition of normal pericardial fluid and its implications for diagnosing pericardial effusions, Am. J. Med. 118 (2005) 636–640. doi:10.1016/j.amjmed.2005.01.066.
[127] A. Balfe, S. Barry, O. Blake, D. Cannon, M. Healy, M. Kilbane, The biochemistry of body fluids, ACBI Sci. Comm. Guidel. (2009) 15–16. http://www.acbi.ie/downloads/guidelines-of-body-fluids.pdf.
[128] M. Bhargava, O.M. Wazni, W.I. Saliba, Interventional Pericardiology, Curr. Cardiol. Rep. 18 (2016) 1–11. doi:10.1007/s11886-016-0698-9.
[129] A. Honda, Y. Ohashi, Y. Mori, Hyaluronic acid in rabbit pericardial fluid and its production by pericardium, FEBS Lett. 203 (1986) 273–278. doi:10.1016/0014-5793(86)80757-8.
[130] A. Honda, T. Iwai, Y. Mori, Insulin-like growth factor I (IGF-I) enhances hyaluronic acid synthesis in rabbit pericardium, Biochim. Biophys. Acta - Mol. Cell Res. 1014 (1989) 305–312. doi:10.1016/0167-4889(89)90227-9.
[131] F.W. Maurer, M.F. Warren, C.K. Drinker, The composition of mammalian pericardial and peritoneal fluids, Am. J. Physiol. Content. 129 (1940) 635–644. doi:10.1152/ajplegacy.1940.129.3.635.
[132] A.T. Gibson, M.B. Segal, A study of the composition of pericardial fluid, with special reference to the probable mechanism of fluid formation., J. Physiol. 277 (1978) 367–377. doi:10.1113/jphysiol.1978.sp012277.
[133] R.H. Stewart, D.A. Rohn, S.J. Allen, G.A. Laine, Basic determinants of epicardial transudation, Am. J. Physiol. - Hear. Circ. Physiol. 273 (1997) H1408–H1414.

doi:10.1152/ajpheart.1997.273.3.H1408.
[134] A.T. Gibson, M.B. Segal, A study of the routes by which protein passes from the pericardial cavity to the blood in rabbits., J. Physiol. 280 (1978) 423–433. doi:10.1113/jphysiol.1978.sp012392.
[135] J.H. Kuh, K.S. Kim, S.H. Kim, K.W. Cho, K.H. Seul, G.Y. Koh, Presence of immunoreactive atrial natriuretic peptides in pericardial fluid of human subjects with congenital heart diseases, Life Sci. 46 (1990) 1977–1983. doi:10.1016/0024-3205(90)90514-R.
[136] T. Tanaka, K. Hasegawa, M. Fujita, S.-I. Tamaki, A. Yamazato, Y. Kihara, R. Nohara, S. Sasayama, Marked Elevation of Brain Natriuretic Peptide Levels in Pericardial Fluid Is Closely Associated With Left Ventricular Dysfunction, J. Am. Coll. Cardiol. 31 (1998) 399–403. doi:10.1016/S0735-1097(97)00482-8.
[137] T. Nishikimi, H. Asakawa, H. Iida, Y. Matsushita, I. Shibasaki, K. Tadokoro, Y. Mori, H. Mori, Y. Mochizuki, Y. Okamura, S. Miyoshi, K. Kangawa, H. Matsuoka, Different secretion patterns of two molecular forms of cardiac adrenomedullin in pressure- and volume-overloaded human heart failure, J. Card. Fail. 10 (2004) 321–327. doi:10.1016/j.cardfail.2003.12.002.
[138] J.-J. Santiago, L.J. McNaughton, N. Koleini, X. Ma, B. Bestvater, B.E. Nickel, R.R. Fandrich, J.T. Wigle, D.H. Freed, R.C. Arora, E. Kardami, High Molecular Weight Fibroblast Growth Factor-2 in the Human Heart Is a Potential Target for Prevention of Cardiac Remodeling, PLoS One. 9 (2014) e97281. doi:10.1371/journal.pone.0097281.
[139] J.-Y. Liou, P.-L. Kuan, K.-G. Shyu, M.-J. Lu, H.-H. Chao, B.-W. Wang, Pericardial Fluid and Serum Levels of Vascular Endothelial Growth Factor and Endostatin in Patients With or Without Coronary Artery Disease, J. Formos. Med. Assoc. 105 (2006) 377–383. doi:10.1016/S0929-6646(09)60133-9.
[140] M. Fujita, M. Ikemoto, M. Kishishita, H. Otani, R. Nohara, T. Tanaka, S. Tamaki, A. Yamazato, S. Sasayama, Elevated Basic Fibroblast Growth Factor in Pericardial Fluid of Patients With Unstable Angina, Circulation. 94 (1996) 610–613. doi:10.1161/01.CIR.94.4.610.
[141] T. Miyazaki, H.P. Pride, D.P. Zipes, Prostaglandins in the pericardial fluid modulate neural regulation of cardiac electrophysiological properties., Circ. Res. 66 (1990) 163–175. doi:10.1161/01.RES.66.1.163.
[142] T. Ege, S. Canbaz, V. Yuksel, E. Duran, Effect of pericardial fluid pro-inflammatory cytokines on hemodynamic parameters, Cytokine. 23 (2003) 47–51. doi:10.1016/S1043-4666(03)00180-7.
[143] A.D. Ristić, S. Pankuweit, R. Maksimović, R. Moosdorf, B. Maisch, Pericardial cytokines in neoplastic, autoreactive, and viral pericarditis, Heart Fail. Rev. 18 (2013) 345–353. doi:10.1007/s10741-012-9334-y.
[144] I. Kiris, S. Kapan, H. Okutan, C. Narin, M. Ozaydin, M.C. Cure, R. Sutcu, Relationship between site of myocardial infarction, left ventricular function and cytokine levels in patients undergoing coronary artery surgery, Cardiovasc. J. Afr. 27 (2016) 299–306. doi:10.5830/CVJA-2016-027.
[145] R.W. Troughton, C.R. Asher, A.L. Klein, Pericarditis, Lancet. 363 (2004) 717–727. doi:10.1016/S0140-6736(04)15648-1.
[146] S.E. Leeds, H.N. Uhley, R.B. Meister, K.R. McCormack, Lymphatic pathways and rate of absorption of 131I-albumin from pericardium of dogs, Lymphology. 10 (1977) 166–172. doi:N/a.
[147] G. Szabo, Z. Magyar, Protein absorption from the pericardial cavity, Res. Exp. Med. 165 (1975) 41–47. doi:10.1007/BF01856447.
[148] B. Boulanger, Z. Yuan, M. Flessner, J. Hay, M. Johnston, Pericardial Fluid Absorption into Lymphatic Vessels in Sheep, Microvasc. Res. 57 (1999) 174–186. doi:10.1006/mvre.1998.2127.
[149] H.J. Stewart, N.F. Crane, J.E. Deitrick, Absorption from the pericardial cavity in man, Am. Heart J. 16 (1938) 198–202. doi:10.1016/S0002-8703(38)90695-7.
[150] C.K. Drinker, M.E. Field, Absorption from the pericardial cavity, J. Exp. Med. 53 (1931) 143–150. doi:10.1084/jem.53.1.143.
[151] K. Takada, Y. Otsuki, S. Magari, Lymphatics and pre-lymphatics of the rabbit pericardium and epicardium with special emphasis on particulate absorption and milky spot-like structures, Lymphology. 24 (1991) 116–124. https://journals.uair.arizona.edu/index.php/lymph/article/view/17671.
[152] K.W. Cho, S.H. Kim, Y.H. Hwang, K.H. Seul, Extracellular fluid translocation in perfused rabbit

atria: implication in control of atrial natriuretic peptide secretion., J. Physiol. 468 (1993) 591–607. doi:10.1113/jphysiol.1993.sp019790.
[153] N/A, Chapter 1: Definition and classification of CKD, Kidney Int. Suppl. 3 (2013) 19–62. doi:10.1038/kisup.2012.64.
[154] R.B. Mellins, O.R. Levine, A.P. Fishman, Effect of systemic and pulmonary venous hypertension on pleural and pericardial fluid accumulation, J. Appl. Physiol. 29 (1970) 564–569. doi:10.1152/jappl.1970.29.5.564.
[155] L.M. Kopcinovic, J. Culej, Pleural, peritoneal and pericardial effusions–a biochemical approach, Biochem. Medica. 24 (2014) 123–137. doi:10.11613/BM.2014.014.
[156] D.M. Dudzinski, G.S. Mak, J.W. Hung, Pericardial Diseases, Curr. Probl. Cardiol. 37 (2012) 75–118. doi:10.1016/j.cpcardiol.2011.10.002.
[157] K.K. Koh, E.J. Kim, C.H. Cho, M.J. Choi, S.K. Cho, S.S. Kim, M.H. Kim, C.J. Lee, S.H. Jin, J.M. Kim, Adenosine deaminase and carcinoembryonic antigen in pericardial effusion diagnosis, especially in suspected tuberculous pericarditis., Circulation. 89 (1994) 2728–2735. doi:10.1161/01.CIR.89.6.2728.
[158] R.M. Segura, C. Pascual, I. Ocaña, J.M. Martínez-Vázquez, E. Ribera, I. Ruiz, M.D. Pelegrí, Adenosine deaminase in body fluids: A useful diagnostic tool in tuberculosis, Clin. Biochem. 22 (1989) 141–148. doi:10.1016/S0009-9120(89)80013-X.
[159] C. Aggeli, C. Pitsavos, S. Brili, D. Hasapis, A. Frogoudaki, C. Stefanadis, P. Toutouzas, Relevance of Adenosine Deaminase and Lysozyme Measurements in the Diagnosis of Tuberculous Pericarditis, Cardiology. 94 (2000) 81–85. doi:10.1159/000047296.
[160] J.-H. Lee, C.W. Lee, S.-G. Lee, H.S. Yang, M.-K.. Hong, J.-J. Kim, S.-W. Park, H.-S. Chi, S.-J. Park, Comparison of polymerase chain reaction with adenosine deaminase activity in pericardial fluid for the diagnosis of tuberculous pericarditis, Am. J. Med. 113 (2002) 519–521. doi:10.1016/S0002-9343(02)01261-5.
[161] K.K. Koh, H.H. In, K.H. Lee, E.J. Kim, C.H. Cho, S.K. Cho, S.S. Kim, S.S. Cho, W.K. Baek, S.H. Jin, Y.C. Ju, J.J. Kim, C.S. Park, H.S. Nam, Y.H. Lee, New scoring system using tumor markers in diagnosing patients with moderate pericardial effusions, Int. J. Cardiol. 61 (1997) 5–13. doi:10.1016/S0167-5273(97)02943-4.
[162] G.I. Cubero, J. Rubin, M. Martín, J. Rondan, E. Simarro, Pericardial effusion: Clinical and analytical parameters clues, Int. J. Cardiol. 108 (2006) 404–405. doi:10.1016/j.ijcard.2005.03.037.
[163] B. Komsuoglu, Ö. Göldeli, K. Kulan, S.S. Komsuoglu, The diagnostic and prognostic value of adenosine deaminase in tuberculous pericarditis, Eur. Heart J. 16 (1995) 1126–1130. doi:10.1093/oxfordjournals.eurheartj.a061057.
[164] O.P. Mishra, S. Yusuf, Z. Ali, G. Nath, Brief report. Lysozyme levels for the diagnosis of tuberculous effusions in children, J. Trop. Pediatr. 46 (2000) 296–300. doi:10.1093/tropej/46.5.296.
[165] H. Reuter, L. Burgess, W. van Vuuren, A. Doubell, Diagnosing tuberculous pericarditis, QJM An Int. J. Med. 99 (2006) 827–839. doi:10.1093/qjmed/hcl123.
[166] K. Matthews, K.A. Wilkinson, B. Kalsdorf, T. Roberts, A. Diacon, G. Walzl, J. Wolske, M. Ntsekhe, F. Syed, J. Russell, B.M. Mayosi, R. Dawson, K. Dheda, R.J. Wilkinson, W.A. Hanekom, T.J. Scriba, Predominance of interleukin-22 over interleukin-17 at the site of disease in human tuberculosis, Tuberculosis. 91 (2011) 587–593. doi:10.1016/j.tube.2011.06.009.
[167] H. Emadi Koochak, S. Davoudi, A. Salehi Omran, R. Mohsenipour, K. Hajifathalian, B. Saeidi, A.A. Amirzargar, M. Sotoudeh, S. Seifirad, Diagnostic value of interferon-gamma assay in tuberculosis pericardial effusions: study on a cohort of Iranian patients., Acta Med. Iran. 51 (2013) 449–453. doi:N/A.
[168] S. Pandie, J.G. Peter, Z.S. Kerbelker, R. Meldau, G. Theron, U. Govender, M. Ntsekhe, K. Dheda, B.M. Mayosi, Diagnostic accuracy of quantitative PCR (Xpert MTB/RIF) for tuberculous pericarditis compared to adenosine deaminase and unstimulated interferon-γ in a high burden setting: a prospective study, BMC Med. 12 (2014) 2–11. doi:10.1186/1741-7015-12-101.
[169] M. Tatsuta, H. Yamamura, R. Yamamoto, M. Ichii, H. Iishi, S. Noguchi, Carcinoembryonic antigens in the pericardial fluid of patients with malignant pericarditis, Oncology. 41 (1984) 328–330. doi:10.1159/000225848.
[170] K. Karatolios, S. Pankuweit, B. Maisch, Diagnostic value of biochemical biomarkers in

malignant and non-malignant pericardial effusion, Heart Fail. Rev. 18 (2013) 337–344. doi:10.1007/s10741-012-9327-x.
[171] S. Lamparter, M. Schoppet, M. Christ, S. Pankuweit, B. Maisch, Matrix Metalloproteinases and Their Inhibitors in Malignant and Autoreactive Pericardial Effusion, Am. J. Cardiol. 95 (2005) 1065–1069. doi:10.1016/j.amjcard.2004.12.059.
[172] J. Liu, Y. Zeng, W. Ma, S. Chen, Y. Zheng, S. Ye, L. Lan, H.-J. Weig, Q. Liu, Preliminary Investigation of the Clinical Value of Vascular Endothelial Growth Factor and Hypoxia-Inducible Factor-1α in Pericardial Fluid in Diagnosing Malignant and Tuberculous Pericardial Effusion, Cardiology. 116 (2010) 37–41. doi:10.1159/000313465.
[173] K. Karatolios, S. Pankuweit, R.G. Moosdorf, B. Maisch, Vascular Endothelial Growth Factor in Malignant and Benign Pericardial Effusion, Clin. Cardiol. 35 (2012) 377–381. doi:10.1002/clc.21967.
[174] K. Karatolios, S. Pankuweit, C. Goettsch, L.C. Hofbauer, N. Timmesfeld, N. Al-Fakhri, B. Maisch, M. Schoppet, Osteoprotegerin (OPG) and TNF-related apoptosis-inducing ligand (TRAIL) levels in malignant and benign pericardial effusions, Clin. Biochem. 45 (2012) 237–242. doi:10.1016/j.clinbiochem.2011.12.003.
[175] S. Yavuz, M. Kasap, G. Akpinar, E. Ozbudak, D. Ural, T. Berki, Analysis of pericardial effusion from idiopathic pericarditis patients by two-dimensional gel electrophoresis, Biomed Res. Int. 2014 (2014) 942718. doi:10.1155/2014/942718.
[176] K. Karatolios, R. Moosdorf, B. Maisch, S. Pankuweit, Cytokines in pericardial effusion of patients with inflammatory pericardial disease, Mediators Inflamm. 2012 (2012) 382082. doi:10.1155/2012/382082.
[177] A.L. Fernández, J.B. García-Bengochea, J. Alvarez, J.R. González Juanatey, Biochemical markers of myocardial injury in the pericardial fluid of patients undergoing heart surgery, Interact. Cardiovasc. Thorac. Surg. 7 (2008) 373–377. doi:10.1510/icvts.2007.168302.
[178] S. Amjad, S.A. Sami, M.N. Basir, K. Hameed, M. Fujita, H.R. Ahmad, Pericardial fluid and serum biomarkers equally predict ventricular dysfunction, Asian Cardiovasc. Thorac. Ann. 21 (2013) 160–165. doi:10.1177/0218492312450292.
[179] K. Tambara, M. Fujita, N. Nagaya, S. Miyamoto, A. Iwakura, K. Doi, G. Sakaguchi, K. Nishimura, K. Kangawa, M. Komeda, Increased pericardial fluid concentrations of the mature form of adrenomedullin in patients with cardiac remodelling, Heart. 87 (2002) 242–246. doi:10.1136/heart.87.3.242.
[180] T. Nishikimi, I. Shibasaki, H. Iida, H. Asakawa, Y. Matsushita, H. Mori, Y. Mochizuki, Y. Okamura, S. Horinaka, K. Kangawa, K. Shimada, H. Matsuoka, Molecular forms of adrenomedullin in pericardial fluid and plasma in patients with ischaemic heart disease, Clin. Sci. 102 (2002) 669–677. doi:10.1042/cs1020669.
[181] N. Abe, T. Matsunaga, K. Kameda, H. Tomita, T. Fujiwara, H. Ishizaka, H. Hanada, K. Fukui, I. Fukuda, T. Osanai, K. Okumura, Increased Level of Pericardial Insulin-Like Growth Factor-1 in Patients With Left Ventricular Dysfunction and Advanced Heart Failure, J. Am. Coll. Cardiol. 48 (2006) 1387–1395. doi:10.1016/j.jacc.2006.06.048.
[182] S. Miyamoto, N. Nagaya, M. Ikemoto, K. Tambara, Y. Kihara, Y. Onozawa, K. Hasegawa, A. Yamazato, M. Fujita, Elevation of matrix metalloproteinase-2 level in pericardial fluid is closely associated with left ventricular remodeling, Am. J. Cardiol. 89 (2002) 102–105. doi:10.1016/S0002-9149(01)02179-8.
[183] Z. Nemeth, A. Cziraki, S. Szabados, B. Biri, S. Keki, A. Koller, Elevated Levels of Asymmetric Dimethylarginine (ADMA) in the Pericardial Fluid of Cardiac Patients Correlate with Cardiac Hypertrophy, PLoS One. 10 (2015) e0135498. doi:10.1371/journal.pone.0135498.
[184] P. Turbucz, P. Kiss, F. Horkay, I. Szokodi, L. Selmeci, A. Juhász-Nagy, I. Karádi, M. Tóth, High pericardial fluid levels of endothelin are not caused by altered neutral endopeptidase activity in cardiac patients, J. Cardiovasc. Pharmacol. 31 (1998) S287–S289. https://insights.ovid.com/pubmed?pmid=9595461.
[185] B. Sax, B. Merkely, K. Túri, A. Nagy, A. Ahres, I. Hartyánszky, T. Hüttl, Z. Szabolcs, K. Cseh, V. Kékesi, Characterization of pericardial and plasma ghrelin levels in patients with ischemic and non-ischemic heart disease, Regul. Pept. 186 (2013) 131–136. doi:10.1016/j.regpep.2013.08.003.
[186] K. Tambara, M. Fujita, S. Miyamoto, K. Doi, K. Nishimura, M. Komeda, Pericardial fluid level of heart-type cytoplasmic fatty acid-binding protein (H-FABP) is an indicator of severe myocardial ischemia, Int. J. Cardiol. 93 (2017) 281–284. doi:10.1016/S0167-5273(03)00219-

5.
[187] O. Guclu, O. Karahan, M. Karabacak, V. Yuksel, S. Huseyin, B. Mavitas, Evaluation of Pericardial Fluid C-Type Natriuretic Peptide Levels in Patients Undergoing Coronary Bypass Surgery, Thorac. Cardiovasc. Surg. 65 (2017) 311–314. doi:10.1055/s-0036-1579626.
[188] T. Yoneda, M. Fujita, Y. Kihara, K. Hasegawa, T. Sawamura, T. Tanaka, M. Inanami, R. Nohara, S. Sasayama, Pericardial Fluid From Patients With Ischemic Heart Disease Accelerates the Growth of Human Vascular Smooth Muscle Cells, Jpn. Circ. J. 64 (2000) 495–498. doi:10.1253/jcj.64.495.
[189] L. Selmeci, M. Antal, F. Horkay, B. Merkely, I. Szokodi, L. Bíró, M. Székely, J. Jobbágy, J. Szépvölgyi, M. Tóth, Enhanced accumulation of pericardial fluid ferritin in patients with coronary artery disease, Coron. Artery Dis. 11 (2000) 53–56. doi:10.1097/00019501-200002000-00010.
[190] M. Ikemoto, K. Hasegawa, Y. Kihara, A. Iwakura, M. Komeda, A. Yamazato, M. Fujita, Development of enzyme-linked immunosorbent assay for acidic fibroblast growth factor and its clinical application, Clin. Chim. Acta. 283 (1999) 171–182. doi:10.1016/S0009-8981(99)00045-5.
[191] L. Fazekas, F. Horkay, V. Kékesi, É. Huszár, E. Barát, R. Fazekas, T. Szabó, A. Juhász-Nagy, A. Naszlady, Enhanced accumulation of pericardial fluid adenosine and inosine in patients with coronary artery disease, Life Sci. 65 (1999) 1005–1012. doi:10.1016/S0024-3205(99)00331-8.
[192] E. Page, J. Upshaw-Earley, G. Goings, Permeability of rat atrial endocardium, epicardium, and myocardium to large molecules. Stretch-dependent effects., Circ. Res. 71 (1992) 159–173. doi:10.1161/01.RES.71.1.159.
[193] J. Amano, A. Suzuki, M. Sunamori, M. Shichiri, F. Marumo, Atrial Natriuretic Peptide in the Pericardial Fluid of Patients with Heart Disease, Clin. Sci. 85 (1993) 165–168. doi:10.1042/cs0850165.
[194] J. Oyama, H. Shimokawa, S. Morita, H. Yasui, A. Takeshita, Elevated interleukin-1β in pericardial fluid of patients with ischemic heart disease, Coron. Artery Dis. 12 (2001) 567–571. doi:10.1097/00019501-200111000-00007.
[195] T. Matsunaga, W.M. Chilian, K. March, Angiostatin is negatively associated with coronary collateral growth in patients with coronary artery disease, Am. J. Physiol. - Hear. Circ. Physiol. 288 (2005) H2042–H2046. doi:10.1152/ajpheart.00669.2004.
[196] V.R. Panchal, J. Rehman, A.T. Nguyen, J.W. Brown, M.W. Turrentine, Y. Mahomed, K.L. March, Reduced pericardial levels of endostatin correlate with collateral development in patients with ischemic heart disease, J. Am. Coll. Cardiol. 43 (2004) 1383–1387. doi:10.1016/j.jacc.2003.10.063.
[197] J.-L. Fellahi, P. Léger, E. Philippe, M. Arthaud, B. Riou, I. Gandjbakhch, P. Coriat, Pericardial cardiac troponin I release after coronary artery bypass grafting, Anesth. Analg. 89 (1999) 829–834. doi:10.1213/00000539-199910000-00004.
[198] H.B. Cihan, O. Gulcan, A. Hazar, R. Turkoz, E. Olmez, Determination of the pericardial to serum myoglobin ratio for the early diagnosis of perioperative myocardial infarction after coronary artery bypass grafting, Pharmacol. Res. 50 (2004) 247–251. doi:10.1016/j.phrs.2004.03.009.
[199] T. Ege, M.H. Us, M. Cikirikcioglu, C. Arar, E. Duran, Analysis of C-reactive protein and biochemical parameters in pericardial fluid, Yonsei Med. J. 47 (2006) 372–376. doi:10.3349/ymj.2006.47.3.372.
[200] K. Kameda, T. Matsunaga, N. Abe, T. Fujiwara, H. Hanada, K. Fukui, I. Fukuda, T. Osanai, K. Okumura, Increased Pericardial Fluid Level of Matrix Metalloproteinase-9 Activity in Patients With Acute Myocardial Infarction, Circ. J. 70 (2006) 673–678. doi:10.1253/circj.70.673.
[201] A. Iwakura, M. Fujita, M. Ikemoto, K. Hasegawa, R. Nohara, S. Sasayama, S. Miyamoto, A. Yamazato, K. Tambara, M. Komeda, Myocardial ischemia enhances the expression of acidic fibroblast growth factor in human pericardial fluid, Heart Vessels. 15 (2000) 112–116. doi:10.1007/PL00007264.
[202] A.G. Driver, C.A. Kukoly, P.A. Spence, W.R. Chitwood, S.J. Mustafa, Pericardial Fluid Adenosine in Ischemic and Valvular Heart Disease, Chest. 107 (1995) 346–351. doi:10.1378/chest.107.2.346.
[203] F. Trindade, R. Vitorino, A. Leite-Moreira, I. Falcão-Pires, Pericardial fluid: an underrated

molecular library of heart conditions and a potential vehicle for cardiac therapy, Basic Res. Cardiol. 114 (2019) 10. doi:10.1007/s00395-019-0716-3.
[204] R.D. Nolan, G.J. Dusting, J. Jakubowski, T.J. Martin, The pericardium as a source of prostacyclin in the dog, ox and rat, Prostaglandins. 24 (1982) 887–902. doi:10.1016/0090-6980(82)90068-5.
[205] G.J. Dusting, R.D. Nolan, Stimulation of prostacyclin release from the epicardium of anaesthetized dogs., Br. J. Pharmacol. 74 (1981) 553–562. doi:10.1111/j.1476-5381.1981.tb10464.x.
[206] O.L. Woodman, G.J. Dusting, R.D. Nolan, Pericardial release of prostacyclin induced by bradykinin and angiotensin II: effects on coronary blood flow in the dog., J. Cardiovasc. Pharmacol. 5 (1983) 954–960. doi:10.1097/00005344-198311000-00007.
[207] R.M. Knabb, S.W. Ely, A.N. Bacchus, R. Rubio, R.M. Berne, Consistent parallel relationships among myocardial oxygen consumption, coronary blood flow, and pericardial infusate adenosine concentration with various interventions and beta-blockade in the dog., Circ. Res. 53 (1983) 33–41. doi:10.1161/01.RES.53.1.33.
[208] Z. Nemeth, A. Cziraki, S. Szabados, I. Horvath, A. Koller, Pericardial fluid of cardiac patients elicits arterial constriction: role of endothelin-1, Can. J. Physiol. Pharmacol. 93 (2015) 779–785. doi:10.1139/cjpp-2015-0030.
[209] V. Kékesi, E. Zima, E. Barát, É. Huszár, A. Nagy, L. Losonczi, B. Merkely, F. Horkay, A. Juhász-Nagy, Pericardial concentrations of adenosine, inosine and hypoxanthine in an experimental canine model of spastic ischaemia, Clin. Sci. 103 (2002) 198S-201S. doi:10.1042/CS103S198S.
[210] Z. Endre, V. Kékesi, N. Andrea, L. Losonczi, T. Ildikó, S. Pál, E. Barát, É. Huszár, B. Merkely, F. Horkay, Endothelin-1-induced elevations in purine metabolite concentrations—autoregulatory protection in the canine pericardium?, Clin. Sci. 103 (2002) 202S-205S. doi:10.1042/CS103S202S.
[211] A. Nagy, I. Toma, M. Rusvai, E. Barát, É. Huszár, A. Juhász-Nagy, V. Kékesi, Intrapericardial adenine nucleosides induce elevation of endothelin-1 concentration in the pericardial space of the dog heart., J. Cardiovasc. Pharmacol. 44 (2004) S227–S230. doi:10.1097/01.fjc.0000166257.89357.7d.
[212] T. Miyazaki, H.P. Pride, D.P. Zipes, Modulation of cardiac autonomic neurotransmission by epicardial superfusion. Effects of hexamethonium and tetrodotoxin., Circ. Res. 65 (1989) 1212–1219. doi:10.1161/01.RES.65.5.1212.
[213] I. Toma, A. Nagy, C. Jánosi, M. Rusvai, A. Juhász-Nagy, V. Kékesi, Effects of intrapericardially administered endothelin-1 on pericardial natriuretic peptide concentrations of the in situ dog heart., J. Cardiovasc. Pharmacol. 44 (2004) S231–S233. doi:10.1097/01.fjc.0000166254.04605.ad.
[214] L. Geller, B. Merkely, I. Szokodi, T. Szabo, T. Vecsey, A. Juhász-Nagy, M. Toth, F. Horkay, Electrophysiological effects of intrapericardial infusion of endothelin-1, Pacing Clin. Electrophysiol. 21 (1998) 151–156. doi:10.1111/j.1540-8159.1998.tb01079.x.
[215] F. Horkay, I. Szokodi, B. Merkely, F. Solti, L. Gellér, P. Kiss, L. Selmeci, I. Horváth, V. Kékesi, A. Juhász-Nagy, Potential pathophysiologic role of endothelin-1 in canine pericardial fluid, J. Cardiovasc. Pharmacol. 31 (1998) S401–S402. doi:10.1097/00005344-199800001-00115.
[216] I. Szokodi, F. Horkay, B. Merkely, F. Solti, L. Gellér, P. Kiss, L. Selmeci, V. Kékesi, O. Vuolteenaho, H. Ruskoaho, A. Juhász-Nagy, M. Tóth, Intrapericardial infusion of endothelin-1 induces ventricular arrhythmias in dogs, Cardiovasc. Res. 38 (1998) 356–364. doi:10.1016/S0008-6363(98)00018-2.
[217] J. Nativi-Nicolau, C.H. Selzman, J.C. Fang, J. Stehlik, Pharmacologic therapies for acute cardiogenic shock, Curr. Opin. Cardiol. 29 (2014) 250–257. doi:10.1097/HCO.0000000000000057.
[218] V. Kékesi, I. Toma, A. Nagy, M. Rusvai, E. Barát, É. Huszár, A. Juhász-Nagy, Cardiovascular responses to catecholamines and interactions with endothelin-1 and adenine nucleosides in the pericardium of the dog heart., J. Cardiovasc. Pharmacol. 44 (2004) S234–S238. doi:10.1097/01.fjc.0000166256.12229.d6.
[219] I. Toma, B. Sax, A. Nagy, L. Entz Jr, M. Rusvai, A. Juhasz-Nagy, V. Kekesi, Intrapericardial angiotensin II stimulates endothelin-1 and atrial natriuretic peptide formation of the in situ dog heart, Exp. Biol. Med. 231 (2006) 847–851. doi:10.3181/00379727-231-2310847.
[220] F. Limana, C. Bertolami, A. Mangoni, A. Di Carlo, D. Avitabile, D. Mocini, P. Iannelli, R. De

Mori, C. Marchetti, O. Pozzoli, C. Gentili, A. Zacheo, A. Germani, M.C. Capogrossi, Myocardial infarction induces embryonic reprogramming of epicardial c-kit+ cells: Role of the pericardial fluid, J. Mol. Cell. Cardiol. 48 (2010) 609–618. doi:10.1016/j.yjmcc.2009.11.008.

[221] A. Iwakura, M. Fujita, K. Hasegawa, T. Sawamura, R. Nohara, S. Sasayama, M. Komeda, Pericardial fluid from patients with unstable angina induces vascular endothelial cell apoptosis, J. Am. Coll. Cardiol. 35 (2000) 1785–1790. doi:10.1016/S0735-1097(00)00651-3.

[222] A. Iwakura, M. Fujita, K. Hasegawa, S. Toyokuni, T. Sawamura, R. Nohara, S. Sasayama, M. Komeda, Pericardial Fluid from Patients with Ischemic Heart Disease Induces Myocardial Cell Apoptotis via an Oxidant Stress-sensitive p38 Mitogen-activated Protein Kinase Pathway, J. Mol. Cell. Cardiol. 33 (2001) 419–430. doi:10.1006/jmcc.2000.1314.

[223] Y. Adler, P. Charron, M. Imazio, L. Badano, G. Barón-Esquivias, J. Bogaert, A. Brucato, P. Gueret, K. Klingel, C. Lionis, B. Maisch, B. Mayosi, A. Pavie, A.D. Ristić, M. Sabaté Tenas, P. Seferovic, K. Swedberg, W. Tomkowski, 2015 ESC Guidelines for the diagnosis and management of pericardial diseases: The Task Force for the Diagnosis and Management of Pericardial Diseases of the European Society of Cardiology (ESC)Endorsed by: The European Association for Cardio-Thoracic Surg, Eur. Heart J. 36 (2015) 2921–2964. doi:10.1093/eurheartj/ehv318.

Chapter II

Characterization of the myocardial proteome and phosphoproteome in aortic stenosis patients with complete or incomplete reverse remodeling

Contents

Abstract

The number of aortic valve replacement interventions grows every year [1], although the number of patients with incomplete myocardial reverse remodeling continue challengingly high. Many risk factors have been proposed (***Chapter I***), but the exact molecular mechanisms underscoring the phenotypical divergence after left ventricle unloading remain obscure. The access to myocardial biopsies during valve replacement provides the perfect chance to dig into the dysregulated biological processes and molecular pathways that are on the root of an incomplete response. Proteomics approaches provide the means to comprehensively characterize the proteins regulating such pathways, not to mention that label-free quantification may deliver surrogate markers with prognostic impact. Based on these premises, in this chapter, the proteome and phosphoproteome of the human myocardium in aortic stenosis patients with complete and incomplete reverse remodeling is characterized. Gene ontology and pathway enrichment analyses to the myocardial proteome suggest that changes in transcription, metabolism (especially in protein metabolism), activation of the acute-phase response and of innate immune response (particularly of the complement system), the latter two confirmed by multivariate analysis, may explain the opposing phenotypes. Phosphoproteome analysis further elicited the activation of the interferon γ and of the proapoptotic tumor necrosis factor-related apoptosis-inducing ligand pathways as critical events in the progression towards a complete or an incomplete response. Dysregulated phosphopeptides were used further for kinase prediction. Higher activity of casein kinase 2, transcription initiation factor TFIID and of the family of IκB kinases as well as lower activity of glycogen synthase kinase 3 (α and β) as well as of dual-specificity tyrosine-regulated kinase 1A and 2 are anticipated in patients with poor left ventricle mass regression. These kinases arise as promising surrogate targets for therapy. In addition, the complement C3 β chain and the anti-hypertrophic kinase dual-specificity tyrosine-regulated kinase 1A showed potential prognostic value.

1. Background

In spite of the instant hemodynamic relief provided by AVR, many AS patients do not achieve the desirable complete myocardial structural and functional normalization [2–4]. Patients often show postoperative LV hypertrophy (incomplete RR) being at higher risk for adverse cardiac and cerebrocardiovascular events, requiring prolonged hospital stays and displaying reduced survival in the long-term [5,6]. Age, sex, patient-prosthesis mismatch, fibrosis and several co-morbidities, such as hypertension, obesity, CAD or diabetes mellitus have all been proposed as risk factors for incomplete RR [4,7–12]. However, reported associations are frequently contradicted [3,13–18]. For instance, Biederman *et al*. [2] showed that >85% of the patients presented LV hypertrophy 4 years after AVR and could not explain this finding based on age, sex, existing CAD, valve type or pre-AVR transvalvular gradient. Therefore, a better comprehension of the mechanisms triggering an incomplete recovery phenotype is urgently required. Moreover, apart from the medical management of the deemed risk factors, today there is no adjuvant pharmacological therapy available that may help improving the outcome of patients enrolled in AVR.

By looking at the complete set of cardiac proteins and, specifically, phosphoproteins, regulating most, if not all, signaling circuitries in cardiomyocytes, fibroblasts and other heart cell types; proteomics and, particularly, phosphoproteomics approaches have shown their merits in cardiovascular research, specifically in mechanistic research, biomarker discovery and identification of potential therapeutic targets (reviewed in [19]). In what regards AS-induced myocardial remodeling, (phospho)proteomics studies with animal models of aortic banding have provided some clues regarding the biological and molecular phenomena underlying myocardial remodeling. As discussed in ***Chapter I***, proteomics studies support the activation of a pro-hypertrophic program [20], bioenergetic adaptations, such as reduced lipolysis and increased flux through the glycolytic pathway [21,22], mitochondrial dysfunction [22–24] as well as the fibrotic response to enhanced mechanical stress [20,23,24]. Phosphoproteomics, in particular, has identified specific protein modifications with functional consequences. For example, a reduction in the phosphorylation of Thr 282 and Ser 283 in α-tropomyosin in mice has been associated with reduced sarcomeric tension and ATPase activity [25]. In the same study, it was demonstrated that the inhibition of Ser 622 phosphorylation in the mitochondrial fission dynamin-related protein 1 halted the

progression of hypertrophy two weeks after banding [25], attesting that new routes for therapy in incomplete RR may be identified through myocardial (phospho)proteomics.

The input of proteomics to the understanding of myocardial RR after AVR is, to this day, lesser than to myocardial remodeling. In the human setting, in particular, proteomics has been limited to the study of RR in patients with LVADs. Besides, the enthusiasm in animal models studies is minimized considering that these rather focus on systemic hypertension as the trigger of pressure overload [26–28], and hypertension, despite recapitulating the hemodynamic overload on the LV, is associated with remarkable neurohumoral activation, which may directly interfere in the process of LV remodeling [29]. In turn, those that resort to aortic banding models, which more closely resemble the consequences of AS on the myocardium, have not yet reported the effects of aortic debanding, akin to the mechanical benefits of AVR. Instead, these studies focus on either the effects of anti-hypertensive [30] or antioxidant therapies [31] on the pressure-overloaded heart. Still, animal studies confirm that anti-hypertensive therapy may target some phenomena associated with myocardial remodeling. For instance, proteomics shows that anti-hypertensive drugs could attenuate hypertrophy [26,30] and rescue fatty acid oxidation [27]. The same drugs could also normalize the pressure overload-induced changes in the expression of some mitochondrial respiratory chain complexes [26] and in some antioxidant and proteostasis defenses [26]. The most promising therapeutic avenue so far seems to be with the use of mitochondria-targeted antioxidant peptides, as these have shown the ability to normalize or, at least, attenuate the dysregulation of 52 out of 53 biological pathways on aortic banding-induced myocardial remodeling [31]. Although, in this study the therapy was initiated right after surgery, which may preclude clinical translation since the extent of RR (e.g. LV mass regression) is determined some months after AVR. In the human case, RR-induced molecular changes have only been studied in patients with LVADs, as these devices are used many times as a bridge to heart transplantation, and, thus, myocardial material may be analyzed before and after mechanical unloading. Traditionally, the study of the myocardial changes in the course of RR has been performed with genomic approaches (e.g. [32]). Albeit, the observation that not always the genetic expression is corroborated by validation at the protein level has motivated some researchers to study molecular changes in the course of RR through proteomics. For instance, Weger *et al*. [33] demonstrated specific changes in cytoskeleton and in mitochondria subproteomes upon LVAD implantation in ischemic heart disease and in dilated cardiomyopathy patients with heart failure. In turn, Shahinian and colleagues reported a decrease of ECM proteins, such as periostin, fibulin and versican, in addition to a reduction in complement system components

and in cardiac hormones with myocardial unloading of dilated cardiomyopathy patients [34]. Nevertheless, LVADs are used to treat patients with already failing hearts, usually displaying patterns of eccentric remodeling (e.g. chamber dilatation and myocardial wall thinning). AS patients, on the contrary, commonly display a pattern of concentric remodeling (myocardial wall thickening without dilatation) [35]. Therefore, the insights of those proteomics studies may not be reliably translated to the case of AS.

Acknowledging the impossibility to analyze myocardial biopsies in AS patients after AVR, we are still able to study the relationship between the proteome profile of the myocardial obtained perioperatively and the outcome of patients (LV mass regression), based on standard and affordable echocardiographic postoperative evaluations. By performing an *in-depth* characterization of the myocardial (phospho)proteome, one may also identify new surrogate markers of an incomplete response that may help physicians to anticipate preventive medical and pharmacological care. Furthermore, by resorting to bioinformatics to predict which kinases are dysregulated in incomplete RR, one may as well elicit new therapeutic targets for further research. Hence, this work aimed to characterize, for the first time, the myocardial proteome and phosphoproteome in AS patients undergoing AVR i) to decipher the dysregulated biological processes and molecular pathways leading to incomplete RR; ii) to uncover candidate prognostic biomarkers and iii) to identify new therapeutic targets to improve the outcome of these patients.

2. Material and Methods

2.1. Study design, patients selection and clinical characterization

AS patients were selected based on retrospective clinical data, and the respective myocardial samples were gathered from the local biobank. The local ethics committee approved the study protocol and written informed consent was obtained from all patients.

Only patients undergoing AVR with clinical predominance of AS, without severe aortic insufficiency or severe forms of other extra-aortic valve diseases and with no more than one stenotic coronary vessel were selected. Clinical evaluation of AS severity and myocardial

structure and function was based on transthoracic echocardiography. Peak aortic valve velocity (Peak Ao), mean aortic transvalvular pressure gradient and indexed aortic valve area (AVAi) were derived from Doppler echocardiography. Mean pressure gradient was obtained with the modified Bernoulli equation and AVAi with the standard continuity equation. In turn, LV end-diastolic dimension (LVEDD), LV posterior wall thickness (PWT) and interventricular septal thickness (IVST) were derived from 2D-echocardiograms during diastole. Relative wall thickness (RWT) was calculated as 2×PWT/LVEDD. Correct orientation of imaging planes, cardiac chambers dimension and function measurements were performed according to the European Association of Echocardiography (EAE)/American Society of Echocardiography (ASE) recommendations [36].

LV mass was estimated according to the joint recommendations of the ASE and EAE using Devereux's formula for ASE measurements in diastole: LV mass = 0.8 x (1.04 x ([LV internal dimension + posterior wall thickness + interventricular septal thickness]^3 – [LV internal dimension]^3) + 0.6 g. LV mass (LVM) index (LVMi) was calculated according to the recent recommendations for cardiac chamber quantification [36]. LVMi greater than 115 g/m^2 in men and greater than 95 g/m^2 in women were considered indicative of LV hypertrophy.

Ten patients were initially selected for shotgun proteomics, however two could not be enrolled since the myocardial biopsies did not provide enough protein for phosphopeptide enrichment (protein mass <500 µg). The demographics and echocardiographic parameters of the final eight patients is summarized in **Table 1**. Eight extra patients were selected for validation assays. One patient was excluded after observation of an ensanguined myocardial biopsy. The remaining seven were adjoined to seven patients initially selected, from which protein was still available for immunoblot experiments. The characteristics of the final 14 subjects included for validation purposes is also found in **Table 1**.

All patients enrolled in this study were free of dilated or hypertrophic cardiomyopathies. Upon preoperative echocardiographic assessment, all subjects showed LVEF >50% (n = 12) or had clinical indication of normal/good systolic function (n = 3). Hence, the evaluation of RR was based on the echocardiographic assessment of LV hypertrophy. LVM regression (%) was defined as the difference between pre- and postoperative LVMi. Patients with LVM regression ≥15% were included in the complete RR (cRR) group, while those with LVM regression ≤5% were integrated into the incomplete RR (iRR) group. A 10% gap was deliberately set in a way to exclude intermediate phenotypes and to separate proteome and phosphoproteome changes between cRR and iRR.

Table 1. Clinical data of the study population.

Parameters	**Discovery (phospho)proteomics population**			**Western Blot validation population**		
Degree of Reverse Remodeling	Complete (ΔLVM≥15%)	Incomplete (ΔLVM≤5%)	*p*	Complete (ΔLVM≥15%)	Incomplete (ΔLVM≤5%)	*p*
Demographics						
N	4	4	n.s.	7	7	n.s.
Age	75.5±4.3	65.5±4.1	n.s.	69.7±10.6	72.9±9.5	n.s.
Gender (male:female)	2:2	0:4	n.s.	4:3	1:6	n.s.
BMI (kg/m^2)	25.3±1.2	37.0±3.2	*	30.2±9.7	32.7±7.9	n.s.
Obesity (n)	0	4	#	2	4	n.s.
Hypertension (n)	4	3	n.s.	6	6	n.s.
Diabetes mellitus (n)	3	1	n.s.	5	4	n.s.
CAD (≤1 vessel) (n)	0	1	n.s.	1	1	n.s.
Smoking history (n)	1	0	n.s.	2	1	n.s.
COPD (n)	1	1	n.s.	1	1	n.s.
Mild-to-moderate aortic insufficiency (n)	4	3	n.s.	6	5	n.s.
Mild-to-moderate mitral stenosis (n)	0	0	n.s.	0	0	n.s.
Mild-to-moderate mitral insufficiency (n)	4	4	n.s.	6	5	n.s.
Mild-to-moderate tricuspid insufficiency (n)	3	3	n.s.	6	4	n.s.
Preoperative parameters						
AVAi, cm^2/m^2	0.43±0.09	0.45±0.09	n.s.	0.41±0.09	0.43±0.08	n.s.
Peak Ao, m/s	4.8±0.7	4.4±0.5	n.s.	4.7±0.6	4.5±0.5	n.s.
Max ATPG, mmHg	93.5±28.1	79.0±18.7	n.s.	88.1±23.0	81.6±19.3	n.s.
Mean ATPG, mmHg	56.8±16.5	49.8±9.5	n.s.	54.0±13.3	52.6±13.9	n.s.
LVEDD, cm	5.2±0.2	5.1±0.4	n.s.	5.1±0.4	4.6±0.6	n.s.
IVST, cm	1.4±0.1	1.3±0.2	n.s.	1.4±0.2	1.4±0.3	n.s.
PWT, cm	1.3±0.1	1.2±0.1	n.s.	1.3±0.1	1.1±0.2	n.s.
RWT	0.48±0.04	0.48±0.08	n.s.	0.51±0.07	0.50±0.14	n.s.
LVMi, g/m^2	174.5±29.9	144.8±21.4	n.s.	162.5±36.9	130.9±23.2	n.s.
Postoperative parameters						
LVEDD, cm	5.0±0.9	5.2±0.3	n.s.	4.9±0.7	4.9±0.5	n.s.
IVST, cm	1.3±0.2	1.4±0.2	n.s.	1.3±0.2	1.5±0.3	n.s.
PWT, cm	0.9±0.1	1.2±0.1	**	1.0±0.1	1.1±0.2	a
RWT	0.38±0.09	0.45±0.06	n.s.	0.41±0.09	0.48±0.10	n.s.
LVMi, g/m^2	120.2±23.5	157.1±21.5	a	114.8±23.3	149.5±35.5	c
ΔLVM, %	30.8±11.6	-8.7±5.1	b	28.5±9.4	-13.8±16.5	b

* p <0.05 ** p <0.01 (unpaired two-tailed t-test); # p <0.05 (Fisher's exact two-sided test); a) p = 0.06; b) Independent variable; c) p = 0.05.

Abbreviations: ATPG: aortic transvalvular pressure gradient; AVAi: aortic valve area, indexed to body surface area; BMI: body mass index; CAD: coronary artery disease; COPD: chronic obstructive pulmonary disease; IVST: interventricular septal thickness; LVEDD: left ventricle end-diastolic dimension; LVMi: left ventricle mass, indexed to body surface area; n.s.: non-significant; Peak Ao: peak aortic valve velocity; PWT: posterior wall thickness; RWT: relative wall thickness; ΔLVM: left ventricle mass regression.

2.2. Sample collection and processing

During AVR, LV myocardial biopsies were collected and immediately frozen at -80 °C. LV biopsy material consisted of endomyocardial tissue resected from the LV outflow tract (Morrow procedure) because of concomitant LV outflow tract hypertrophy.

Tissue homogenization and protein extraction was carried out with a Precellys bead-beating system using 1.4 mm zirconium oxide beads. A lysis buffer with 7.1 M urea, 45 mM HEPES pH 8, supplemented with 1 mM EDTA, protease inhibitors (1.2 mM AEBSF, 0.46 µM aprotinin, 14 µM bestatin, 12.3 µM E-64, 112 µM leupeptin and 1.16 µM pepstatin, mammalian cocktail VWR®) and phosphatase inhibitors (PhosStop, Roche®) was added to the tissue (10 µL/mg). Tissue grinding and protein extraction was carried out in 2 cycles of 30 seconds at 6500 rpm, with a 5-min interval on ice. Samples were then centrifuged at 12,000 rpm, 4 ºC for 15 min to remove debris, and the supernatants were collected and immediately stored at -80 °C until further processing. Protein concentration was determined by the BCA method, using bovine serum albumin (BSA) as a standard.

2.3. Characterization of the myocardial proteome and phosphoproteome

2.3.1. In-solution digestion, peptide cleanup and phosphopeptide enrichment

500 µg of each sample was reduced with 1500 nmols of dithiothreitol (DTT, 1 h, 37 °C) and alkylated in the dark with 3000 nmol iodoacetamide (IAA, 30 min, 25 ºC). The resulting protein extract was first diluted 1:3 with 200 mM NH_4HCO_3 and digested with 50 µg LysC (Wako, cat #129-02541) overnight at 37 ºC and then diluted 1:2 and digested further with 50 µg of trypsin (Promega, cat #V5113) for eight hours at 37 ºC. The peptide mix was acidified with formic acid (FA) and desalted with a MacroSpin C18 column (The Nest Group, Inc). 5 µg was preserved for the proteome analysis and 495 µg of each sample was enriched in phosphopeptides with the Pierce TiO_2 Phosphopeptide Enrichment kit (Thermo Scientific, cat #88301).

2.3.2. LC-MS/MS analysis

The peptide mixes, proteome and phosphoproteome, were analyzed in different runs, using an Orbitrap Fusion Lumos mass spectrometer (Thermo Scientific, San Jose, CA, USA) coupled to an EasyLC (Thermo Scientific (Proxeon), Odense, Denmark). Peptides were loaded directly onto the analytical column and were separated by reversed-phase chromatography using a 50-cm column with an inner diameter of 75 µm, packed with 2 µm C18 particles spectrometer (Thermo Scientific, San Jose, CA, USA). Chromatographic gradients started at 95% buffer A (0.1% FA in water) and 5% buffer B (0.1% FA in acetonitrile) with a flow rate of 300 nL/min and gradually increased to 22% buffer B in 79 min and then to 35% buffer B in 11 min. After each analysis, the column was washed for 10 min with 5% buffer A and 95% buffer B.

The mass spectrometer was operated in DDA mode and full MS scans with 1 micro scans at resolution of 120.000 were used over a mass range of *m/z* 350-1500 with detection in the Orbitrap. Auto gain control (AGC) was set to 2e5 and dynamic exclusion to 60 seconds. In each cycle of DDA analysis, following each survey scan Top Speed ions with charges 2 to 7 above a threshold ion count of 1e4 were selected for fragmentation at a normalized collision energy of 28%. Fragment ion spectra produced via high-energy collision dissociation were acquired in the Ion Trap, AGC was set to 3e4, isolation window of 1.6 *m/z* and maximum injection time of 40 ms was used. All data were acquired with Xcalibur software v3.0.63.

2.3.3. Data analysis

The MaxQuant software suite (v1.6.0.16) was used for peptide identification and quantification. The data was searched against an in-house generated database containing all proteins corresponding to human in the Swissprot database plus a list of common contaminants and all the corresponding decoy entries (release April 2018, 42.518 entries). A precursor ion mass tolerance of 4.5 ppm at the MS1 level was used, and up to three missed cleavages for trypsin were allowed. The fragment ion mass tolerance was set to 0.5 Da. Oxidation of methionine, protein acetylation at the N-terminal and phosphorylation in Serine, Threonine and Tyrosine were defined as variable modifications; whereas

carbamidomethylation of cysteines was set as a fix modification. Identified peptides have been filtered using a 1% FDR. Only proteins identified with ≥2 peptides were considered.

The proteome and the phosphoproteome data have been deposited to the ProteomeXchange Consortium via PRIDE [37] partner repository, respectively with the dataset identifiers PXD015497 and PXD015498.

2.4. Bioinformatics analysis

MaxQuant's label-free quantification (LFQ) algorithm (MaxLFQ) was used to calculate the fold-change of protein variation between patients with complete and incomplete RR. MaxLFQ normalizes data based on peptide intensities [38]. After filtering out contaminants, reversed sequences and proteins identified only by site, data was transformed by computing log2 and the differences detected with t-test. As an additional validation step of the differentially expressed proteins (DEPs) between cRR and iRR patients, the effect size was calculated using Cohen's d (standardized mean difference).

Next, a first GOEA and pathway enrichment analysis was undertaken with FunRich (v.3.1.3), providing the main differences in biological processes, pathways, molecular functions and protein distribution across cellular components [39]. For this analysis, the DEPs and cRR- and iRR-exclusive proteins were selected. The top 10 terms were selected based on the highest differences between cRR and iRR in the percentage of genes covering each of the enlisted terms, using the whole proteome as reference and the FunRich database. To provide a deeper screen of the dysregulated biological processes in (in)complete RR a second GOEA was performed with Cytoscape's plugins ClueGO (v.2.5.3) [40] and Cluepedia (v.1.5.3). For this purpose, two clusters were defined (cRR and iRR) comprising the same proteins. The GO range was fixed between levels 5 and 15 and a minimum of three genes per cluster was defined to map GO terms. The GO library, from the Gene Ontology consortium, was updated on January 22nd, 2019.

A multivariate analysis, considering also the relationship between proteins, was pursued with MetaboAnalyst v4.0. To that end, normalized LFQ and log2-transform data were uploaded and mean-centered, to provide the best bell-shaped distribution. Then, a partial least square discriminant analysis (PLS-DA) was performed to identify the most important proteins in separating cRR and iRR patients (variables importance in projection, VIP).

The identification of dysregulated phosphopeptides was also ensued through t-test analysis. This was done after excluding contaminants, reversed sequences and peptides that were only identified by site. Peptides that were present in less than three of samples, per group, were not considered. Quantification was also ensued through MaxLFQ algorithm. Pathway enrichment analysis was performed again with FunRich, using the proteins whose phosphosites were found differentially expressed between the two subsets of patients.

Next, motif analysis was performed using WebLogo (https://weblogo.berkeley.edu/logo.cgi) tool, using the differentially expressed phosphopeptides and setting six flanking amino acid residues in each of the phosphosite's *termini*. A small sample correction feature was used to compensate entropy overestimation. In order to identify potentially dysregulated kinases and affected pathways, kinase prediction was performed through the Group-based Prediction System (GPS) 3.0 tool [41]. Both GPS features, namely the species-specific (*Homo sapiens*) and the dual-specificity (designed for kinases that can phosphorylate Ser/Thr and Tyr residues) modalities were used. Kinase prediction was carried out with the highest threshold (a false positive rate of 2% and 4%, respectively for Ser/Thr and Tyr kinases) and comprising only phosphosites with a probability of occurrence >0.9, as defined by MaxLFQ. Predicted kinases were ranked according to the difference in the percentage of all phosphorylation events associated to cRR and iRR. The 10^{th} percentile was used to extract the most important kinases in both phenotypes. Finally, network analysis was undertaken with Cytoscape v.3.7.1 to decipher kinase-substrate interactions. In this analysis, the top 3 kinases in each group and the respective phosphosites were selected. The phosphosite's node size was defined to represent the fold-change of variation between complete and incomplete RR.

2.5. Western blot validation

30 µg of protein obtained from myocardium lysates of cRR and iRR and from a technical control (collected from a patient with CAD) were resolved by SDS-PAGE (12%), essentially as described by Laemmli [42]. Due to the high concentration of urea (7.2M) in the myocardial lysates, reduced by half (3.6 M) when mixing with the loading buffer, samples were not boiled, but rather incubated at 37 °C, for 10 min, to prevent non-enzymatic protein carbamylation and the subsequent undesired band mobility upon detection. Gels were run at constant current (120V to 200V), for about one hour. Then proteins were blotted onto

0.45 µm nitrocellulose membranes (Amersham™ Protan™, GE Healthcare) in transfer buffer (25 mM Tris(hydroxymethyl)aminomethane, 192 mM glycine, pH 8.3, 20% methanol v/v), for two hours at 200 mA. Protein loading was normalized by Ponceau S staining (0.1% in 5% acetic acid v/v), because previous studies have demonstrated that total protein detection is more reliable than commonly used housekeeping proteins (glyceraldehyde 3-phosphate dehydrogenase, α- and γ-tubulins, α-actinin and β-actin) to control protein loading in hypertrophy models [43]. After completely removing Ponceau S staining with TBS-T (Tris buffer saline-Tween 20: 10 mM Tris(hydroxymethyl)aminomethane, 240 mM NaCl, pH 8.0, 0.05% Tween-20), the membranes were blocked with either nonfat dry milk or BSA. Then, the membranes were incubated with the specific primary antibody, washed thrice with TBS-T for 10 min, incubated with the respective secondary horseradish peroxidase-linked antibody and washed again thrice with TBS-T for 10 min. **Table 2** compiles the specific conditions (blocking solution, blocking time, primary and secondary antibody incubations) and the antibody references. The detection was carried out with enhanced chemiluminescence reagents (Western Bright™, Advansta), with support of ChemiDoc™ Touch Imaging System. Blot scans were analyzed with ImageLab 5.1 software (Bio-Rad). Optical density (OD) of each band was normalized to lane's total OD, obtained from Ponceau S staining scan, and then to the OD of the technical control.

2.6. Statistical analysis

Categorical clinical data is presented as absolute frequencies. Fisher's exact test was applied to detect differences between both groups (cRR and iRR). Continuous demographical and molecular expression data are presented as mean ± standard deviation. The normality of the distribution was tested by the D'Agostino & Pearson omnibus method. The differences between groups in normally distributed variables were tested with the unpaired two-tailed t-test, otherwise the Mann-Whitney test was used. Correlation between clinical parameters and the relative expression of the proteins was evaluated with Pearson's test if data presented a normal distribution and with Spearman's test, if otherwise. All statistical tests were done with GraphPad Prism 6 and, in any case, $p < 0.05$ was considered significant.

Table 2. Western blot specific conditions.

Protein target	UniProt ID and Gene Name	Blocking conditions	Primary antibody	Incubation conditions	Secondary antibody	Incubation conditions
NLR family member X1	Q86UT6 NLRX1 or NOD9	1 hour in 5% nonfat milk in TBS	Mouse mAb 1:1000; sc-7294	Overnight 4 °C	HRP-linked sheep anti-mouse 1:5000; GE Amersham NA931	1 hour RT
26S proteasome non-ATPase regulatory subunit 1	Q99460 PSMD1	1 hour in 5% nonfat milk in TBS	Mouse mAb 1:1000; sc-166038	Overnight 4 °C	HRP-linked sheep anti-mouse 1:5000; GE Amersham NA931	1 hour RT
Complement C3	P01024 C3	1 hour in 5% nonfat milk in TBS-T	Mouse mAb 1:1000; sc-28294	Overnight 4 °C	HRP-linked sheep anti-mouse 1:5000; GE Amersham NA931	1 hour RT
Transcription initiation factor TFIID subunit 1*	P21675 TAF1	1 hour in 5% BSA in TBS-T	Mouse mAb 1:250; sc-735	Overnight 4 °C	HRP-linked sheep anti-mouse 1:5000; GE Amersham NA931	1 hour RT
Glycogen synthase kinase-3 α and β*	P49840/ P49841 GSK3A/GSKB	Overnight in 5% nonfat milk in TBS-T	Mouse mAb 1:500; Invitrogen #44-610	2 hours RT	HRP-linked sheep anti-mouse 1:5000; GE Amersham NA931	1 hour RT
Calcium/calmodulin-dependent protein kinase type II*	Not specific to a CAMK2 isoform	2 hours in 5% nonfat milk in TBS-T	Mouse mAb 1:1000; ab22609	Overnight 4 °C	HRP-linked sheep anti-mouse 1:5000; GE Amersham NA931	1 hour RT
Nuclear factor of activated T-cells, cytoplasmic 1*	O95644 NFATC1	1 hour in 5% BSA in TBS-T	Mouse mAb 1:500; sc-7294	Overnight 4 °C	HRP-linked sheep anti-mouse 1:5000; GE Amersham NA931	1 hour RT
Dual specificity tyrosine-phosphorylation-regulated kinase 1A	Q13627 DYRK1A	1 hour in 5% nonfat milk in TBS-T	Mouse mAb 1:1000; sc-100376	Overnight 4 °C	HRP-linked sheep anti-mouse 1:5000; GE Amersham NA931	1 hour RT

* Reprobing was attempted after mild stripping (200 mM Gly, 0.1% SDS, 1% Tween 20, pH 2.2). Membranes were washed twice for 10 min with the stripping buffer, twice with phosphate-buffered saline (10 min) and twice with TBS-T (5 min).

Abbreviations: BSA: bovine serum albumin; HRP: horseradish peroxidase; mAb: monoclonal antibody; RT: room temperature; TBS: Tris(hydroxymethyl)aminomethane buffer saline; TBS-T: TBS-Tween-20.

3. Results

All subjects included in this study presented moderate-to-severe AS, according to ESC's and AHA's guidelines [44]. In all cases, the AVAi was below 0.60 cm^2/m^2 and the peak Ao was over 4 m/s, except one case with a velocity of 3.9 m/s. The mean aortic transvalvular pressure gradient ranged between 40 and 80 mmHg. The patients with cRR and iRR were not significantly different with concern to the degree of valve stenosis, potential risk factors, such as age, gender, hypertension, diabetes mellitus, CAD, smoking history or co-existing mild-to-moderate extra-aortic valve disorders. The only difference resided in BMI, which was significantly higher in patients with iRR in the discovery cohort, but not in the validation group. Beyond the demographics, the patients were quite homogeneous with respect to myocardial remodeling and systolic function. Overall, the study population presented concentric remodeling (RWT >0.42, except two subjects, with 0.34 and 0.41), and all displayed preserved systolic function. Therefore, in the following sections, the characterization of the myocardial proteome and phosphoproteome differences between patients with cRR and iRR reflect the higher or lower likelihood to post-AVR LVM regression.

3.1. The myocardial proteome profile in aortic stenosis patients with complete and incomplete reverse remodeling

From over 1800 proteins quantified in human myocardium, 1% (18 proteins) was identified exclusively in AS with cRR and 2.5% (46 proteins) was identified only in AS patients with iRR (**Figure 1A**). Apart from these exclusive proteins, 83 common proteins were found dysregulated between cRR with iRR patients (**Figure 1B** and **Table 3**). All these proteins (with *p*-value <0.05) presented a large effect-size (Cohen's d >0.8), corroborating a consistent variation in RR (**Supplementary Figure S1, Appendix**). This shows that the sample size of n = 4 per group is, with 95% confidence, suitable to study the molecular differences between AS patients with complete or incomplete RR. 39 out of 83 proteins were downregulated in iRR (green dots in **Figure 1B**), and the remaining 44 proteins were found upregulated in iRR (red dots in **Figure 1B**). Moreover, 15 out of the 39 downregulated proteins and 25 out of the 44 upregulated proteins changed over 1.5-fold and are depicted respectively as darker green and darker red dots in the volcano plot. For instance, there is

a downregulation of the slow-twitch skeletal muscle isoform of troponin I (ssTnI), proteostasis-associated proteins, such as the non-ATPase regulatory subunit 1 of the 26S proteasome (PSMD1), the E3 ubiquitin ligase HUWE1 and the NLR family member X1 (NLRX1), which promotes autophagy, according to UniProt. In turn, there is a remarkable upregulation of angiotensinogen, complement system elements (e.g. complement C3, C4-A, C4-B and factor H-related protein 1) and of the eukaryotic translation initiation factor 3 (subunit H).

The dysregulated biological processes and pathways, molecular functions and the protein localization were initially screened with FunRich (**Figure 1C**). In all cases, the percentage of proteins covering each of the FunRich terms in each group is given, together with the *p*-value for the enrichment in relation to the whole proteome. Overall, the enrichment analysis suggests for iRR a decrease in the metabolic (-15.7%), energetic pathways (-14.0%) and, specifically, in protein metabolism (-7.3%), an increase in immune response (+9.4%, $p < 0.03$) and in the regulation of the nucleic acid metabolism (+19.5%). Of note, proteins involved in apoptosis (+2.0%) were only mapped from proteins increased or exclusively identified in the iRR group. From the pathway analysis, one can notice in iRR the great representation of transcription (+12.5%, $p < 0.01$), closely followed by the innate immune system (+6.4%, $p < 0.01$). In turn, cRR is associated to a higher metabolic activity (+5.2%), particularly of amino acids and their derivatives (+6.0%). Regarding the molecular functions, there is a clear overrepresentation of DNA-binding proteins in iRR (+13.5%, $p < 0.001$) and of proteins with catalytic activity in cRR (+20.1%, $p < 0.01$). Finally, dysregulated proteins in iRR are more easily found inside the nucleus/nucleolus/nucleoplasm (+9.9 to +20.8%, $p < 0.01$), in the centrosome (+24.3%, $p < 0.01$) or outside the cell (+26.1%, $p < 0.01$), probably in part through exosome release (+28.2%, $p < 0.01$). Given the generalized nature of the terms provided by FunRich analysis, a deeper analysis was undertaken through a second GOEA with ClueGO. **Figure 2** shows a network representing all the predicted up- and downregulated biological processes from a specific GO level range (5-15). Remarkably, it was predicted downregulation of NADH metabolism and of lysine catabolism in iRR and upregulation of complement system activation, TGF-β production regulation and of apoptotic cell clearance.

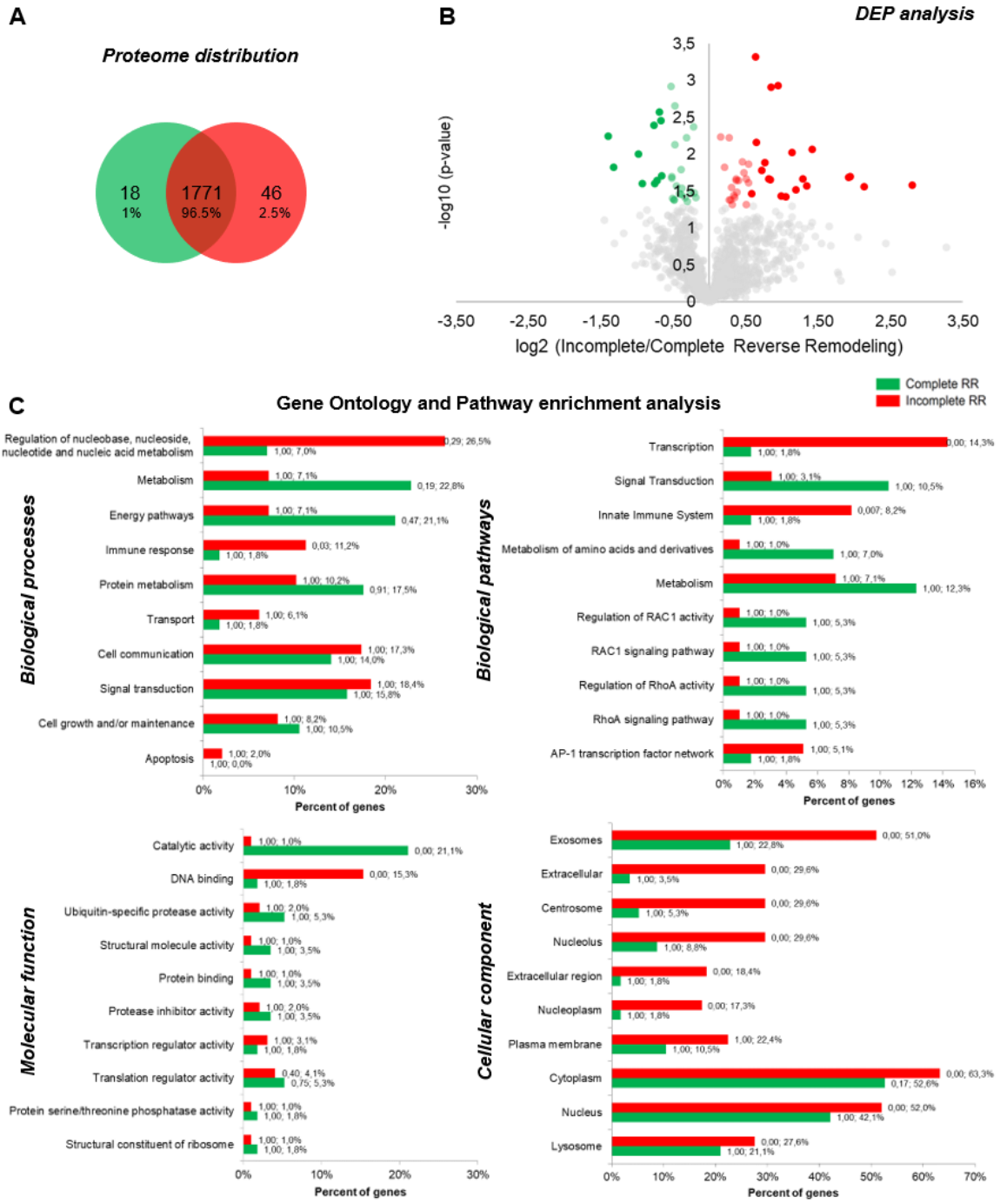

Figure 1. Characterization of the myocardial proteome in aortic stenosis patients with complete (green) and incomplete (red) reverse remodeling. **A.** Venn chart showing the distribution of the proteins identified in both groups. **B.** Volcano plot representing differentially expressed proteins in patients with complete and incomplete reverse remodeling. Gray dots represent proteins with no significant differences between both groups. Darker green and darker red dots depict proteins that are, at least, 1.5-fold lower or higher in incomplete reverse remodeling, respectively. **C.** FunRich enrichment analysis of gene ontology terms (biological processes, molecular function and cellular component) and biological pathways. The percentage of proteins (associated genes) covering each term and the Bonferroni-corrected *p*-value for the enrichment with respect to the whole proteome are indicated ahead of each bar.

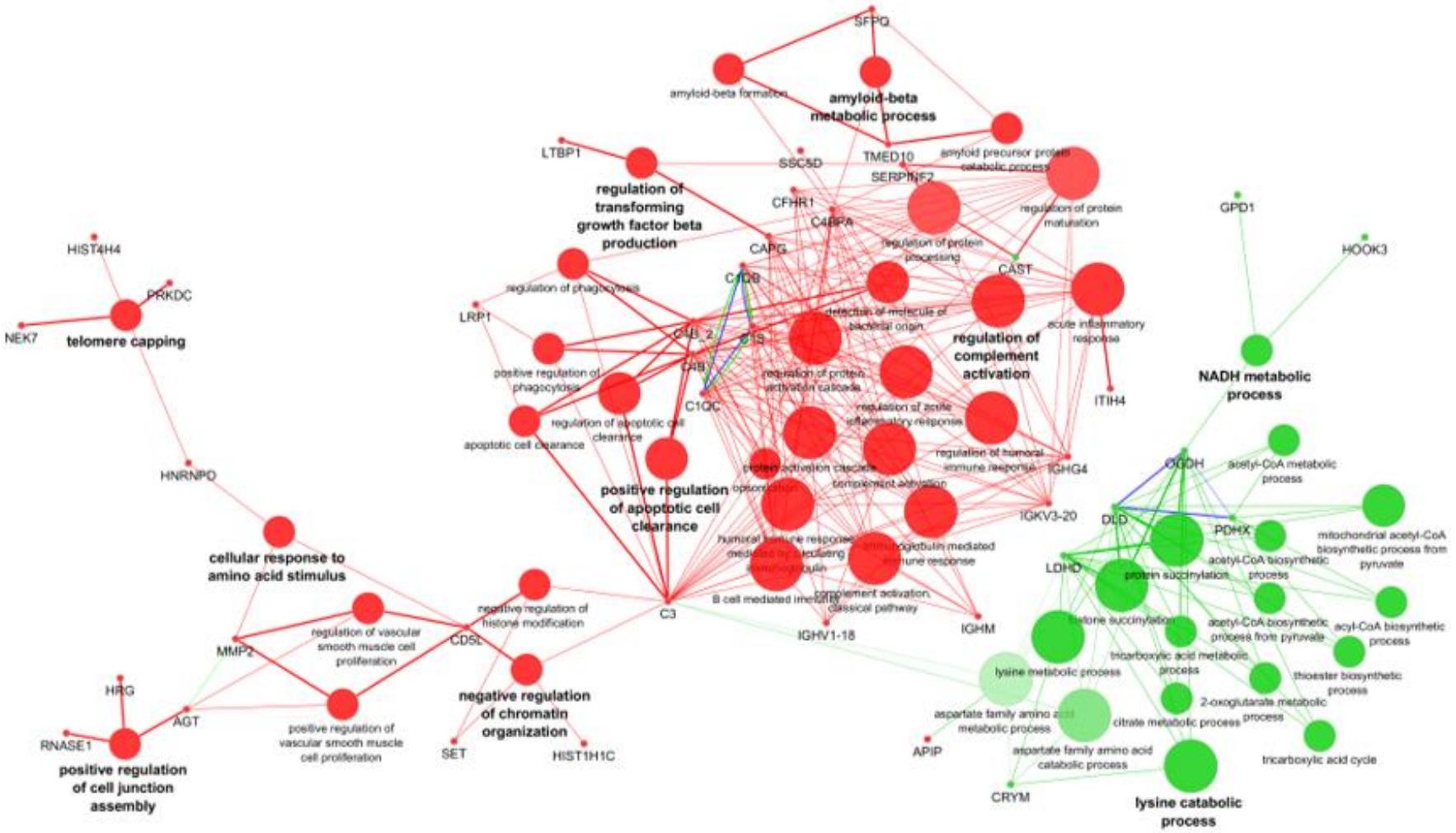

Figure 2. Network representing the dysregulated biological processes in incomplete (and complete) reverse remodeling, according to ClueGO+CluePedia enrichment analysis. Red nodes represent incomplete reverse remodeling and the green nodes represent complete reverse remodeling. GO range was set between 5 and 15 as to provide detailed biological information. Proteins are identified through the respective gene name.

Acknowledging that, in a systems level, a response to a stimulus (e.g. pressure overload) is reflected in protein modules changing in the same direction (increasing or decreasing), a multivariate analysis was also performed, as to identify the most important proteins that can separate cRR from iRR. **Figure 3A** depicts a PLS-DA analysis of the myocardial proteome in complete and incomplete RR, showing a complete separation of the two study groups in the two components, together explaining over 50% of data variability. The most important proteins to explain the variability in the first component are shown in **Figure 3B**. Notably, all proteins presented a VIP score >3.0. These proteins can be grouped in immune system (three immunoglobulin chains, high in iRR), complement system (factor D, C4-B and complement factor H-related protein 1, high in iRR), sarcomere contraction regulation (tropomyosin α-3 chain and troponin I, high in cRR) and acute-phase response (haptoglobin and α-1-antichymotrypsin, high in iRR).

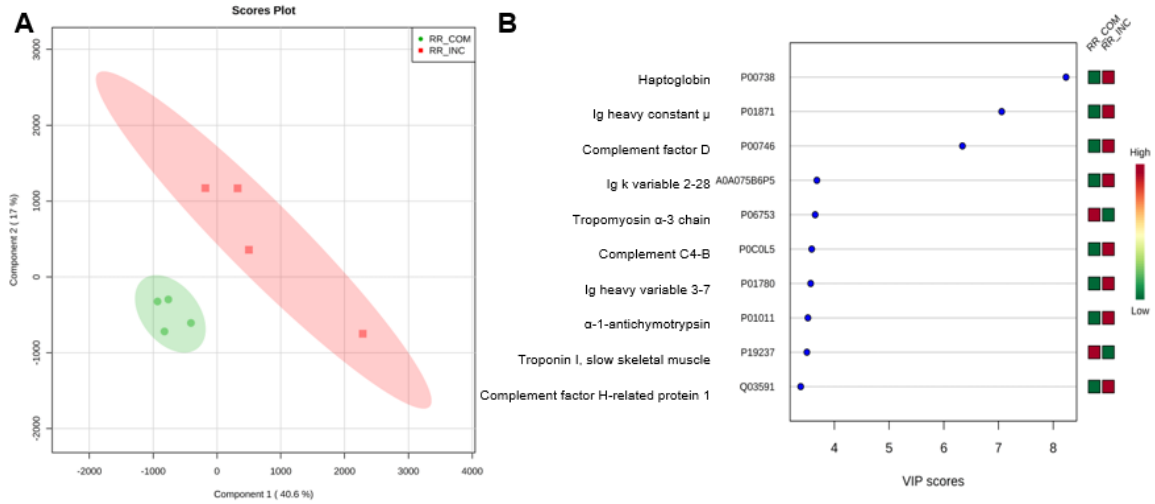

Figure 3. A. PLS-DA plot showing the separation of patients with complete (green) and incomplete (red) reverse remodeling. **B.** Top 10 proteins with the highest VIP (variable importance in projection) score.

Table 3. Differentially expressed proteins in incomplete reverse remodeling. Proteins are sorted in descending order of the fold-change.

UniProt ID	Gene Name	Full name	# Pep.	Seq. Cov. (%)	n (cRR)	n (iRR)	FC	Cohen's d	*p*
P01871	IGHM	Immunoglobulin heavy constant μ	13	34.7	4	4	7.0	2.08	0.026
P04003	C4BPA	C4b-binding protein α chain	5	12.7	3	3	4.4	2.76	0.028
P01019	AGT	Angiotensinogen	6	18.1	4	3	4.2	1.90	0.046
P08697	SERPINF2	α-2-antiplasmin	3	9	4	3	3.8	2.41	0.020
P01861	IGHG4	Immunoglobulin heavy constant γ 4	10	52	3	4	3.8	2.48	0.021
P0C0L5	C4B	Complement C4-B	50	43.2	4	4	2.7	2.72	0.009
Q03591	CFHR1	Complement factor H-related protein 1	9	32.7	4	4	2.5	2.07	0.027
Q14624	ITIH4	Inter-α-trypsin inhibitor heavy chain H4	18	24.1	4	4	2.5	2.18	0.022
P01024	C3	Complement C3	82	55.7	4	4	2.3	2.00	0.030
P0C0L4	C4A	Complement C4-A	50	43.2	4	4	2.2	2.65	0.009
P00450	CP	Ceruloplasmin	29	42.3	4	4	2.2	1.78	0.046
O95782	AP2A1	AP-2 complex sub. α-1	3	5.7	4	4	2.1	1.88	0.038
P04196	HRG	Histidine-rich glycoprotein	11	27.6	4	4	2.0	1.89	0.037
P53814	SMTN	Smoothelin	4	6.3	3	4	1.9	5.11	0.001
O43390	HNRNPR	Heterogeneous nuclear ribonucleoprotein R	5	11.4	4	4	1.8	1.75	0.048
Q9Y263	PLAA	Phospholipase A-2-activating protein	3	6.3	3	4	1.8	4.72	0.001
P36578	RPL4	60S ribosomal protein L4	6	25.1	4	4	1.8	2.16	0.022
O15372	EIF3H	Eukaryotic translation initiation factor 3 sub. H	3	14.5	3	3	1.8	2.99	0.022
Q86UP2	KTN1	Kinectin	11	10.1	4	4	1.7	2.48	0.013
P10155	RO60	60 kDa SS-A/Ro ribonucleoprotein	2	5	4	4	1.7	1.85	0.040
P61952	GNG11	Guanine nucleotide-binding protein G(I)/G(S)/G(O) sub. γ-11	2	27.4	4	3	1.7	2.94	0.016
O94905	ERLIN2	Erlin-2	3	13.9	2	3	1.7	3.56	0.041
P27105	STOM	Erythrocyte band 7 integral membrane protein	5	30.2	4	4	1.6	2.85	0.007
P43487	RANBP1	Ran-specific GTPase-activating protein	3	14.9	4	4	1.6	4.83	0.000

Q6H8Q1	ABLIM2	Actin-binding LIM protein 2	4	9	4	3	1.5	2.38	0.034
Q8TDX7	NEK7	Serine/threonine-protein kinase Nek7	3	13.9	4	4	1.5	2.44	0.014
Q13162	PRDX4	Peroxiredoxin-4	8	32.1	4	4	1.5	2.11	0.024
Q9NZA1	CLIC5	Chloride intracellular channel protein 5	5	19	3	3	1.4	2.99	0.022
Q9NZN4	EHD2	EH domain-containing protein 2	18	49.9	4	4	1.4	1.75	0.048
O14744	PRMT5	Protein arginine N-methyltransferase 5	2	6.9	3	2	1.4	4.41	0.018
P22314	UBA1	Ubiquitin-like modifier-activating enzyme 1	26	40.8	4	4	1.4	2.48	0.013
Q9Y696	CLIC4	Chloride intracellular channel protein 4	14	79.8	4	4	1.3	2.15	0.023
Q9UHD8	SEPTIN9	Septin-9	5	17.4	4	4	1.3	1.96	0.032
P49354	FNTA	Protein farnesyltransferase/geranylgeranyltransferase type-1 sub. α	2	7.4	4	4	1.3	2.16	0.022
P62805	HIST*H#[a)]	Histone H4	8	56.3	4	4	1.3	2.18	0.022
P16403	HIST1H1C	Histone H1.2	8	31.9	4	4	1.3	1.86	0.039
P55884	EIF3B	Eukaryotic translation initiation factor 3 sub. B	3	3.8	3	4	1.3	2.35	0.036
Q01105	SET	Protein SET	3	17.2	4	4	1.2	1.75	0.048
P24534	EEF1B2	Elongation factor 1-β	7	44	4	4	1.2	2.03	0.028
Q14103	HNRNPD	Heterogeneous nuclear ribonucleoprotein D0	8	24.5	4	4	1.2	1.83	0.041
P49755	TMED10	Transmembrane emp24 domain-containing protein 10	4	28.8	4	4	1.2	2.94	0.006
P11277	SPTB	Spectrin β chain, erythrocytic	36	22.8	4	4	1.2	1.83	0.041
P23246	SFPQ	Splicing factor, proline- and glutamine-rich	8	15.8	4	4	1.2	2.38	0.015
Q14204	DYNC1H1	Cytoplasmic dynein 1 heavy chain 1	72	20.7	4	4	1.1	2.96	0.006
Q9NSE4	IARS2	Isoleucine--tRNA ligase, mitochondrial	17	23.2	4	4	-1.1	1.86	0.039
Q05639	EEF1A2	Elongation factor 1-α 2	23	65.2	4	4	-1.2	1.92	0.035
P61026	RAB10	Ras-related protein Rab-10	5	24.5	4	4	-1.2	3.16	0.004
Q02218	OGDH	2-oxoglutarate dehydrogenase, mitochondrial	60	60.5	4	4	-1.2	1.74	0.049
Q14894	CRYM	Ketimine reductase μ-crystallin	17	69.4	4	4	-1.2	1.97	0.032
Q6UXV4	APOOL	MICOS complex sub. MIC27	10	57.1	4	4	-1.2	1.81	0.043
P11766	ADH5	Alcohol dehydrogenase class-3	15	50.3	4	4	-1.2	2.94	0.006
Q86TD4	SRL	Sarcalumenin	28	28.9	4	4	-1.3	1.86	0.039

O15371	EIF3D	Eukaryotic translation initiation factor 3 sub. D	3	7.7	2	2	-1.3	4.39	0.048
P20810	CAST	Calpastatin	16	43.5	4	4	-1.3	2.03	0.029
O60739	EIF1B	Eukaryotic translation initiation factor 1b	5	54	4	4	-1.3	2.34	0.016
Q9UHQ9	CYB5R1	NADH-cytochrome b5 reductase 1	15	60.7	4	4	-1.3	1.93	0.035
Q9UL46	PSME2	Proteasome activator complex sub. 2	4	24.7	4	4	-1.3	1.95	0.033
P83111	LACTB	Serine β-lactamase-like protein LACTB, mitochondrial	8	21.4	4	4	-1.3	1.74	0.049
Q6P5Q4	LMOD2	Leiomodin-2	9	22.9	4	4	-1.4	2.06	0.027
O43615	TIMM44	Mitochondrial import inner membrane translocase sub. TIM44	6	18.8	4	4	-1.4	3.62	0.002
P10916	MYL2	Myosin regulatory light chain 2, ventricular/cardiac muscle isoform	30	93.4	4	4	-1.4	1.77	0.046
O00330	PDHX	Pyruvate dehydrogenase protein X component, mitochondrial	15	36.9	4	4	-1.4	2.80	0.007
P55822	SH3BGR	SH3 domain-binding glutamic acid-rich protein	8	38.9	4	4	-1.4	1.83	0.042
Q9H0R4	HDHD2	Haloacid dehalogenase-like hydrolase domain-containing protein 2	2	13.1	4	4	-1.4	1.83	0.042
P09622	DLD	Dihydrolipoyl dehydrogenase, mitochondrial	26	67.6	4	4	-1.4	1.85	0.040
Q86WU2	LDHD	Probable D-lactate dehydrogenase, mitochondrial	15	57	4	4	-1.4	2.19	0.021
Q86VS8	HOOK3	Protein Hook homolog 3	3	4.9	4	4	-1.4	2.23	0.020
Q6PIU2	NCEH1	Neutral cholesterol ester hydrolase 1	8	30.6	4	4	-1.4	4.07	0.001
Q7Z6Z7	HUWE1	E3 ubiquitin-protein ligase HUWE1	4	1.5	3	3	-1.6	3.07	0.020
Q96CN7	ISOC1	Isochorismatase domain-containing protein 1	5	27.9	4	4	-1.6	3.28	0.004
Q5BKX8	CAVIN4	Caveolae-associated protein 4	5	14.6	4	4	-1.6	1.74	0.049
Q9P2B2	PTGFRN	Prostaglandin F2 receptor negative regulator	4	5.9	4	4	-1.6	3.47	0.003
P26196	DDX6	Probable ATP-dependent RNA helicase DDX6	3	9.5	3	3	-1.6	2.70	0.030
O75128	COBL	Protein cordon-bleu	2	2.2	4	3	-1.6	2.54	0.022
Q9GZT3	SLIRP	SRA stem-loop-interacting RNA-binding protein, mitochondrial	4	45.9	4	4	-1.7	1.79	0.044
P51687	SUOX	Sulfite oxidase, mitochondrial	5	18.3	4	4	-1.7	2.10	0.025
Q86UT6	NLRX1	NLR family member X1	5	5.7	4	4	-1.7	3.19	0.004
O14548	COX7A2L	Cytochrome c oxidase sub. 7A-related protein, mitochondrial	2	40.4	4	4	-1.9	1.91	0.036
P21266	GSTM3	Glutathione S-transferase μ 3	9	51.6	4	4	-1.9	2.11	0.025
Q99460	PSMD1	26S proteasome non-ATPase regulatory sub. 1	3	4.5	4	3	-2.0	2.91	0.010

Q15370	ELOB	Elongin-B	3	39	4	4	-2.3	2.09	0.025
Q8IXI1	RHOT2	Mitochondrial Rho GTPase 2	3	7.4	2	2	-2.5	8.06	0.015
P19237	TNNI1	Troponin I, slow skeletal muscle	10	47.1	4	4	-2.6	2.96	0.006

a) Several genes: HIST1H4A, HIST1H4B, HIST1H4C, HIST1H4D, HIST1H4E, HIST1H4F, HIST1H4H, HIST1H4I, HIST1H4J, HIST1H4K, HIST1H4L, HIST2H4A, HIST2H4B, HIST4H4
Abbreviations: FC: fold-change; Pep.: peptides; Seq. Cov.: sequence coverage.

3.2. The myocardial phosphoproteome profile in aortic stenosis patients with complete and incomplete reverse remodeling

After taking a snapshot of the dysregulated biological and molecular processes in patients with cRR and iRR through proteomics, the myocardial phosphoproteome was characterized aiming principally to predict potentially dysregulated kinases. After phosphopeptides enrichment and analysis, over 22,000 phosphopeptides were identified and over 2,600 could be quantified in, at least, three subjects per group. 108 phosphopeptides were found differentially expressed in the myocardium of patients with cRR or iRR (**Table 4**). Specifically, 73 phosphopeptides showed an upregulation and 35 a downregulation in patients with an incomplete response. An initial screen of the biological pathways regulated by these phosphopeptides was undertaken with FunRich (**Figure 4A**). The enrichment analysis evidenced a higher activation of immune system pathways in iRR, such as the TNF-related apoptosis-inducing ligand (TRAIL) signaling pathway (+7.5%) and the IFN γ pathway (+6.0%) and reduced metabolic activity (-6.7%), corroborating the proteomics findings.

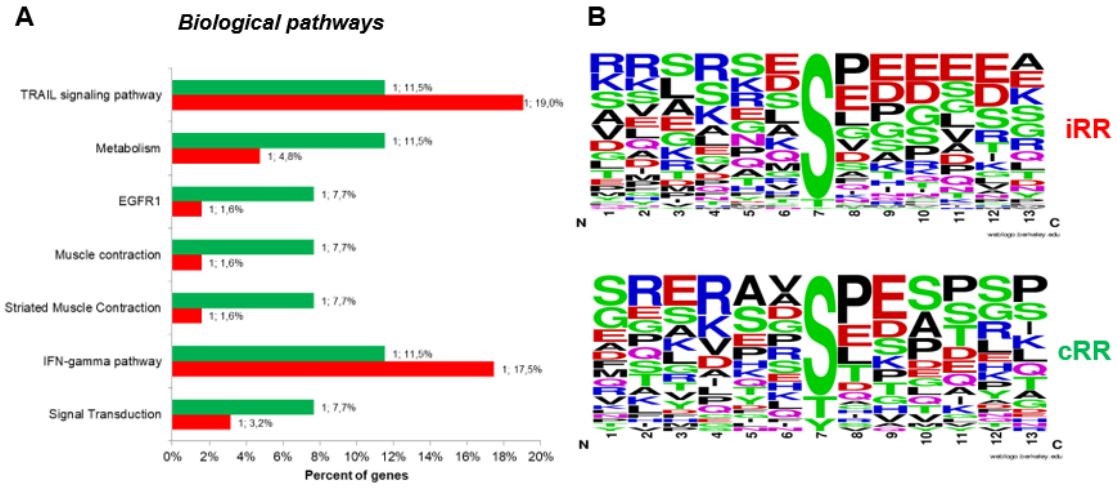

Figure 4. A. FunRich enrichment analysis of the biological pathways related to the significantly dysregulated phosphoproteins in reverse remodeling. Green and red bars correspond to complete and incomplete reverse remodeling, respectively. The percentage of proteins (associated genes) covering each term and the Bonferroni-corrected *p*-value for the enrichment with respect to the whole proteome is given ahead of each bar. **B.** WebLogo motif analysis of the phosphosite's neighboring sequence in incomplete (top) and complete (bottom) reverse remodeling.

Table 4. Differentially expressed phosphopeptides in incomplete reverse remodeling. Phosphopeptides are sorted in descending order of the fold-change.

UniProt ID	Gene Name	Protein name	Phosphopeptide	Seq. pos.	AA	FC	*p*
P41208	CETN2	Centrin-2	RMpSPKPELTEEQK	20	S	3.7	0.003
Q8IYB7	DIS3L2	DIS3-like exonuclease 2	RPGTQGHLGPEKEEEEpSDGEPEDSSTS	875	S	3.6	0.004
Q13459	MYO9B	Unconventional myosin-IXb	VQEKPDpSPGGSTQIQR	1290	S	3.5	0.003
Q15842	KCNJ8	ATP-sensitive inward rectifier potassium channel 8	pSIIPEEYVLAR	6	S	3.4	0.036
P02765	AHSG	α-2-HS-glycoprotein	CDSSPDpSAEDVRK	138	S	3.3	0.015
Q7Z5L9	IRF2BP2	Interferon regulatory factor 2-binding protein 2	RKPpSPEPEGEVGPPK	360	S	3.3	0.022
P46976	GYG1	Glycogenin-1	ERWEQGQADYMGADpSFDNIK	337	S	3.1	0.028
P08559	PDHA1	Pyruvate dehydrogenase E1 component sub. α, somatic form, mitochondrial	VLSGApSQKPASR	16	S	3.1	0.043
O94811	TPPP	Tubulin polymerization-promoting protein	AANRTPPKpSPGDPSK	18	S	2.8	0.010
O94811	TPPP	Tubulin polymerization-promoting protein	AANRpTPPKSPGDPSK	14	T	2.8	0.010
Q9UHD8	SEPT9	Septin-9	pSVQPTSEERIPK	327	S	2.8	0.007
Q8WZ42	TTN	Titin	RLpSDHSVEPGK	6920	S	2.8	0.049
O95359	TACC2	Transforming acidic coiled-coil-containing protein 2	DLSRSpSDSEEAFETPESTTPVK	1947	S	2.8	0.028
Q13557	CAMK2D	Calcium/calmodulin-dependent protein kinase type II sub. δ	KPDGVKEpSTESSNTTIEDEDVK	330	S	2.8	0.004
P08670	VIM	Vimentin	QVQpSLTCEVDALK	325	S	2.5	0.025
O00192	ARVCF	Armadillo repeat protein deleted in velo-cardio-facial syndrome	DGEMDRNFDpTLDLPK	642	T	2.4	0.031
O15234	CASC3	Protein CASC3	STVTGERQpSGDGQESTEPVENK	148	S	2.2	0.024
Q8IYB3	SRRM1	Serine/arginine repetitive matrix protein 1	KVELpSESEEDKGGK	463	S	2.2	0.047
Q14151	SAFB2	Scaffold attachment factor B2	VVTNARpSPGAR	444	S	2.2	0.040
Q5UIP0	RIF1	Telomere-associated protein RIF1	SNEpSVDIQDQEEK	1579	S	2.2	0.003
Q01082	SPTBN1	Spectrin β chain, non-erythrocytic 1	ESpSPIPSPTSDRK	2165	S	2.1	0.039

P29590	PML	Protein PML	VIKMEpSEEGK	493	S	2.1	0.020
Q9UHB6	LIMA1	LIM domain and actin-binding protein 1	QQpSPQEPK	698	S	2.1	0.016
Q96CB8	INTS12	Integrator complex sub. 12	SVpSCDNVSK	378	S	2.1	0.017
P61981	YWHAG	14-3-3 protein γ	VISSIEQKTpSADGNEK	71	S	2.0	0.015
P02545	LMNA	Prelamin-A/C	ASSHSpSQTQGGGSVTK	407	S	2.0	0.022
Q09666	AHNAK	Neuroblast differentiation-associated protein AHNAK	MpSLPDVDLDLK	1068	S	2.0	0.010
Q13557	CAMK2D	Calcium/calmodulin-dependent protein kinase type II sub. δ	ESTEpSSNTTIEDEDVK	333	S	2.0	0.008
Q99759	MAP3K3	Mitogen-activated protein kinase kinase kinase 3	AQpSFPDNRQEYSDRETQLYDK	250	S	1.9	0.021
P13637	ATP1A3	Sodium/potassium-transporting ATPase sub. α-3	YNTDCVQGLTHpSK	56	S	1.9	0.029
Q13428	TCOF1	Treacle protein	AALAPAKEpSPRK	906	S	1.9	0.040
O15021	MAST4	Microtubule-associated serine/threonine-protein kinase 4	SQALGQpSAPSLTASLK	206	S	1.9	0.043
O15021	MAST4	Microtubule-associated serine/threonine-protein kinase 4	SQALGQSAPSLTApSLK	213	S	1.9	0.043
Q99549	MPHOSPH8	M-phase phosphoprotein 8	GAEAFGDpSEEDGEDVFEVEK	51	S	1.9	0.010
P43003	SLC1A3	Excitatory amino acid transporter 1	NRDVEMGNpSVIEENEMK	512	S	1.8	0.042
Q14157	UBAP2L	Ubiquitin-associated protein 2-like	STSAPQMpSPGSSDNQSSSPQPAQQK	467	S	1.8	0.006
Q9GZR7	DDX24	ATP-dependent RNA helicase DDX24	AQAVpSEEEEEEEGK	82	S	1.8	0.022
Q9UGV2	NDRG3	Protein NDRG3	SRTHSTSSpSLGSGESPFSR	335	S	1.8	0.026
P23497	SP100	Nuclear autoantigen Sp-100	KRVIGQDHDFpSESSEEEAPAEASSGALR	407	S	1.8	0.021
Q3KQU3	MAP7D1	MAP7 domain-containing protein 1	RSpSQPSPTAVPASDSPPTK	113	S	1.8	0.033
Q6GYQ0	RALGAPA1	Ral GTPase-activating protein sub. α-1	pTVDIDDAQILPR	754	T	1.8	0.042
Q9Y2X7	GIT1	ARF GTPase-activating protein GIT1	HGpSGADSDYENTQSGDPLLGLEGK	592	S	1.8	0.029
Q9Y2X7	GIT1	ARF GTPase-activating protein GIT1	LSRHGSGADSDpYENTQSGDPLLGLEGK	598	Y	1.8	0.029
Q9UQ35	SRRM2	Serine/arginine repetitive matrix protein 2	THTTALAGRSPpSPASGR	297	S	1.8	0.042

Q9UQ35	SRRM2	Serine/arginine repetitive matrix protein 2	THTTALAGRSPSPApSGRR	300	S	1.8	0.042
Q9NYL9	TMOD3	Tropomodulin-3	DLDEDELLGNLpSETELK	25	S	1.8	0.039
Q29RF7	PDS5A	Sister chromatid cohesion protein PDS5 homolog A	RAAVGQEpSPGGLEAGNAK	1305	S	1.8	0.005
Q92609	TBC1D5	TBC1 domain family member 5	SEpSMPVQLNK	522	S	1.7	0.050
Q9UIG0	BAZ1B	Tyrosine-protein kinase BAZ1B	FPDRLAEDEGDpSEPEAVGQSR	1468	S	1.7	0.045
Q14195	DPYSL3	Dihydropyrimidinase-related protein 3	NLHQSGFSLpSGTQVDEGVR	541	S	1.7	0.027
Q9UKJ3	GPATCH8	G patch domain-containing protein 8	SQpSPHYFR	1035	S	1.7	0.034
O60271	SPAG9	C-Jun-amino-terminal kinase-interacting protein 4	SASQSpSLDKLDQELK	733	S	1.7	0.047
P02545	LMNA	Prelamin-A/C	pSNEDQSMGNWQIK	458	S	1.7	0.002
O14974	PPP1R12A	Protein phosphatase 1 regulatory sub. 12A	SApSSPRLSSSLDNK	472	S	1.7	0.003
Q9Y5K6	CD2AP	CD2-associated protein	pSVDFDSLTVR	458	S	1.7	0.035
O75475	PSIP1	PC4 and SFRS1-interacting protein	EDTDHEEKApSNEDVTK	129	S	1.7	0.046
Q8IYB3	SRRM1	Serine/arginine repetitive matrix protein 1	KVELpSESEEDKGGK	463	S	1.6	0.016
Q8IYB3	SRRM1	Serine/arginine repetitive matrix protein 1	KVELSEpSEEDKGGK	465	S	1.6	0.016
P62328	TMSB4X	Thymosin β-4	pSDKPDMAEIEKFDK	2	S	1.6	0.014
O95453	PARN	Poly(A)-specific ribonuclease PARN	ELpSPAGSISK	619	S	1.6	0.000
Q8NE71	ABCF1	ATP-binding cassette sub-family F member 1	KLpSVPTpDEEDEVPAPKPR	105	S	1.5	0.020
Q13557	CAMK2D	Calcium/calmodulin-dependent protein kinase type II sub. δ	ESTESSNTpTIEDEDVK	337	T	1.5	0.037
Q01813	PFKP	ATP-dependent 6-phosphofructokinase, platelet type	GRpSFAGNLNTYK	386	S	1.5	0.005
Q9H0B6	KLC2	Kinesin light chain 2	TLSSpSSMDLSR	610	S	1.5	0.047
P16284	PECAM1	Platelet endothelial cell adhesion molecule	YSRTEGpSLDGT	734	S	1.4	0.013
Q92597	NDRG1	Protein NDRG1	TApSGSSVTSLDGTR	330	S	1.4	0.029
Q9H246	C1orf21	Uncharacterized protein C1orf21	GRDYCpSEEEDIT	115	S	1.4	0.021

Q7Z6E9	RBBP6	E3 ubiquitin-protein ligase RBBP6	WDKDDFEpSEEEDVK	1328	S	1.4	0.039
O75351	VPS4B	Vacuolar protein sorting-associated protein 4B	GNDpSDGEGESDDPEKK	102	S	1.4	0.021
O95070	YIF1A	Protein YIF1A	AYHpSGYGAHGSK	5	S	1.3	0.049
O95070	YIF1A	Protein YIF1A	AYHSGYGAHGpSK	12	S	1.3	0.049
Q86VM9	ZC3H18	Zinc finger CCCH domain-containing protein 18	LGVSVpSPSR	534	S	1.2	0.049
P08648	ITGA5	Integrin α-5	LLESSLSpSSEGEEPVEYK	127	S	1.2	0.039
P30566	ADSL	Adenylosuccinate lyase	AAGGDHGpSPDSYRSPLASR	9	S	-1.4	0.032
Q09666	AHNAK	Neuroblast differentiation-associated protein AHNAK	VDVEVPDVpSLEGPEGK	1298	S	-1.5	0.045
Q9HBL0	TNS1	Tensin-1	SGpSLGQPSPSAQR	1119	S	-1.6	0.047
Q9HBL0	TNS1	Tensin-1	SGSLGQPpSPSAQR	1124	S	-1.6	0.047
Q8WX93	PALLD	Palladin	RAIADSETEDFDpSEK	60	S	-1.6	0.038
Q4G0J3	LARP7	La-related protein 7	RKRSSpSEDAESLAPR	300	S	-1.9	0.036
Q6PKG0	LARP1	La-related protein 1	ETESAPGSPRAVpTPVPTK	526	T	-1.9	0.011
O75151	PHF2	Lysine-specific demethylase PHF2	EDKPKPVRDEYEYVpSDDGELK	681	S	-1.9	0.040
Q2M3C7	SPHKAP	A-kinase anchor protein SPHKAP	QSpSCESITDEFSR	1121	S	-1.9	0.041
Q9H1B7	IRF2BPL	Interferon regulatory factor 2-binding protein-like	RKApSPEPPDSAEGALK	547	S	-1.9	0.007
P12883	MYH7	Myosin-7	NLpTEEMAGLDEIIAK	979	T	-1.9	0.028
Q9UN36	NDRG2	Protein NDRG2	pSRTASLTSAASVDGNRSR	328	S	-2.0	0.030
Q9UN36	NDRG2	Protein NDRG2	LSRSRpTASLTSAASVDGNR	330	T	-2.0	0.030
Q9BXK5	BCL2L13	Bcl-2-like protein 13	pSSPATSLFVELDEEEVK	370	S	-2.0	0.027
Q8N3K9	CMYA5	Cardiomyopathy-associated protein 5	LVAQpSIEDK	291	S	-2.0	0.016
Q14247	CTTN	Src substrate cortactin	TQpTPPVSPAPQPTEER	401	T	-2.1	0.025
P21397	MAOA	Amine oxidase [flavin-containing] A	VLGpSQEALHPVHYEEK	383	S	-2.1	0.011
Q6PKG0	LARP1	La-related protein 1	EpTESAPGSPRAVTPVPTKTEEVSNLK	515	T	-2.2	0.005
Q9UBB9	TFIP11	Tuftelin-interacting protein 11	KGAAEEAELEDpSDDEEKPVKQDDFPK	98	S	-2.2	0.046

P19237	TNNI1	Troponin I, slow skeletal muscle	MFDAAKpSPTSQ	183	S	-2.3	0.013
Q14247	CTTN	Src substrate cortactin	TQTPPVpSPAPQPTEERLPSSPVYEDAASFK	405	S	-2.3	0.020
Q96AG3	SLC25A46	Solute carrier family 25 member 46	SFpSTGSDLGHWVTTPPDIPGSR	34	S	-2.5	0.037
Q15772	SPEG	Striated muscle preferentially expressed protein kinase	AApSVELPQRR	2037	S	-2.6	0.008
Q6JBY9	RCSD1	CapZ-interacting protein	SSEEVDGQHPAQEEVPEpSPQTSGPEAENR	284	S	-2.6	0.029
P62070	RRAS2	Ras-related protein R-Ras2	FQEQECPPpSPEPTRK	186	S	-2.7	0.039
Q99959	PKP2	Plakophilin-2	WGRGTAQYSpSQK	132	S	-2.7	0.044
Q9UN36	NDRG2	Protein NDRG2	TApSLTSAASVDGNR	332	S	-3.0	0.001
Q8N3K9	CMYA5	Cardiomyopathy-associated protein 5	GLpSEEVSHPADFK	1752	S	-3.0	0.048
P10644	PRKAR1A	cAMP-dependent protein kinase type I-α regulatory sub.	EDEIpSPPPPNPVVK	83	S	-3.1	0.027
P40763	STAT3	Signal transducer and activator of transcription 3	YCRPESQEHPEADPGSAAPpYLK	705	Y	-3.5	0.043
Q99959	PKP2	Plakophilin-2	RLEISPDSSPERAHpYTHSDYQYSQR	161	Y	-5.8	0.027
Q99959	PKP2	Plakophilin-2	RLEISPDSSPERAHpYTHSDYQYSQR	161	Y	-8.5	0.027
O14639	ABLIM1	Actin-binding LIM protein 1	MIHRpSTSQGSINSPVYSR	450	S	-8.6	0.000
O14639	ABLIM1	Actin-binding LIM protein 1	MIHRSTSQGSINpSPVYSR	458	S	-8.6	0.000
Q14896	MYBPC3	Myosin-binding protein C, cardiac-type	RISDpSHEDTGILDFSSLLK	286	S	-281.2	0.002

Abbreviations: AA: amino acid residue; FC: fold-change.

Some differences in kinase activity between iRR and cRR were soon suggested by motif analysis (**Figure 4B**). First, in iRR, the dysregulated kinases show an apparently higher preference for proteins with more acidic residues flanking the phosphorylated residue at the C-*terminus* side, mainly Glu or Asp in the second, third and fifth positions. Second, in cRR, most kinases seem to prefer nonpolar residues at the first flanking position at the N-*terminus* side (Val and Ala preferred over Glu or Asp). Third, also in cRR, a higher predilection for Pro residues in the C-*terminus* flanking sequence is noticeable, mainly at first, fourth and sixth positions. Despite these main traces of amino acid preferences, motif analysis suggests the existence of heterogeneous sets of kinases in cRR and iRR, as shown by a somewhat balanced amino acid composition of the phosphosite's flanking positions (compare central Ser's height with that of the neighboring amino acids). This diversity was witnessed by performing kinase prediction with GPS 3.0. **Figure 5** illustrates the most important kinases (predicted to be the most active) in cRR and iRR, according to the difference in the percentage of assigned phosphorylation events. **Figure 5A** depicts the kinase rank, including only those kinases predicted to be responsible for >0.5% of the phosphorylation events (the whole range of kinases, spanning from 0 to 2.1% of assigned phosphorylation is shown in **Supplementary Figure S2, Appendix**). The kinases at the 10^{th} percentile (≥ 0.9% of assigned phosphorylation events) were regarded as the kinases with the highest probability of being active in cRR (green bars) and iRR (red bars). Apart from some kinase families, including the tyrosine kinase-like (TKL) and mitogen activated protein kinase (MAPK) families and the mixed lineage kinases (MLK); the dual specificity tyrosine-phosphorylation-regulated kinase (DYRK) 1A and 2 as well as the glycogen synthase kinase (GSK, including isoforms α and β) were found associated to cRR. In turn, the serine threonine kinase receptors (STKR), IκB kinase (IKK), vaccinia related kinase (VRK) families as well as casein kinase II (CK2), transcription initiation factor TFIID subunit 1 (TAF1) and the phosphorylase kinase (PHK) were deemed the most active kinases in iRR. **Figure 5B** shows the segregation of the most important kinases, according to the respective kinase class (left panel) and highlights the three most important kinases for cRR and iRR and the respective phosphosites (right panel). Note that kinase families were left out of the analysis and that IKK was represented instead of STKR family, as the latter comprise kinases phylogenetically more diverse than the former. A high degree of kinase-substrate overlap in both phenotypes could be observed through network analysis (the reader should see the interconnectivity between phosphoproteins, represented by gene name, and the central kinases), suggesting co-regulation or participation in convergent pathways.

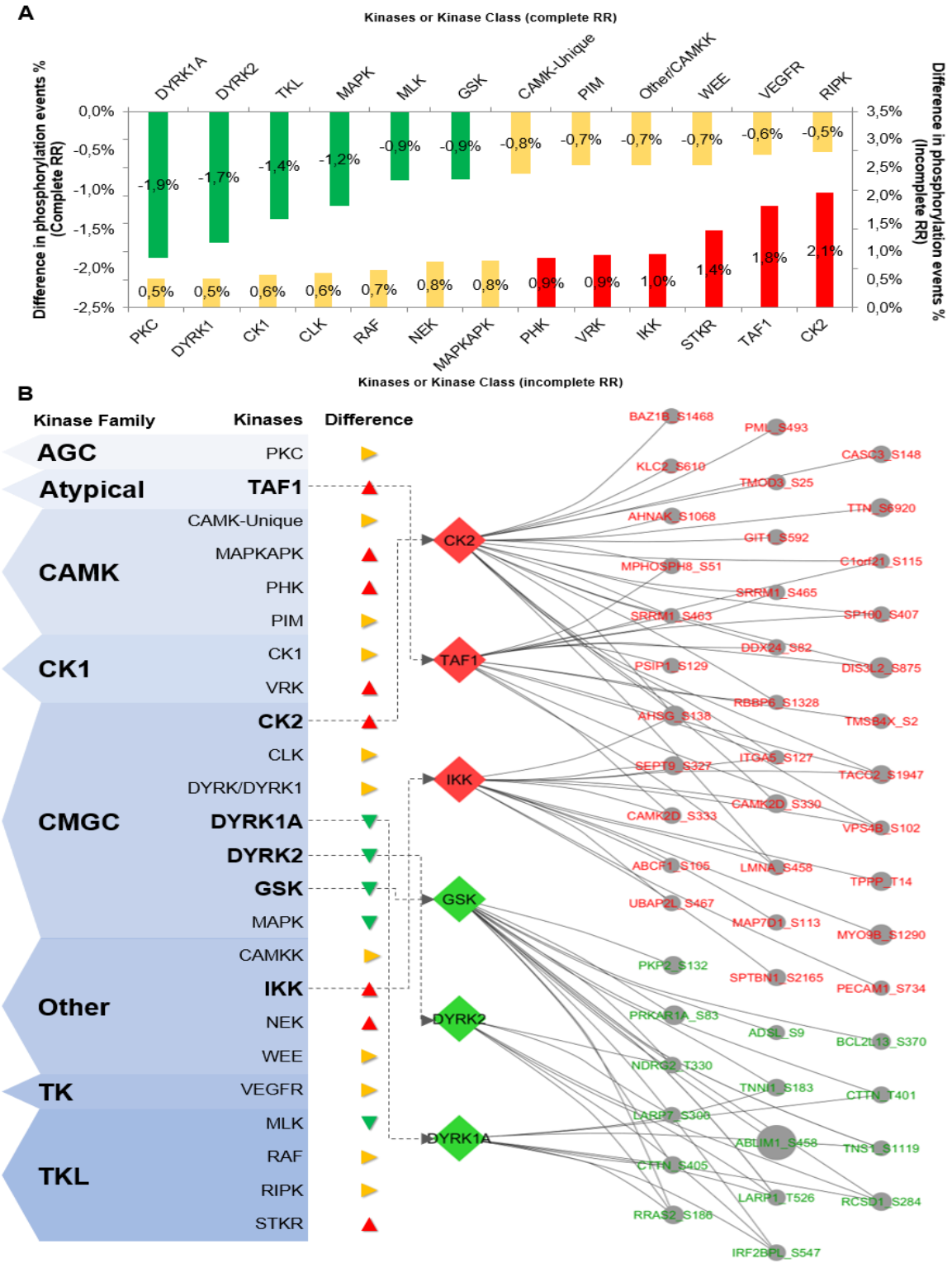

Figure 5. A. Kinase rank. Kinases were predicted with GPS 3.0 and sorted according to the percentage of associated phosphorylation events. Kinases (or families) in the 10th percentile associated with complete and incomplete reverse remodeling are marked in green and red, respectively. **B.** Distribution of kinases by family (left) and respective phosphopeptides (right). Kinase-substrate relationships were represented for the six most important kinases, through network analysis. Each phosphopeptide (gray nodes) is identified by the respective gene name of the associated protein and, in any case, the phosphosite is identified. Node size reflects fold-change of variation. Abbreviation of the represented kinases and their families is found in Appendix (Supplementary Table S1).

3.3. Western blot validation of the dysregulated proteins and kinases

Some of the most important DEPs as determined by LFQ were selected for validation through western blot in a larger cohort of AS patients (**Figure 6**). The protein NLRX1, which was found upregulated in cRR, was selected due to the reported protective effect against apoptosis [45] that may involve autophagy stimulation [46], beyond its inhibitory effects on the innate immune response and inflammation (GO annotation). Notwithstanding the observed decreased expression of NLRX1 in iRR patients through proteomics, the assessment in the larger cohort did not support this finding. In turn, the proteasome subunit PSMD1 could not be successfully detected through western blot (data not shown). Still with the regard to the myocardial proteome, while the intact complement C3 (α + β chain, ~185 kDa) could not be immunodetected, an increase of the C3 β chain (which remains intact in the activated forms of C3: C3b, iC3b and C3c [47]), was found tendentiously higher in iRR, almost reaching significance (p = 0.12). Next, the expression of some of the most important predicted kinases and their targets was investigated (**Figure 6**). If the atypical kinase TAF1 could not be detected in the human myocardial samples, this was not the case of the pro-hypertrophic kinase calcium/calmodulin-dependent protein kinase type II (CAMK2), predicted to be a target of CK2, TAF1 and the IKK family of kinases in the phosphosites Ser 330 and Ser 333. Still, no differences in the expression were found between cRR and iRR. In turn, the nuclear factor of activated T-cells (NFAT), which is primed by DYRK1A and 2 for GSK3β-mediated phosphorylation, leading to its nuclear export [48], could be detected, but the labeling was very unspecific to draw any reliable conclusions. Two of the kinases with the highest association to cRR, GSK3 and DYRK1A, could successfully be analyzed through immunoblot. Using an antibody simultaneously targeting the GSK3 α and β isoforms, the protein levels of these two kinases could be measured in the validation cohort. In spite of the predicted higher activity of GSK3 in cRR, the amount of GSK3α and β did not differ between the two groups. Finally, the expression of DYRK1A was found to be 1.4-fold higher (p <0.05) in iRR patients, despite higher predicted activity in cRR patients.

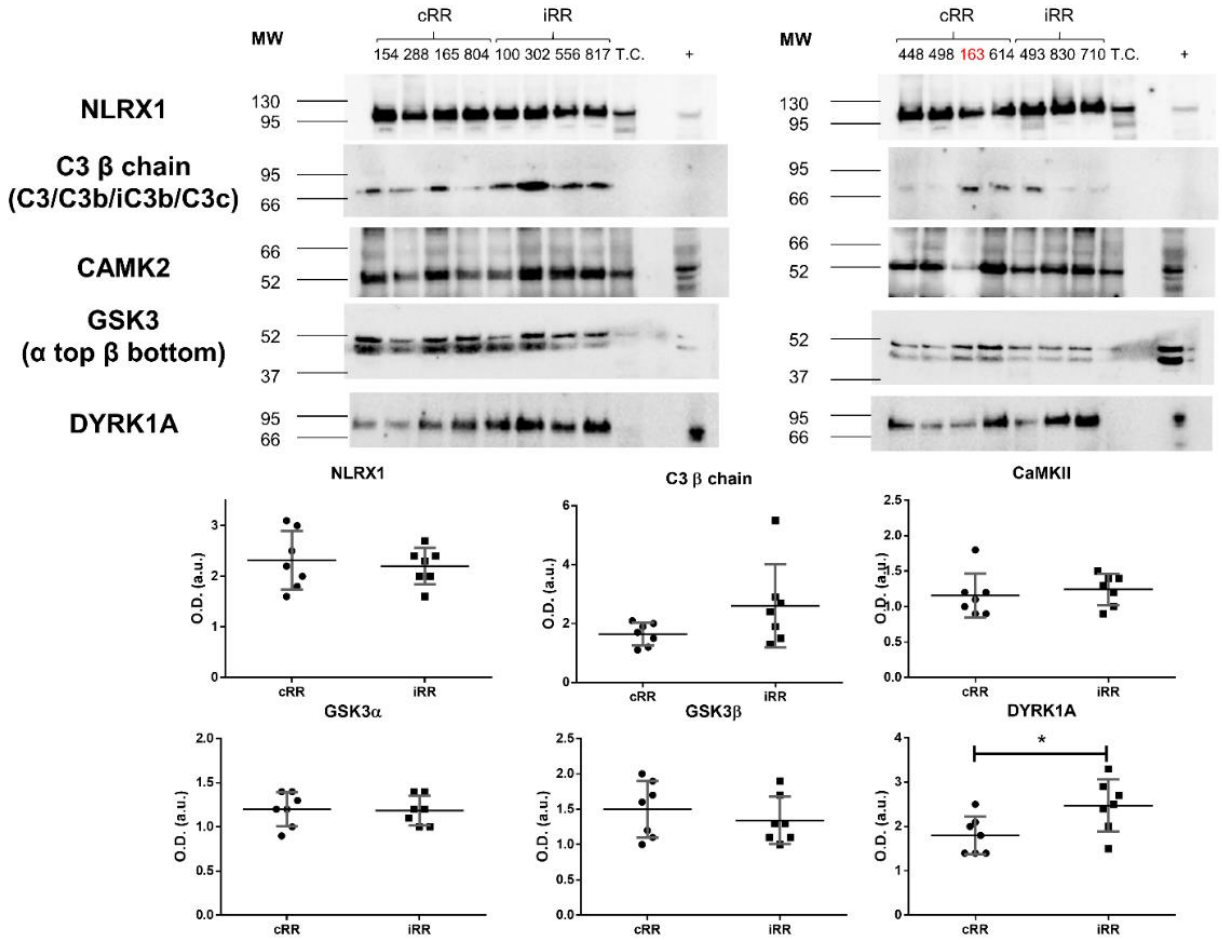

Figure 6. Western blot quantification of NLR family member X1 (NLRX1), complement C3b (C3b), calcium/calmodulin-dependent protein kinase type II (CAMK2), glycogen synthase kinase 3 (GSK3) α and β, and dual-specificity tyrosine-regulated kinase 1A (DYRK1A) in patients with complete (cRR) and incomplete (iRR) reverse remodeling. The molecular weight of the protein ladder is shown on the right of each blot. T.C. designates a technical control, and "+" the positive control. A HeLa cell extract was used as positive control for NLRX1, GSK3 and CAMK2, and a Hep G2 cell lysate was used for C3 and DYRK1A. The sample 163 is marked in red, because it was excluded from the assay *a posteriori* (aortic insufficiency was found more severe than AS). NLRX1 was detected on the reported MW (108 kDa). Complement C3 β chain was found around 75 kDa range as expected. CAMK2 was detected at the predicted 56 kDa position. GSK3α corresponds to the top band (51 kDa) and GSK3β to the bottom band (47 kDa). DYRK1A was detected on the reported region ~86 kDa. The respective optical density quantification is shown at the bottom. * p <0.05.

3.4. Correlation analysis

Aiming to identify possible associations between AS patients' phenotype and protein expression, the correlation between protein levels as measured by western blot and clinical variables was tested. These included age, BMI, Peak Ao, maximum and mean transvalvular pressure gradients, AVAi, preoperative and postoperative LVEDD, IVST, PWT, RWT and LVMi, in addition to LVM regression. **Figure 7A-E** displays the variables pairs with significant correlations. An age-associated decrease of the autophagy-promoter NLRX1 was observed (r = -0.64). A positive association between CAMK2 and DYRK1A was also found (r = 0.55). Furthermore, important protein-clinical correlates with potential prognostic implications were encountered. High levels of CAMK2 was associated with lower PWT (r = -0.66) and RWT (r = -0.61). Finally, the preoperative myocardial expression (but not the activity) of DYRK1A was associated with a higher propensity for iRR, as demonstrated by the positive correlation with postoperative LVMi (r = 0.63) and the negative correlation with LVM regression (r = -0.62).

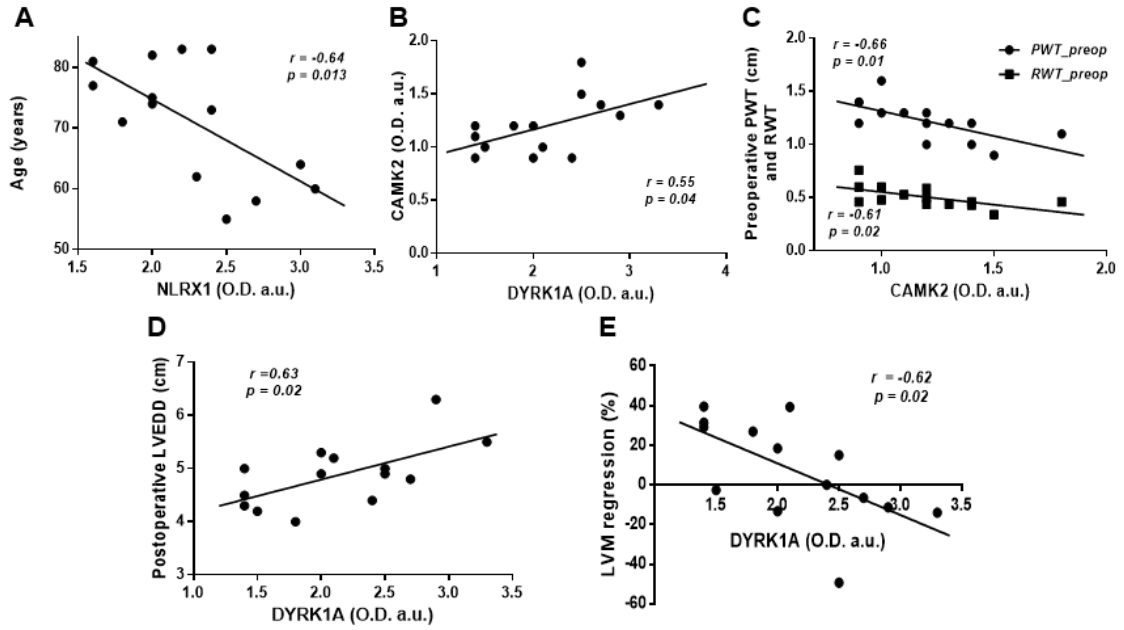

Figure 7. Correlation analysis between clinical and molecular data. In all cases, data was normally distributed, and "r" denotes the correlation coefficient as calculated by Pearson's test. **A.** Negative relationship between age and myocardial NLR family member X1 (NLRX1) levels. **B.** Positive association between the protein levels of calcium/calmodulin-dependent kinase type II (CAMK2) and dual-specificity tyrosine-regulated kinase 1A (DYRK1A). **C**. Negative correlation between CAMK2 and preoperative posterior wall thickness (PWT) and relative wall thickness (RWT). **D.** Positive association between DYRK1A and postoperative left ventricle end-diastolic dimension (LVEDD). **E.** Negative correlation between DYRK1A and left ventricle mass (LVM) regression.

4. Discussion

A patient with AS is typically a frail, older subject that often remains undiagnosed for extended periods of time due to the prolonged non-symptomatic phase of the disease. Besides, when referred to AVR (or TAVI) there is currently no way to doubtlessly predict whether this patient will show a good (cRR) or poor (iRR) outcome. This is worrisome since patients with iRR showing post-AVR hypertrophy present almost three times higher risk of hospitalization, due to cardiovascular events, and of all-cause death [4]. Therefore, a deeper investigation of the molecular mechanisms taking place during myocardial RR and the development of ancillary therapies to improve the outcome of iRR patients are imperative. To help bridge this gap, the myocardial proteome and phosphoproteome were characterized for the first time in AS patients, with different degrees of RR. Although exploratory, this study generates several hypotheses concerning the molecular processes on the root of divergent post-AVR phenotypes, which will be discussed onwards.

The increased workload experienced by cardiomyocytes with progressively stenotic aortic valves is compensated by hypertrophy, mainly driven by parallel sarcomere addition and sided with the reactivation of the fetal gene program (e.g. α- to β-MHC isoform shift) [49,50]. Upon AVR-driven myocardial unloading, hypertrophy reversal is set in motion through the recycling of sarcomeric components. Protein turnover in the heart is carried out essentially through two systems: the ubiquitin-proteasome system (UPS) and the autophagy pathway [51,52]. It is envisaged that a higher flux through the UPS and autophagy pathways favors LVM regression. Indeed, an increased expression of the E3 ubiquitin-protein ligase HUWE1 (HUWE1), the proteasome activator complex subunit 2 (PSME2) and the 26S proteasome non-ATPase regulatory subunit 1 (PSMD1) was found in cRR (**Table 3**), suggesting higher rates of protein recycling through the UPS in these patients. In turn, upregulation of NLRX1 in the same subjects may be related to protection from apoptosis, probably through stimulation of autophagy [46]. To validate the association between NLRX1 and PSMD1 expression and cRR, immunodetection was carried out in a larger cohort of patients. Even though no significant changes were found for NLRX1, a significant negative correlation between NLRX1 and age was observed. This may be explained by the age-dependent decline of autophagic activity, which is paramount to deal with higher protein cargoes for recycling [53]. In fact, some have described higher mortality in older patients undergoing AVR [11,54]. Concerning PSMD1, detection was unsuccessful,

thus the hypothesis of higher propensity for protein recycling through UPS and autophagy in patients with cRR remains to demonstrate. However, with respect to HUWE1, reduced levels of this E3 ubiquitin ligase were reported in patients with end-stage heart failure due to ischemic or idiopathic dilated cardiomyopathies [55]. Furthermore, the same authors described pathological hypertrophy in HUWE1 knockout mice and attributed this finding, at least in part, to the accumulation of its target, the pro-hypertrophic transcription factor c-myc [55]. Of note, GOEA showed an association of the term “amyloid-beta metabolic processing” to iRR (**Figure 2**). Although exuberant β-amyloid accumulation is rather unlikely in the heart, this points to the presence of protein agglomerates that might be degraded by similar mechanisms to those implicated in neurodegenerative conditions. This idea is supported by the work of Ayyadevara *et al*. [56], who have profiled the proteome of cardiac aggregates in a mouse model of hypertension (also inducing pressure overload), reporting a very strong association to Alzheimer’s, Parkinson’s and Huntington’s diseases, by GOEA (in all cases >20-fold, FDR $<10^{-37}$). Besides the apparently lower rate of protein recycling in iRR patients indicated by DEP analysis, FunRich analysis show a much higher enrichment of proteins related to transcription in iRR, suggesting active protein synthesis that may as well feed the hypertrophy phenotype in these subjects.

Apart from the overall decrease of the sarcomere components during RR, specific isoform adaptations occur due to the activation of the fetal gene program, and this may have important functional consequences. In this regard, a prominent upregulation of the ssTnI was observed in patients showing a good regression. Studies with transgenic mice expressing this troponin I isoform have shown an improved myofilamentary calcium sensitivity in isolated cardiomyocytes when compared to wild-type mice expressing the post-natal cardiac troponin I isoform [57]. The slow-twitch isoform is restricted to skeletal muscle in adult life, and it is not PKA-responsive (it lacks the N-terminal phosphorylation sites). Besides, the PKA pathway is activated soon after the onset of pressure overload [20]. Therefore, the proteome data suggests that patients with higher expression of ssTnI may display better myocardial contractility. The relevance of this troponin I isoform for a complete recovery could be further demonstrated by multivariate analysis. In fact, the latter and the tropomyosin α-3 chain together were the only proteins increased in cRR figuring in the top 10 most important variables in distinguishing the two groups of patients. Similarly to troponin I, a isoform-specific regulation of tropomyosin α-chain is apparent in the context of AS-induced myocardial remodeling. While studies with animal models reported an upregulation of the α-4 chain and 2 isoforms (α-1 chain dysregulation is conflicting) upon pressure overload-induced LV hypertrophy [21,26], this study adds suggesting that an

increase of α-3 chain (also a slow isoform) may favor a complete regression after pressure overload relief.

As judged by GOEA, patients with overall higher utilization of the energetic pathways and higher metabolic rates, particularly of proteins and amino acids, have higher chances of achieving a complete recovery. For instance, the cRR group presented higher expression of the protein X component of the mitochondrial pyruvate dehydrogenase complex, which delivers the energetic substrate acetyl-coenzyme A to the Krebs cycle. These patients also showed higher expression of the Krebs cycle enzyme 2-oxoglutarate dehydrogenase and of the complex IV (cytochrome c oxidase) subunit 7A-related protein. In a previous study with spontaneously hypertensive rats, it was found that anti-hypertensive therapy could rescue the downregulation of some complex IV protein subunits [26], pointing to a selective advantage of these individuals. Since the myocardial remodeling process is associated to a gradual worsening of tissue perfusion [50], the utilization of alternative substrates, such as amino acids, may also be beneficial for cardiomyocyte bioenergetics [58]. The downregulation of amino acid metabolism, specifically the degradation of branched-chain amino acids (Val, Leu and Ile) has been previously reported in animal models of pathological hypertrophy, due to pressure overload [21,24]. This study further suggests that upregulation of Lys catabolism, a ketogenic amino acid, may also contribute to a complete recovery. Hence, in the future, the specific role of diet and amino acid supplementation in AS should be further explored with respect to the outcome of AVR.

Previous studies have shown the association between pressure overload-induced LV hypertrophy and oxidative stress, showing that improving the antioxidant defenses attenuates heart failure (e.g. by rescuing fractional shortening) [31,59]. Herein, two antioxidant proteins were found dysregulated in RR. Somewhat unexpected, it was found an increased expression of peroxiredoxin-4 in iRR. According to UniProt knowledgebase, this enzyme catalyzes the neutralization of hydrogen peroxides, although it may also be responsible for the activation of the pro-hypertrophic, pro-inflammatory and pro-fibrotic nuclear factor kappa B (NF-κB) transcription factor. Therefore, its protective role might be limited. In turn, the enzyme glutathione S-transferase was found close to two times higher in cRR. Curiously, the expression of this antioxidant protein is repressed by the transcription factor c-Myc, in the absence of the HUWE1 ubiquitin ligase [55]. Thus, either targeting the glutathione S-transferase or, perhaps upstream, the HUWE1 ubiquitin ligase, may be relevant avenues for the development of therapies for iRR.

The higher UPS activity, favoring sarcomere turnover, a specific configuration of sarcomeric proteins isoforms, an improved mitochondrial function, the utilization of alternative energetic substrates and a better antioxidant depot are among the potential protective mechanisms proposed by proteomics to favor a complete recovery. Therewithal, this approach elicited relevant dysregulated processes associated with an incomplete LV mass regression, meriting further research. A remarkable activation of the immune system, particularly of the innate immune response was pointed out by FunRich analysis. GOEA further showed an upregulation of the complement system in the myocardium of iRR patients, which is an important arm of the innate immune system. The complement might probably be involved in clearing apoptotic cardiomyocytes, a biological process also mapped by GOEA (see the term “positive regulation of apoptotic cell clearance” in **Figure 2**). This is corroborated by DEP analysis, showing significant upregulation of complement component elements, such as complement C3 and by multivariate analysis, showing that complement factors D, C4-b and H-related protein are among the top 10 most important variables to discriminate iRR from cRR. While cardiomyocyte apoptosis is a well-established hallmark of LV remodeling in AS patients, due to the poor myocardial perfusion (the vasculature growth cannot keep up with cardiomyocyte growth) [50], the specific role of complement system in the setting of post-AVR RR requires more attention. Indeed, it has been previously reported the human heart itself can generate all elements of the complement system and that these increase and become activated after myocardial infarction [60], which is also the result of an ischemic insult. The same authors also concluded that complement activation may lead to chronic damage, as the expression of complement elements is perpetuated. Hence, it was hypothesized that AS patients with higher expression (and activity) of complement components had higher chances of showing iRR. The immunoblot detection in the validation cohort, although not confirmatory, provided reason to believe that high complement activity at the time of surgery, may be indicative of poorer outcomes, as C3 β chain was found tendentiously higher in patients with iRR. The influence of the complement system in the extent of RR will need further research, but current data points to a detrimental role. For instance, Hein and colleagues [61] reported that AS patients undergoing AVR with worse systolic function presented higher levels of complement C9-associated cell oncosis (ischemic cell death). The authors proposed that the reduced coronary flow reserve might underscore cardiomyocyte oncosis. Thus, it is conceivable that local complement activation and associated oncosis can be an important switcher between a complete and incomplete response to AVR. This idea is corroborated by the prevention of cardiac remodeling (hypertrophy, inflammation and fibrosis) in an

angiotensin II-induced model of hypertension with a complement C5a receptor antagonist [62]. Also supporting the deleterious effect of complement, it was reported that the terminal complement complex C5b-9 is capable of activating *in vitro* the NF-κB transcription factor [63], whose prolonged activation is associated to exacerbation of the inflammation and cell death [64].

The inflammatory process is indeed a relevant hallmark of myocardial remodeling. For example, the characterization of the myocardial proteome in a murine model of pressure overload shows an early upregulation of acute phase response signaling early after aortic constriction and a sustained organ inflammation with perpetuation of the constriction up to 42 days [20]. The present data points to the degree of acute phase response activation yet as another factor weighing on the development of iRR. As judged by PLS-DA, two acute phase proteins, haptoglobin and α-1-antichymotrypsin are among the ten most important proteins in discriminating subjects with cRR and iRR. Remarkably, haptoglobin presented with a VIP score >8, being the protein with the highest discrimination potential. This association with iRR may be related to increased oxidative stress, as haptoglobin displays antioxidant activity (UniProt). Curiously, a reduced level of circulating haptoglobin has been associated with hypertrophic cardiomyopathy [65]. While at a first glance this may seem contradictory, one should mind the comparison of two different biological samples (serum versus myocardium). The authors propose that serum depletion of haptoglobin is a consequence of outflow tract gradient induced-hemolysis, as haptoglobin rapidly scavenges free hemoglobin and the complexes are engulfed by macrophages. Furthermore, the main role of haptoglobin in myocardium should be to protect against oxidative stress and to promote adapative hypertrophy. In fact, haptoglobin knockout mice develop skeletal muscle atrophy, aggravated by oxidative stress [66]. Notwithstanding, the importance of haptoglobin in the setting of RR should be clarified, through animal models of aortic constriction-induced pressure overload as well as through serum screening in AS patients with different degrees of RR. In turn, the positive association between α-1-antichymotrypsin and iRR might also be regarded as a compensatory mechanism. This is because the conversion of angiotensinogen (4-fold higher in iRR, see **Table 3**) to angiotensin II (a major mediator of pressure overload deleterious effects) in heart relies mainly on chymase (and less on ACE) [67,68], and the α-1-antichymotrypsin specifically inhibits this enzyme. Still, as evidenced by FunRich and GOEA, the protective effects of haptoglobin and of α-1-antichymotrypsin may not suffice as patients with iRR appear to have higher levels of apoptosis and fibrosis. First, as opposed to iRR proteome, none of the proteins in cRR was mapped to “apoptosis”. Second, the term “regulation of transforming growth factor beta

production" was associated to iRR, which may result from cardiac fibroblast stimulation by angiotensin II [69]. Therefore, the proteome data is consistent with the view that marked replacement fibrosis (substitution of dead cardiomyocytes by ECM) is the point of no return for a poor outcome [50,69,70], in this case, post-AVR hypertrophy.

To gain insight into the signaling pathways and dysregulated kinases associated to iRR, the myocardial phosphoproteome was also characterized. Over 100 phosphopeptides were deemed dysregulated in RR, varying somewhere between 1.2- and 8.6-fold, except for the cardiac isoform of the myosin-binding protein C (cMyBP-C), whose Ser 286 phosphorylation was found astonishingly 280 times decreased in patients with iRR. This endorses the findings of Kooij *et al*. [71] who have reported reduced phosphorylation of Ser 284, Ser 286 and Thr 290 in end-stage heart failure patients. All these phosphorylation sites are localized in the M-domain and reduce binding to F-actin, thus likely affecting myocardial contractility. This study adds by showing that early pronounced cMyBP-C dephosphorylation on Ser 286 in AS patients undergoing AVR has great potential for prognosis purposes. Hence, large-scale validation of this finding is imperative.

Aiming to shed light into the mechanisms underlying the phenotypical divergence observed in cRR and iRR, FunRich pathway enrichment analysis was undertaken. In great agreement with proteome data, it was found a higher enrichment of proteins (12 versus 3) associated with the pro-apoptotic TRAIL signaling in patients that have developed iRR. The cytokine TRAIL activates the death receptor promoting FAS-associated death domain protein (FADD)-mediated caspase 8 activation, which may directly or indirectly (through the mitochondrial pathway) trigger apoptosis [72]. In an *in vitro* model of cardiomyocyte stretch-induced apoptosis, the involvement of TRAIL was evidenced, leading to direct and mitochondria-mediated apoptosis [73]. Due to the reported crosstalk of both death signaling routes, it is tempting to speculate that additional activation of the TRAIL pathway in AS patients may be a determinative factor for incomplete regression. Further research is needed to elucidate the relative relevance of both pathways in the context of iRR. Another interesting finding of pathway screening was the association of IFN γ pathway to patients with iRR. The IFN γ has been shown to mitigate cardiac hypertrophy in pressure overloaded models [74,75]. The superior activation of IFN γ may be interpreted as a compensatory mechanism. This is because IFN γ has been found to inhibit prostaglandin F2-α-induced hypertrophy observed in adult rat cardiomyocytes [74]. The myocardial release of prostaglandin F2-α is a consequence of pressure overload and may be stimulated by angiotensin II at least partly due to protein kinase C (PKC) activation [76]. Since cRR

patients presented a marked upregulation (>1.5-fold) of the negative regulator of the prostaglandin F2-α receptor (PTGFRN), it is plausible to hypothesize that this receptor inhibitor confers superior protection from hypertrophy than IFN γ. In fact, increased expression of IFN γ in PF is associated with chronic heart failure [77]. The prognostic potential of PTGFRN and of IFN γ should, thus, be further scrutinized in the future.

Beyond the association of TRAIL and IFN γ signaling cascades to iRR, pathway enrichment analysis also demonstrates a higher relevance of the pro-survival epidermal growth factor (EGF) receptor (erbB/EGFR) pathway in cRR. The protection conferred by EGF or neuregulins has been verified in an animal model of AS. Rohrbach and colleagues showed that erbB2 and erbB4 expression is similar to sham animals at early stages of myocardial remodeling (6 weeks), but are later depressed at the beginning of heart failure development (22 weeks) [78], thus implying that reduced flux through this pathway may underscore maladaptive remodeling.

The ultimate goal of the phosphoproteome analysis was to pinpoint potentially dysregulated kinases in iRR that may become surrogate therapeutic targets for iRR. Motif analysis readily envisioned what turned out to be a heterogeneous set of kinases associated with each phenotype (cRR and iRR), anticipating the involvement of a multitude of signaling events underscoring an incomplete response to AS treatment. Kinase prediction confirmed the implication of distinct kinase types. Hence, the analysis strategy consisted of extracting kinases with the highest number of associated phosphorylation events (10^{th} percentile for cRR and iRR). Through this approach, CK2, TAF and the family of IKK were associated to iRR, while GSK3 (α/β), DYRK2 and DYRK1A were deemed more active in cRR.

The CK2 is a pleiotropic kinase that regulates a myriad of cellular processes, such as cell cycle progression, apoptosis and transcription (UniProt), making hard to extrapolate its role in the context of RR. Different studies pertaining to heart pathology suggest an initially protective effect of CK2, that if maintained at the long-term, may become harmful. For instance, CK2 can phosphorylate the cytoplasmic tail of the ACE, promoting retention at the plasma membrane [79]. This mechanism may be a way to reduce local load of the pernicious angiotensin II, balancing the effects of pressure overload. However, as previously stated, chymase may be more relevant in this context [67,68] The activation of CK2 has also been demonstrated in a leporine model of myocardial ischemia, but it was found not to be related with the benefits provided by ischemic preconditioning in limiting infarct size [80]. Others have shown an upregulation of CK2 in non-infarcted heart and a concomitant downregulation in the infarct scar in a rat model of infarction. The same authors

proposed indeed that CK2 activation may drive the process of pathological hypertrophy [81]. Besides, different hypertrophic stimuli promote CK2 activation, leading to histone deacetylase (HDAC) 2 phosphorylation (Ser 394), which repress the expression of anti-hypertrophic genes [82]. Consistent with this, Chang and colleagues found a new highly phosphorylated motif (pSDxD) in hypertrophied hearts of a mouse model of aortic banding, which is easily recognized by CK2 (pS/TxxD/E) [25]. Based on the above motif analysis, it is likely that CK2 plays equally an important role in the human setting, specifically favoring an incomplete regression. This is because Glu (E) and Asp (D) represented the most frequent residues in the third C-terminal position of the peptide sequences associated to iRR, in obvious contrast with cRR, where the neutral amino acids Ser (S) and Ala (A) occupy the same position. The literature and the current work altogether point to the hypothesis of initial protection derived by CK2 activation in the compensated state of AS-induced myocardial remodeling that, if sustained in time, should favor an incomplete regression through the perpetuation of hypertrophic signaling. To date, no one has explored the roles of CK2 in the context of pressure overload-induced myocardial remodeling. Therefore, in the future, the effects of CK2 inhibition should be evaluated in the course of RR, since a therapeutic benefit is expected.

TAF1 followed as the second most important kinase in iRR. TAF1 is also the core scaffold of the transcription factor TFIID, which is part of the family of general transcription factors. Specifically, TFIID is important for the recognition of the promoter DNA and for the assembly of the pre-initiation complex required for RNA polymerase II-mediated transcription [83]. This is in line with the marked enrichment of proteins involved in “transcription” observed for iRR proteome (**Figure 1**). High rates of transcription probably sustain the expression of sarcomeric proteins explaining the exaggerated hypertrophic response observed in iRR patients. The relevance of TAF1 in keeping high transcriptional activity is corroborated by TAF1-mediated phosphorylation p53 on Thr 55, priming to murine double minute 2 (MDM2)-mediated degradation [84] and abrogating its cell growth inhibitory function. Furthermore, cardiac-specific p53 ablation results in hypertrophy and in heart failure, especially in older mice [85]. On the other hand, phenylephrine, a well-known pro-hypertrophic agent, induces TAF1 expression, suggesting once more that TAF1 regulates pro-hypertrophic gene expression [86]. Considering the potential detrimental role of TAF1 in RR, validation was attempted in a larger population. Unfortunately, this kinase could not be detected in the amount of protein available, likely due to its low expression.

The IKK family of kinases complete the group of kinases associated to iRR. This family comprise four kinases, the inhibitors of NF-κB (IκB) kinases α, β and ε, in addition to the TANK-binding kinase 1 (TBK1). In a steady-state, some NF-κB transcription factors are bound to IκB, which is responsible for their cytoplasmic sequestration. However, in response to a stimulus, all four, but mainly IKKα and IKKβ, can phosphorylate IκB, thereby promoting its UPS-mediated degradation and releasing NF-κB. This transcription factor can, thus, translocate to the nucleus where it regulates transcription of pro-inflammatory genes (e.g. TNF-α, interleukins 1 and 6) and pro-hypertrophic genes (e.g. c-myc) [64,87]. Hence, sustained activation of this pathway may be another reason why some patients end up showing iRR. This hypothesis is supported by a previous study showing activation of the NF-κB in a mouse model of hypertension-induced pressure overload and LV hypertrophy, partially mitigated by anti-hypertensive therapy [28]. Another evidence of the detrimental effects of NF-κB comes from a study showing that ablation of p65 (one of two NF-κB subunits) reduces hypertrophy and pathological remodeling as well as preserves heart's contractile performance in a mouse model of pressure overload [88]. From the study, it was also clear that NF-κB synergizes with NFAT in the activation of pro-hypertrophic genes.

Among the many common substrates of CK2, TAF1 and IKK, CAMK2 popped up because it is a key enzyme in the regulation of cardiomyocyte activity. Thus, its expression was validated in a larger population. Even though no differences between cRR and iRR were observed, a significant negative correlation with preoperative PWT and RWT became evident. This suggests that initial CAMK2 activation should be beneficial, by limiting hypertrophy. However, if short-term activation of CAMK2 is deemed protective, sustained activation is detrimental and is associated with maladaptive remodeling [89]. For instance, this kinase can activate the heat shock factor 1 transcription factor, leading to increased expression of the anti-apoptotic heat shock protein 70. However, permanent activation leads to the phosphorylation of the HDAC4, derepressing the myocyte enhancer factor 2 (MEF2) and leading to the expression of fetal genes. A final example is the ability of CAMK2 to activate the IKK-NFκB pathway, translating into increased expression of chemokines and, hence, inflammation and fibrosis [89,90]. Therefore, an emerging hypothesis is that patients with sustained activation of CAMK2 will have more chances of showing a poor outcome (iRR). The specific phosphorylated residues should explain the regulation of CAMK2 in the setting of AS-induced myocardial remodeling. Until now, from the three phosphosites identified, only Ser330 was found to be regulated under ischemia, according to PhosphoSitePlus database. Thus, it will be interesting to understand the pathological

significance of the remaining phosphosites (Ser 333 and Thr 337), particularly whether these PTMs perpetuate activation of CAMK2 in patients with iRR.

In the opposite side, the GSK3 kinases were associated to cRR. The GSK3 family comprises the kinases GSK3α and GSK3β, sharing a highly identical kinase domain, but not the entire set of substrates nor their function. As opposed to many kinases, the GSK3 are constitutively active and their inhibition may result from different stimuli [91]. Consequently, the association of GSK3 to cRR should be rather viewed as inhibition of GSK3 in iRR. This should explain why no differences were found between cRR and iRR in terms of total levels of GSK3α and β. In the future, the levels of phosphorylated GSK3α (Ser 21) and GSK3β (Ser 9) should be evaluated in AS patients, as this PTM is inhibitory [91]. An increased level of the phosphorylated levels is anticipated in patients showing a poor LV mass regression. Still, while some studies show that active GSK3α and GSK3β may reduce hypertrophy in the setting of pressure overload-induced LV hypertrophy [92,93], some controversy does exist regarding the protection conferred by these kinases (as reviewed by [91]) and, thus, the signaling mechanisms conferring protection require clarification.

Finally, the closely related kinases DYRK2 and DYRK1A emerged as the most important kinases in cRR. In addition to DYRK1B, 3 and 4, the kinases above complete the family of the dual-specificity tyrosine-regulated kinases, a group of pleiotropic, but highly conserved, proteins, also known as proline-directed (preference for Pro (P) in the P+1 position) kinases that regulate cell survival, differentiation and gene transcription [94,95]. In line with this, motif analysis showed a higher relative occupancy of Pro in the first C-terminal position to the phosphosite in the cRR. DYRK1A also detains some specificity for Arg (R) in the third N-terminal position to the phosphosite [94], and this amino acid configuration was more frequently found in the cRR motif logo. Evidence has been accumulating on the hypertrophy-limiting role of DYRK2 and DYRK1A. For instance, DYRK2 overexpression leads to reduced cardiomyocyte size and in halted hypertrophy in response to phenylephrine, by priming the eukaryotic initiation factor 2B to GSK3β-mediated inhibition, thereby blocking protein synthesis [96]. In turn, hyperhomocysteinemia-induced cardiac hypertrophy was sided with DYRK1A downregulation [97]. DYRK1A downregulation *de facto* promotes cardiac hypertrophy [98]. Besides, DYRK1A inhibits cardiomyocyte hypertrophy in response to phenylephrine and calcineurin (CaN) overexpression [98]. Intriguingly, a significant increase in DYRK1A protein levels was found in iRR patients. In fact, LVMi was tendentiously lower (p = 0.08) in iRR patients (130.9 versus 162.5 g/m^2 in cRR) before AVR. Hence, the association between high levels of DYRK1A and lower

hypertrophy is consistent. Notwithstanding, how can we explain the worse outcome in these patients? The explanation may be more complex than anticipated. It is well established that DYRK1A accumulates in response to NFAT activation (one of the most important hypertrophic transcription factors), leading to its cytosolic translocation, in a negative feedback loop [94,98]. The mechanism likely involves DYRK1A (or DYRK2)-mediated NFAT priming for GSK3 phosphorylation and subsequent inhibition [94]. To test a possible association between DYRK1A and NFAT, the protein levels of NFAT were also measured in the same population, but detection was inconclusive. Still, a significant correlation was found between CAMK2 and DYRK1A protein levels. CAMK2 is also known to inhibit NFAT, in a CaN-dependent manner [90], but protection is limited, since sustained activation promotes adverse remodeling through HDAC4 inhibition and MEF2-mediated derepression [99]. Thus, it is tempting to speculate that despite the continuous stimulation of DYRK1A expression, its protection is overridden in some individuals by inhibitory cues that are now starting to be disclosed (e.g. miR-199b [100]). This is because kinase prediction points to a lower activity of DYRK1A in iRR (the reader should recall that kinase ranking was based on the number of deemed phosphorylation events, an indirect approach for activity estimation), in spite of higher protein expression. Consequently, the clarification of DYRK1A inhibition mechanisms are required to understand the definitive role in the setting of iRR. Particularly, phosphatases targeting DYRK's activation loop (a conserved YxY motif) remain to identify [94], but the modulation of DYRK1A activity looks a promising approach to treat iRR. This idea is further explored in ***Chapter IV***. Last, but not least, DYRK1A relevance was also evidenced by a significant positive correlation with postoperative LVEDD and, more importantly, by a negative correlation with LV mass regression. Hence, DYRK1A myocardial expression might have prognostic value.

Notwithstanding the valuable insights into the mechanisms (and key molecular players) driving to iRR provided by the characterization of the myocardial (phospho)proteome, this work also has some limitations. First, a relatively small number of subjects was enrolled in the proteomics experiments. In spite of the access to a biobank of human samples, the population at scope is mainly composed by older patients showing several comorbidities. It is, thus, difficult to retrieve patients with isolated AS due to the high prevalence of coexistent CAD and other valve disorders. Still, an effort was made to minimize the interference of concurring pathologies, by excluding patients with severe forms of other valve diseases, with more than one stenotic coronary and/or that have experienced myocardial infarction. After the clinical constraints, there is also a technical limitation, regarding phosphopeptide enrichment. This technique requires a large amount of starting protein (typically 500 µg to

1 mg) and often myocardial biopsies are minute, not yielding enough protein material to proceed with the analysis. Anyhow, this work addressed the first characterization of the human myocardial (phospho)proteome in AS, comparing patients with different degrees of RR, and for the sake of discovery proteomics a high number of samples is not essential. Nonetheless, proteins emerging with high potential prognostic value or those that were considered surrogate targets of therapeutic modulation were validated in a larger number of patients (n = 14). Even so, these should be further scrutinized in an independent and larger cohort. A second limitation of this work is related to patients' follow-up. The evaluation of the post-AVR outcome relies on echocardiographic assessment of myocardial structure and function. Since this was a retrospective study it was not possible to compare echocardiographic at the same time-point. Data available spanned from four months up to three years (median was 9 months) after AVR, although it was previously reported that most of LV mass regression occurs within the first six months post-AVR [2,101]. Third, while AS patients included in proteomics analysis were quite homogenous concerning clinical variables and demographics, iRR patients presented higher BMI. Therefore, it is not possible to categorically exclude a potential implication of obesity in the process of RR. Although, protein validation was carried out in a population that did not present such difference. Finally, while kinase prediction was very important to identify potentially dysregulated kinases in the setting of RR, one has to acknowledge that implicated pathways depend on the cell type (cardiomyocytes, cardiac fibroblasts, smooth muscle cells …). Also, kinase *in silico* prediction with GPS is based on knowledge gathered *a priori*, precluding the identification of novel kinases and substrate relationships. Furthermore, no information on active/repressed phosphatases, equally important in the regulation of the signaling cascades, is possible to collect from this approach, but their role is acknowledged to be as important as kinases.

5. Conclusions

Myocardial proteome and phosphoproteome were characterized, for the first time, in AS patients with complete and incomplete RR. From over 1800 proteins and 22,000 phosphopeptides identified, a systems-level portrayal of dysregulated proteins, kinases, biological processes and pathways could be sketched. In much agreement with previous animal model studies of pressure overload-induced myocardial (reverse) remodeling, the

present approach suggests that patients with higher basal rates of transcription, lower protein metabolism and UPS activity, favoring hypertrophy, are in higher risk for an iRR. Moreover, greater activation of the acute-phase response and of the innate immune system and, remarkably, of the complement system, may also jeopardize the process of RR. In this regard, the activation of the TRAIL and IFN γ pathways deserve further attention. Considering the role of complement in clearing apoptotic cells, the prognostic role of complement C3 should be tested. Higher levels of this protein (and, most probably, of the membrane attack complex proteins – C5b-C9) may mark pronounced apoptosis and oncosis, favoring replacement fibrosis and, thus, a "point of no return" in the development of iRR. The association between complement and apoptotic cardiomyocytes in AS patients warrants, thus, more investigation. With the present approach it was also possible to pinpoint kinases that may regulate the process of RR and that may become important nodes of therapeutic regulation. These included CK2, TAF1 and the IKK family associated with a poor outcome and GSK3(α/β), DYRK2 and DYRK1A associated with a good outcome. DYRK1A, in particular, adds to C3 β chain as a protein with a potential prognostic role. DYRK1A has been established as an anti-hypertrophic kinase in other settings, but the increased levels found in iRR patients, despite higher predicted activity in cRR, challenges the idea of DYRK1A overexpression being protective. So, the identification of the specific mechanisms controlling the expression and activity of this kinase in the (reverse) remodeling myocardium is needed.

The present work was presented at the biennial meeting of the European Society of Cardiology Working Groups on Myocardial Function & Cellular Biology of the Heart that took place on May 9th-11th (2019) in Naples, Italy, under the title "Human myocardial phospho-proteome analysis evidences complement activation and deregulated kinases in post-aortic valve replacement incomplete reverse remodeling" (poster session).

6. References

[1] S.D. Culler, D.J. Cohen, P.P. Brown, A.D. Kugelmass, M.R. Reynolds, K. Ambrose, M.L. Schlosser, A.W. Simon, M.R. Katz, Trends in Aortic Valve Replacement Procedures Between 2009 and 2015: Has Transcatheter Aortic Valve Replacement Made a Difference?, Ann. Thorac. Surg. 105 (2018) 1137–1143. doi:10.1016/j.athoracsur.2017.10.057.

[2] R.W.W. Biederman, J.A. Magovern, S.B. Grant, R.B. Williams, J.A. Yamrozik, D.A. Vido, V.K.

Rathi, G. Rayarao, K. Caruppannan, M. Doyle, LV reverse remodeling imparted by aortic valve replacement for severe aortic stenosis; is it durable? A cardiovascular MRI study sponsored by the American Heart Association, J Cardiothorac Surg. 6 (2011) 1–8. doi:10.1186/1749-8090-6-53.

[3] T. Waszyrowski, J.D. Kasprzak, M. Krzemińska-Pakuła, J. Droż, A. Dziatkowiak, J. Zasłonka, Regression of left ventricular dilatation and hypertrophy after aortic valve replacement, Int. J. Cardiol. 57 (1996) 217–225. doi:10.1016/S0167-5273(96)02803-3.

[4] C. Gavina, I. Falcão-Pires, P. Pinho, M.-C. Manso, A. Gonçalves, F. Rocha-Gonçalves, A. Leite-Moreira, Relevance of residual left ventricular hypertrophy after surgery for isolated aortic stenosis, Eur. J. Cardio-Thoracic Surg. 49 (2015) 952–959. doi:10.1093/ejcts/ezv240.

[5] J.M. Beach, T. Mihaljevic, J. Rajeswaran, T. Marwick, S.T. Edwards, E.R. Nowicki, J. Thomas, L.G. Svensson, B. Griffin, A.M. Gillinov, E.H. Blackstone, Ventricular hypertrophy and left atrial dilatation persist and are associated with reduced survival after valve replacement for aortic stenosis, J. Thorac. Cardiovasc. Surg. 147 (2014) 362–369. doi:10.1016/j.jtcvs.2012.12.016.

[6] T. Hatani, T. Kitai, R. Murai, K. Kim, N. Ehara, A. Kobori, M. Kinoshita, S. Kaji, T. Tani, Y. Sasaki, T. Yamane, T. Koyama, M. Nasu, Y. Okada, Y. Furukawa, Associations of residual left ventricular and left atrial remodeling with clinical outcomes in patients after aortic valve replacement for severe aortic stenosis, J. Cardiol. 68 (2016) 241–247. doi:10.1016/j.jjcc.2015.09.017.

[7] C. Gavina, I. Falcão-Pires, J. Rodrigues, B. Marinho, N. Gonçalves, R. Lopes, M.J. Amorim, J. Almeida, P. Pinho, A. Gonçalves, F. Rocha-Gonçalves, A. Leite-Moreira, Load independent impairment of reverse remodeling after valve replacement in hypertensive aortic stenosis patients, Int. J. Cardiol. 170 (2014) 324–330. doi:10.1016/j.ijcard.2013.11.006.

[8] V.D. Bruno, P. Chivasso, F. Rapetto, G. Guida, E. Di Tommaso, H.M. Chau, H. Vohra, Impact of Body Mass Index on Short- and Long-Term Outcomes After Isolated First-Time Surgical Aortic Valve Replacement for Aortic Stenosis, J. Cardiothorac. Vasc. Anesth. (2019). doi:10.1053/j.jvca.2019.02.015.

[9] J.A.L. Vicente, I.L. Blasco, P.P. Perez, B.S. Sanchez, M.R.O. Nadal, J.R.R. Arroyo, M.G. Carretero, A.D.R. Ligorit, Impact of moderate coronary atherosclerosis on long-term left ventricular remodeling after aortic valve replacement, Cardiol. J. 18 (2011) 277–281.

[10] A. Kulik, I.G. Burwash, V. Kapila, T.G. Mesana, M. Ruel, Long-Term Outcomes After Valve Replacement for Low-Gradient Aortic Stenosis, Circulation. 114 (2006) I-553-I–558. doi:10.1161/CIRCULATIONAHA.105.001180.

[11] R.E. Zybach-Benz, B.C. Aeschbacher, M. Schwerzmann, Impact of left ventricular hypertrophy late after aortic valve replacement for aortic stenosis on cardiovascular morbidity and mortality, Int. J. Cardiol. 109 (2006) 41–47. doi:10.1016/j.ijcard.2005.05.050.

[12] N. Hanayama, G.T. Christakis, H.R. Mallidi, V. Rao, G. Cohen, B.S. Goldman, S.E. Fremes, C.D. Morgan, C.D. Joyner, Determinants of Incomplete Left Ventricular Mass Regression Following Aortic Valve Replacement for Aortic Stenosis, J. Card. Surg. 20 (2005) 307–313. doi:10.1111/j.1540-8191.2005.200485.x.

[13] K. Linhartová, J. Filipovský, R. Čerbák, G. Štěrbáková, I. Hanišová, V. Beránek, Severe aortic stenosis and its association with hypertension: Analysis of clinical and echocardiographic parameters, Blood Press. 16 (2007) 122–128. doi:10.1080/08037050701343241.

[14] H.W. Chang, K.H. Kim, J.S. Kim, K.H. Kim, Y.J. Kim, Relationship between morphologic features of myocardial tissue and left ventricular function in patients with aortic valve disease and left ventricular hypertrophy, J. Heart Valve Dis. 22 (2013) 476–483.

[15] O. Lund, K. Emmertsen, I. Dørup, F.T. Jensen, C. Flø, Regression of left ventricular hypertrophy during 10 years after valve replacement for aortic stenosis is related to the preoperative risk profile, Eur. Heart J. 24 (2003) 1437–1446. doi:10.1016/S0195-668X(03)00316-6.

[16] M. Vaduganathan, R. Lee, A.J. Beckham, A.-C. Andrei, B. Lapin, N.J. Stone, E.C. McGee, S.C. Malaisrie, P. Kansal, R.A. Silverberg, D.M. Lloyd-Jones, P.M. McCarthy, Relation of Body Mass Index to Late Survival After Valvular Heart Surgery, Am. J. Cardiol. 110 (2012) 1667–1678. doi:10.1016/j.amjcard.2012.07.041.

[17] N.J. Howell, B.E. Keogh, V. Barnet, R.S. Bonser, T.R. Graham, S.J. Rooney, I.C. Wilson, D. Pagano, Patient-prosthesis mismatch does not affect survival following aortic valve replacement, Eur. J. Cardio-Thoracic Surg. 30 (2006) 10–14.

doi:10.1016/j.ejcts.2006.03.046.
[18] T. Nakamura, K. Toda, T. Kuratani, S. Miyagawa, Y. Yoshikawa, S. Fukushima, S. Saito, D. Yoshioka, N. Kashiyama, T. Daimon, Y. Sawa, Diabetes Mellitus Impairs Left Ventricular Mass Regression after Surgical or Transcatheter Aortic Valve Replacement for Severe Aortic Stenosis, Hear. Lung Circ. 25 (2016) 68–74. doi:10.1016/j.hlc.2015.05.019.
[19] M.P.Y. Lam, P. Ping, E. Murphy, Proteomics Research in Cardiovascular Medicine and Biomarker Discovery, J. Am. Coll. Cardiol. 68 (2016) 2819–2830. doi:10.1016/j.jacc.2016.10.031.
[20] J. Rüdebusch, A. Benkner, A. Poesch, M. Dörr, U. Völker, K. Grube, E. Hammer, S.B. Felix, Dynamic adaptation of myocardial proteome during heart failure development, PLoS One. 12 (2017) e0185915. doi:10.1371/journal.pone.0185915.
[21] K. Kotlo, K.R. Johnson, J.M. Grillon, D.L. Geenen, P. DeTombe, R.S. Danziger, Phosphoprotein abundance changes in hypertensive cardiac remodeling, J. Proteomics. 77 (2012) 1–13. doi:10.1016/j.jprot.2012.05.041.
[22] H. Bugger, M. Schwarzer, D. Chen, A. Schrepper, P.A. Amorim, M. Schoepe, T.D. Nguyen, F.W. Mohr, O. Khalimonchuk, B.C. Weimer, T. Doenst, Proteomic remodelling of mitochondrial oxidative pathways in pressure overload-induced heart failure, Cardiovasc. Res. 85 (2009) 376–384. doi:10.1093/cvr/cvp344.
[23] T. Köcher, P. Pichler, M. Schutzbier, C. Stingl, A. Kaul, N. Teucher, G. Hasenfuss, J.M. Penninger, K. Mechtler, High Precision Quantitative Proteomics Using iTRAQ on an LTQ Orbitrap: A New Mass Spectrometric Method Combining the Benefits of All, J. Proteome Res. 8 (2009) 4743–4752. doi:10.1021/pr900451u.
[24] H.K. Kwon, H. Jeong, D. Hwang, Z.-Y. Park, Comparative proteomic analysis of mouse models of pathological and physiological cardiac hypertrophy, with selection of biomarkers of pathological hypertrophy by integrative proteogenomics, Biochim. Biophys. Acta - Proteins Proteomics. 1866 (2018) 1043–1054. doi:10.1016/j.bbapap.2018.07.006.
[25] Y.-W. Chang, Y.-T. Chang, Q. Wang, J.J.-C. Lin, Y.-J. Chen, C.-C. Chen, Quantitative Phosphoproteomic Study of Pressure-Overloaded Mouse Heart Reveals Dynamin-Related Protein 1 as a Modulator of Cardiac Hypertrophy, Mol. &Amp; Cell. Proteomics. 12 (2013) 3094–3107. doi:10.1074/mcp.M113.027649.
[26] J. Gallego-Delgado, A. Lazaro, J.I. Osende, M.G. Barderas, M.C. Duran, F. Vivanco, J. Egido, Comparison of the Protein Profile of Established and Regressed Hypertension-Induced Left Ventricular Hypertrophy, J. Proteome Res. 5 (2006) 404–413. doi:10.1021/pr0503275.
[27] X. Jin, L. Xia, L.-S. Wang, J.-Z. Shi, Y. Zheng, W.-L. Chen, L. Zhang, Z.-G. Liu, G.-Q. Chen, N.-Y. Fang, Differential protein expression in hypertrophic heart with and without hypertension in spontaneously hypertensive rats, Proteomics. 6 (2006) 1948–1956. doi:10.1002/pmic.200500337.
[28] J. Gallego-Delgado, A. Lazaro, J.I. Osende, V. Esteban, M.G. Barderas, C. Gomez-Guerrero, R. Vega, F. Vivanco, J. Egido, Proteomic Analysis of Early Left Ventricular Hypertrophy Secondary to Hypertension: Modulation by Antihypertensive Therapies, J. Am. Soc. Nephrol. 17 (2006) S159–S164. doi:10.1681/ASN.2006080937.
[29] A. Rassa, F. Zahr, Hypertension and Aortic Stenosis: A Review, Curr. Hypertens. Rev. 14 (2018) 6–14. doi:10.2174/1573402114666180416161326.
[30] L. Liu, W. Wang, X. Meng, J. Gao, H. Wu, P. Wang, W. Wu, L. Wang, L. Ma, W. Zhang, Left ventricular hypertrophy induced by abdominal aortic banding and its prevention by angiotensin receptor blocker telmisartan—a proteomic analysis, J. Physiol. Biochem. 66 (2010) 329–338. doi:10.1007/s13105-010-0039-1.
[31] D. Dao-Fu, H.E. J., C. Tony, M.L. G., B.N. B., T. Lauren, B.R. P., C.D. A., S.N. J., S.H. H., T. Rong, M.M. J., R.P. S., Global Proteomics and Pathway Analysis of Pressure-Overload–Induced Heart Failure and Its Attenuation by Mitochondrial-Targeted Peptides, Circ. Hear. Fail. 6 (2013) 1067–1076. doi:10.1161/CIRCHEARTFAILURE.113.000406.
[32] A. Rodrigue-Way, D. Burkhoff, B.J. Geesaman, S. Golden, J. Xu, M.J. Pollman, M. Donoghue, R. Jeyaseelan, S. Houser, R.E. Breitbart, A. Marks, S. Acton, Sarcomeric genes involved in reverse remodeling of the heart during left ventricular assist device support, J. Hear. Lung Transplant. 24 (2005) 73–80. doi:10.1016/j.healun.2003.10.016.
[33] R.A. de Weger, M.E.I. Schipper, E.S. Koning, P. van der Weide, M.F.M. van Oosterhout, R. Quadir, H. Steenbergen-Nakken, J.R. Lahpor, N. de Jonge, N. Bovenschen, Proteomic profiling of the human failing heart after left ventricular assist device support, J. Hear. Lung

Transplant. 30 (2011) 497–506. doi:10.1016/j.healun.2010.11.011.
[34] J.H. Shahinian, B. Mayer, S. Tholen, K. Brehm, M.L. Biniossek, H. Füllgraf, S. Kiefer, U. Heizmann, C. Heilmann, F. Rüter, M. Grapow, O.T. Reuthebuch, F. Eckstein, F. Beyersdorf, O. Schilling, M. Siepe, Proteomics highlights decrease of matricellular proteins in left ventricular assist device therapy, Eur. J. Cardio-Thoracic Surg. 51 (2017) 1063–1071. doi:10.1093/ejcts/ezx023.
[35] I. Shimizu, T. Minamino, Physiological and pathological cardiac hypertrophy, J. Mol. Cell. Cardiol. 97 (2016) 245–262. doi:10.1016/j.yjmcc.2016.06.001.
[36] R.M. Lang, L.P. Badano, V. Mor-Avi, J. Afilalo, A. Armstrong, L. Ernande, F.A. Flachskampf, E. Foster, S.A. Goldstein, T. Kuznetsova, P. Lancellotti, D. Muraru, M.H. Picard, E.R. Rietzschel, L. Rudski, K.T. Spencer, W. Tsang, J.-U. Voigt, Recommendations for Cardiac Chamber Quantification by Echocardiography in Adults: An Update from the American Society of Echocardiography and the European Association of Cardiovascular Imaging, Eur. Hear. J. - Cardiovasc. Imaging. 16 (2015) 233–271. doi:10.1093/ehjci/jev014.
[37] Y. Perez-Riverol, A. Csordas, J. Bai, M. Bernal-Llinares, S. Hewapathirana, D.J. Kundu, A. Inuganti, J. Griss, G. Mayer, M. Eisenacher, E. Pérez, J. Uszkoreit, J. Pfeuffer, T. Sachsenberg, S. Yilmaz, S. Tiwary, J. Cox, E. Audain, M. Walzer, A.F. Jarnuczak, T. Ternent, A. Brazma, J.A. Vizcaíno, The PRIDE database and related tools and resources in 2019: improving support for quantification data, Nucleic Acids Res. 47 (2019) D442–D450. doi:10.1093/nar/gky1106.
[38] J. Cox, M.Y. Hein, C.A. Luber, I. Paron, N. Nagaraj, M. Mann, Accurate Proteome-wide Label-free Quantification by Delayed Normalization and Maximal Peptide Ratio Extraction, Termed MaxLFQ, Mol. Cell. Proteomics. 13 (2014) 2513–2526. doi:10.1074/mcp.M113.031591.
[39] M. Pathan, S. Keerthikumar, C.-S. Ang, L. Gangoda, C.Y.J. Quek, N.A. Williamson, D. Mouradov, O.M. Sieber, R.J. Simpson, A. Salim, A. Bacic, A.F. Hill, D.A. Stroud, M.T. Ryan, J.I. Agbinya, J.M. Mariadason, A.W. Burgess, S. Mathivanan, FunRich: An open access standalone functional enrichment and interaction network analysis tool, Proteomics. 15 (2015) 2597–2601. doi:10.1002/pmic.201400515.
[40] G. Bindea, B. Mlecnik, H. Hackl, P. Charoentong, M. Tosolini, A. Kirilovsky, W.-H. Fridman, F. Pagès, Z. Trajanoski, J. Galon, ClueGO: a Cytoscape plug-in to decipher functionally grouped gene ontology and pathway annotation networks., Bioinformatics. 25 (2009) 1091–1093. doi:10.1093/bioinformatics/btp101.
[41] Y. Xue, F. Zhou, M. Zhu, K. Ahmed, G. Chen, X. Yao, GPS: a comprehensive www server for phosphorylation sites prediction, Nucleic Acids Res. 33 (2005) W184–W187. doi:10.1093/nar/gki393.
[42] U.K. Laemmli, Cleavage of structural proteins during the assembly of the head of bacteriophage T4, Nature. 227 (1970) 680–685. doi:10.1038/227680a0.
[43] M.A.S. Fortes, G.N. Marzuca-Nassr, K.F. Vitzel, C.H. da Justa Pinheiro, P. Newsholme, R. Curi, Housekeeping proteins: How useful are they in skeletal muscle diabetes studies and muscle hypertrophy models?, Anal. Biochem. 504 (2016) 38–40. doi:10.1016/j.ab.2016.03.023.
[44] H. Baumgartner, J. Hung, J. Bermejo, J.B. Chambers, A. Evangelista, B.P. Griffin, B. Iung, C.M. Otto, P.A. Pellikka, M. Quiñones, Echocardiographic Assessment of Valve Stenosis: EAE/ASE Recommendations for Clinical Practice, J. Am. Soc. Echocardiogr. 22 (2009) 1–23. doi:10.1016/j.echo.2008.11.029.
[45] K. Sugiyama, Anti-lipopolysaccharide activity of histatins, peptides from human saliva, Experientia. 49 (1993) 1095–1097.
[46] Y. Lei, H. Wen, J.P.Y. Ting, The NLR protein, NLRX1, and its partner, TUFM, reduce type I interferon, and enhance autophagy, Autophagy. 9 (2013) 432–433. doi:10.4161/auto.23026.
[47] E. Łukawska, M. Polcyn-Adamczak, Z.I. Niemir, The role of the alternative pathway of complement activation in glomerular diseases, Clin. Exp. Med. 18 (2018) 297–318. doi:10.1007/s10238-018-0491-8.
[48] Y. Gwack, S. Sharma, J. Nardone, B. Tanasa, A. Iuga, S. Srikanth, H. Okamura, D. Bolton, S. Feske, P.G. Hogan, A. Rao, A genome-wide Drosophila RNAi screen identifies DYRK-family kinases as regulators of NFAT, Nature. 441 (2006) 646–650. doi:10.1038/nature04631.
[49] H. Taegtmeyer, S. Sen, D. Vela, Return to the fetal gene program, Ann. N. Y. Acad. Sci. 1188 (2010) 191–198. doi:10.1111/j.1749-6632.2009.05100.x.
[50] B.R. Lindman, M.-A. Clavel, P. Mathieu, B. Iung, P. Lancellotti, C.M. Otto, P. Pibarot, Calcific

aortic stenosis, Nat. Rev. Dis. Prim. 2 (2016) 16006. doi:10.1038/nrdp.2016.6.
[51] M.S. Willis, A. Bevilacqua, T. Pulinilkunnil, P. Kienesberger, M. Tannu, C. Patterson, The role of ubiquitin ligases in cardiac disease, J. Mol. Cell. Cardiol. 71 (2014) 43–53. doi:10.1016/j.yjmcc.2013.11.008.
[52] M. Willis, C. Patterson, Proteotoxicity and Cardiac Dysfunction — Alzheimer's Disease of the Heart?, N Engl J Med. 368 (2013) 455–464. doi:doi: 10.1056/nejmra1106180.
[53] H. Shih, B. Lee, R.J. Lee, A.J. Boyle, The Aging Heart and Post-Infarction Left Ventricular Remodeling, J. Am. Coll. Cardiol. 57 (2011) 9–17. doi:10.1016/j.jacc.2010.08.623.
[54] M. Gaudino, F. Alessandrini, F. Glieca, N. Luciani, C. Cellini, C. Pragliola, M. Morelli, C. Canosa, G. Nasso, G. Possati, Survival after aortic valve replacement for aortic stenosis: does left ventricular mass regression have a clinical correlate?, Eur Hear. J. 26 (2005) 51–57. doi:10.1093/eurheartj/ehi012.
[55] K. Dadson, L. Hauck, Z. Hao, D. Grothe, V. Rao, T.W. Mak, F. Billia, The E3 ligase Mule protects the heart against oxidative stress and mitochondrial dysfunction through Myc-dependent inactivation of Pgc-1α and Pink1, Sci. Rep. 7 (2017) 41490. doi:10.1038/srep41490.
[56] S. Ayyadevara, F. Mercanti, X. Wang, S.G. Mackintosh, A.J. Tackett, S.V.S. Prayaga, F. Romeo, R.J. Shmookler Reis, J.L. Mehta, Age- and Hypertension-Associated Protein Aggregates in Mouse Heart Have Similar Proteomic Profiles., Hypertension. 67 (2016) 1006–1013. doi:10.1161/HYPERTENSIONAHA.115.06849.
[57] R.C. Fentzke, S.H. Buck, J.R. Patel, H. Lin, B.M. Wolska, M.O. Stojanovic, A.F. Martin, R.J. Solaro, R.L. Moss, J.M. Leiden, Impaired cardiomyocyte relaxation and diastolic function in transgenic mice expressing slow skeletal troponin I in the heart, J. Physiol. 517 (1999) 143–157. doi:10.1111/j.1469-7793.1999.0143z.x.
[58] K.J. Drake, V.Y. Sidorov, O.P. Mcguinness, D.H. Wasserman, J.P. Wikswo, Amino acids as metabolic substrates during cardiac ischemia, Exp. Biol. Med. 237 (2012) 1369–1378. doi:10.1258/ebm.2012.012025.
[59] D.-F. Dai, E.J. Hsieh, Y. Liu, T. Chen, R.P. Beyer, M.T. Chin, M.J. MacCoss, P.S. Rabinovitch, Mitochondrial proteome remodelling in pressure overload-induced heart failure: the role of mitochondrial oxidative stress, Cardiovasc. Res. 93 (2011) 79–88. doi:10.1093/cvr/cvr274.
[60] Y. Koji, S. Claudia, M.E. G., M.P. L., Human Heart Generates Complement Proteins That Are Upregulated and Activated After Myocardial Infarction, Circ. Res. 83 (1998) 860–869. doi:10.1161/01.RES.83.8.860.
[61] H. Stefan, A. Eyal, K. Sawa, S. Markus, E. Albrecht, P. Victoria, B.E. P., K. Wolf-Peter, S. Jutta, Progression From Compensated Hypertrophy to Failure in the Pressure-Overloaded Human Heart, Circulation. 107 (2003) 984–991. doi:10.1161/01.CIR.0000051865.66123.B7.
[62] C. Zhang, Y. Li, C. Wang, Y. Wu, J. Du, Antagonist of C5aR Prevents Cardiac Remodeling in Angiotensin II–Induced Hypertension, Am. J. Hypertens. 27 (2014) 857–864. doi:10.1093/ajh/hpt274.
[63] T.P. Zwaka, D. Manolov, C. Özdemir, N. Marx, Z. Kaya, M. Kochs, M. Höher, V. Hombach, J. Torzewski, Complement and Dilated Cardiomyopathy: A Role of Sublytic Terminal Complement Complex-Induced Tumor Necrosis Factor-α Synthesis in Cardiac Myocytes, Am. J. Pathol. 161 (2002) 449–457. doi:10.1016/S0002-9440(10)64201-0.
[64] J.W. Gordon, J.A. Shaw, L.A. Kirshenbaum, Multiple Facets of NF-κB in the Heart, Circ. Res. 108 (2011) 1122–1132. doi:10.1161/CIRCRESAHA.110.226928.
[65] E. Orenes-Piñero, D. Hernández-Romero, C. De Torre, J.A. Vilchez, M. Martínez, A.I. Romero-Aniorte, V. Climent, A. García-Honrubia, M. Valdés, F. Marín, Identification and confirmation of haptoglobin as a potential serum biomarker in hypertrophic cardiomyopathy using proteomic approaches, Ann. Med. 45 (2013) 341–347. doi:10.3109/07853890.2013.792555.
[66] E. Bertaggia, G. Scabia, S. Dalise, F. Lo Verso, F. Santini, P. Vitti, C. Chisari, M. Sandri, M. Maffei, Haptoglobin Is Required to Prevent Oxidative Stress and Muscle Atrophy, PLoS One. 9 (2014) e100745. doi:10.1371/journal.pone.0100745.
[67] S.J. Forrester, G.W. Booz, C.D. Sigmund, T.M. Coffman, T. Kawai, V. Rizzo, R. Scalia, S. Eguchi, Angiotensin II Signal Transduction: An Update on Mechanisms of Physiology and Pathophysiology, Physiol. Rev. 98 (2018) 1627–1738. doi:10.1152/physrev.00038.2017.
[68] M. Shimizu, R. Tanaka, T. Fukuyama, R. Aaoki, K. Orito, Y. Yamane, Cardiac Remodeling and Angiotensin II-Forming Enzyme Activity of the Left Ventricle in Hamsters with Chronic

Pressure Overload Induced by Ascending Aortic Stenosis, J. Vet. Med. Sci. 68 (2006) 271–276. doi:10.1292/jvms.68.271.
[69] C. Gavina, I. Falcão-Pires, F. Rocha-Goncalves, A. Leite-Moreira, Left Ventricular Hypertrophy in Isolated Aortic Stenosis: Primetime for the Ventricle, Curr. Pharm. Biotechnol. 13 (2012) 2503–2514. doi:10.2174/1389201011208062503.
[70] M.R. Dweck, N.A. Boon, D.E. Newby, Calcific Aortic Stenosis: A Disease of the Valve and the Myocardium, J. Am. Coll. Cardiol. 60 (2012) 1854–1863. doi:10.1016/j.jacc.2012.02.093.
[71] V. Kooij, R.J. Holewinski, A.M. Murphy, J.E. Van Eyk, Characterization of the cardiac myosin binding protein-C phosphoproteome in healthy and failing human hearts, J. Mol. Cell. Cardiol. 60 (2013) 116–120. doi:10.1016/j.yjmcc.2013.04.012.
[72] A. Thorburn, Tumor Necrosis Factor-Related Apoptosis-Inducing Ligand (TRAIL) Pathway Signaling, J. Thorac. Oncol. 2 (2007) 461–465. doi:10.1097/JTO.0b013e31805fea64.
[73] X. Liao, X. Wang, Y. Gu, Q. Chen, L.-Y. Chen, Involvement of death receptor signaling in mechanical stretch-induced cardiomyocyte apoptosis, Life Sci. 77 (2005) 160–174. doi:10.1016/j.lfs.2004.11.029.
[74] H. Jin, W. Li, R. Yang, A. Ogasawara, H. Lu, N.F. Paoni, Inhibitory effects of interferon-γ on myocardial hypertrophy, Cytokine. 31 (2005) 405–414. doi:10.1016/j.cyto.2005.06.013.
[75] K. Akihiko, I. Yuko, F. Machi, N. Mizuho, K. Yumi, T. Akira, M. Naofumi, K. Toshikazu, Protective Roles of Interferon-γ in Cardiac Hypertrophy Induced by Sustained Pressure Overload, J. Am. Heart Assoc. 7 (2019) e008145. doi:10.1161/JAHA.117.008145.
[76] G.K. Oriji, Angiotensin II stimulates hypertrophic growth of cultured neonatal rat ventricular myocytes: roles of PCK and PGF2alpha, Prostaglandins, Leukot. Essent. Fat. Acids. 62 (2000) 233–237. doi:10.1054/plef.2000.0148.
[77] R. Iskandar, S. Liu, F. Xiang, W. Chen, L. Li, W. Qin, F. Huang, X. Chen, Expression of pericardial fluid T-cells and related inflammatory cytokines in patients with chronic heart failure, Exp. Ther. Med. 13 (2017) 1850–1858. doi:10.3892/etm.2017.4202.
[78] R. Susanne, Y. Xinhua, W.E. O., H. Faisal, B. Jozef, M.M. A., L.B. H., Neuregulin in Cardiac Hypertrophy in Rats With Aortic Stenosis , Circulation. 100 (1999) 407–412. doi:10.1161/01.CIR.100.4.407.
[79] K. Karin, S. Firouzeh, M.-E. Werner, B. Rudi, F. Ingrid, CK2 Phosphorylates the Angiotensin-Converting Enzyme and Regulates Its Retention in the Endothelial Cell Plasma Membrane, Circ. Res. 91 (2002) 749–756. doi:10.1161/01.RES.0000038114.17939.C8.
[80] S.O. Kim, C.P. Baines, S.D. Critz, S.L. Pelech, S. Katz, J.M. Downey, M. V Cohen, Ischemia induced activation of heat shock protein 27 kinases and casein kinase 2 in the preconditioned rabbit heart, Biochem. Cell Biol. 77 (1999) 559–567. doi:10.1139/o99-065.
[81] Y.-J. Xu, D. Chapman, I.M.C. Dixon, R. Sethi, X. Guo, N.S. Dhalla, Differential gene expression in infarct scar and viable myocardium from rat heart following coronary ligation, J. Cell. Mol. Med. 8 (2004) 85–92. doi:10.1111/j.1582-4934.2004.tb00262.x.
[82] E.G. Hyeon, C.Y. Kuk, K. Jeong-Hyeon, S. Sera, C. Nakwon, K. Yoojung, J. Hosouk, K. Hyung-Seok, N. Kwang-Il, K.H. Jin, K. Hyun, Casein Kinase-2α1 Induces Hypertrophic Response by Phosphorylation of Histone Deacetylase 2 S394 and its Activation in the Heart, Circulation. 123 (2011) 2392–2403. doi:10.1161/CIRCULATIONAHA.110.003665.
[83] R.K. Louder, Y. He, J.R. López-Blanco, J. Fang, P. Chacón, E. Nogales, Structure of promoter-bound TFIID and model of human pre-initiation complex assembly, Nature. 531 (2016) 604. doi:10.1038/nature17394.
[84] H.-H. Li, A.G. Li, H.M. Sheppard, X. Liu, Phosphorylation on Thr-55 by TAF1 Mediates Degradation of p53: A Role for TAF1 in Cell G1 Progression, Mol. Cell. 13 (2004) 867–878. doi:10.1016/S1097-2765(04)00123-6.
[85] J. Wiley, Antimicrobial peptides of the oral cavity, 51 (2009) 152–180.
[86] T. Santalucía, M. Sánchez-Feutrie, L.E. Felkin, P.K. Bhavsar, P.J.R. Barton, A. Zorzano, M.H. Yacoub, N.J. Brand, Phenylephrine requires the TATA box to activate transcription of GLUT1 in neonatal rat cardiac myocytes, J. Mol. Cell. Cardiol. 38 (2005) 677–684. doi:10.1016/j.yjmcc.2005.02.013.
[87] H. Häcker, M. Karin, Regulation and Function of IKK and IKK-Related Kinases, Sci. STKE. 2006 (2006) re13. doi:10.1126/stke.3572006re13.
[88] L. Qinghang, C. Yi, A.-M. Mannix, M.J. D., Interaction Between NFκB and NFAT Coordinates Cardiac Hypertrophy and Pathological Remodeling, Circ. Res. 110 (2012) 1077–1086. doi:10.1161/CIRCRESAHA.111.260729.

[89] J. Beckendorf, M.M.G. van den Hoogenhof, J. Backs, Physiological and unappreciated roles of CaMKII in the heart, Basic Res. Cardiol. 113 (2018) 29. doi:10.1007/s00395-018-0688-8.
[90] D. Matthias, von der L. Albert, K.H. A., B. Johannes, Calcium Signaling and Transcriptional Regulation in Cardiomyocytes, Circ. Res. 121 (2017) 1000–1020. doi:10.1161/CIRCRESAHA.117.310355.
[91] L. Hind, A. Firdos, W. James, F. Thomas, The GSK-3 Family as Therapeutic Target for Myocardial Diseases, Circ. Res. 116 (2015) 138–149. doi:10.1161/CIRCRESAHA.116.303613.
[92] A. Tateishi, M. Matsushita, T. Asai, Z. Masuda, M. Kuriyama, K. Kanki, K. Ishino, M. Kawada, S. Sano, H. Matsui, Effect of inhibition of glycogen synthase kinase-3 on cardiac hypertrophy during acute pressure overload, Gen. Thorac. Cardiovasc. Surg. 58 (2010) 265–270. doi:10.1007/s11748-009-0505-2.
[93] P. Zhai, S. Gao, E. Holle, X. Yu, A. Yatani, T. Wagner, J. Sadoshima, Glycogen Synthase Kinase-3α Reduces Cardiac Growth and Pressure Overload-induced Cardiac Hypertrophy by Inhibition of Extracellular Signal-regulated Kinases, J. Biol. Chem. 282 (2007) 33181–33191. doi:10.1074/jbc.M705133200.
[94] S. Aranda, A. Laguna, S. de la Luna, DYRK family of protein kinases: evolutionary relationships, biochemical properties, and functional roles, FASEB J. 25 (2010) 449–462. doi:10.1096/fj.10-165837.
[95] U. Soppa, W. Becker, DYRK protein kinases, Curr. Biol. 25 (2015) R488–R489. doi:10.1016/j.cub.2015.02.067.
[96] C.S. Weiss, M.M. Ochs, M. Hagenmueller, M.R. Streit, P. Malekar, J.H. Riffel, S.J. Buss, K.H. Weiss, J. Sadoshima, H.A. Katus, S.E. Hardt, DYRK2 Negatively Regulates Cardiomyocyte Growth by Mediating Repressor Function of GSK-3β on eIF2Bε, PLoS One. 8 (2013) e70848. doi:10.1371/journal.pone.0070848.
[97] L. Raaf, C. Noll, M. Cherifi, Y. Benazzoug, J.-M. Delabar, N. Janel, Hyperhomocysteinemia-induced Dyrk1a downregulation results in cardiomyocyte hypertrophy in rats, Int. J. Cardiol. 145 (2010) 306–307. doi:10.1016/j.ijcard.2009.10.043.
[98] C. Kuhn, D. Frank, R. Will, C. Jaschinski, R. Frauen, H.A. Katus, N. Frey, DYRK1A Is a Novel Negative Regulator of Cardiomyocyte Hypertrophy, J. Biol. Chem. . 284 (2009) 17320–17327. doi:10.1074/jbc.M109.006759.
[99] K.M. M., L.L. H., K. Stanislav, H. Marc-Oscar, O. Ulrike, K. Michael, R. Jan-Christian, N. Kay, S.M. D., H.J. A., D. Dobromir, M. Christoph, M.L. S., G. Hermann-Josef, K.H. A., O.E. N., B. Johannes, Cardiac CaM Kinase II Genes δ and γ Contribute to Adverse Remodeling but Redundantly Inhibit Calcineurin-Induced Myocardial Hypertrophy, Circulation. 130 (2014) 1262–1273. doi:10.1161/CIRCULATIONAHA.114.006185.
[100] P.A. da Costa Martins, K. Salic, M.M. Gladka, A.-S. Armand, S. Leptidis, H. el Azzouzi, A. Hansen, C.J. Coenen-de Roo, M.F. Bierhuizen, R. van der Nagel, J. van Kuik, R. de Weger, A. de Bruin, G. Condorelli, M.L. Arbones, T. Eschenhagen, L.J. De Windt, MicroRNA-199b targets the nuclear kinase Dyrk1a in an auto-amplification loop promoting calcineurin/NFAT signalling, Nat. Cell Biol. 12 (2010) 1220–1227. doi:10.1038/ncb2126.
[101] U.C. Sharma, P. Barenburg, S. Pokharel, W.R.M. Dassen, Y.M. Pinto, J.G. Maessen, Systematic review of the outcome of aortic valve replacement in patients with aortic stenosis, Ann Thorac Surg. 78 (2004) 90–95. doi:10.1016/j.athoracsur.2004.02.020.

Chapter III

Preoperative myocardial expression of E3 ubiquitin ligases in aortic stenosis patients undergoing valve replacement and their clinical correlates

Contents

Abstract

The process of myocardial structure and function normalization, or reverse remodeling, initiated by aortic valve replacement is shaped by a multitude of factors that, in combination, determine a complete or incomplete response. In the previous ***Chapter II***, the profiling of myocardial proteome evoked the dysregulation of some biological processes as potential brakes in myocardial recovery. These included, for example, higher transcriptional activity, the activation of the innate immune (and complement) response or the activation of the acute-phase response. In addition, proteome analysis evoked that the extent of reverse remodeling may as well depend on how well ubiquitin-proteasome system tackle hypertrophy. To further explore this idea, the total levels of ubiquitin-tagged protein and ubiquitin ligases were assessed in the left ventricle collected from patients undergoing valve replacement and their association to the degree of reverse remodeling was tested. Correlation analysis with clinical data demonstrated that Muscle Ring Finger 1 is negatively associated with postoperative interventricular septum thickness, a marker of hypertrophy. No significant correlations were found with left ventricle mass regression. Nonetheless, a trend for a negative association between the ligase Murine Double Minute 2 and mass regression points to the need for confirmatory animal models studies on whether this activation is protective or detrimental. The association between the preoperative myocardial levels of ubiquitin and its ligases and hypertrophy echocardiographic parameters corroborates the proteomics findings, strengthening the hypothesis that targeting this system in incomplete reverse remodeling may be of therapeutic relevance.

1. Background

As terminally differentiated, post-mitotic cells, the cardiomyocytes have low regenerative capacity. Therefore, the ubiquitin-proteasome system (UPS) is, in addition to the autophagic pathway, essential for protein turnover; ergo for the regulation of cardiac mass [1,2]. Three enzyme classes belong to the UPS quality control team, namely the E1 (ubiquitin-activating enzymes), E2 (ubiquitin-conjugating enzymes) and the E3 ubiquitin

ligases. E3 ligases confer substrate-specificity, delivering one or several ubiquitin tags to the target protein, that may or may not be degraded in the proteasome [1,3].

If left untreated, AS promotes myocardial maladaptive remodeling which may lead to the development of heart failure [4]. Therefore, AS patients need to undergo valve replacement, to set in motion the opposite process (reverse remodeling). Nonetheless, even with AVR, many subjects fail to achieve complete restoration of the myocardial structure and function [5–7]. Among the factors that may influence the degree of RR is the activity of the UPS. In the previous chapter, it is described a higher preoperative myocardial expression of UPS players, such as the E3 ubiquitin ligase HUWE1, the subunit 2 of the proteasome activator complex or the 26S proteasome non-ATPase regulatory subunit 1, in patients with a complete response. GOEA further suggested a higher flux through the UPS, reflected by higher coverage of the terms “protein metabolism” and “metabolism of amino acids and derivatives”, anticipating a higher degree of protein turnover in complete RR.

The association between UPS, in particular, the E3 ubiquitin ligases, and cardiac disease is not new. A growing body of evidence shows the relationship between these enzymes and cardiac disease, particularly with hypertrophy. For instance, patients with compound Muscle Ring Finger (MuRF)1 deficiency and a deleterious MuRF3 missense mutation develop cardiomyopathy [8]. Similarly, MuRF1/MuRF3 double knockout mice develop extreme muscle hypertrophy [9]. Mice overexpressing atrogin-1 in the heart display a blunted hypertrophy phenotype and decreased apoptosis when subjected to pressure overload [10]. Finally, MDM2 overexpression in cardiomyocytes stimulated with pro-hypertrophic α-agonists (phenylephrine and endothelin-1) mitigates hypertrophy and inhibits the fetal gene program [11].

Thus, since i) hypertrophy reversal is a necessary requisite for complete RR, ii) the myocardial proteome suggests a reduced UPS activity in incomplete RR and iii) E3 ubiquitin ligases have been implicated in the regulation of hypertrophy, the association between preoperative LV levels of total protein ubiquitination and of the ligases MuRF1, MuRF3, atrogin-1 and MDM2 with the degree of RR was tested.

2. Material and Methods

2.1. Study design, patients selection and clinical characterization

AS patients were selected based on retrospective clinical data, and the respective myocardial samples were gathered from the local biobank. The local ethics committee approved the study protocol and written informed consent was obtained from all patients.

Only patients undergoing AVR with clinical predominance of AS, without severe aortic insufficiency or severe forms of other extra-aortic valve diseases and with no more than one stenotic coronary vessel were selected. Clinical evaluation of AS severity and myocardial structure and function was based on transthoracic echocardiography. Peak aortic valve velocity (Peak Ao), mean aortic transvalvular pressure gradient and indexed aortic valve area (AVAi) were derived from Doppler echocardiography. Mean pressure gradient was obtained with the modified Bernoulli equation and AVAi with the standard continuity equation. In turn, LV end-diastolic dimension (LVEDD), LV posterior wall thickness (PWT) and interventricular septal thickness (IVST) were derived from 2D-echocardiograms during diastole. Relative wall thickness (RWT) was calculated as 2×PWT/LVEDD. Correct orientation of imaging planes, cardiac chambers dimension and function measurements were performed according to the EAE/ASE recommendations [12].

LV mass (LVM) index was estimated according to the joint recommendations of the ASE and EAE using Devereux's formula for ASE measurements in diastole: LV mass = 0.8 x (1.04 x ([LV internal dimension + posterior wall thickness + interventricular septal thickness]^3 – [LV internal dimension]^3) + 0.6 g. LV mass (LVM) index (LVMi) was calculated according to the recent recommendations for cardiac chamber quantification [12]. LVMi greater than 115 g/m^2 in men and greater than 95 g/m^2 in women were considered indicative of LV hypertrophy.

Table 1. summarizes the clinical and demographical of the study population (n = 15).

Table 1. Clinical data of the study population.

Parameters			
Degree of Reverse Remodeling	Complete (ΔLVM≥15%)	Incomplete (ΔLVM≤5%)	*p*
Demographics			
N	8	7	n.s.
Age	68.7±3.2	68.8±3.4	n.s.
Gender (male:female)	4:3	1:6	n.s.
BMI (kg/m^2)	30.2±9.2	33.6±6.3	n.s.
Obesity (n)	3	5	n.s.
Hypertension (n)	5	5	n.s.
Diabetes mellitus (n)	3	2	n.s.
CAD (≤1 vessel) (n)	1	2	n.s.
Smoking history (n)	4	1	n.s.
COPD (n)	2	1	n.s.
Mild-to-moderate aortic insufficiency (n)	8	5	n.s.
Mild-to-moderate mitral stenosis (n)	0	0	n.s.
Mild-to-moderate mitral insufficiency (n)	7	5	n.s.
Mild-to-moderate tricuspid insufficiency (n)	6	4	n.s.
Preoperative parameters			
AVAi, cm^2/m^2	0.44±0.04	0.44±0.04	n.s.
Peak Ao, m/s	4.7±0.6	4.5±0.5	n.s.
Max ATPG, mmHg	89.6±22.1	80.6±17.9	n.s.
Mean ATPG, mmHg	56.3±13.5	51.0±11.8	n.s.
LVEDD, cm	5.2±0.2	4.8±0.5	n.s.
IVST, cm	1.4±0.2	1.3±0.2	n.s.
PWT, cm	1.3±0.1	1.2±0.2	n.s.
RWT	0.50±0.05	0.50±0.09	n.s.
LVMi, g/m^2	164.9±32.0	130.1±26.8	*
Postoperative parameters			
LVEDD, cm	4.8±0.4	5.0±0.5	n.s.
IVST, cm	1.3±0.2	1.4±0.1	n.s.
PWT, cm	1.0±0.2	1.1±0.1	a
RWT	0.41±0.07	0.45±0.06	n.s.
LVMi, g/m^2	110.6±23.8	139.6±27.9	*
ΔLVM, %	32.9±7.2	-7.9±9.9	b

* p <0.05 (unpaired two-tailed t-test); a) p = 0.06; b) Independent variable

Abbreviations: ATPG: aortic transvalvular pressure gradient; AVAi: aortic valve area, indexed to body surface area; BMI: body mass index; CAD: coronary artery disease; COPD: chronic obstructive pulmonary disease; IVST: interventricular septal thickness; LVEDD: left ventricle end-diastolic dimension; LVMi: left ventricle mass, indexed to body surface area; n.s.: non-significant; Peak Ao: peak aortic valve velocity; PWT: posterior wall thickness; RWT: relative wall thickness; ΔLVM: left ventricle mass regression.

All patients enrolled in this study were free of dilated or hypertrophic cardiomyopathies. Upon preoperative echocardiographic assessment, patients presented with a mean RWT >0.42, indicative of a more concentric remodeling, typical of pressure overload-induced myocardial remodeling. These patients showed LVEF >50% (n = 12) or had clinical indication of normal/good systolic function (n = 2). Only one patient showed a borderline

LVEF (42%). Hence, the evaluation of RR was based on echocardiographic assessment of LV hypertrophy. LVM regression (%) was defined as the difference between pre- and postoperative LVMi. Patients with LVM regression (ΔLVM) ≥15% were included in the complete RR (cRR) group, while those with LVM regression ≤5% were integrated into the incomplete RR (iRR) group. Complete and incomplete RR groups were not different regarding risk factors such as age, hypertension, obesity, diabetes and smoking. All patients displayed severe or were borderline between moderate to severe AS, according to the ESC/AHA guidelines [13].

2.2. Sample collection and processing

During AVR, LV myocardial biopsies were collected and immediately frozen at -80 °C. LV biopsy material consisted of endomyocardial tissue resected from the LV outflow tract (Morrow procedure) because of concomitant LV outflow tract hypertrophy. The myocardial tissue of AS patients and from a healthy donor heart (technical control) were homogenized in RIPA buffer (40 µL/mg tissue; Thermo Scientific™ cat #89900), supplemented with a cocktail of protease inhibitors (1:100; Sigma-Aldrich® cat #8340), by mechanical disruption using a tissue homogenizer. Protein-rich, debris-free supernatants were recovered after centrifugation for 30 min at 13,000 × *g* (4 °C), aliquoted and stored in liquid nitrogen. Protein concentration was estimated with a BCA assay kit, using BSA as standard.

2.3. Western blot validation

Protein extracts (10 µg) were separated by SDS-PAGE on 8-16% or 4-20% (for atrogin-1 only) gradient TGX stain-free gels, essentially as described by Laemmli [14], and gels were scanned on a ChemiDoc MP imager (BioRad). Next, proteins were transferred to low fluorescence polyvinylidene difluoride membranes using BioRad's Trans-Blot® Turbo™ system with a customized setting (2.5 A, 25 V, 8 min). Transfer efficiency was evaluated by scanning the membranes and rescanning the gels. All membranes were blocked with 1% BSA for 30 min and incubated overnight (4 °C) with the primary antibodies. Following

several washes with TBS-T, membranes were incubated for one hour with the respective secondary antibodies and washed again with TBS-T. **Table 2** compiles all the antibodies used. Chemiluminescence-based detection was carried out with an enhanced chemiluminescence system kit (Clarity Max^{TM} Western ECL, BioRad), using ChemiDoc MP imaging system. Fluorescence-based detection was performed with the same imaging system. Acknowledging the findings of Curi *et al*. [15] (as in the previous chapter), OD normalization was made in relation to total protein levels. Although, instead of the standard Ponceau S staining, protein's signal OD was normalized to total lane OD after transfer. This was possible due to the utilization of the stain-free technology, with greater linear dynamic range than the typical Ponceau S method (Bio-Rad). To compare samples in different blots, the OD signal was also normalized to the technical control sample. Blot scans were analyzed with ImageLab 5.1 software (Bio-Rad).

Table 2. List of antibodies used in western blot.

Protein target	UniProt ID and Gene Name	Primary antibody	Secondary antibody
Ubiquitin	Not applying - the antibody targets ubiquitin and polyubiquitin chains	Mouse mAb 1:500; sc-166553	Peroxidase-AffiniPure Goat pAb anti-mouse 1:10000; Jackson Immunoresearch lab. 115-035-062
Muscle Ring Finger 1	Q969Q1 TRIM63	Goat pAb 1:200; ab4125	HRP-linked Donkey pAb anti-goat 1:10000; sc-2020
Muscle Ring Finger 3	Q9BYV2 TRIM54	Goat pAb 1:500; ab4351	HRP-linked Donkey pAb anti-goat 1:10000; sc-2020
Atrogin-1	Q969P5 FBXO32	Mouse mAb 1:500; sc-166806	DyLight 800-conjugated Goat pAb anti-mouse; Bio-Rad STAR117D800GA
Murine Double Minute 2	Q00987 MDM2	Mouse mAb 1:500; sc-965	Peroxidase-AffiniPure Goat pAb anti-mouse 1:10000; Jackson Immunoresearch lab. 115-035-062

Abbreviations: HRP: horseradish peroxidase; mAb: monoclonal antibody; pAb: polyclonal antibody.

2.4. Statistical analysis

Categorical clinical data are presented as absolute frequencies. Fisher's exact test was applied to detect differences between both groups (cRR and iRR). Continuous demographical and molecular expression data are presented as mean ± standard deviation. The normality of the distribution was tested by the D'Agostino & Pearson omnibus method.

The differences between groups were tested with the unpaired two-tailed t-test, if the variables were normally distributed, or with the Mann-Whitney test, if otherwise. Correlation between clinical parameters and the relative expression of the proteins was evaluated with Pearson's test if data presented a normal distribution and with Spearman's test, if otherwise. All statistical tests were done with GraphPad Prism 6 and, in any case, p <0.05 was considered significant.

3. Results

3.1. Characterization of the preoperative levels of ubiquitin and of hypertrophy-associated ubiquitin ligases in the left ventricle

Protein recycling by the proteasome requires prior ubiquitination. In the previous chapter, proteome analysis supported the idea that despite higher levels of E1 ubiquitin-activating enzyme in iRR, ubiquitination and proteasomal degradation are more likely in cRR. Therefore, it was hypothesized that cRR patients present higher preoperative levels of total protein ubiquitination. Immunodetection of ubiquitinated proteins, however, showed no significant difference in total ubiquitin levels between the two groups (**Figure 1A and 1E** depicts representative blots. The remaining blots can be found in **Supplementary Figure S3, Appendix**). Perhaps, ubiquitination of rather specific substrates may underscore the difference between these groups. Moreover, an incomplete response may also arise from dysregulation of the E3 ubiquitin ligases involved in marking proteins towards proteasome turnover. In this sense, the relative expression of three muscle-specific ubiquitin ligases, namely MuRF1 (**Figure 1B and 1G**), MuRF3 (**Figure 1C and 1H**) and atrogin-1 (**Figure 1D and 1I**), which are known to stimulate atrophy or blunt hypertrophy [8–10] were assessed. Additionally, the ubiquitous MDM2 was also measured (**Figure 1E and 1J**), due to previously reported cardioprotective effects in a different pathological setting [11]. Surprisingly, no differences were found for these UPS players, despite the apparently higher levels of MuRF3 (1.3-fold, p = 0.17) in cRR patients that did not reach statistical significance.

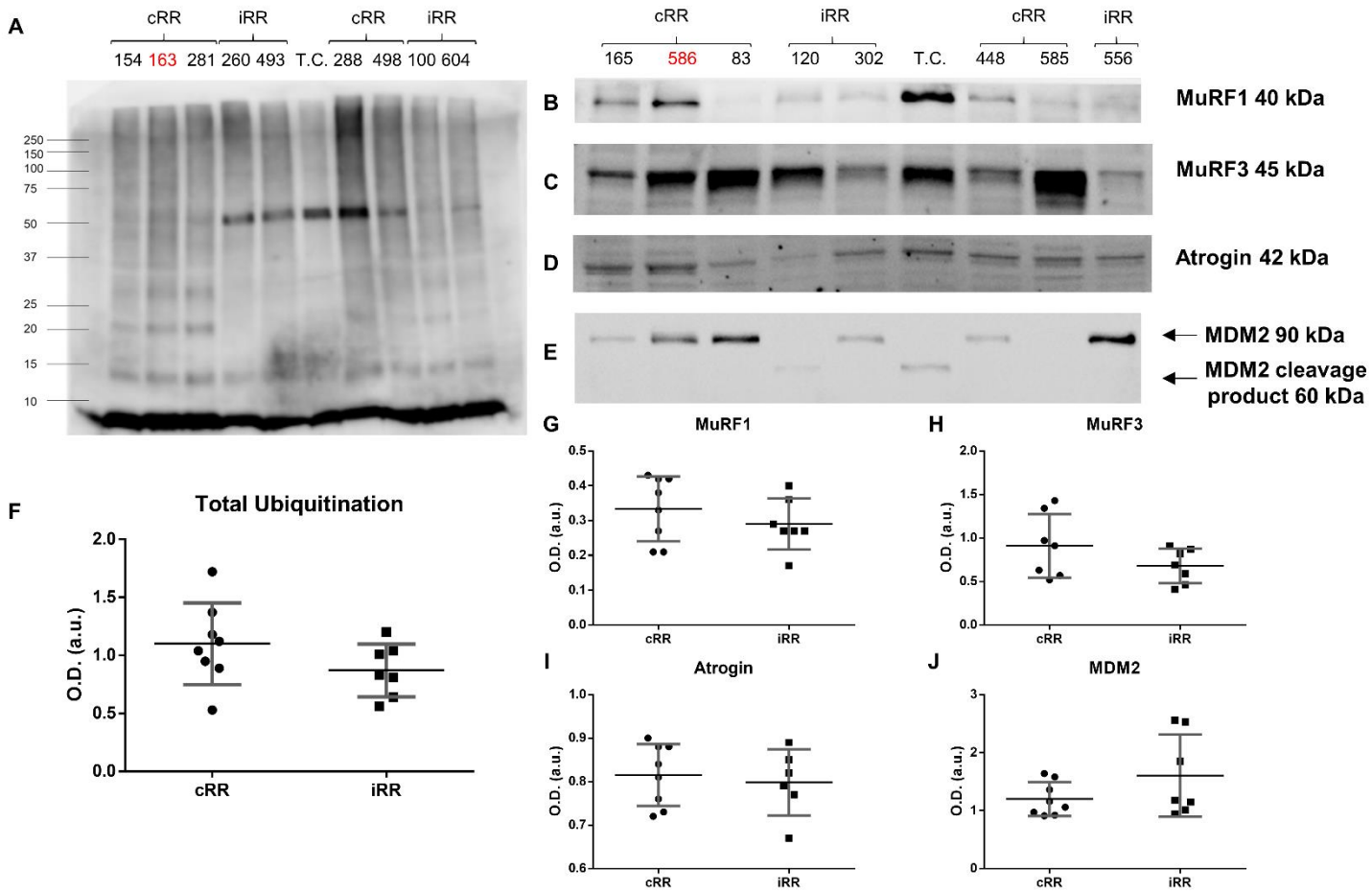

Figure 1. Ubiquitination profile and expression of ubiquitin ligases in the human myocardium collected from patients with complete (cRR) or incomplete (iRR) reverse remodeling. Representative western blot scans are depicted for ubiquitin-tagged proteins (**A**) and for the E3 ubiquitin ligases Muscle Ring Finger (MuRF) 1 (**B**), MuRF3 (**C**), atrogin-1 (**D**) and Murine Double Minute 2 (MDM2) (**E**). In the latter, two bands are identified with arrows, referring to intact MDM2 (upper arrow) and its cleavage product (lower arrow), as reported in the datasheet. Quantification was based on the intact band only. The respective optical density-based semi-quantification is shown in (**F**), (**G**), (**H**), (**I**) and (**J**). T.C. designates the technical control. Samples 163 and 586 are marked in red because these were excluded from the study *a posteriori* (aortic insufficiency was found to be more or as severe as aortic stenosis).

3.2. Correlation analysis

Considering that most of the clinical parameters measured are continuous variables, correlation analysis was performed to foresee potential associations between preoperative levels of ubiquitin and its ligases with patients' outcomes. Comparison between clinical parameters showed that patients with higher preoperative LVMi displayed a higher tendency to LVM regression, as demonstrated by a positive association with ∆LVM (**Table 3**). Besides, LVM regression should rely mainly on the normalization of the PWT, since this parameter was out of the three echocardiographic indexes of chamber geometry (LVEDD, IVST and PWT), the one more closely associated to ∆LVM (r = 0.49, *p* = 0.07). This is expected considering the pattern of concentric remodeling commonly found in AS patients [16]. Furthermore, AVAi correlated negatively with preoperative IVST (r = -0.69, *p* = 0.01) and both Peak Ao and the maximal transvalvular pressure gradient correlated positively with LVMi (r = 0.55, *p* = 0.03), showing that the magnitude of hypertrophy is associated with AS severity. Altogether, these results reassure the consistency of clinical data.

Also presented in **Table 3** are the correlations between the levels of protein ubiquitination and ligases with several clinical parameters. **Figure 2** shows the linear relationship between variables with normal distribution. Concerning total ubiquitin, a significant correlation was found with preoperative IVST (r = 0.55, *p* = 0.03, **Figure 2B**) and PWT (r = 0.65, *p* = 0.009, **Figure 2C**), both markers of hypertrophy. Besides, ubiquitin was inversely correlated to AVAi (r = -0.63, *p* = 0.03, **Figure 2A**), as opposed to MuRF1 (r = 0.59, *p* = 0.04, **Figure 2D**). MuRF1 also showed a negative association with preoperative RWT (r = -0.56, *p* = 0.03, **Figure 2E**). Somehow unexpected, though, a strong positive association of atrogin-1 with preoperative LVMi (r = 0.70, *p* = 0.006, **Figure 2G**) is evident. Since it is unethical to collect LV from patients after AVR, the variation of total protein ubiquitination and of ligases during RR cannot be evaluated. Still, their association with several post-clinical parameters may be analyzed. Regarding MuRF1, adding to its inverse association with preoperative RWT, this ligase showed a negative association to postoperative PWT (r = -0.68, *p* = 0.005, **Table 3**). Atrogin, in turn, was positively associated with postoperative IVST (r = 0.71, *p* = 0.005, **Figure 2F**). No correlations were found between MuRF3 and any of the pre- or postoperative parameters analyzed. Concerning LVM regression, the most important parameter to determine the success of AVR in patients' outcome, out of the five UPS elements analyzed, MDM2 showed the strongest association

(r = -0.44, **Table 3**), approaching significance (*p* = 0.10). Curiously, MDM2, unlike the remaining ligases, is the only one showing an inverse relationship with ΔLVM.

Table 3. Correlation analysis between clinical and molecular data.

Clinical Parameters	ΔLVM	Molecular Data				
		Ubiquitin[a)]	**MuRF1**	**MuRF3**	**Atrogin-1**	**MDM2[b)]**
AVAi		r = -0.63 *p* = 0.03	r = 0.59 *p* = 0.04			
IVST (preop.)		r = 0.55 *p* = 0.03				
IVST (postop.)					r = 0.71 *p* = 0.005	
PWT (preop.)		r = 0.65 *p* = 0.009				
PWT[b)] (postop.)			r = -0.68 *p* = 0.005			
RWT (preop.)			r = -0.56 *p* = 0.03			
RWT (postop.)						
LVMi (preop.)	r = 0.55 *p* = 0.04				r = 0.70 *p* = 0.006	
LVMi (postop.)	r = -0.56 *p* = 0.03					
	ΔLVM	r = 0.34 *p* = 0.22	r = 0.16 *p* = 0.56	r = 0.37 *p* = 0.20	r = 0.26 *p* = 0.37	**r = -0.44** ***p* = 0.10**

a) Total protein ubiquitination; b) Non-normal distribution; Spearman's test was used instead

No correlations were found for age, body mass index, peak aortic valve velocity or to mean/maximal aortic transvalvular pressure gradients.

Abbreviations: MuRF; Muscle Ring Finger Protein; MDM2: Murine Double Minute 2; AVAi: indexed aortic valve area; LVEDD: left ventricle end-diastolic dimension; IVST: interventricular septal thickness; PWT: posterior wall thickness; LVMi; indexed left ventricle mass, indexed to body surface area; ΔLVM: left ventricle mass variation.

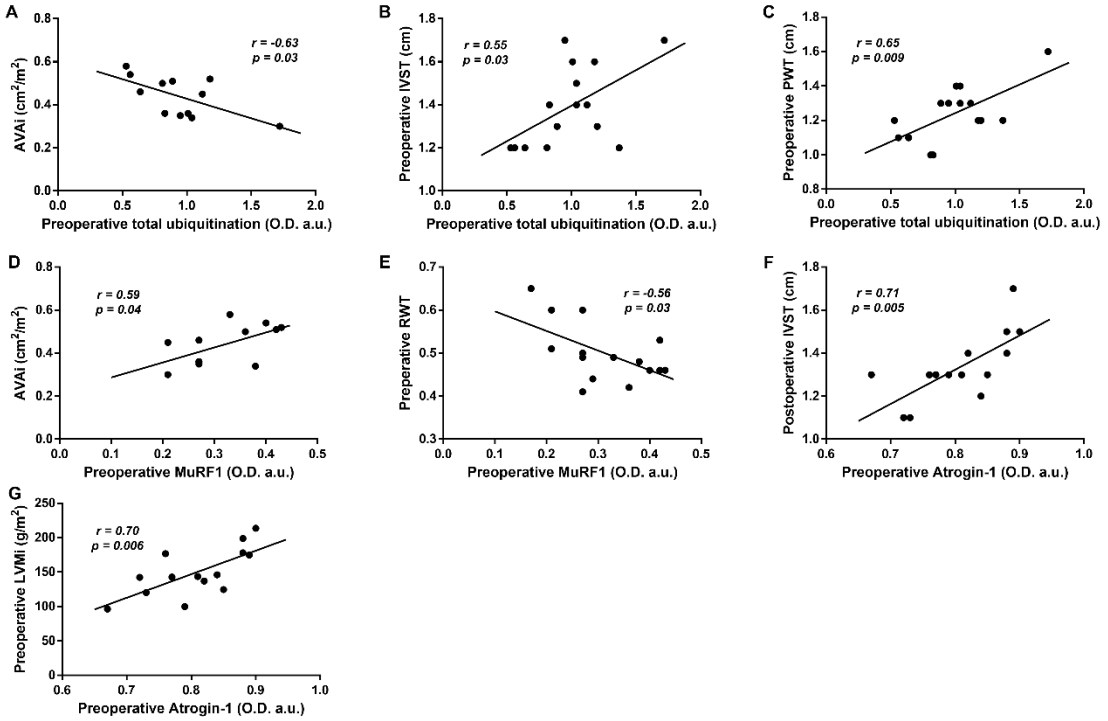

Figure 2. Correlation analysis between clinical and molecular data. In all cases, data was normally distributed, and "r" denotes the correlation coefficient as calculated by Pearson's test. **A.** Negative relationship between total ubiquitination and indexed aortic valve area (AVAi). **B.** and **C.** Positive association between total ubiquitination and, respectively, preoperative interventricular septal thickness (IVST) and posterior wall thickness. **D.** Positive relationship between Muscle Ring Finger (MuRF) 1 and AVAi. **E.** Negative correlation between MuRF1 and preoperative relative wall thickness. **F.** and **G.** Positive relationship between atrogin-1 and postoperative IVST and preoperative left ventricle mass, indexed to body surface area (LVMi).

4. Discussion

Despite directly addressing AS' superimposed pressure overload, AVR may not always be an effective treatment. In fact, some patients still exhibit LV hypertrophy after surgery and demand further clinical attention and care. In this regard, identifying potential novel therapeutic targets to maximize the outcome of patients displaying iRR can be helpful. Based on the premise that UPS plays a central role in sarcomere recycling and is required for the management of hypertrophy [2], the association between the preoperative levels of ubiquitin and of its ligases with the degree of RR was tested. When comparing the two study groups, it was clear that no significant differences were present. This may be explained by the high standard deviation of the protein levels, which, in turn, should reflect the high variation in LVM regression. For that reason, and acknowledging that clinical parameters

were continuous variables, correlation analysis was performed, in an effort to uncover associations between UPS elements and markers of AS severity, hypertrophy and RR.

Proteasome-based degradation of proteins relies on the serial addition of ubiquitin chains [3]. Thus, the global ubiquitination profile in the LV was studied. Interestingly, an association between the amount of ubiquitinated proteins and the severity of AS was observed, as patients with lower valve area (AVAi) presented higher ubiquitin expression. Besides, positive correlations between hypertrophy (preoperative IVST and PWT) and total levels of ubiquitinated proteins were found. Therefore, it is tempting to suggest that the more stenotic the valves are, the higher will be the magnitude of LV hypertrophy and, consequently, the levels of ubiquitinated proteins. Perhaps depending on the specificity of the ubiquitination, conferred by E3 ligases, and the (dys)regulation of E3 ligases itself, such proteins may or may not be recycled on the proteasome. This may be one of the reasons why some patients present complete and others incomplete RR.

Many ubiquitin ligases have been studied in the heart and reported to regulate cell trophic response [1,3]. Since RR relies heavily on the reversal of hypertrophy, the levels of post-natal muscle-specific ubiquitin ligases, MuRF1, MuRF3 and atrogin-1, were studied. MuRF1 has been reported to regulate hypertrophy by downregulation of the CaN A-NFAT axis, through ubiquitination and consequent proteasomal delivery [17]. The relevance of MuRF1 and of MuRF3 is also demonstrated by extreme hypertrophy in a MuRF1 and MuRF3 double knockout model [9]. MuRF1 was found negatively associated with postoperative PWT. Thus, although, not directly associated with LVM regression, MuRF1 may be important for the normalization of LV chamber geometry, by limiting LV's posterior wall thickening. This is corroborated by a previous study showing increased MuRF1 levels in atrophied LV samples collected after implantation of LVADs [18]. Intriguingly, though, MuRF1 levels were lower in patients with narrower aortic valves (positive correlation with AVAi), suggesting a possible downregulation with increased AS severity that requires confirmation. Despite the deemed relevance of MuRF3 in hypertrophy management [9], in this setting it seems that MuRF3 activity may not be as important as the remaining ligases, since, no correlation was found with any of the clinical parameters. Atrogin-1 expression was also hypothesized to be an important factor in determining LVM regression after AVR. The rationale is supported by, for instance reduced hypertrophy and apoptosis in atrogin-1 overexpressing mice subjected to myocardial pressure overload [10]. Surprisingly, though, atrogin-1 showed a strong positive correlation with preoperative LVMi and with postoperative IVST. If, at one hand, the association with LVMi suggests that atrogin-1

expression is a response to growing cardiomyocytes; at the other hand, the association to postoperative IVST (a hypertrophy marker) suggests that such induction might not be beneficial. In fact, some reports challenge the idea of atrogin-1 being cardioprotective in AS-induced myocardial remodeling. While the expression of this enzyme rises in response to pressure overload-induced hypertrophy [19], atrogin also shows a profibrotic role. This is corroborated by the fact that atrogin-1 knockout mice show smaller hearts and reduced interstitial fibrosis when subjected to aortic constriction-induced pressure overload [20]. Mechanistically, this is explained by lower activation of the transcription factor NF-κB, because transgenic mice presented higher levels of its cytoplasmic inhibitor (IκBα). Given the contradictory findings [10,19,20], more research is required to understand the definitive role of atrogin-1 in cardiac hypertrophy induced by AS.

Although MDM2 (a.k.a. HDM2, double minute 2 protein) is traditionally associated with tumorigenesis, due to its p53 suppressing activities, it also targets sarcomeric proteins for degradation, such as telethonin [21]. Previous experiments have shown a cardioprotective role of MDM2. Overexpression of MDM2 efficiently mitigated the development of hypertrophy and fetal gene program activation in cardiomyocytes stimulated *in vitro* with phenylephrine and endothelin-1 [11]. Others reported that MDM2 increases in response to treatment with insulin-like growth factor-1, protecting from stretch-mediated apoptosis, through the arrest of p53 function [22]. Finally, ablation of cardiac MDM2 resulted in concentric hypertrophy, wall thickening and interstitial fibrosis. This was translated into lower fractional shortening and higher mortality in a Mdm2-knockout mouse model [23]. Therefore, despite the ubiquitous expression, MDM2 expression was also hypothesized to affect the degree of myocardial RR after AVR. Even though only a trend, MDM2 was of all ubiquitin ligases, the one showing the closest association to LVM regression ($r = -0.44$, $p = 0.1$). Curiously, though, a negative relationship was observed, suggesting that patients with higher levels of MDM2 are at higher risk of post-AVR iRR. One hypothesis to explain this observation is that, despite being initially protective, persistent activation can be detrimental. In fact, MDM2 inhibits p53 transcriptional activity and promotes its degradation through direct ubiquitination and targeting to proteasome, preventing apoptosis [24]. Notwithstanding, other pathways can be activated by MDM2 and negatively regulate RR. Upregulation of MDM2 leads to sustained inflammation and fibrosis also through the degradation of the IκBα [25], favoring hypertrophy as well [26]. Thus, the present data and the existing evidence together suggest that long-term activation of MDM2 may not be beneficial for myocardial recovery. Anyhow, since only a trend for an association between MDM2 and LVM regression was observed, a screen in a bigger population will be

necessary. If confirmed, the definitive role of MDM2, in the context of RR, should be elucidated in animal models of Mdm2 overexpression/ablation, considering that current evidence is conflicting.

5. Conclusions

In summary, studying human cardiac tissue is challenging. Heart biopsies are only available upon surgery, and the collected material is scarce but highly valuable. The biggest limitation of the present work was the impossibility to perform molecular analysis on LV after surgery. Consequently, the assessment of myocardial recovery was limited to echocardiographic examination, and no causal relationships could be determined between variation of UPS players and the incompleteness of RR. Nonetheless, by assessing proteins governing proteostasis in heart muscle and testing their association with clinical parameters some ubiquitin ligases arose as important players in the process of RR, meriting further scrutiny. This is the case for MuRF1, herein showing a negative correlation with a hypertrophy marker, the postoperative PWT. MuRF1 prognostic role requires tests in larger cohorts and, if possible, in a longitudinal manner. Also worthy of further focus of research is MDM2, the ubiquitin ligase with the highest association with LVM regression. Current evidence points to a rather adverse role of MDM2 in the progression of RR. MDM2 may, thus, become an important therapeutic target, though, only by performing animal studies a definitive conclusion will be achieved.

The present work was developed in a Short-Term Scientific Mission, granted by European COST Action BM1307 Proteostasis, which took place at the University of Skövde, Sweden, in collaboration with Prof. Homa Tajsharghi.

6. References

[1] M.S. Willis, A. Bevilacqua, T. Pulinilkunnil, P. Kienesberger, M. Tannu, C. Patterson, The role

of ubiquitin ligases in cardiac disease, J. Mol. Cell. Cardiol. 71 (2014) 43–53. doi:10.1016/j.yjmcc.2013.11.008.
[2] M. Willis, C. Patterson, Proteotoxicity and Cardiac Dysfunction — Alzheimer's Disease of the Heart?, N Engl J Med. 368 (2013) 455–464. doi:doi: 10.1056/nejmra1106180.
[3] D.I. Brown, T.L. Parry, M.S. Willis, Ubiquitin Ligases and Posttranslational Regulation of Energy in the Heart: The Hand that Feeds, Compr. Physiol. 7 (2017) 841–862. doi:10.1002/cphy.c160024.
[4] C. Gavina, I. Falcão-Pires, F. Rocha-Goncalves, A. Leite-Moreira, Left Ventricular Hypertrophy in Isolated Aortic Stenosis: Primetime for the Ventricle, Curr. Pharm. Biotechnol. 13 (2012) 2503–2514. doi:10.2174/1389201011208062503.
[5] R.W.W. Biederman, J.A. Magovern, S.B. Grant, R.B. Williams, J.A. Yamrozik, D.A. Vido, V.K. Rathi, G. Rayarao, K. Caruppannan, M. Doyle, LV reverse remodeling imparted by aortic valve replacement for severe aortic stenosis; is it durable? A cardiovascular MRI study sponsored by the American Heart Association, J Cardiothorac Surg. 6 (2011) 1–8. doi:10.1186/1749-8090-6-53.
[6] T. Waszyrowski, J.D. Kasprzak, M. Krzemińska-Pakuła, J. Droż, A. Dziatkowiak, J. Zasłonka, Regression of left ventricular dilatation and hypertrophy after aortic valve replacement, Int. J. Cardiol. 57 (1996) 217–225. doi:10.1016/S0167-5273(96)02803-3.
[7] C. Gavina, I. Falcão-Pires, P. Pinho, M.-C. Manso, A. Gonçalves, F. Rocha-Gonçalves, A. Leite-Moreira, Relevance of residual left ventricular hypertrophy after surgery for isolated aortic stenosis, Eur. J. Cardio-Thoracic Surg. 49 (2015) 952–959. doi:10.1093/ejcts/ezv240.
[8] M. Olivé, S. Abdul-Hussein, A. Oldfors, J. González-Costello, P.F.M. van der Ven, D.O. Fürst, L. González, D. Moreno, B. Torrejón-Escribano, J. Alió, A. Pou, I. Ferrer, H. Tajsharghi, New cardiac and skeletal protein aggregate myopathy associated with combined MuRF1 and MuRF3 mutations, Hum. Mol. Genet. 24 (2015) 6264. doi:10.1093/hmg/ddv311.
[9] J. Fielitz, M.-S. Kim, J.M. Shelton, S. Latif, J.A. Spencer, D.J. Glass, J.A. Richardson, R. Bassel-Duby, E.N. Olson, Myosin accumulation and striated muscle myopathy result from the loss of muscle RING finger 1 and 3, J. Clin. Invest. 117 (2007) 2486–2495. doi:10.1172/JCI32827.
[10] H.-H. Li, M.S. Willis, P. Lockyer, N. Miller, H. McDonough, D.J. Glass, C. Patterson, Atrogin-1 inhibits Akt-dependent cardiac hypertrophy in mice via ubiquitin-dependent coactivation of Forkhead proteins, J. Clin. Invest. 117 (2007) 3211–3223. doi:10.1172/JCI31757.
[11] A. Toth, P. Nickson, L.L. Qin, P. Erhardt, Differential Regulation of Cardiomyocyte Survival and Hypertrophy by MDM2, an E3 Ubiquitin Ligase, J. Biol. Chem. . 281 (2006) 3679–3689. doi:10.1074/jbc.M509630200.
[12] R.M. Lang, L.P. Badano, V. Mor-Avi, J. Afilalo, A. Armstrong, L. Ernande, F.A. Flachskampf, E. Foster, S.A. Goldstein, T. Kuznetsova, P. Lancellotti, D. Muraru, M.H. Picard, E.R. Rietzschel, L. Rudski, K.T. Spencer, W. Tsang, J.-U. Voigt, Recommendations for Cardiac Chamber Quantification by Echocardiography in Adults: An Update from the American Society of Echocardiography and the European Association of Cardiovascular Imaging, Eur. Hear. J. - Cardiovasc. Imaging. 16 (2015) 233–271. doi:10.1093/ehjci/jev014.
[13] H. Baumgartner, J. Hung, J. Bermejo, J.B. Chambers, A. Evangelista, B.P. Griffin, B. Iung, C.M. Otto, P.A. Pellikka, M. Quiñones, Echocardiographic Assessment of Valve Stenosis: EAE/ASE Recommendations for Clinical Practice, J. Am. Soc. Echocardiogr. 22 (2009) 1–23. doi:10.1016/j.echo.2008.11.029.
[14] U.K. Laemmli, Cleavage of structural proteins during the assembly of the head of bacteriophage T4, Nature. 227 (1970) 680–685. doi:10.1038/227680a0.
[15] M.A.S. Fortes, G.N. Marzuca-Nassr, K.F. Vitzel, C.H. da Justa Pinheiro, P. Newsholme, R. Curi, Housekeeping proteins: How useful are they in skeletal muscle diabetes studies and muscle hypertrophy models?, Anal. Biochem. 504 (2016) 38–40. doi:10.1016/j.ab.2016.03.023.
[16] I. Shimizu, T. Minamino, Physiological and pathological cardiac hypertrophy, J. Mol. Cell. Cardiol. 97 (2016) 245–262. doi:10.1016/j.yjmcc.2016.06.001.
[17] Y. Maejima, S. Usui, P. Zhai, M. Takamura, S. Kaneko, D. Zablocki, M. Yokota, M. Isobe, J. Sadoshima, Muscle-Specific RING Finger 1 Negatively Regulates Pathological Cardiac Hypertrophy Through Downregulation of Calcineurin A, Circ. Hear. Fail. 7 (2014) 479–490. doi:10.1161/CIRCHEARTFAILURE.113.000713.
[18] M.S. Willis, M. Rojas, L. Li, C.H. Selzman, R.-H. Tang, W.E. Stansfield, J.E. Rodriguez, D.J.

Glass, C. Patterson, Muscle ring finger 1 mediates cardiac atrophy in vivo, Am. J. Physiol. Circ. Physiol. 296 (2009) H997–H1006. doi:10.1152/ajpheart.00660.2008.
[19] G. Kamalov, W. Zhao, T. Zhao, Y. Sun, R.A. Ahokas, T.N. Marion, F. Al Darazi, I.C. Gerling, S.K. Bhattacharya, K.T. Weber, Atrophic cardiomyocyte signaling in hypertensive heart disease, J. Cardiovasc. Pharmacol. 62 (2013) 497–506. doi:10.1097/FJC.0000000000000011.
[20] S. Usui, Y. Maejima, J. Pain, C. Hong, J. Cho, J.Y. Park, D. Zablocki, B. Tian, D.J. Glass, J. Sadoshima, Endogenous Muscle Atrophy F-Box Mediates Pressure Overload–Induced Cardiac Hypertrophy Through Regulation of Nuclear Factor-κB, Circ. Res. 109 (2011) 161–71. doi:10.1161/CIRCRESAHA.110.238717.
[21] L.-F. Tian, H.-Y. Li, B.-F. Jin, X. Pan, J.-H. Man, P.-J. Zhang, W.-H. Li, B. Liang, H. Liu, J. Zhao, W.-L. Gong, T. Zhou, X.-M. Zhang, MDM2 interacts with and downregulates a sarcomeric protein, TCAP, Biochem. Biophys. Res. Commun. 345 (2006) 355–361. doi:10.1016/j.bbrc.2006.04.108.
[22] A. Leri, Y. Liu, P.P. Claudio, J. Kajstura, X. Wang, S. Wang, P. Kang, A. Malhotra, P. Anversa, Insulin-Like Growth Factor-1 Induces Mdm2 and Down-Regulates p53, Attenuating the Myocyte Renin-Angiotensin System and Stretch-Mediated Apoptosis, Am. J. Pathol. 154 (1999) 567–580. doi:10.1016/S0002-9440(10)65302-3.
[23] L. Hauck, S. Stanley-Hasnain, A. Fung, D. Grothe, V. Rao, T.W. Mak, F. Billia, Cardiac-specific ablation of the E3 ubiquitin ligase Mdm2 leads to oxidative stress, broad mitochondrial deficiency and early death, PLoS One. 12 (2017) e0189861. doi:10.1371/journal.pone.0189861.
[24] Y. Haupt, R. Maya, A. Kazaz, M. Oren, Mdm2 promotes the rapid degradation of p53, Nature. 387 (1997) 296–299. doi:10.1038/387296a0.
[25] H. Zhao, R. Shen, X. Dong, Y. Shen, Murine Double Minute-2 Inhibition Attenuates Cardiac Dysfunction and Fibrosis by Modulating NF-κB Pathway After Experimental Myocardial Infarction, Inflammation. 40 (2017) 232–239. doi:10.1007/s10753-016-0473-5.
[26] S. Gaspar-Pereira, N. Fullard, P.A. Townsend, P.S. Banks, E.L. Ellis, C. Fox, A.G. Maxwell, L.B. Murphy, A. Kirk, R. Bauer, J.H. Caamaño, N. Figg, R.S. Foo, J. Mann, D.A. Mann, F. Oakley, The NF-κB Subunit c-Rel Stimulates Cardiac Hypertrophy and Fibrosis, Am. J. Pathol. 180 (2012) 929–939. doi:10.1016/j.ajpath.2011.11.007.

Chapter IV

The impact of the dual specificity tyrosine-phosphorylation-regulated kinase 1A (DYRK1A) on cardiomyocytes' function

Contents

Abstract

Alongside with the resolution of hypertrophy, the process of reverse remodeling requires the normalization of myocardial function. In this sense, the surrogate targets elicited by myocardial (phospho)proteomics, in the previous ***Chapter II***, require further attention. In particular, the dual specificity tyrosine-phosphorylation-regulated kinase 1A (DYRK1A) popped out, because it was found overexpressed in patients with incomplete reverse remodeling, while a higher predicted activity was found for those with a complete response. Moreover, this constitutively active kinase interacts with many myofibrillar proteins. Therefore, it was hypothesized that the dual specificity tyrosine-phosphorylation-regulated kinase 1A regulates cardiomyocyte function. Thus, a proof-of-concept was designed to test the influence of its expression on sarcomeric mechanical properties. Cardiomyocytes from haploinsufficient mice ($Dyrk1a^{+/-}$) and from wild-type littermates were isolated, permeabilized and glued between a motor and a force transducer. The passive tension-sarcomere length, the maximal developed tension and the force-pCa relationships were recorded to assess myofilaments' stiffness, contractility and Ca^{2+} sensitivity. Cardiomyocytes from mutant mice showed a different response to stretch, presenting higher passive tension when sarcomeres were stretched over 2.2 µm. Although no changes were detected in myofilamentary calcium sensitivity, skinned mutant cardiomyocytes showed higher residual force (at 2.2 µm) and developed less force under saturating calcium conditions. Collectively, the results suggest that the dysregulation of the dual specificity tyrosine-phosphorylation-regulated kinase 1A favors the development of diastolic dysfunction. This preliminary study reinforces the idea that this kinase may be modulated to treat incomplete reverse remodeling, demonstrating the usefulness of myocardial phosphoproteomics to extract relevant therapeutic targets.

1. Background

Traditionally associated with neurodegenerative diseases, DYRK1A is the product of a homonymous gene located in the chromosome 21 and a part of the so-called "Down

syndrome critical region" [1,2]. The DYRK1A belongs to the group of the highly conserved DYRK kinases [3] and is composed by a nuclear localization signal at the N-terminal, a DH (DYRK homology) box rich in acidic residues, a catalytic domain containing a YxY motif, a PEST region (rich in Pro, Glu, Ser and Thr), a stretch of 13 consecutive His and a Ser/Thr repeat close to the C-terminal [1] (**Figure 1**). Similarly to GSK3, DYRK1A is auto-phosphorylated in the YxY motif (Y321) during translation, becoming constitutively active. Its regulation is, thus, done at the levels of gene expression, protein-protein interaction and subcellular localization [4]. For instance, while the β-amyloid peptide induces [4], the miR-199b inhibits DYRK1A expression [5]. Despite the presence of a nuclear localization signal, in physiological conditions, DYRK1A is mainly found in the cytoskeleton (~79%) and only ~12% is found in the nucleus, being also present in the cytosol (~8%). When overexpressed, though, DYRK1A accumulates in the nucleus [2,6,7]. Therefore, the cytoplasmic-nuclear shuttling should be important to regulate its activity. Besides, the intracellular localization of this kinase seems to be also determined by different phosphorylation patterns, with the nuclear localization being associated with a higher degree of phosphorylation (DYRK1A pI in nucleus 5.5-6.5 versus 7.2-8.2 in cytoskeleton and 8.7 in the cytosol) [7]. Thus, DYRK1A activity should be regulated by other kinases or phosphatases, that are yet to identify. This scenario illustrates the incomplete understanding of DYRK1A function and operability.

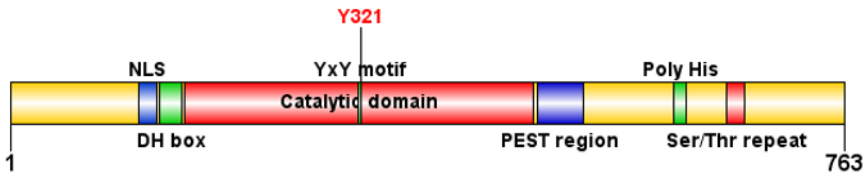

Figure 1. Representation of DYRK1A structural domains, from the N- to the C-*terminus*: the nuclear localization signal (NLS), DYRK homology box (DH), catalytic domain (containing the YxY motif), PEST region, poly His region and the Ser/Thr repeat. Y321 corresponds to the amino acid that is phosphorylated to activate DYRK1A.

The study of DYRK1A's biological activity has started with a great focus on neurodegenerative diseases [2]. Although, evidence has been accumulating on the crucial role of this kinase in other pathological settings, such as in cancer. Depending on the type of cancer, DYRK1A may have either a tumor suppressive or oncogenic role (reviewed in [8]). Concerning cardiovascular diseases, a major role of DYRK1A is readily forecasted by the existence of alternatively-spliced DYRK1A transcripts (containing exon 1 instead of exon 2) that are restricted to the heart and skeletal muscle [1]. Furthermore, patients with Down syndrome (trisomy 21), which express 1.5 times more DYRK1A than healthy subjects, are predisposed to congenital heart disease [1]. In addition, DYRK1A anti-

hypertrophic role has been demonstrated, involving NFAT inhibition and subsequent cytosolic translocation [5,9,10]. The pro-hypertrophic transcription factor NFAT itself induces DYRK1A expression, describing a negative feedback loop [4]. Albeit, judging by the high number of genes (>230) that are dysregulated upon DYRK1A overexpression [2], the relevance of this kinase for cardiomyocyte activity should not be circumscribed to the regulation of cell growth. In fact, Lu and Yin [11] show that DYRK1A interacts (and potentially phosphorylates) the splicing factor SRp55, promoting a fetal-like expression of cardiac troponin T isoforms 1 and 2 (containing exon 5) that exhibit higher calcium sensitivity. Just recently, over 40 proteins have been identified as interactors of DYRK1A in physiological conditions, most being cytosolic and cytoskeletal proteins, including the myofibrillar proteins caldesmon and tropomodulin-3 as well as the Z-disc proteins, protein AHNAK2, palladin and the PDZ and LIM domain protein 5 [6].

In the previous ***Chapter II***, a higher expression of DYRK1A was found in patients with iRR, despite lower predicted activity (measured as the percentage of associated phosphorylated events). The concomitant dysregulation at the expression and activity levels anticipates an important role during the process of RR, meriting further scrutiny. Since i) DYRK1A interacts with several cytoskeleton proteins including myofibrillar proteins and Z disc proteins [6], ii) it is constitutively active [4], pleiotropic [3], and iii) when overexpressed, DYRK1A accumulates in the nucleus [2,6,7]; the increased DYRK1A expression observed in iRR, might explain the reduction in the basal activity taking place in the cytoskeleton, where most interaction partners (ergo, phosphorylation reactions as well) take place [6]. Thus, the concomitant nuclear gain-of-function and cytoplasmic loss-of-function, may have functional repercussions, which might contribute to the poor outcome of AS patients. To clarify a potential role of DYRK1A in cardiomyocyte functional properties, a proof-of-principle study was conducted with permeabilized cardiomyocytes isolated from a mouse model of Dyrk1a haploinsufficiency ($Dyrk1a^{+/-}$). Relevant mechanic properties such as myofibrillar stiffness, developed force and myofilamentary calcium sensitivity were studied and compared between wild-type (WT) and $Dyrk1a^{+/-}$ mice.

2. Material and Methods

2.1. Animal model

Animal experiments were approved by the Ethics Committee of the Spanish Research Council (CSIC) and were carried out according to the guidelines from Directive 2010/63/EU of the European Parliament on the protection of animals used for scientific purposes. Mice were housed in a controlled environment (temperature = 20±1 °C; humidity = 60%) with unlimited access to food and water on 12-hours light/dark cycle. The number of mice and suffering were minimized as possible.

Hearts from six weeks-old haploinsufficient mice (Dyrk1a$^{+/-}$, n = 5), maintained on a CD1 background, and the respective wild type littermates (WT, n = 5) were kindly provided by Dr. Mariona Arbonés (Institut de Biologia Molecular de Barcelona - CSIC). All mice were genotyped by PCR analysis using tail genomic DNA. Details on the generation of the mutant mice and on the genotyping is described elsewhere [12]. The experiments were conducted with sex-matched animals (3:2 male/female).

2.2. Isolation and permeabilization of cardiomyocytes

Around 5 mg of myocardial samples were defrosted in cold relaxing solution (5.95 mM Na_2ATP, 6.04 mM $MgCl_2.6H_2O$, 2 mM (tritriplex) ethylene glycol-bis(2-aminoethyl ether)-N,N,N',N'-tetraacetic acid, EGTA, 139.6 mM KCl and 10 mM imidazole) and mechanically disrupted in a Potter-Elvehjem glass, using a tissue grinder paced at 30-40 rpm (three strokes, 2 seconds each). Triton® X-100 10% was added to the cell suspension to a final concentration of 0.5%, and the cells were incubated for 5 min as to remove the membrane structures. The skinned cardiomyocytes were then washed out of detergent by adding cold relaxing solution and removing the supernatant fraction obtained after centrifugation (1 min, 4 °C, 1,500 rpm). This procedure was repeated five times to ensure complete elimination of the detergent.

2.3. Force measurements and calcium sensitivity

Aliquots of skinned cardiomyocytes suspended in relaxing solution were poured onto coverslips, and the cells allowed to set. Single rod-shaped cardiomyocytes showing a good striation pattern were selected and attached with silicon glue (Marineland, #31003) between a force transducer and an electromagnetic motor on an inverted microscope. After the glue has cured, two subsequent protocols were followed. In the first, passive tension-sarcomere length relationships ranging between 1.8 and 2.3 µm were acquired at 15 °C, with 0.1 µm step increases. In the latter, the sarcomere length was set at 2.2 µm and the development of active force was monitored indirectly by assessing total force ($F_{active} = F_{total} - F_{passive}$) in activating solutions with different calcium concentrations (pCa: 5.0, 5.2, 5.4, 5.6, 5.8 and 6.0; diluted from a stock of 5.97 mM Na_2ATP, 6.28 Mm $MgCl_2$, 40.64 mM propionic acid, 100 mM N,N-Bis(2-hydroxyethyl)taurine, 7 mM Ca-EGTA and 14.5 mM phosphocreatine dissodium salt hydrate, Na_2PCr). In any case, passive force was measured through a “slack” test (cells shortening was set to 80% of initial length) in relaxing solution (5.89 mM Na_2ATP, 6.48 mM $MgCl_2$, 6.97 mM EGTA, 40.76 mM propionic acid, 100 mM N,N-Bis(2-hydroxyethyl)taurine and 14.5 mM phosphocreatine dissodium salt hydrate, Na_2PCr). Several cardiomyocytes from each animal were used, and the data were pooled in each group (WT vs. Dyrk1a$^{+/-}$). Force was normalized for myocyte cross-sectional area, which was calculated after measuring width and length, assuming an elliptical shape of the cell.

2.4. Data and statistical analysis

Force recordings in the two protocols were analyzed through an in-house created program (Cellprog) to extract data on total, passive and active tensions, rate of force redevelopment, Ktr, and residual force. An exponential growth curve (Equation 1, below) was used to fit the relationship between sarcomere length and passive tension. From this equation, the constant β was collected, as an indicator of cardiomyocyte stiffness. In turn, a modified Hill equation (Equation 2, below) was used to fit the (sigmoidal) relationship between relative active force ($F_{relative}$, i.e. the fraction of the maximal force, obtained at pCa 4.5) and pCa. From this equation, the cooperativity (nHill) and the myofilamentary calcium

sensitivity (pCa_{50}, defined as the midpoint of the curve, corresponding to the pCa where developed force is half of the maximal) were obtained.

$$Passive\ tension\ (sarcomere\ length) = a \times e^{(\beta \times (sarcomere\ length))}\ (Equation\ 1)$$

$$F_{relative}(Ca^{2+}) = \frac{[Ca^{2+}]^{nHill}}{[pCa_{50}^{2+}]^{nHill} + [Ca^{2+}]^{nHill}}\ (Equation\ 2)$$

Data is presented as mean ± standard deviation. The normality of the distribution was tested by the D'Agostino & Pearson omnibus method. In the sarcomere length-passive tension protocol, a two-way ANOVA with repeated measures (RM) was used to detect differences between WT and Dyrk1a$^{+/-}$ cardiomyocytes. Specific differences at different sarcomere lengths were interrogated with Bonferroni's multiple comparisons test. In the calcium sensitivity protocol, tensions were log transformed to obtain a normal distribution. The differences between groups were tested with an unpaired two-tailed t-test, if the variables were normally distributed, or with the Mann-Whitney test, if otherwise. All statistical tests were done with GraphPad Prism 6 and, in any case, p <0.05 was considered significant.

3. Results

In order to test the hypothesis that DYRK1A contributes to the regulation of cardiomyocyte contractile function, the mechanical properties (passive and active) of isolated skinned cardiomyocytes (**Figure 2A** and **2B**) were studied in a murine model of DYRK1A haploinsufficiency (Dyrk1a$^{+/-}$) and compared to wild-type littermates (Dyrk1a$^{+/+}$, referred to as WT). Two protocols were followed. In the first (section 3.1), the relationship between sarcomere length and passive tension was obtained. In the second (section 3.2) the force developed with increasing concentrations of calcium was measured.

3.1. Sarcomere length-passive tension relationship

The passive tension of each cardiomyocyte was recorded at increasing sarcomere lengths (1.8, 1.9, 2.0, 2.1, 2.2 and 2.3 µm), to obtain the sarcomere length-passive tension relationship (**Figure 2C**). As expected, a length-dependent increase in passive tension was observed in both WT and Dyrk1a$^{+/-}$ cardiomyocytes. Despite no apparent differences in cardiomyocytes' stiffness were observed between WT and mutant mice (β constant: 4.5 ± 1.5 µm^{-1} in WT *versus* 5.2 ± 2.0 µm^{-1} in mutant cells, non-significant), 2W ANOVA RM highlighted a significant interaction ($p < 0.01$), between genotype and sarcomere length-passive tension relationship. This points towards relevant differences in the cardiomyocytes' response to stretch. This is clear when sarcomeres are stretched beyond 2.2 µm, where mutant cardiomyocytes show a significantly higher passive tension.

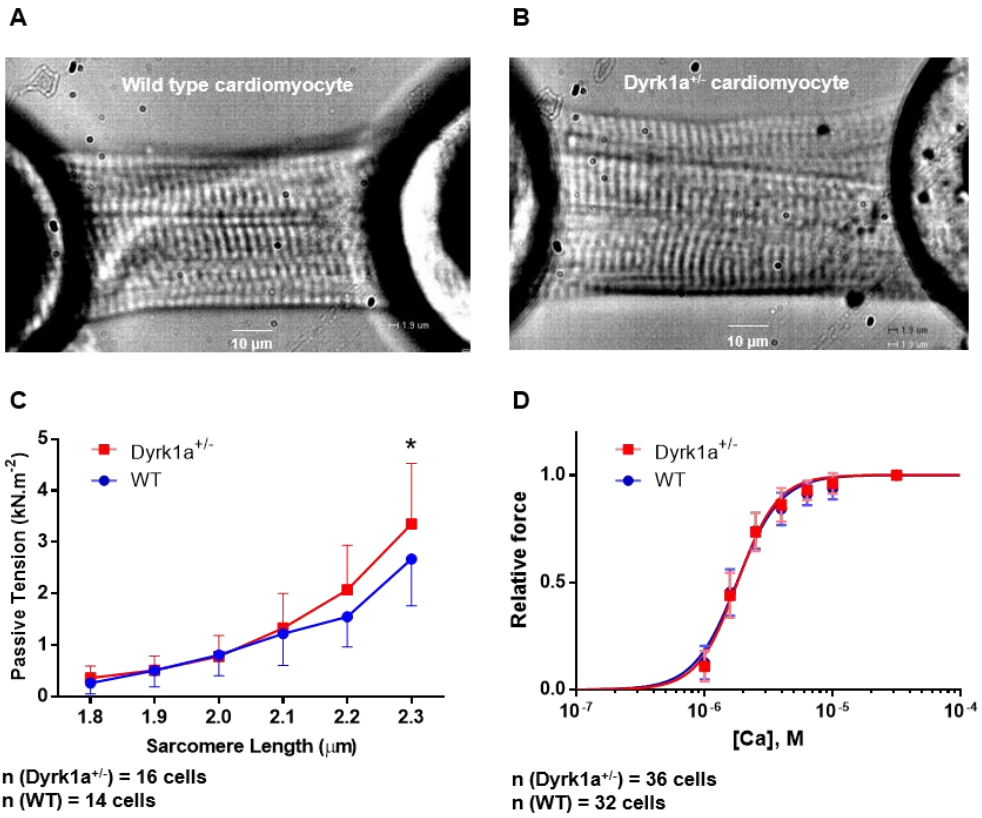

Figure 2. Cardiomyocyte mechanical properties in Dyrk1a$^{+/+}$ (wild-type) and Dyrk1a$^{+/-}$ (mutant) mice. **A.** and **B.** Snapshots of skinned cardiomyocytes obtained, respectively, from WT and Dyrk1a$^{+/-}$ mice. Cells were glued between a force transducer (left) and a motor (right), to perform the force-recording experiments. **C.** Sarcomere length-passive tension relationship. Wild-type mice are represented with a blue curve and the mutant mice with a red curve. To improve readability, only top (Dyrk1a$^{+/-}$) or bottom (WT) error bars are displayed. **D.** Calcium sensitivity on isometric (2.2 µm) force development. Force was normalized to control force at saturating calcium concentration (pCa 4.5). Again, wild-type mice are represented with a blue curve and the mutant mice with a red curve. * p <0.05

3.2. Development of force and calcium sensitivity

The force developed by each cardiomyocyte was also recorded, at increasing calcium concentrations (pCa 6.0, 5.8, 5.6, 5.4, 5.2, 5.0 and 4.5) on a fixed sarcomere length (2.2 µm), to trace the force-pCa relationship and to assess myofilaments' Ca^{2+}-sensitivity. As one can see in **Figure 2D**, there is no apparent change in force dependency of calcium concentration, judging by the overlap of the sigmoidal curves, between WT and mutant mice. Moreover, as shown in **Table 1**, no significant changes were observed in myofilamentary calcium sensitivity (pCa_{50}) nor in cooperativity (nHill) in both groups. Although, the downregulation of Dyrk1a seems to tendentiously decrease the rate of force redevelopment, Ktr (p = 0.14) and significantly increase sarcomeres' residual force (1.3-fold, p <0.05). Importantly, $Dyrk1a^{+/-}$-derived myocytes show a significant decrease in the developed (active) tension (17.1±10.4 $kN.m^{-2}$ *versus* 23.0±11.8 $kN.m^{-2}$ in WT mice, p <0.05), in calcium-saturating conditions (pCa 4.5).

Table 1. Mechanical properties of the skinned cardiomyocytes retrieved from the force development (calcium sensitivity) protocol.

Mechanical properties	WT (n = 32, 5 animals)	DYRK1A$^{+/-}$ (n = 36, 5 animals)	*p*-value
Total Tension ($kN.m^{-2}$)	24.2±12.1	18.1±11.5	**
Active Tension ($kN.m^{-2}$)	23.0±11.8	17.1±10.4	*
Ktr (s^{-1})	15.3±2.4	14.4±4.0	
Residual Force	0.67±0.10	0.86±0.82	#
pCa_{50}	5.74±0.01	5.73±0.01	
nHill	2.71±0.11	2.85±0.08	

* $p < 0.05$ ** $p < 0.01$ (data was log-transformed; unpaired two-tailed t-test); # $p < 0.05$ (Mann-Whitney test)
Abbreviations: Ktr: rate of force redevelopment; nHill: steepness of the force-pCa relationship; pCa_{50}: -log([Ca^{2+}]), for which developed force is half of maximal.

4. Discussion

Severe phenotypical consequences arise from changes in DYRK1A gene dosage. For instance, $Dyrk1a^{-/-}$ mice die during embryogenesis stages E10.5 to E13.5, and up to 30% of $Dyrk1a^{+/-}$ mice die in the first post-natal days [2]. In humans, the rare genetic syndrome

known as DYRK1A haploinsufficiency results in microcephaly and mental retardation [13]. Despite ubiquitously expressed during development, DYRK1A is found highly expressed in the adult brain, lungs, skeletal muscle and in the heart [8]. In the latter, a role has been suggested in troponin T splicing [11], and many sarcomeric-related proteins have been identified as interactors [6]. Based on this evidence and considering the significantly different myocardial expression of DYRK1A between AS patients with cRR and iRR, it was hypothesized that altered cardiomyocyte DYRK1A expression would affect this cell's functional properties.

Force-recording experiments demonstrated that reduced Dyrk1a expression influences mechanical properties of the heart, in comparison to WT littermates. This was observed right after tracing the sarcomere length-passive tension relationship. Despite no apparent differences in the steepness of the curve could be observed, 2W ANOVA RM shows significant differences in the interaction between genotype and sarcomere length-passive tension relationships, corroborating a different response of the mutant cardiomyocytes with stretch. Indeed, haploinsufficient mice exhibited increased passive tension when sarcomeres were stretched over 2.2 µm, suggesting, at least, a tendentiously higher myofibrillar stiffness. Then, through the calcium sensitivity protocol, it was found that sarcomeres fixed at a 2.2 µm length show a higher residual force when Dyrk1a expression is decreased. This may reflect greater difficulty in the process of actomyosin detachment, i.e., impaired relaxation [14]. In fact, according to the results of ***Chapter II*** (**Figure 5**), DYRK1A might target troponin I (slow-twitch skeletal isoform, ssTnI) on Ser 183, which is increased in cRR patients. Considering that troponin I interacts with all known regulatory proteins in the thin filament (troponins T and C, tropomyosin and actin) [15], it is possible that phosphorylation of such residue interferes with the stabilization of the troponin complex, required to prevent the formation of the actomyosin complex, at diastolic calcium concentrations [16]. The increase in residual force is congruent with the different response of mutant cardiomyocytes to stretch. Still, it should be noted that the greater passive tension recorded beyond 2.2 µm might also reflect changes at the level of sarcomeric elastic elements, provided with the fact that DYRK1A interacts with other myofibrillar proteins [6]. Anyway, these data insinuate that DYRK1A dysregulation may contribute to the diastolic dysfunction, a common observation in AS patients [17].

Apart from the changes in the passive properties, a significant drop in the developed (active) force at 2.2 µm in mutant mice was noticed. The lower active tension may be explained, at least in part, by the hypertrophic effect of Dyrk1a haploinsufficiency [5]. So far,

available literature is conflicting concerning the association of hypertrophy with active tension development, with some reports showing that hypertrophy lowers force development, others showing that it augments, and others reporting no effect [18–21]. Nevertheless, this is likely the reflection of the study of different animal models, human diseases or time-points. For instance, Pedroni *et al*. [18] demonstrated that, in comparison with normotensive control animals, papillary muscles isolated from deoxycorticosterone (DOCA)-induced hypertensive rats, as opposed to one/two kidney(s)-one clip-induced hypertensive rats, showed an increase in developed tension. In turn, in a model of aorta constriction-induced pressure overload, papillary muscle's developed tension was found to decrease in the first 15 days post-surgery and then to normalize 28 days later, when hypertrophy had been stabilized [19]. In the case of studies with human material there is also controversy regarding the possible effect of hypertrophy. For instance, permeabilized cardiomyocytes collected from patients with dilated cardiomyopathies (either of idiopathic or ischemic region) showed similar passive and developed force in comparison to normal cardiomyocytes (from transplants) but displayed increased calcium sensitivity [20]. In turn, no differences were detected in cardiomyocytes' maximal tension and calcium sensitivity between patients with different types of overload (pressure, due to AS, or volume, due to aortic or mitral insufficiency) [21]. However, in hypertrophic cardiomyopathy induced by genetic defects in myofilamentary proteins then, the diversity of changes in cardiomyocytes' maximal tension and calcium sensitivity depends on the mutation underlying the phenotype [22–24]. Herein, the hearts have been collected at the same time-point (six weeks), thus one can exclude the effects of different hypertrophy stages. Since the mice were free of any form of heart disease, it is possible to conclude that the limited force development capacity of Dyrk1a$^{+/-}$ is due to a reduced expression of Dyrk1a.

When conciliated with the results of ***Chapter II***, this work suggests that DYRK1A overexpression, and the associated nuclear shuttling [2,6,7], explains the paradoxically reduced predicted activity in iRR patients, which translates into abnormalities in response to stretch and in a lower ability to develop force. The virtually reduced activity (defined by the percentage of phosphorylation events) of DYRK1A in iRR, may be explained by its nuclear import, whereby DYRK1A can no longer bind (and, potentially, phosphorylate) to its many sarcomeric/cytoskeletal interactors. One of these partners could be troponin I whose phosphorylation by DYRK1A (predicted to occur on Ser 183 but requiring validation) may be relevant for proper myocardial relaxation. Thus, either the reduced expression of Dyrk1a in the case of mutant mice, or the relatively reduced cytoskeletal/cytosolic occupancy as

appears to be the case of iRR patients, may deem the myocardium more prone to diastolic dysfunction.

This study has some limitations. First, since myocyte-sized preparations were used, one cannot exclude other actions of DYRK1A on the ECM. However, it should be noted that DYRK1A is not predicted to be secreted (according to SecretomeP 2.0 algorithm [25] and to SignalP 5.0 algorithm [26]); ergo, direct effects on ECM are unlikely. Second, cardiomyocytes were permeabilized and, thus, free of membrane systems, organelles and kinases or phosphatases. While, this provides a simplified model to test the direct effect of DYRK1A in sarcomeres, one cannot exclude indirect effects occurring *in vivo*. Third, only the effect of DYRK1A downregulation was tested in cardiomyocytes function, remaining to address the influence of DYRK1A supplementation.

The present work was designed as a proof-of-concept study to demonstrate that myocardial phosphoproteomics is a valuable tool to pinpoint therapeutic targets. Notwithstanding, this is the first demonstration of the influence of DYRK1A in cardiomyocytes' mechanical properties, with this kinase being identified among a myriad of candidate proteins derived from myocardial (phospho)proteomics. To confirm a positive effect of this kinase in cardiomyocyte mechanical function, in the future, passive and active force must be recorded upon incubation of skinned WT and mutant cells with the recombinant protein. It will also be interesting to understand whether supplementation of DYRK1A to cardiomyocytes collected from iRR patients will exert a positive effect on their function. Moreover, to better elucidate the role of DYRK1A in sarcomere's contractile properties, particularly concerning the molecular mechanisms, the myocardial DYRK1A interactome should be explored in both hypertrophic and non-hypertrophic conditions to identify relevant partners. Then, targeted mutation of DYRK1A substrates will be required to establish which phosphosites will likely impact on cardiomyocyte force generation.

5. Conclusions

In summary, downregulation of DYRK1A has direct effects on cardiomyocytes biomechanics. Mutant cardiomyocytes respond differently to stretch, presenting higher passive tension than WT counterparts at higher sarcomere lengths. Cells from Dyrk1a$^{+/-}$

mice have higher residual force and develop less force than WT mice, under saturating calcium conditions. Although preliminary, this proof-of-concept study suggests that steady cytosolic levels of DYRK1A are important to sustain normal myocardial contractility. In other words, the downregulation of DYRK1A or nuclear accumulation of this kinase, as seems to be the case in iRR patients, may favor the development of diastolic dysfunction.

6. References

[1] J. Galceran, K. De Graaf, F.J. Tejedor, W. Becker, The MNB/DYRK1A protein kinase: genetic and biochemical properties, Adv. Down Syndr. Res. 67 (2003) 139–148. doi:10.1007/978-3-7091-6721-2_12.

[2] J. Wegiel, C.-X. Gong, Y.-W. Hwang, The role of DYRK1A in neurodegenerative diseases, FEBS J. 278 (2011) 236–245. doi:10.1111/j.1742-4658.2010.07955.x.

[3] S. Aranda, A. Laguna, S. de la Luna, DYRK family of protein kinases: evolutionary relationships, biochemical properties, and functional roles, FASEB J. 25 (2010) 449–462. doi:10.1096/fj.10-165837.

[4] W. Becker, W. Sippl, Activation, regulation, and inhibition of DYRK1A, FEBS J. 278 (2011) 246–256. doi:10.1111/j.1742-4658.2010.07956.x.

[5] P.A. da Costa Martins, K. Salic, M.M. Gladka, A.-S. Armand, S. Leptidis, H. el Azzouzi, A. Hansen, C.J. Coenen-de Roo, M.F. Bierhuizen, R. van der Nagel, J. van Kuik, R. de Weger, A. de Bruin, G. Condorelli, M.L. Arbones, T. Eschenhagen, L.J. De Windt, MicroRNA-199b targets the nuclear kinase Dyrk1a in an auto-amplification loop promoting calcineurin/NFAT signalling, Nat. Cell Biol. 12 (2010) 1220–1227. doi:10.1038/ncb2126.

[6] J. Roewenstrunk, C. Di Vona, J. Chen, E. Borras, C. Dong, K. Arató, E. Sabidó, M.S.Y. Huen, S. de la Luna, A comprehensive proteomics-based interaction screen that links DYRK1A to RNF169 and to the DNA damage response, Sci. Rep. 9 (2019) 6014. doi:10.1038/s41598-019-42445-x.

[7] W. Kaczmarski, M. Barua, B. Mazur-Kolecka, J. Frackowiak, W. Dowjat, P. Mehta, D. Bolton, Y.-W. Hwang, A. Rabe, G. Albertini, J. Wegiel, Intracellular distribution of differentially phosphorylated dual-specificity tyrosine phosphorylation-regulated kinase 1A (DYRK1A), J. Neurosci. Res. 92 (2014) 162–173. doi:10.1002/jnr.23279.

[8] P. Fernández-Martínez, C. Zahonero, P. Sánchez-Gómez, DYRK1A: the double-edged kinase as a protagonist in cell growth and tumorigenesis, Mol. Cell. Oncol. 2 (2015) e970048. doi:10.4161/23723548.2014.970048.

[9] C. Kuhn, D. Frank, R. Will, C. Jaschinski, R. Frauen, H.A. Katus, N. Frey, DYRK1A Is a Novel Negative Regulator of Cardiomyocyte Hypertrophy, J. Biol. Chem. . 284 (2009) 17320–17327. doi:10.1074/jbc.M109.006759.

[10] Y. Gwack, S. Sharma, J. Nardone, B. Tanasa, A. Iuga, S. Srikanth, H. Okamura, D. Bolton, S. Feske, P.G. Hogan, A. Rao, A genome-wide Drosophila RNAi screen identifies DYRK-family kinases as regulators of NFAT, Nature. 441 (2006) 646–650. doi:10.1038/nature04631.

[11] S. Lu, X. Yin, Overexpression of Dyrk1A regulates cardiac troponin T splicing in cells and mice, Biochem. Biophys. Res. Commun. 473 (2016) 993–998. doi:10.1016/j.bbrc.2016.04.004.

[12] V. Fotaki, M. Dierssen, S. Alcántara, S. Martínez, E. Martí, C. Casas, J. Visa, E. Soriano, X. Estivill, M.L. Arbonés, Dyrk1A haploinsufficiency affects viability and causes developmental delay and abnormal brain morphology in mice, Mol. Cell. Biol. 22 (2002) 6636–6647. doi:10.1128/mcb.22.18.6636-6647.2002.

[13] R.S. Møller, S. Kübart, M. Hoeltzenbein, B. Heye, I. Vogel, C.P. Hansen, C. Menzel, R.

Ullmann, N. Tommerup, H.-H. Ropers, Z. Tümer, V.M. Kalscheuer, Truncation of the Down Syndrome Candidate Gene DYRK1A in Two Unrelated Patients with Microcephaly, Am. J. Hum. Genet. 82 (2008) 1165–1170. doi:10.1016/j.ajhg.2008.03.001.
[14] V. Sequeira, A. Najafi, M. McConnell, E.D. Fowler, I.A.E. Bollen, R.C.I. Wüst, C. dos Remedios, M. Helmes, E. White, G.J.M. Stienen, J. Tardiff, D.W.D. Kuster, J. van der Velden, Synergistic role of ADP and Ca2+ in diastolic myocardial stiffness, J. Physiol. 593 (2015) 3899–3916. doi:10.1113/JP270354.
[15] J.-J. Sheng, J.-P. Jin, TNNI1, TNNI2 and TNNI3: Evolution, regulation, and protein structure–function relationships, Gene. 576 (2016) 385–394. doi:10.1016/j.gene.2015.10.052.
[16] I.A. Katrukha, Human cardiac troponin complex. Structure and functions, Biochem. 78 (2013) 1447–1465. doi:10.1134/S0006297913130063.
[17] A.N. Rassi, P. Pibarot, S. Elmariah, Left Ventricular Remodelling in Aortic Stenosis, Can. J. Cardiol. 30 (2014) 1004–1011. doi:10.1016/j.cjca.2014.04.026.
[18] P. Pedroni, G.N. Perez, A. Mattiazzi, Calcium sensitivity of isometric tension in intact papillary muscles and chemically skinned trabeculae in different models of hypertensive hypertrophy, Cardiovasc. Res. 24 (1990) 584–590. doi:10.1093/cvr/24.7.584.
[19] P. Jouannot, P.Y. Hatt, Rat myocardial mechanics during pressure-induced hypertrophy development and reversal, Am. J. Physiol. Content. 229 (1975) 355–364. doi:10.1152/ajplegacy.1975.229.2.355.
[20] M.R. Wolff, S.H. Buck, S.W. Stoker, M.L. Greaser, R.M. Mentzer, Myofibrillar calcium sensitivity of isometric tension is increased in human dilated cardiomyopathies: role of altered beta-adrenergically mediated protein phosphorylation., J. Clin. Invest. 98 (1996) 167–176. doi:10.1172/JCI118762.
[21] J. van der Velden, L.J. Klein, M. van der Bijl, M.A.J.. Huybregts, W. Stooker, J. Witkop, L. Eijsman, C.A. Visser, F.C. Visser, G.J.M. Stienen, Isometric tension development and its calcium sensitivity in skinned myocyte-sized preparations from different regions of the human heart, Cardiovasc. Res. 42 (1999) 706–719. doi:10.1016/S0008-6363(98)00337-X.
[22] S. Vasco, W.P. J.M., N.L. L.A.M., K.D. W.D., N. Aref, W.-P.E. Rosalie, R.J. A., B. Nicky, ten C.F. J., G. Tjeerd, C. Lucie, S. Sakthivel, van S.M. A., Z. Ruud, F.D. Brian, M.A. M., P. Corrado, dos R. Cris, S.G. J.M., H.C. Y., M. Michelle, van der V. Jolanda, Perturbed Length-Dependent Activation in Human Hypertrophic Cardiomyopathy With Missense Sarcomeric Gene Mutations, Circ. Res. 112 (2013) 1491–1505. doi:10.1161/CIRCRESAHA.111.300436.
[23] E.R. Witjas-Paalberends, N. Piroddi, K. Stam, S.J. van Dijk, V.S. Oliviera, C. Ferrara, B. Scellini, M. Hazebroek, F.J. ten Cate, M. van Slegtenhorst, C. dos Remedios, H.W.M. Niessen, C. Tesi, G.J.M. Stienen, S. Heymans, M. Michels, C. Poggesi, J. van der Velden, Mutations in MYH7 reduce the force generating capacity of sarcomeres in human familial hypertrophic cardiomyopathy, Cardiovasc. Res. 99 (2013) 432–441. doi:10.1093/cvr/cvt119.
[24] I.A.E. Bollen, M. Schuldt, M. Harakalova, A. Vink, F.W. Asselbergs, J.R. Pinto, M. Krüger, D.W.D. Kuster, J. van der Velden, Genotype-specific pathogenic effects in human dilated cardiomyopathy, J. Physiol. 595 (2017) 4677–4693. doi:10.1113/JP274145.
[25] J.D. Bendtsen, L.J. Jensen, N. Blom, G. von Heijne, S. Brunak, Feature-based prediction of non-classical and leaderless protein secretion, Protein Eng. Des. Sel. 17 (2004) 349–356. doi:10.1093/protein/gzh037.
[26] J.J. Almagro Armenteros, K.D. Tsirigos, C.K. Sønderby, T.N. Petersen, O. Winther, S. Brunak, G. von Heijne, H. Nielsen, SignalP 5.0 improves signal peptide predictions using deep neural networks, Nat. Biotechnol. 37 (2019) 420–423. doi:10.1038/s41587-019-0036-z.

Chapter V

A fractionation approach applying chelating magnetic nanoparticles to characterize pericardial fluid's proteome

Contents

Abstract

If, on the one hand, surgical aortic valve replacement is an invasive procedure that may compromise the survival of aortic stenosis patients, on the other hand, when mandatory, it provides the chance to collect and study biological material that greatly enhances our comprehension of aortic stenosis-induced myocardial remodeling. In the previous ***Chapter II***, ***Chapter III*** and ***Chapter IV***, the usefulness of myocardial biopsies to uncover dysregulated biological processes, surrogate prognostic markers and therapeutic targets for incomplete reverse remodeling was demonstrated. However, there is yet another source of biological information, also accessible during valve replacement, whose molecular characterization may add to the insights provided by myocardial proteomics. This is the fluid confined to the pericardial cavity and, thus, named pericardial fluid. Owing to its proximity, the pericardial fluid proteome should mirror the pathophysiological status of the heart. Despite this potential, the current knowledge of pericardial fluid's proteome is scarce, and its characterization is hurdled by large amounts of albumin, masking the least abundant proteins. Thus, before focusing on the exploration of the pericardial fluid in aortic stenosis patients with complete and incomplete reverse remodeling (***Chapter VI***), the validation of a technique for the fractionation and proteome characterization of this biofluid is demonstrated. Herein, N-(trimethoxysilylpropyl)ethylenediamine triacetic acid (EDTA)-functionalized magnetic nanoparticles (NPs@EDTA) were used to fractionate pericardial fluid and the proteome was characterized by a GeLC-MS/MS approach. Similarly to an albumin-depletion kit, NPs@EDTA-based fractionation was efficient in removing albumin. Both methods displayed comparable inter-individual variability, but NPs@EDTA outperformed the former concerning the protein dynamic range as well as the monitoring of biological processes. Over 50% of the proteins identified (297 in 565) have never been assigned to the pericardial fluid. This NPs@EDTA-based fractionation method also showed good proteome reproducibility, and it has high protein binding capacity, beyond being affordable and rapidly automatable, thus bearing a great potential towards future clinical application.

1. Background

Pericardial fluid (PF) is, in its essence, a plasma ultrafiltrate with important contributions from pericardial mesothelial cells, epicardial capillaries and from the myocardial interstitial space [1,2]. Albeit not commonly used in the clinical routine, the close proximity of the PF to the heart likely holds relevant molecular information, reflecting its pathophysiological status. Even though the molecular knowledge of PF is rather scarce, the need for an invasive collection and the ethical restraints of collecting PF from healthy subjects have been probably discouraging its study. However, PF can be easily and safely collected, for instance, from patients undergoing open-heart surgery [3]. Furthermore, once it is enriched with many bioactive substances, such as cytokines, growth factors or cardiac hormones, governing heart function by autocrine or paracrine activity, PF provides a direct window to the heart. Therefore, the molecular analysis of PF may be an important tool to address the pathophysiological mechanisms underlying cardiac diseases and, simultaneously, to pinpoint potential therapeutic targets [3,4].

Proteomics provides a reliable approach to study PF because the profiling (and quantification) of biofluid proteins allows us to scrutinize directly the pathophysiology of the diseases. Nonetheless, the proteomic characterization of PF can be challenging. First, the albumin content can be even higher than in plasma (71% versus 62%) [4], thus the probability of albumin masking other less abundant proteins needs to be accounted for. Second, PF is expected to bear a high dynamic range of protein concentrations because it is generated by plasma ultrafiltration. The plasma itself displays a range higher than 10^{10}-fold [5]. Third, data integration will be difficult since only one study was published so far, reporting the first in-depth proteomic characterization of PF [6]. In that study the first 1000 PF proteins were identified by removing the 14 most abundant proteins (using Agilent's Multiple Affinity Removal System, MARS) and by following a SDS-PAGE-LC-MS/MS approach. Still, the removal of so many proteins, e.g. albumin, IgM or apolipoprotein AI, was made at the expense of other less abundant small proteins/peptides, which bind to the column-captured proteins. Besides, such method is highly expensive due to the antibody dependency, which readily hampers large-scale use in clinical research.

The N-(trimethoxysilylpropyl)ethylenediamine triacetic acid (EDTA)-functionalized magnetic nanoparticles (NPs@EDTA) have been previously found useful to obtain metal-dependent proteins-enriched salivary fractions from chronic periodontitis subjects to

perform gelatin zymography. In such assay, the enrichment of metalloproteases with NPs@EDTA was evidenced by enhanced metalloproteases-driven gelatinolytic activity [7]. The ability to enrich metalloproteins or metal-dependent proteins is explained by the EDTA's chelating properties, a pentadentate ligand anchored in the surface of magnetic nanoparticles. Additionally, these nanoparticles display tremendous potential for clinical application owing to their affordability, high surface area-to-volume ratio and, thus, sensibility, in addition to the ability to provide a fast separation upon application of an external magnetic field [8].

Hence, it was hypothesized that processing PF with NPs@EDTA would deepen PF's proteome knowledge, by enriching low abundant proteins. This work aimed to validate the use of NPs@EDTA to fractionate and characterize PF proteome and to expand the proteome catalogued to date. In order to do that, the application of these lab-made nanoparticles was compared with a commercial albumin/IgG-depletion kit, regarding the SDS-PAGE profiles as well as to the proteome profile and the trackable biological processes.

2. Material and Methods

2.1. Sample collection, processing and protein quantification

PF was collected from two obese, hypertensive and diabetic female patients during valve surgery (samples were named PF1 and PF2). A third sample was collected from an obese, hypertensive non-diabetic male patient during valve surgery (named PF3). Approximately 15 mL of fluid was collected from each patient immediately after sternotomy and pericardiotomy. Following collection, PF was centrifuged at 5,000 rpm, 4 °C for 15 min to remove cellular components and the supernatant was stored at -80 °C until further processing. Protein quantification was performed with the BCA protein assay kit (Pierce®, Thermo Scientific), using BSA as a standard. The study was approved by the Institutional Ethical Committee, and all patients provided written informed consent.

2.2. Depletion of albumin and immunoglobulin G from pericardial fluid

PF from subjects PF1 and PF2 was processed using an albumin/IgG-depletion kit (Pierce™ Top 2 Abundant Protein Depletion Spin Columns, Thermo Scientific), according to the manufacturer's protocol. The volume corresponding to 600 µg of proteins was used since the spin columns can process up to 10 µL of serum/plasma (~600 µg of protein). An additional elution step was performed in order to collect the albumin/IgG-rich fraction. To collect these fractions, samples were incubated with 300 µL of 0.1 M glycine solution pH 2.4, for 30 min, in an end-over-end mixer, and centrifuged for 2 min at 1,000 ×*g*. Neutralization of samples was achieved with 0.5 M Tris solution pH 8.5.

2.3. Synthesis and characterization of NPs@EDTA

A detailed description of NPs@EDTA (patent register PT107608) preparation has been described elsewhere [8] but, essentially, comprised: i) the synthesis of the magnetic core made of Fe_3O_4 through oxidative hydrolysis of an Iron (II) salt in alkaline medium; ii) surface coating with a shell of amorphous silica (SiO_2) in alkaline environment using tetraethyl ortho-silicate as a precursor; and iii) surface chemical functionalization with N-(trimethoxysilylpropyl)ethylenediamine triacetate trisodium salt (EDTA-TMS), as illustrated in **Supplementary Figure S4, Appendix**.

Morphology and size of NPs@EDTA particles were obtained through transmission electron microscopy (TEM) using a Hitachi H-9000 microscope operated at 300 kV. Sample for TEM analysis was prepared by evaporating dilute suspensions of the nanoparticles on a copper grid coated with an amorphous carbon film. The Fourier Transform Infrared (FTIR) spectrum was collected using a spectrometer Mattson 7000 with 256 scans and 4 cm^{-1} resolution, using a horizontal attenuated total reflectance cell. The surface charge of the NPs was assessed by zeta potential measurements, using a Zetasizer Nanoseries equipment from Malvern Instruments.

2.4. NPs@EDTA assay for fractionation of pericardial fluid proteins

After NPs@EDTA synthesis, a suspension of nanoparticles was prepared in ultrapure water to a known concentration. One mg of NPs@EDTA was used to each sample. Before incubation of samples, magnetic beads were washed with binding buffer [0.01 M 2-(N-Morpholino)ethanesulfonic acid (MES), 0.01 M NaCl, pH 6.5-8.5]. Then, two independent assays were performed, using samples PF1 and PF2. In the first, 0.6 mg (the same amount processed with the commercial kit) and 3 mg of PF protein were incubated with the beads and subjected to mechanical agitation for one hour at room temperature. In the second, to estimate NPs@EDTA saturation, 0.3 mg, 1.5 mg, 3 mg and 4.5 mg of PF proteins were incubated with the beads and subjected to the same agitation conditions. After sample incubation, supernatants were collected, and the beads were washed 3 times by adding 500 µL of MES buffer and performing agitation cycles for 3-5 min. Elution of beads-bound proteins was carried out with 20 µL of Laemmli loading buffer by promoting further mechanical agitation for 10 min.

2.5. Protein separation by SDS-PAGE

Aiming to compare the protein profiles of the fractions collected with the commercial kit and with the NPs@EDTA, protein fractions were separated by SDS-PAGE, following Laemmli procedure [9]. The volume corresponding to 30 µg of protein from total unprocessed sample and from the protein fractions collected by the commercial kit was directly loaded onto the gel. 10 µL of each fraction collected in the first NPs@EDTA assay was also loaded onto the gel. This volume was chosen because, when starting with 600 µg of protein, it corresponds to the same protein amount (30 µg) as in the case of the kit. Finally, in the second (saturation) assay the whole adsorbed protein fractions were loaded onto gel. Proteins were separated under reducing and denaturing conditions in 12.5% gels, applying a 200 V voltage. Gels were then incubated in fixation solution (methanol: acetic acid 40:10 v/v) for 45 min, stained with Colloidal Coomassie Blue G250 and destained with 20% methanol until an optimal contrast was achieved.

2.6. *In gel* digestion and peptide cleanup

Each lane of the gels was cut in 16 pieces and washed with 100 mM NH_4HCO_3 and acetonitrile. Proteins were then reduced with 10 mM DTT (30 min, 60 °C), alkylated in the dark with 55 mM IAA (30 min, 25 ºC) and washed again with 100 mM NH_4HCO_3 and acetonitrile, before being digested with trypsin overnight (37 °C). Peptides were extracted with 10% FA, FA 10%: acetonitrile (1:1) and vacuum-dried. Next, peptides were resuspended in 5% acetonitrile and 0.5% trifluoroacetic acid and purified using Pierce® C18 Spin Columns (Thermo Scientific) following the manufacturer's instructions. Peptides were re-dried and kept frozen (-80 ºC) until MS-based analysis.

2.7. Reproducibility assay

In order to test the reproducibility of the fractionation method employing magnetic nanoparticles, the third sample (PF3) was processed in duplicate following the same procedure used for the former samples (PF1 and PF2, see section 2.4). Three mg of protein were used as this amount was found to saturate 1 mg of NPs@EDTA. The elution of the proteins bound to the nanoparticles, however, was made with a 50 mM NH_4HCO_3 and 0.1% SDS solution.

2.8. *In solution* digestion and peptide cleanup

The protein samples from the reproducibility assay were reduced with 3 µM DTT (30 min, 56 °C), alkylated in the dark with 5 µM IAA (30 min, 25 ºC) and digested with trypsin overnight at 37 ºC, following Wiśniewski *et al*. [10] FASP procedure. After digestion, peptide mix was acidified with FA and desalted with a MicroSpin C18 column (The Nest Group, Inc) prior to LC-MS/MS analysis.

2.9. Protein identification by LC-MS/MS analysis

Samples from PF1 and PF2 were analyzed on a Triple TOF™ 5600 System (ABSciex®) in DDA mode as previously described [11,12]. Peptides were resolved by liquid chromatography (nanoLC Ultra 2D, Eksigent®) on a MicroLC column ChromXP™ C18CL (300 µm internal diameter (ID) × 15 cm length, 3 µm particles, 120 Å pore size, Eksigent®) at 5 µL/min with a multistep gradient: 0-2 min linear gradient from 5 to 10%, 2-45 min linear gradient from 10% to 30% and 45-46 min to 35% of acetonitrile in 0.1% FA. Peptides were ionized into the mass spectrometer using an electrospray ionization source (DuoSpray™ Source, ABSciex®) with a 50 µm ID stainless steel emitter (NewObjective).

For DDA experiments the mass spectrometer was set to scanning full spectra (350-1250 *m/z*) for 250 ms, followed by up to 100 MS/MS scans (100–1500 *m/z* from a dynamic accumulation time – minimum 30 ms for precursor above the intensity threshold of 1000 – in order to maintain a cycle time of 3.3 s). Candidate ions with a charge state between +2 and +5 and counts above a minimum threshold of 10 counts/second were isolated for fragmentation and MS/MS spectra was collected before adding those ions to the exclusion list for 25 seconds (mass spectrometer operated by Analyst® TF 1.7, ABSciex®). Rolling collision was used with a collision energy spread of 5.

Peptide identification and library generation were performed with Protein Pilot software (v5.1, ABSciex®), using the following parameters: i) search against the SwissProt database (March 2016 release); ii) IAA as cysteines alkylating agents as fixed modification; iii) trypsin as digestion type. An independent FDR analysis using the target-decoy approach provided with Protein Pilot software was used to assess the quality of the identifications, and positive identifications were considered when identified proteins and peptides reached a 5% local FDR [13,14].

The peptide mixes from sample PF3 were analyzed using a LTQ-Orbitrap Velos Pro mass spectrometer (Thermo Fisher Scientific, San Jose, CA, USA) coupled to an EasyLC (Thermo Fisher Scientific (Proxeon), Odense, Denmark). Peptides were loaded onto the 2-cm Nano Trap column with an inner diameter of 100 µm packed with C18 particles of 5 µm particle size (Thermo Fisher Scientific) and were separated by reversed-phase chromatography using a 25-cm column with an inner diameter of 75 µm, packed with 1.9 µm C18 particles (Nikkyo Technos Co., Ltd. Japan). Chromatographic gradients started at 93% buffer A and 7% buffer B with a flow rate of 250 nL/min for 5 min and gradually

increased 65% buffer A and 35% buffer B in 120 min. After each analysis, the column was washed for 15 min with 10% buffer A and 90% buffer B. Buffer A: 0.1% FA in water. Buffer B: 0.1% FA in acetonitrile.

The mass spectrometer was operated in DDA mode and full MS scans with 1 micro scans at resolution of 60.000 were used over a mass range of *m/z* 350-2000 with detection in the Orbitrap. AGC was set to 1E6, dynamic exclusion (60 seconds) and charge state filtering disqualifying singly charged peptides was activated. In each cycle of DDA analysis, following each survey scan the top 20 most intense ions with multiple charged ions above a threshold ion count of 5000 were selected for fragmentation at a normalized collision energy of 35%. Fragment ion spectra produced via collision-induced dissociation were acquired in the Ion Trap, AGC was set to 5e4, isolation window of 2.0 *m/z*, activation time of 0.1 ms and maximum injection time of 100 ms was used. All data were acquired with Xcalibur software v2.2.

Proteome Discoverer software suite (v1.4, Thermo Fisher Scientific) and the Mascot search engine (v2.5, Matrix Science [15]) were used for peptide identification and quantification. Samples were searched against a SwissProt database containing entries corresponding to human, a list of common contaminants and all the corresponding decoy entries (20797 entries). Trypsin was chosen as enzyme and a maximum of three miscleavages were allowed. Carbamidomethylation (C) was set as a fixed modification, whereas oxidation (M) and acetylation (N-terminal) were used as variable modifications. Searches were performed using a peptide tolerance of 7 ppm, a product ion tolerance of 0.5 Da. Resulting data files were filtered for FDR <5%.

The proteome data has been deposited to the ProteomeXchange Consortium via PRIDE [16] partner repository with the dataset identifier PXD008620.

2.10. Proteome analysis, bioinformatics and statistical analysis

The differences between protein profiles were explored by Venn diagram analysis with the help of BioVenn webtool [17], using UniProt accessions.

To determine the cellular localization of the proteins, a STRING [18] analysis was performed. Only GO terms with FDR <5% were considered. To get insight into the biological

processes that can be screened with both methods, a ClueGO (v.2.2.6) [19] analysis was performed. For the comparison between methodological approaches a 3-8 GO range was set, while GO was fixed on level 3 for the comparison of the experimental dataset to that reported by Xiang's *et al.* [6] In both cases, the GO library, from the Gene Ontology consortium, was updated on February 9th 2016.

To estimate the dynamic range of the identified proteins, the base-10 logarithm was calculated, for each protein, from the sum of the peptide intensities and its variation, Δ, was calculated from the difference of the highest and lowest logarithms. To calculate the dynamic range of the PF proteome already characterized, the MS/MS raw data available on PRIDE (dataset PXD000194) was used.

Two-proportion z-test was used to test the representativeness of plasma- and heart-derived proteome to overall PF proteome, in comparison to the aforementioned dataset [6]. In all cases, p <0.05 was considered significant.

3. Results

3.1. Preparation and characterization of NPs@EDTA

The NPs@EDTA were synthesized in three steps (**Supplementary Figure S4, Appendix**), as previously described [8]. TEM analysis (**Figure 1A**) shows that these particles present core@shell morphology, comprising a spherical magnetic core of Fe_3O_4 (darker) with an average diameter of 48 ± 8 nm coated with amorphous silica (SiO_2) shells of 14 ± 2 nm in thickness. Owing to Fe_3O_4 core, NPs@EDTA particles are ferrimagnetic and display a magnetization hysteresis loop at room temperature (300 K) with small remnant magnetization and coercivity and a saturation magnetization of 40 emu/g [8]. The FTIR spectrum (**Figure 1B**) shows the typical bands of Fe_3O_4 (556 cm^{-1} (ν(Fe–O))) and amorphous SiO_2 (1060 cm^{-1} (ν_{as}(SiO–Si)), 958 cm^{-1} (ν(Si–OH)) and 799 and 432 cm^{-1} (δ(Si–O–Si))). Although less intense, the bands at 1386 cm^{-1} (ν(C–OH)) and 1635 cm^{-1} (ν(C=O)) support the presence of carboxylic acid groups at the surface of the particles due to the

grafting of EDTA-TMS. Accordingly, the surface of NPs@EDTA particles was strongly negatively charged, with zeta potential values of -65.6 mV (pH 7.1, MES buffer).

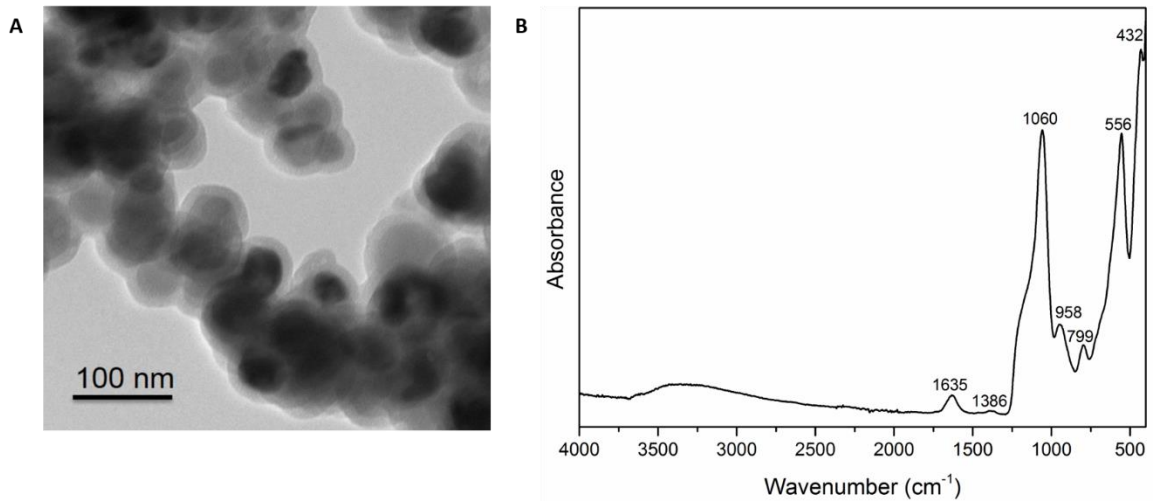

Figure 1. A. TEM image and **B.** FTIR spectrum of NPs@EDTA.

3.2. SDS-PAGE analysis

After processing PF with the commercial kit, the albumin/IgG-poor (F1) and the rich (F2) fractions were obtained for each sample. In turn, after fractionating PF with NPs@EDTA, a non-adsorbed (F3) and an adsorbed (F4) protein fraction were retrieved. All fractions and the total/unprocessed sample (TF) are depicted in **Figure 2**, showing the different protein SDS-PAGE profiles achieved with the depletion (**Figure 2A and 2B**) and the enrichment (**Figure 2C and 2D**) methods. As expected, a dramatic decline in the intensity of the band associated with albumin (~ 69 kDa, HSA in **Figure 2**) was found in F1, corroborating albumin removal. In fact, the majority of albumin was captured by the resin antibodies and collected in F2, as shown by increased intensity of albumin's band in the third lane of **Figure 2A** and **2B**. Immunoglobulin G removal could also be observed in F1 by a decrease in the intensity of its heavy chain band (IgG h.c. in **Figure 2**), whose weight is known to be close to 50 kDa [20]. Accordingly, the majority of this IgG chain could be seen in F2, where the intensity of the band is identical to the respective in TF. Likewise, by fractionating PF with NPs@EDTA we could get rid of a considerable amount of albumin and IgG, as corroborated by increased intensity of the respective bands (HSA and IgG h.c.) in F3 (non-adsorbed protein fraction) in comparison to F4 (adsorbed protein fraction), particularly visible when

processing 3 mg of protein. Therefore, similarly to the commercial columns, NPs@EDTA offer a platform for the depletion of abundant proteins (albumin and IgG, at least) and concomitant enrichment of low abundant proteins.

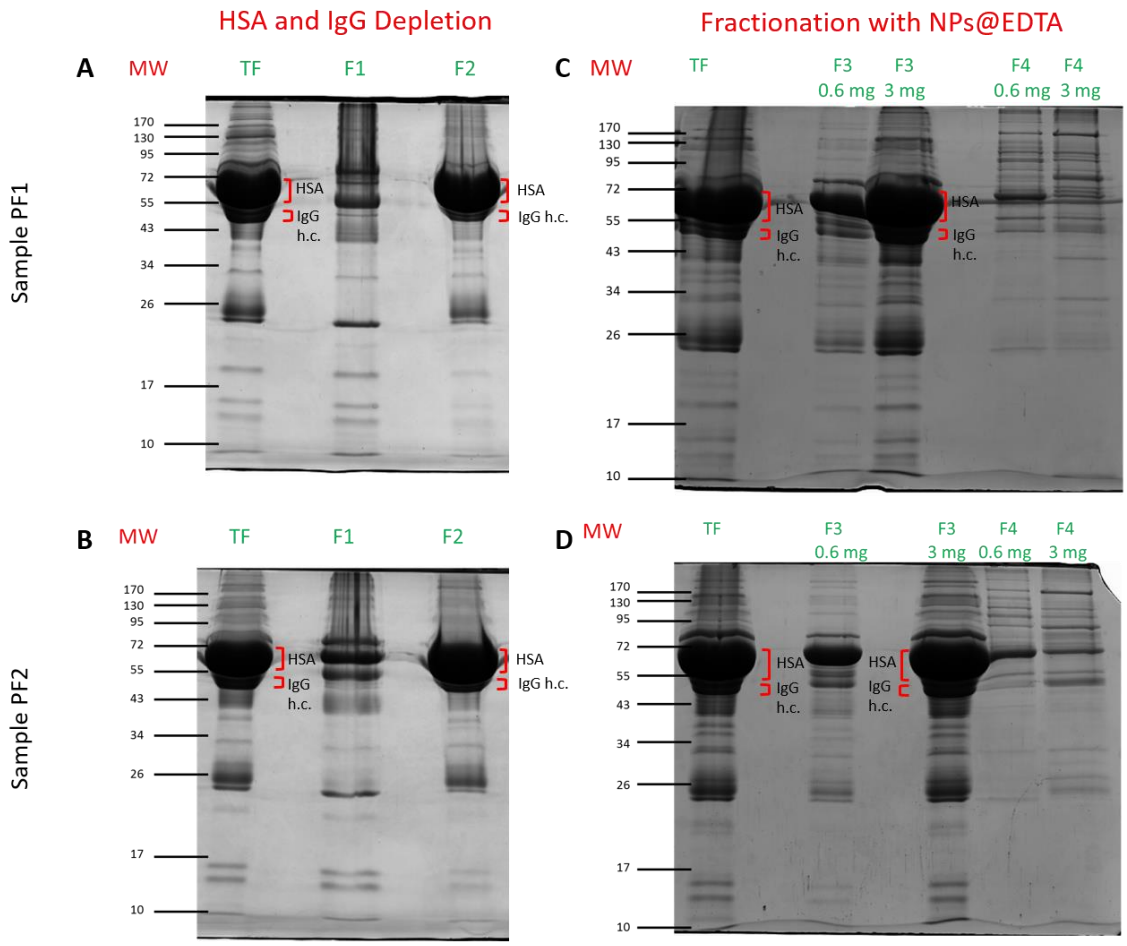

Figure 2. SDS-PAGE profiles of the protein fractions collected with the commercial kit (**A.** and **B.**) and with the NPs@EDTA (**C.** and **D.**), from two individuals (top: PF1, bottom: PF2). The first lane in each gel (TF) corresponds to the total/unprocessed sample. F1: albumin (HSA)/IgG-poor fraction; F2: HSA/IgG-rich fraction; F3: non-adsorbed fraction; F4: adsorbed fraction. Red brackets mark HSA and IgG heavy chain (h.c.) bands.

3.3. Analysis of proteome coverage, dynamic range and inter-individual variability

A bottom-up approach comprising protein trypsinization and peptide identification by LC-MS/MS was followed. **Table 1** summarizes the main proteome data for both methods. Overall, without taking into account the data obtained after performing saturation and

reproducibility assays (see sections 3.4. and 3.5), on a first analysis, 185 proteins could be identified across different samples, fractions and methods (**Figure 3A**). From these, 122 proteins (66%) were identified in both subjects (**Figure 3B**). Importantly, both depletion and nanoparticles-based methods could increase the number of proteins identified, respectively, by 38% and 40%, over PF's direct analysis. Furthermore, both methods combined increased by 59% the number of identified proteins, showing that depletion of high abundant proteins in PF is imperative to enlarge proteome coverage. Notwithstanding, one should acknowledge that such an increase was also a result of the analysis of the albumin/IgG-rich fraction (usually discarded) and of the non-adsorbed protein fraction, which shows that analyzing both fractions in both methods guarantees the deepest proteome coverage. While both methods contributed equally to proteome coverage, the same was not true with respect to the protein dynamic range. In fact, NPs@EDTA-based fractionation achieved a higher range of protein abundances (4.5 versus 3.7 log units, **Table 2**) than the commercial method. Still, such range was found lower when compared to TF (4.8 log units).

With regard to the inter-individual variability, the subjects were found to share 66% of the PF proteome. Furthermore, it was found that either processing PF with the kit or with the NPs@EDTA does not induce important variations in the individual proteome, at least, in the desired fractions. In fact, both individuals shared 62% of the proteins in the albumin-poor fraction (F1) and 60% of the proteins in the adsorbed protein fraction (F4). These data suggest biological rather than technical proteome variations, explaining the percentage of shared proteome between individuals.

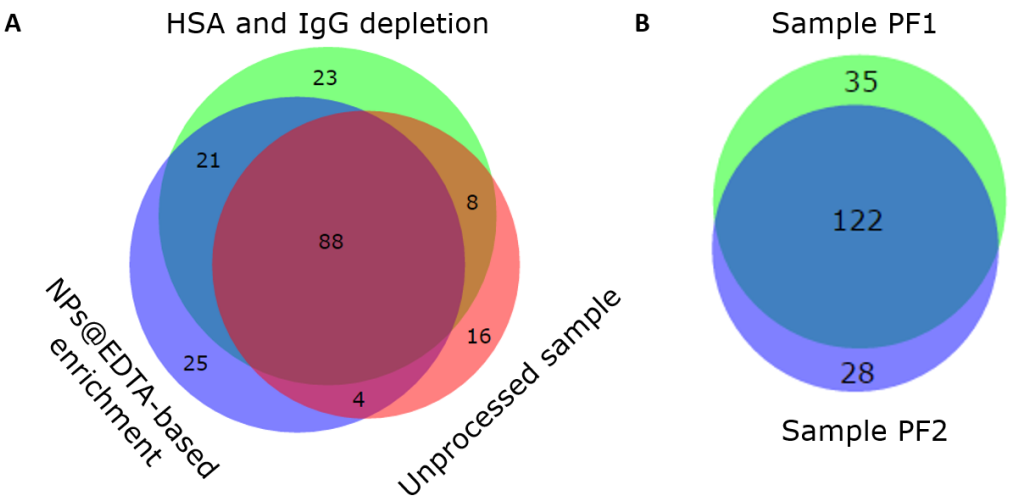

Figure 3. A. Venn's graphical representation of the pericardial fluid proteins identified across the two approaches and in the unprocessed sample and **B.** across the two individuals.

Table 1. Main indicators of proteome data, namely inter-individual variability, proteome coverage and increment of protein identification in comparison to total unprocessed samples.

General Statistics			
Total Number of Identified Proteins	185		
Total Number of Identified Proteins on Sample PF1	157		
Total Number of Identified Proteins on Sample PF2	150	Total Fraction (unprocessed samples)	
Number of Shared Proteins	122	Total Number of Proteins	116
Proteins shared between individuals	66%	Proteins shared between individuals	64%
Method 1: Depletion of HSA and IgG			
HSA- and IgG-rich fraction (F2)		HSA- and IgG-poor fraction (F1)	
Total Number of Proteins	78	Total Number of Proteins	124
Proteins shared between individuals	41%	Proteins shared between individuals	62%
Number of proteins identified exclusively by the method [in comparison to "Total Fraction"]			44
Increment of Protein Identification			38%
Method 2: Enrichment with NPs@EDTA			
Non-adsorbed protein fraction (F3)		Adsorbed protein fraction (F4)	
Total Number of Proteins	86	Total Number of Proteins	92
Proteins shared between individuals	56%	Proteins shared between individuals	60%
Number of proteins identified exclusively by the method [in comparison to "Total Fraction"]			46
Increment of Protein Identification			40%
Comparison between Methods			
Method 1: Depletion of HSA and IgG		Method 2: Enrichment with NPs@EDTA	
Total Number of Proteins	140	Total Number of Proteins	138
Unique Number of Proteins	23	Unique Number of Proteins	25
Unique Coverage	12%	Unique Coverage	14%
Increment of Protein Identification	38%	Increment of Protein Identification	40%
Combined Coverage			37%
Combined Increment in Protein Identification			59%

Table 2. Dynamic range estimation (log_{10} of the peptide intensity sum for each protein identified) in proteome data obtained from total unprocessed samples, fraction 1 (albumin/IgG-poor fraction) and 4 (NPs@EDTA-adsorbed protein fraction); this last in both the standard and in the saturation assays.

Fraction	Log10 Peptide Intensity Sum Range	Δ Log10
Total	1.5 – 6.3	4.8
F1	1.9 – 5.6	3.7
F4 (standard assay)	1.0 – 5.5	4.5
F4 (saturation assay)	1.2 – 6.6	5.4

3.4. Saturation of NPs@EDTA with large volumes of PF increased proteome coverage

Aiming to find the saturation point of NPs@EDTA the experience was repeated, using the same amount of nanoparticles (1 mg), but with increasing amounts of PF protein: 0.3 mg, 1.5 mg, 3 mg and 4.5 mg. **Figure 4** depicts the SDS-PAGE profile of the adsorbed protein fractions collected in the saturation assay for sample PF2 (the same can be found for PF1 in **Supplementary Figure S5, Appendix**). As one can see, there is a gradual increase in nanoparticle saturation, as proven by similar intensities of gel bands across different samples with a concomitant increase of starting protein mass. For instance, when one compares the assays with 3 mg and 4.5 mg, it is noticeable that bands B (~80 kDa), D (~40 kDa) and E (~35 kDa) display similar intensity across two lanes. Additionally, if one compares the assays with 1.5 mg and 3 mg, the same is true for bands A (~170 kDa) and C (~65-72 kDa). Thus, the main differences in bands' intensity are found when we compare the profiles respective to 0.3 mg and 1.5 mg. For instance, band D is nearly absent and bands A, B and E are fainter when processing only 0.3 mg of protein. Together, these data suggest that 1 mg NPs@EDTA can process up to 3 mg of PF proteins.

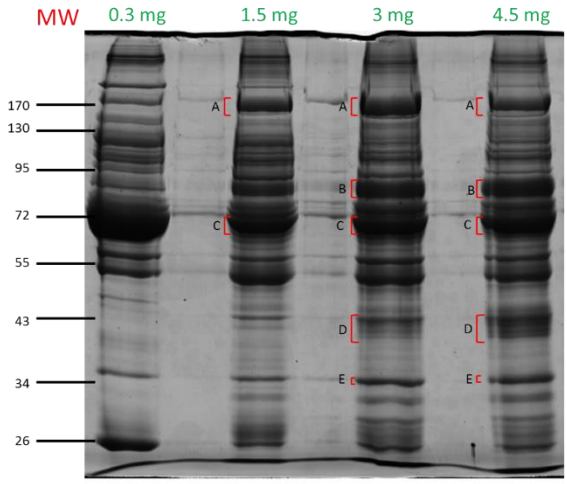

Figure 4. SDS-PAGE profile of the adsorbed protein fractions retrieved after the processing of 0.3 mg, 1.5 mg, 3 mg and 4.5 mg of pericardial fluid protein from sample PF2. Red brackets identify bands A to E, discussed in the text.

Despite the saturation of 1 mg of NPs@EDTA with 3 mg of protein, it was hypothesized that processing a large excess of PF protein (4.5 mg) would still increase proteome coverage and dynamic range. Thus, the proteins belonging to the adsorbed protein fraction

were identified in the assay with 4.5 mg of initial protein. Curiously, 185 proteins were identified again across the two individuals (**Supplementary Figure S6, Appendix**), with similar inter-individual variability – 66% versus 60% in the preliminary assay (**Table 1**). Although, a higher range of protein abundances (5.4 log units) was achieved, outperforming direct PF analysis, i.e. without fractionation/depletion steps. Furthermore, the total number of proteins identified was increased to 247.

3.5. Reproducibility analysis of the NPs@EDTA-based fractionation method

Once the saturation point for the NPs@EDTA was calculated, the reproducibility of the present method was analyzed. Thus, 3 mg of protein of the third PF sample (PF3) was fractionated with the NPs@EDTA in duplicate. The non-adsorbed fraction was then digested in solution, and the peptides were analyzed by a more powerful MS instrument (LTQ-Orbitrap Velos Pro). Overall, 475 proteins could be identified (397 proteins in the first run and 399 proteins in the second run), with 68% of the proteins being identified in both MS/MS runs. Moreover, if one considers the proteins identified with higher confidence (i.e., with 2 or more peptides identified, as in the case of Xiang's work [6]), one can see that 82% of the proteome can be reproducibly identified (271 and 249 proteins identified in the first and second runs, respectively).

3.6. Gene Ontology enrichment analysis

In order to compare protein localization as well as the biological processes between the two methods, a GOEA was performed. To predict protein localization, the STRING webtool was used (**Supplementary Table S2, Appendix**). As expected, both methods allow to explore mainly secreted proteins, as exemplified by "extracellular space" and "extracellular exosome" GO terms. Besides, ClueGO was used to get a glimpse over potentially trackable biological processes (network depicted in **Figure 5**).

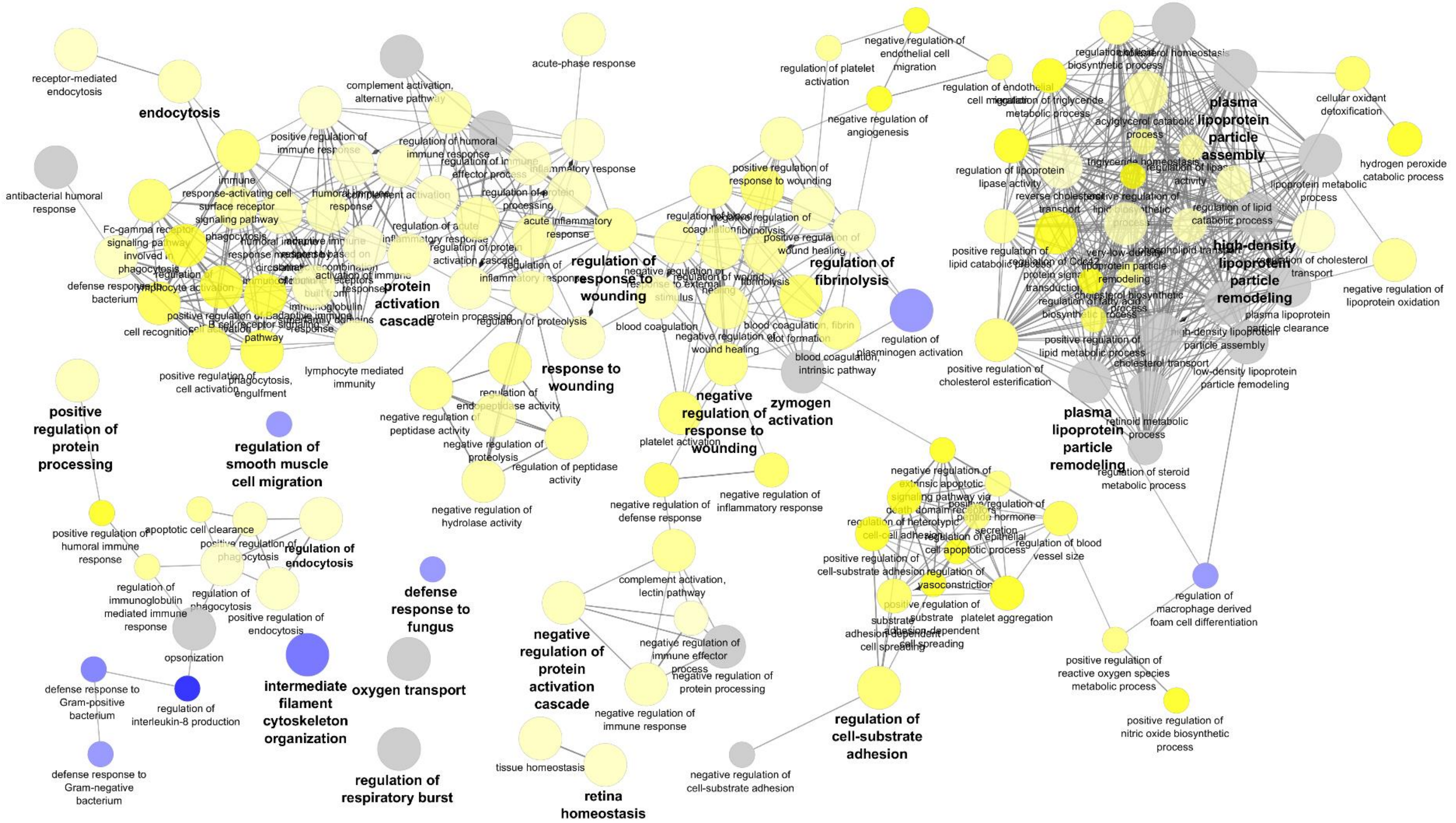

Figure 5. ClueGO network depicting the main biological processes associated to the genes/proteins identified through the kit (green nodes, absent), the NPs@EDTA's-based method (blue nodes) or both (yellow nodes). Gray nodes represent unspecific GO terms. Node size is proportional to each biological phenomenon's relevance.

In this analysis, all proteins exclusively identified in the desired fraction of each method, namely the F1 (24 proteins) and F4 (99 proteins) were compared to those identified by both methods (100 proteins). Interestingly, all processes could be either screened by both methods (**Supplementary Figure S7, Appendix**) or by NPs@EDTA-based fractionation alone (**Figure 6**). Relevant biological phenomena that can be studied using NPs@EDTA alone are, for instance, defense response to fungus, interleukin-8 production and low-density lipoprotein particle remodeling.

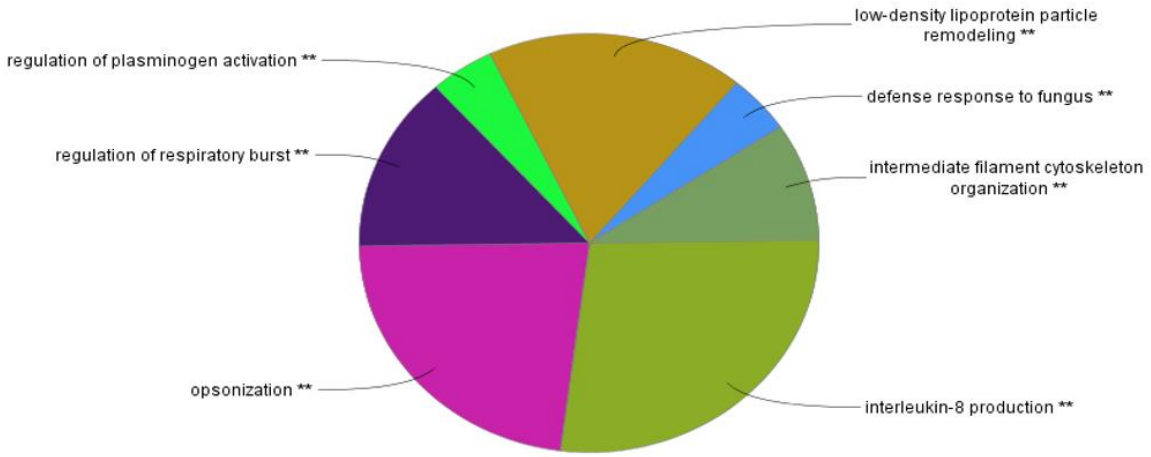

Figure 6. Significant annotated biological processes detectable through NPs@EDTA-based fractionation alone.

3.7. Comparison with known pericardial fluid proteome

Overall 565 proteins were identified, representing 56% of those identified previously [6]. Still, more than half (297) of the identified proteins have not been previously assigned to PF. To analyze the proportion of plasma- and heart-derived proteins in PF's proteome, a comparison was made with the datasets published by Farrah *et al*. [21] (cataloguing over 91 LC-MS/MS datasets) and by Aye *et al*. [22] (analyzing a healthy male's left ventricle tissue following several fractionation, digestion and fragmentation strategies), respectively. When compared to the first PF's proteome reported, a similar proportion of plasma proteins (62% versus 65%, Δ = 3%, n.s.) was found, showing that NPs@EDTA platform does not induce a bias for the plasma subproteome. In turn, heart-derived proteins are slightly less represented (55% versus 62%, Δ = 7%, p <0.05).

Aiming to retrieve the specific biological phenomena detectable with the present dataset, a new GOEA was undertaken in comparison to Xiang's dataset [6]. For instance, phenomena such as humoral immune response, regulation of plasma lipoproteins levels and response to wounding, among others, were found more specifically associated to the dataset obtained by NPs@EDTA-based fractionation (**Figure 7**), showing that the molecular features of this biofluid are not yet completely disclosed.

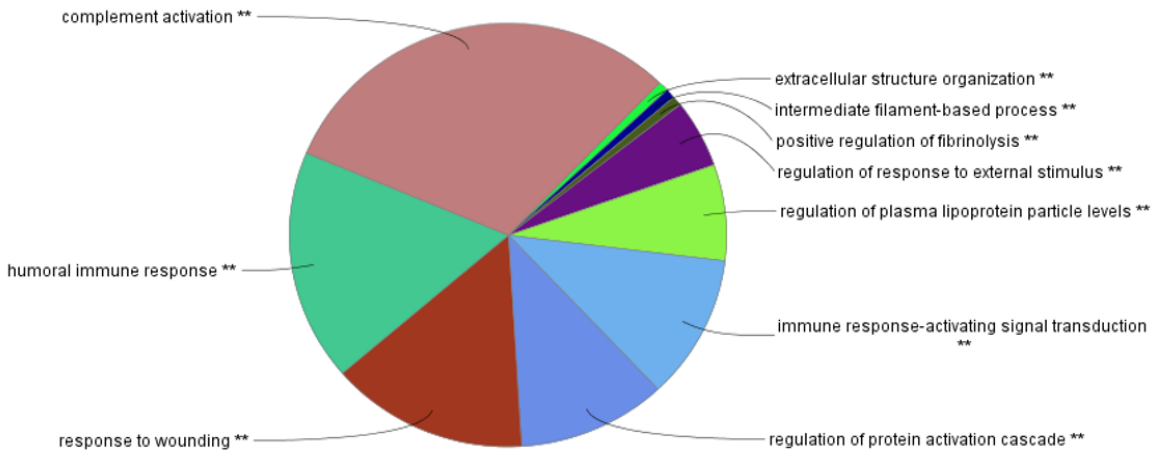

Figure 7. Significant annotated biological processes associated to the experimental dataset as compared to Xiang *et al*. (2013) Proteomics.

4. Discussion

Owing to its anatomical distribution, the PF likely stores relevant molecular information reporting the pathophysiological status of the heart. However, the application of PF for diagnosis purposes is far from being a reality in everyday clinical routine. In fact, PF analysis is often limited to the determination of protein concentration, LDH, ADA (for the diagnosis of tuberculous pericarditis) and the search for malignant markers (such as carcinoembryonic antigen), when patients exhibit pericardial effusion [23]. Before the full exploitation of PF diagnostic or prognostic properties, two major tasks superimpose, namely the complete characterization of PF's proteome and the development of suitable platforms for large-scale analysis. Xiang *et al*. [6] paved the way to fulfill the first, by performing the first in-depth PF proteomic characterization. In their work, 1007 proteins were identified by pooling 10 PF samples from lung bullae patients and by performing two independent LC-

MS/MS runs. Therefore, herein a method to help complete the first task and to accomplish the second is described. An enrichment-based, instead of a depletion-based approach is presented to characterize PF proteome, using affordable lab-made magnetic nanoparticles. Also, this technique was compared to another commercially available and standard method (albumin/IgG-depletion kit) in order to validate the use of NPs@EDTA for PF's proteome fractionation and characterization.

The first challenge in the characterization of PF is, similarly to plasma/serum, the high content in albumin [4]. Thus, proteome fractionation is imperative when one seeks to screen PF's proteome. In fact, by SDS-PAGE, and similarly to the commercial kit, it was found that fractionating PF with NPs@EDTA could decrease the amount of albumin and IgG. By doing so, the NPs@EDTA, like the antibody-based depletion method, increase the odds of identifying other less abundant proteins/peptides, usually undercovered. Moreover, NPs@EDTA-based fractionation was reproducible as corroborated by the presence of the same lane profiles while increasing the protein amount from 0.6 mg to 3 mg (**Figure 2C and 2D**) as well as in the saturation assay (**Figure 4**). Furthermore, NPs@EDTA-based method allowed the identification of a similar number of proteins (138 vs. 140), increased equally (40% vs. 38%) the number of identifications in comparison to the kit, allowed to monitor a higher range of proteins with different abundances (differing somewhere between 10^5 and 10^6-fold) and displayed similar inter-individual variability (60% vs. 62%). For all these reasons, the use of NPs@EDTA to fractionate and characterize PF's proteome was validated.

In order to determine the suitable amount of magnetic beads to process PF, a saturation assay was performed with increasing amounts of protein to a fixed amount of NPs@EDTA. One mg of NPs@EDTA showed the capacity to process up to 3 mg of protein. In a previous assay with urine, a 1:1 ratio was deemed the most appropriate to enrich the urinary proteins of low abundance [24]. Such difference can be explained mainly by the difference in albumin content between the biofluids. In fact, albumin may reach 70% of the total protein content in PF [4], while in urine it represents only 25% [25]. Thus, a lower proportion of NPs@EDTA in PF is needed to collect less abundant proteins. One advantage of using these nanoparticles to fractionate PF prior to proteomic analysis is the chance to adjust the amount of the beads to the protein amount. Contrarily, the commercial columns are limited to 600 µg of protein (~10 µL of serum/plasma). Thus, if one aims to process larger amounts of protein (especially important when the goal is to characterize subproteomes, such as the phosphoproteome) the sample needs to be separated in different columns, increasing

sample manipulation as well as the processing time. Additionally, with magnetic nanoparticles, one can rapidly remove unbound proteins upon application of an external magnetic field.

Another important aspect to consider when designing new proteome fractionation strategies is the reproducibility of protein identification. Therefore, the protocol was performed in duplicate using another sample. Considering the saturation point determined in the previous assay, 1 mg of NPs@EDTA was used to process 3 mg protein. However, in this assay a more powerful MS instrument (LTQ Orbitrap Velos) was used, so that the number of proteins identified could be increased and, thus, the knowledge of the PF proteome. With this approach an inter-run proteome reproducibility of 68% was achieved for overall proteome and of 82% for proteins identified with 2 or more peptides. A study using similar MS instrumentation (LTQ Orbitrap Velos) achieved comparable inter-run reproducibility when processing sera samples with 2 immunodepletion methods. When using the MARS14 system, 79-85% of the proteins (≥2 peptides) were consistently identified. In turn, with the Prot20 system, 76-84% of the proteins (≥2 peptides) were always identified [26]. Using the same criteria for protein identification, Xiang *et al*. [6] could achieve a reproducibility of 80% for the proteins identified in the 2 separate MS/MS runs. Thus, it is possible to conclude that the present method displays a fairly good reproducibility, with proteomes differences being intrinsically associated with the LC-MS/MS technology applied.

The use of NPs@EDTA is also made valid by GO analysis. First, no relevant changes in cell localization were found between the two methods. Second, even though some proteins could only be identified through the kit [e.g. attractin (ATRN), hemoglobin subunit gamma-1 (HBG1) and subunit epsilon (HBE1)], all biological processes were tracked by NPs@EDTA (blue nodes in **Figure 5**) or by both methods (yellow or gray nodes in **Figure 5**). Theoretically, these data show that using NPs@EDTA to fractionate PF one may screen relevant phenomena played by PF proteins exclusively identified through the depletion approach and prompts it to high throughput applications. Furthermore, some relevant biological processes were exclusively tracked with NPs@EDTA, e.g. IL-8 production, LDL particle remodeling and regulation of respiratory burst. The monitoring of these processes in PF can be important to answer relevant questions in cardiovascular research, with the additional advantage of PF being closer to the heart and more likely reflecting the onset of cardiovascular diseases. For instance, tracking of IL-8 production can be important to investigate the predictive power of this cytokine regarding the mortality of acute coronary

syndrome patients [27]. In turn, tracking the regulation of the respiratory burst may provide important clues regarding the metabolic state of the myocardium during remodeling, which may be an important factor in determining a complete or incomplete response to AVR (see ***Chapter II***, **Figure 1C**).

Notwithstanding the ability of NPs@ETDA to replace the traditional kit-based method, both helped expand the known PF proteome. Collectively, 565 proteins could be identified with the two methods and sample fractions and 53% of those (297 proteins) have not been described before [6]. Moreover, specific biological phenomena could be tracked with the attained proteome, less represented or without representation in the referential proteome (**Figure 7**), namely the regulation of response to external stimulus, humoral immune response, response to wounding, positive regulation of fibrinolysis, regulation of protein activation cascade and regulation of plasma lipoprotein particle levels. This can be explained, at least in part, by the main disadvantage of MARS, in which not only the targeted proteins but others are indirectly removed (depletome) due to unspecific binding [5]. Also, such phenomena can also be explained by a larger number of proteins identified playing such roles, through the methods used herein. Additionally, even though MARS targets the 14 most abundant proteins in plasma/PF, removing up to 94% of the total protein mass [5], the protein dynamic range is not as high, as one would envision. In fact, while in the first proteomic study performed with this system the protein abundance ranged in about 6.4 log units, herein, with a much more affordable system, it was possible to screen a set of proteins whose abundance ranged 5.4 log units. Besides, even targeting the proteins of low abundance, a similar representation of heart- and plasma-derived PF's subproteomes was achieved. Together, these observations demonstrate the application potential of NPs@EDTA in the clinical investigation.

The present work enrolled 3 PF samples, with the first 2 being analyzed by a Triple TOF spectrometer and the latter by a LTQ Orbitrap spectrometer. At the end of the first experiment, 247 proteins were identified. At a first glance, this can be considered a limitation, as this is a small number when compared to the 1007 proteins identified by others [6]. However, one should realize that such authors made use of a mass analyzer with higher resolving power (LTQ-Orbitrap with 100,000 – 240,000 versus Triple TOF with 40,000) [28], besides performing two MS/MS runs (873 and 937 proteins were identified in the first and second runs, respectively). Indeed, when using a similar strategy, the number of identified proteins increased to 565. The remaining difference can be explained by the depletion of the 14 most abundant proteins found in plasma (and probably in PF) and also by the pooling

of 10 samples from different individuals [6]. Hence, increasing the number of enrolled subjects would likely increase these numbers (see ***Chapter VI***). Also, the identification of a similar number of proteins (138) as compared to a depletion strategy (employing a HSA- and IgG-depletion kit) similar to that reported in [6], allowing the identification of 140 proteins using the same experimental and instrumentation conditions, corroborates such findings. Additionally, because the samples were not pooled prior to LC-MS/MS analysis, one can evaluate inter-individual variability and set a reference to future studies (60 – 66% of the proteins were shared between individuals when using NPs@EDTA), which was not possible in the former. Moreover, PF was collected from three patients with the same clinical background (AS). Thus, it is likely that enrolling patients with different conditions (e.g. CAD, congenital heart disease) will diversify PF's proteome and even point out potential markers for such pathologies.

5. Conclusions

Taken together, this work validates the use of NPs@EDTA to characterize PF's proteome. NPs@EDTA can be especially useful in large-scale applications such as in cohort studies due to their easy handling and affordability. Furthermore, together with the commercial kit, the known PF repertoire could be increased by 297 proteins, showing how obscure it still is and warranting the analysis from patients with different clinical backgrounds.

*This chapter was adapted from the paper: **F. Trindade**, P. Bastos, A. Leite-Moreira, I. B. Manadas, R. Ferreira, S. F. Soares, A. L. Daniel-da-Silva, I. Falcão-Pires, R. Vitorino. A fractionation approach applying chelating magnetic nanoparticles to characterize pericardial fluid's proteome. Archives of Biochemistry and Biophysics. 634 (2017): 1-10. doi: 10.1016/j.abb.2017.09.016.*

6. References

[1] K. Vogiatzidis, S.G. Zarogiannis, I. Aidonidis, E.I. Solenov, P.-A. Molyvdas, K.I. Gourgoulianis, C. Hatzoglou, Physiology of pericardial fluid production and drainage, Front. Physiol. 6 (2015) 1–6. doi:10.3389/fphys.2015.00062.

[2] F. Trindade, R. Vitorino, A. Leite-Moreira, I. Falcão-Pires, Pericardial fluid: an underrated molecular library of heart conditions and a potential vehicle for cardiac therapy, Basic Res. Cardiol. 114 (2019) 10. doi:10.1007/s00395-019-0716-3.

[3] M. Fujita, M. Komeda, K. Hasegawa, Y. Kihara, R. Nohara, S. Sasayama, Pericardial fluid as a new material for clinical heart research, Int. J. Cardiol. 77 (2016) 113–118. doi:10.1016/S0167-5273(00)00462-9.

[4] S. Ben-Horin, A. Shinfeld, E. Kachel, A. Chetrit, A. Livneh, The composition of normal pericardial fluid and its implications for diagnosing pericardial effusions, Am. J. Med. 118 (2005) 636–640. doi:10.1016/j.amjmed.2005.01.066.

[5] E. Gianazza, I. Miller, L. Palazzolo, C. Parravicini, I. Eberini, With or without you — Proteomics with or without major plasma/serum proteins, J. Proteomics. 140 (2016) 62–80. doi:10.1016/j.jprot.2016.04.002.

[6] F. Xiang, X. Guo, W. Chen, J. Wang, T. Zhou, F. Huang, C. Cao, X. Chen, Proteomics analysis of human pericardial fluid, Proteomics. 13 (2013) 2692–2695. doi:10.1002/pmic.201200317.

[7] F. Trindade, F. Amado, R.P. Oliveira-Silva, A.L. Daniel-da-Silva, R. Ferreira, J. Klein, R. Faria-Almeida, P.S. Gomes, R. Vitorino, Toward the definition of a peptidome signature and protease profile in chronic periodontitis, PROTEOMICS – Clin. Appl. 9 (2015) 917–927. doi:10.1002/prca.201400191.

[8] R. Oliveira-Silva, J. Pinto da Costa, R. Vitorino, A.L. Daniel-da-Silva, Magnetic chelating nanoprobes for enrichment and selective recovery of metalloproteases from human saliva, J. Mater. Chem. B. 3 (2015) 238–249. doi:10.1039/C4TB01189A.

[9] U.K. Laemmli, Cleavage of structural proteins during the assembly of the head of bacteriophage T4, Nature. 227 (1970) 680–685. doi:10.1038/227680a0.

[10] J.R. Wiśniewski, A. Zougman, N. Nagaraj, M. Mann, Universal sample preparation method for proteome analysis., Nat. Methods. 6 (2009) 359–362. doi:10.1038/nmeth.1322.

[11] S.I. Anjo, C. Santa, B. Manadas, Short GeLC-SWATH: A fast and reliable quantitative approach for proteomic screenings, Proteomics. 15 (2015) 757–762. doi:10.1002/pmic.201400221.

[12] C. Silva, C. Santa, S.I. Anjo, B. Manadas, A reference library of peripheral blood mononuclear cells for SWATH-MS analysis, PROTEOMICS – Clin. Appl. 10 (2016) 760–764. doi:10.1002/prca.201600070.

[13] L. Sennels, J.-C. Bukowski-Wills, J. Rappsilber, Improved results in proteomics by use of local and peptide-class specific false discovery rates, BMC Bioinformatics. 10 (2009) 1–11. doi:10.1186/1471-2105-10-179.

[14] W.H. Tang, I. V Shilov, S.L. Seymour, Nonlinear Fitting Method for Determining Local False Discovery Rates from Decoy Database Searches, J. Proteome Res. 7 (2008) 3661–3667. doi:10.1021/pr070492f.

[15] J.S. Cottrell, U. London, Probability-based protein identification by searching sequence databases using mass spectrometry data, Electrophoresis. 20 (1999) 3551–3567. doi:10.1002/(SICI)1522-2683(19991201)20:18<3551::AID-ELPS3551>3.0.CO;2-2.

[16] Y. Perez-Riverol, A. Csordas, J. Bai, M. Bernal-Llinares, S. Hewapathirana, D.J. Kundu, A. Inuganti, J. Griss, G. Mayer, M. Eisenacher, E. Pérez, J. Uszkoreit, J. Pfeuffer, T. Sachsenberg, S. Yilmaz, S. Tiwary, J. Cox, E. Audain, M. Walzer, A.F. Jarnuczak, T. Ternent, A. Brazma, J.A. Vizcaíno, The PRIDE database and related tools and resources in 2019: improving support for quantification data, Nucleic Acids Res. 47 (2019) D442–D450. doi:10.1093/nar/gky1106.

[17] T. Hulsen, J. de Vlieg, W. Alkema, BioVenn – a web application for the comparison and visualization of biological lists using area-proportional Venn diagrams, BMC Genomics. 9

(2008) 488. doi:10.1186/1471-2164-9-488.
[18] D. Szklarczyk, A. Franceschini, S. Wyder, K. Forslund, D. Heller, J. Huerta-Cepas, M. Simonovic, A. Roth, A. Santos, K.P. Tsafou, M. Kuhn, P. Bork, L.J. Jensen, C. von Mering, STRING v10: protein-protein interaction networks, integrated over the tree of life., Nucleic Acids Res. 43 (2015) D447-452. doi:10.1093/nar/gku1003.
[19] G. Bindea, B. Mlecnik, H. Hackl, P. Charoentong, M. Tosolini, A. Kirilovsky, W.-H. Fridman, F. Pagès, Z. Trajanoski, J. Galon, ClueGO: a Cytoscape plug-in to decipher functionally grouped gene ontology and pathway annotation networks., Bioinformatics. 25 (2009) 1091–1093. doi:10.1093/bioinformatics/btp101.
[20] M. Page, R. Thorpe, Analysis of IgG Fractions by Electrophoresis, in: J.M. Walker (Ed.), Protein Protoc. Handb., Humana Press, Totowa, NJ, 2002: pp. 1005–1007. doi:10.1385/1-59259-169-8:1005.
[21] T. Farrah, E.W. Deutsch, G.S. Omenn, D.S. Campbell, Z. Sun, J.A. Bletz, P. Mallick, J.E. Katz, J. Malmström, R. Ossola, J.D. Watts, B. Lin, H. Zhang, R.L. Moritz, R. Aebersold, A High-Confidence Human Plasma Proteome Reference Set with Estimated Concentrations in PeptideAtlas, Mol. Cell. Proteomics. 10 (2011) 1–14. doi:10.1074/mcp.M110.006353.
[22] T.T. Aye, A. Scholten, N. Taouatas, A. Varro, T.A.B. Van Veen, M.A. Vos, A.J.R. Heck, Proteome-wide protein concentrations in the human heart, Mol. Biosyst. 6 (2010) 1917–1927. doi:10.1039/C004495D.
[23] L.J. Burgess, Biochemical analysis of pleural, peritoneal and pericardial effusions, Clin. Chim. Acta. 343 (2004) 61–84. doi:10.1016/j.cccn.2004.02.002.
[24] P. Bastos, F. Trindade, R. Ferreira, A. Leite-Moreira, I. Falcão-Pires, B. Manadas, A.L. Daniel-da-Silva, R. Vitorino, EDTA-functionalized magnetic nanoparticles: A suitable platform for the analysis of low abundance urinary proteins, Talanta. 170 (2017) 81–88. doi:10.1016/j.talanta.2017.03.087.
[25] N. Nagaraj, M. Mann, Quantitative analysis of the intra- and inter-individual variability of the normal urinary proteome., J. Proteome Res. 10 (2011) 637–645. doi:10.1021/pr100835s.
[26] M.P.W. Smith, S.L. Wood, A. Zougman, J.T.C. Ho, J. Peng, D. Jackson, D.A. Cairns, A.J.P. Lewington, P.J. Selby, R.E. Banks, A systematic analysis of the effects of increasing degrees of serum immunodepletion in terms of depth of coverage and other key aspects in top-down and bottom-up proteomic analyses, Proteomics. 11 (2011) 2222–2235. doi:10.1002/pmic.201100005.
[27] E. Cavusoglu, J.D. Marmur, S. Yanamadala, V. Chopra, S. Hegde, A. Nazli, K.P. Singh, M. Zhang, C. Eng, Elevated baseline plasma IL-8 levels are an independent predictor of long-term all-cause mortality in patients with acute coronary syndrome, Atherosclerosis. 242 (2015) 589–594. doi:10.1016/j.atherosclerosis.2015.08.022.
[28] Z. Zhang, S. Wu, D.L. Stenoien, L. Paša-Tolic, High-throughput proteomics, Annu. Rev. Anal. Chem. 7 (2014) 427–454. doi:10.1146/annurev-anchem-071213-020216.

Chapter VI

Pericardial fluid proteome profile in aortic stenosis patients with complete or incomplete reverse remodeling

Contents

Abstract

Biomarker discovery has been traditionally pursued by proteomic characterization of easily accessed biofluids such as plasma or urine. Although, there are cases where less easily accessed biofluids can offer a direct window to the diseased organ, serving as a pool to fish biomarkers with higher predicted specificity for a given condition. This is the case of pericardial fluid. If previously considered a mere plasma ultrafiltrate, today it is clear that pericardial fluid also stores many heart-derived proteins. Therefore, the screening of pericardial fluid proteome may uncover surrogate prognostic markers for incomplete myocardial reverse remodeling. Despite the potential of pericardial fluid as a platform for prognosis, two limitations arise when one aims at characterizing this biofluid's proteome in aortic stenosis. First, the contribution of albumin should be eliminated or minimized, to disclose proteins of lower abundance. This has been addressed in the previous ***Chapter V***, through the fractionation with NPs@EDTA, herein applied on a larger scale. Second, the enrollment of healthy control individuals is unethical. To bypass this problem and, thus, improve the specificity of the analysis, pericardial fluid from other cardiac pathologies/surgeries lacking the variable/stress of interest (pressure overload) is used. In this case, coronary artery disease patients are used to control the differences between patients with complete or incomplete reverse remodeling. By following a shotgun approach, over 750 proteins could be identified in the pericardial fluid of patients undergoing valve replacement or coronary artery bypass grafting. Seven proteins were found dysregulated in patients showing complete or incomplete reverse remodeling. Interestingly, the pericardial fluid proteome points to an apparent complement C8 consumption in patients with incomplete reverse remodeling. Gene ontology enrichment analysis shows a significant representation of proteins with mitochondrial origin in patients with an incomplete response, suggesting higher levels of cell death in the myocardium of these patients. Although no prognostic markers could be encountered, new clues on the pathology of incomplete myocardial reverse remodeling emerged with this proteomics approach. Particularly, complement activation comes out as a key event in myocardial remodeling, and new questions arise in this regard: is the complement system promoting cardiomyocyte cell death or instead does the loss of cardiomyocyte intracellular contents activate this arm of the innate immune system? Anyway, targeting the complement system in patients with incomplete reverse remodeling may become a valuable therapy to improve the postoperative outcome.

1. Background

The assessment of myocardial hypertrophy after AVR is of extreme importance because patients showing incomplete regression of LV mass are at greater risk for long-term complications, such as myocardial infarction, stroke or heart failure, leading to prolonged hospitalizations and reduced survival [1–3]. In this regard, the prediction of iRR would be of great interest for the clinician, to tighten patients' surveillance and to initiate adjuvant therapies designed to mitigate the development of heart failure and improve their survival. So far, many clinical parameters, such as age, sex, hypertension, diabetes, CAD, valve hemodynamics and size or patient-prosthesis mismatch have failed to predict iRR [4,5]. Preoperative LVM, a measure of the extent of hypertrophy, is perhaps the best predictor of iRR available today [5]. However, not all patients with higher preoperative LVM show worse regression (for examples, the reader is referred to **Table 1** in ***Chapter II*** and ***Chapter III***). Therefore, more reliable prognostic markers of iRR are needed.

In the quest to identify new and more specific tools of iRR prognosis, the PF holds great potential. First, the PF collects many heart-derived factors, including from the myocardial interstitial space [6], such as growth factors [7–9], prostaglandins [10] and cytokines [11–13], which are involved in the paracrine regulation of the heart, modulating vasodilation, contractility and sympathetic tone [10,14]. Second, PF has low clearance rates [15], increasing the probability of detecting molecules that may more rapidly be eliminated in other biofluids. Third, the variation of molecular species in PF is more strongly associated with echocardiographic parameters of cardiac structure and function than blood-derived biofluids (see **Table 3**, ***Chapter I*** or [16]). Fourth, the process of translating surrogate markers to plasma (or serum) monitoring is easier than from myocardium, since the PF is a plasma ultrafiltrate. Fifth, the proximity to the heart brings the additional advantage of identifying new molecular mechanism of disease and potential therapeutic targets, when high throughput approaches, such as proteomics, are followed.

Currently, the use of PF's diagnostic/prognostic properties is mainly limited to pericardial diseases often leading to pronounced fluid buildup [17]. In the context of valve disease and myocardial remodeling, though, the full potential of PF is yet to explore, and few reports have been published addressing the molecular characterization of PF in this setting. For instance, increased levels of asymmetric dimethylarginine [18] and decreased levels of adenosine, LDH, ferritin and ghrelin [19–21] are observed in valvular heart disease when

compared to CAD. It was also found that natriuretic peptides (ANP and BNP) and the ADM (a peptide with anti-hypertrophic and anti-fibrotic properties) are increased in AS, when compared with other valve disorders that, unlike AS, induce LV volume overload, namely aortic or mitral regurgitation [22]. Concerning LV remodeling, it was found a strong positive association of MMP2 with LV systolic and diastolic volumes and a negative correlation with LVEF [23], although this was observed in a population of CAD patients. Hence, much is yet to uncover regarding PF molecular features in heart diseases, especially in AS and the subsequent myocardial remodeling.

Therefore, in order to help fill the gap in the knowledge of PF molecular features in AS and to identify potential prognostic markers of iRR, the PF proteome was characterized for the first time in this condition.

2. Material and Methods

2.1. Study design, patients selection and clinical characterization

Patients were selected based on retrospective clinical data, and the respective PF samples were gathered from the local biobank. The local ethics committee approved the study protocol and written informed consent was obtained from all patients.

Clinical evaluation of AS severity and myocardial structure and function was based on transthoracic echocardiography. Peak aortic valve velocity (Peak Ao), mean aortic transvalvular pressure gradient and indexed aortic valve area (AVAi) were derived from Doppler echocardiography. Mean pressure gradient was obtained with the modified Bernoulli equation and AVAi with the standard continuity equation. In turn, LV end-diastolic dimension (LVEDD), LV posterior wall thickness (PWT) and interventricular septal thickness (IVST) were derived from 2D-echocardiograms during diastole. Relative wall thickness (RWT) was calculated as 2×PWT/LVEDD. Correct orientation of imaging planes, cardiac chambers dimension and function measurements were performed according to the EAE/ASE recommendations [24].

LV mass (LVM) index (LVMi) was estimated according to the joint recommendations of the ASE and EAE using Devereux's formula for ASE measurements in diastole: LV mass = 0.8 x (1.04 x ([LV internal dimension + posterior wall thickness + interventricular septal thickness]^3 – [LV internal dimension]^3) + 0.6 g. LV mass (LVM) index (LVMi) was calculated according to the recent recommendations for cardiac chamber quantification [24]. LVMi greater than 115 g/m^2 in men and greater than 95 g/m^2 in women were considered indicative of LV hypertrophy.

Thirteen AS patients were initially selected for the characterization of PF proteome. Only patients undergoing AVR with moderate-to-severe AS (according to ESC/AHA guidelines [25]) and with no more than one stenotic coronary vessel were selected. One AS patient was excluded because there was clinical indication of severe depression of the systolic function. Six additional CAD patients with ≥2 stenotic coronaries, but without clinical evidence of AS, were selected as controls. For validation assays, 20 extra patients with moderate-to-severe AS, with no more than one stenotic coronary vessel were selected. From these only 14 patients could be considered because they either missed postoperative echocardiography (n = 5) or presented reduced LVEF (34%, n = 1).

The clinical and demographical of the final selection of patients for discovery proteomics (n = 12) and validation cohort (n = 14) is summarized in **Table 1**. All patients enrolled in this study were free of dilated or hypertrophic cardiomyopathies. Upon preoperative echocardiographic assessment, all patients from the validation cohort showed LVEF >50% (n = 23) or had clinical indication of normal/good systolic function (n = 3). Hence, the evaluation of RR was based on echocardiographic assessment of LV hypertrophy. LVM regression (%) was defined as the difference between pre- and postoperative LVMi. Patients with LVM regression (ΔLVM) ≥15% were included in the complete RR (cRR) group, while those with LVM regression ≤5% were integrated into the incomplete RR (iRR) group. Complete and incomplete RR groups were not different regarding risk factors such as age, hypertension, obesity, diabetes and smoking. Patients from the validation cohort were collected blindly in relation to the extent of RR. Four patients presented cRR, four presented iRR and the remaining six showed an intermediate phenotype (5%< ΔLVM <15%).

Table 1. Clinical data of the study population.

Parameters	**Discovery proteomics population**			**Slot blot validation population**
Degree of Reverse Remodeling	Complete (ΔLVM≥15%)	Incomplete (ΔLVM≤5%)	*p*	Blind
Demographics				
N	5	7	n.s.	14
Age	67.6±18.9	71.6±6.6	n.s.	70.7±8.5
Gender (male:female)	2:3	2:5	n.s.	6:8
BMI (kg/m^2)	25.3±5.9	32.8±6.8	n.s.	29.8±3.8
Obesity (n)	1	6	n.s.	8
Hypertension (n)	5	5	n.s.	8
Diabetes mellitus (n)	1	3	n.s.	5
CAD (≤1 vessel) (n)	0	1	n.s.	1
Smoking history (n)	1	1	n.s.	6
COPD (n)	2	2	n.s.	2
Mild-to-moderate aortic insufficiency (n)	4[a]	4	n.s.	12
Mild-to-moderate mitral stenosis (n)	0[b]	1	n.s.	2
Mild-to-moderate mitral insufficiency (n)	5	5[c]	n.s.	13
Mild-to-moderate tricuspid insufficiency (n)	4	5	n.s.	11
Preoperative parameters				
AVAi, cm^2/m^2	0.43±0.12	0.45±0.08	n.s.	0.43±0.12
Peak Ao, m/s	4.7±0.7	4.4±0.6	n.s.	4.7±0.3
Max ATPG, mmHg	91.0±28.5	80.1±22.0	n.s.	88.1±11.7
Mean ATPG, mmHg	56.4±16.8	49.0±11.7	n.s.	55.9±6.0
LVEDD, cm	5.0±0.3	5.1±0.4	n.s.	4.9±0.5
IVST, cm	1.4±0.1	1.3±0.1	n.s.	1.3±0.3
PWT, cm	1.2±0.0	1.1±0.1	n.s.	1.1±0.2
RWT	0.47±0.04	0.41±0.04	*	0.46±0.10
LVMi, g/m^2	150.4±21.6	126.6±21.6	n.s.	126.0±33.1
Postoperative parameters				
LVEDD, cm	4.9±0.8	5.1±0.4	n.s.	4.7±0.5
IVST, cm	1.2±0.2	1.4±0.2	n.s.	1.3±0.2
PWT, cm	0.8±0.2	1.1±0.1	*	1.0±0.1
RWT	0.35±0.09	0.41±0.06	n.s.	0.42±0.08
LVMi, g/m^2	107.4±28.2	138.5±27.1	n.s.	113.2±22.3
ΔLVM, %	29.2±12.3	-9.5±11.1	[d]	7.1±19.1

* *p* <0.05 (unpaired two-tailed t-test); a) One patient presented with severe aortic insufficiency; b) One patient presented with severe mitral stenosis; c) One patient presented with severe mitral insufficiency; d) Independent variable

Abbreviations: ATPG: aortic transvalvular pressure gradient; AVAi: aortic valve area, indexed to body surface area; BMI: body mass index; CAD: coronary artery disease; COPD: chronic obstructive pulmonary disease; IVST: interventricular septal thickness; LVEDD: left ventricle end-diastolic dimension; LVMi: left ventricle mass, indexed to body surface area; Peak Ao: peak aortic valve velocity; PWT: posterior wall thickness; RWT: relative wall thickness; ΔLVM: left ventricle mass regression.

2.2. Sample collection and processing

Immediately after sternotomy and pericardiotomy, around 15 mL of PF was collected from each patient. Following collection, PF was centrifuged at 5,000 rpm, 4 °C for 15 min to remove cellular components, and the supernatant was aliquoted and stored at -80 °C until further processing. Protein concentration was estimated by the DC method (BioRad®), using BSA as standard.

PF samples used for proteomics were fractionated with NPs@EDTA, essentially as described in [26] (also in ***Chapter V***). Briefly, 3 mg of protein was incubated with 1 mg of magnetic nanoparticles (NPs@EDTA) in continuous agitation for 1h at room temperature. Subsequently, the albumin-rich supernatant was removed, and the beads were washed 3 times with 500 µL of MES buffer (0.01 M MES, 0.01 M NaCl, pH 6.5-8.5) for 5 min. Finally, the beads were incubated with 30 µL of Laemmli loading buffer and agitated for 10 min to elute the desired albumin-poor fraction. These fractions were readily processed and resolved by SDS-PAGE in denaturing and reducing conditions, applying a 200 V voltage. Gels were then incubated in fixation solution (methanol: acetic acid 40:10 v/v) for 45 min, stained with Colloidal Coomassie Blue G250 and destained with 20% methanol until an optimal contrast was achieved.

2.3. In-gel digestion and peptide cleanup

Each lane of the gels was cut in 16 pieces and washed with 100 mM NH_4HCO_3 and acetonitrile. Proteins were then reduced with 10 mM DTT (30 min, 60 °C), alkylated in the dark with 55 mM IAA (30 min, 25 ºC) and washed again with 100 mM NH_4HCO_3 and acetonitrile, before being digested with trypsin overnight (37 °C). Peptides were extracted first with 10% FA and with FA 10%: acetonitrile (1:1) and then vacuum-dried. Next, peptides were resuspended in 2% acetonitrile and 1% FA and purified using OMIX Tip C18 columns C18 Spin Columns (Agilent) following the manufacturer's instructions. Peptides were re-dried and kept frozen (-80 ºC) until MS-based analysis.

2.4. LC-MS/MS analysis

The peptide mixtures were re-suspended in 20 µL loading solvent (0.1% trifluoroacetic acid in water/ acetonitrile, 2/98 (v/v)). 10 µL of the peptide mixtures were analyzed by LC−MS/MS system on an Ultimate 3000 RSLC nano LC (Thermo Fisher Scientific, Bremen, Germany) in-line connected to a Q Exactive HF mass spectrometer (Thermo Fisher Scientific). The peptides were first loaded on a trapping column (made in-house, 100 µm ID × 20 mm, 5 µm beads C18 Reprosil-HD, Dr. Maisch, Ammerbuch-Entringen, Germany) and after flushing from the trapping column, peptides were loaded on an analytical column (made in-house, 75 µm ID × 400 mm, 1.9 µm beads C18 Reprosil-HD, Dr. Maisch) using a non-linear 150 min gradient of 2-56% solvent B (0.1% FA in water/acetonitrile, 20/80 (v/v)) at a flow rate of 250 nL/min. This was followed by a 10 min wash reaching 99% solvent B and re-equilibration with solvent A (0.1% FA in water). Column temperature was kept constant at 50 °C (CoControl 3.3.05, Sonation).

The mass spectrometer was operated in DDA, positive ionization mode, automatically switching between MS and MS/MS acquisition for the 16 most abundant peaks in a given MS spectrum. The source voltage was set to 2.8 kV and the capillary temperature was 250 °C. One MS1 scan (*m/z* 375-1500, AGC target 3E6 ions, maximum ion injection time of 60 ms) acquired at a resolution of 60,000 (at 200 *m/z*) was followed by up to 16 tandem MS scans (resolution 15,000 at 200 *m/z*) of the most intense ions fulfilling predefined selection criteria (AGC target 1E5 ions, maximum ion injection time of 80 ms, isolation window of 1.5 *m/z*, fixed first mass of 145 *m/z*, spectrum data type: centroid, under fill ratio 1%, intensity threshold 1.3E4, exclusion of unassigned, singly charged precursors, peptide match preferred, exclude isotopes on, dynamic exclusion time of 12 s). The higher collision energy dissociation was set to 28% Normalized Collision Energy, and the polydimethylcyclosiloxane background ion at 445.12002 Da was used for internal calibration (lock mass).

2.5. Data analysis

Data analysis was performed with MaxQuant (version 1.6.1.0) using the Andromeda search engine. Spectra were searched against the human proteins in the Swissprot database (release March 2018, www.uniprot.org). The mass tolerance for precursor and fragment ions was set to 20 and 4.5 ppm, respectively, during the main search. Enzyme specificity was set to C-terminal to arginine and lysine, also allowing cleavage at arginine/lysine-proline bonds with a maximum of two missed cleavages. Carbamidomethylation on cysteines was set as a fix modification. Variable modifications were set to oxidation of methionine, acetylation of protein N-termini and phosphorylation of serine, threonine or tyrosine. Matching between runs was allowed using a 0.7 min match time window and a 20 min alignment time window. Proteins were quantified by the MaxLFQ algorithm integrated in the MaxQuant software. Identified peptides have been filtered using a 1% FDR. Only proteins identified with 2 or more peptides were considered.

The proteome data has been deposited to the ProteomeXchange Consortium via PRIDE [27] partner repository, with the dataset identifier PXD015607.

2.6. Bioinformatics analysis

MaxQuant's LF algorithm (MaxLFQ) was used to calculate the fold-change of protein variation between AS and CAD patients and, then, between patients with cRR and iRR. MaxLFQ normalizes data based on peptide intensities [28]. After filtering out contaminants, reversed sequences and proteins identified only by site, data was transformed by computing log2 and the differences detected with t-test. As an additional validation step of the dysregulated proteins, the effect size was calculated using Cohen's d (standardized mean difference).

To inquire the potential prognostic value of the significantly changed proteins between cRR and iRR, a univariate receiver operating characteristic (ROC) curve analysis was performed with MetaboAnalyst v4.0, to compute the area under the curve (AUC) and infer about sensitivity and specificity of each hypothetical marker.

Next, a first GOEA and pathway enrichment analysis was undertaken with FunRich (v.3.1.3), providing the main differences in biological processes, pathways, molecular functions and protein distribution across cellular components [29]. For this analysis, the proteins showing significant changes between cRR and iRR as well as the exclusive proteins were selected. The top 10 terms were selected based on the highest differences between cRR and iRR in the percentage of genes covering each of the enlisted terms, using the whole proteome as reference and the FunRich database. To provide a deeper screen of the dysregulated biological processes in (in)complete RR a second GOEA was performed with Cytoscape's plugins ClueGO (v.2.5.4) [30] and Cluepedia (v.1.5.4). For this purpose, two clusters were defined (cRR and iRR) comprising the same proteins. The GO range was fixed between levels 3 and 8 and a minimum of three genes per cluster was defined to map GO terms. The GO library, from the Gene Ontology consortium, was updated on February 27th, 2019.

A multivariate analysis, considering also the relationship between proteins, was pursued with MetaboAnalyst v4.0. To that end, normalized LFQ and log2-transform data was uploaded and scaled by Pareto's method, to provide the best bell-shaped distribution. Then, a PLS-DA was undertaken to identify the most important variables (proteins) to separate AS from CAD (controls) and, then, cRR from iRR patients (VIP).

2.7. Immunoblot validation

All proteins except for complement C3 were analyzed through slot blot. From each PF sample, 10 µg of protein diluted in TBS buffer (10 mM Tris(hydroxymethyl)aminomethane, 240 mM NaCl, pH 8.0) was loaded into the wells in a slot blot apparatus. Protein was transferred with vacuum onto 0.45 µm nitrocellulose membranes (Amersham™ Protan™, GE Healthcare). In the case of C3, the quantification was performed by western blot, essentially as described in ***Chapter II*** (section 2.5), with minor modifications: 20 µg of PF protein were diluted with 0.5 M Tris(hydroxymethyl)aminomethane pH 6.8, before mixing with Laemmli loading buffer and boiled for 5 min at 95 °C before loading in a 10% polyacrylamide gel. In order to normalize total protein levels after the transfer, membranes (slot or western blot) were stained with Ponceau S and digitalized in a GS-800™ Calibrated Imaging Densitometer (Bio-Rad). To remove the staining, membranes were washed with

TBS-T (TBS buffer with 0.05% Tween-20). Then, membranes were blocked with 5% (w/v) nonfat dry milk in TBS for 30 min, except for cytochrome C, where blocking was done with 5% BSA. Incubation with the primary antibody was done overnight. In the next day, membranes were washed thrice with TBS-T, for 10 min, and incubated with the respective secondary peroxidase-conjugated antibodies for one hour (**Table 2** compiles all the antibodies used). The membranes were washed again thrice with TBS-T solution for 3 x 10 min before protein detection. The detection was carried out with enhanced chemiluminescence reagents (Western Bright™, Advansta), with support of ChemiDoc™ Touch Imaging System. Blot scans were analyzed with ImageLab 5.1 software (Bio-Rad). OD of each band was normalized to the OD obtained with Ponceau S staining.

Table 2. List of antibodies used in slot blot and western blot.

Protein target	UniProt ID and Gene Name	Primary antibody	Secondary antibody
Protein AMBP	P02760 AMBP	Mouse mAb 1:1000; sc-81948	HRP-linked sheep anti-mouse 1:5000; GE Amersham NA931
Cytochrome C	P99999 CYCS	Rabbit mAb 1:1000; 136F3 Cell Signaling #4280	HRP-linked donkey anti-rabbit 1:10000; GE Amersham NA934
Adrenomedullin	P35318 ADM	Mouse mAb 1:1000; sc-80462	HRP-linked sheep anti-mouse 1:5000; GE Amersham NA931
72 kDa type IV collagenase (Matrix Metalloproteinase 2)	P08253 MMP2	Rabbit pAb 1:1000; ab37150	HRP-linked donkey anti-rabbit 1:10000; GE Amersham NA934
Metalloproteinase inhibitor 1	P01033 TIMP1	Rabbit pAb 1:1000; ab38978	HRP-linked donkey anti-rabbit 1:10000; GE Amersham NA934
Metalloproteinase inhibitor 2	P16035 TIMP2	Mouse mAb 1:1000; ab1828	HRP-linked sheep anti-mouse 1:5000; GE Amersham NA931
Complement C3	P01024 C3	Mouse mAb 1:1000; sc-28294	HRP-linked sheep anti-mouse 1:5000; GE Amersham NA931

Abbreviations: HRP: horseradish peroxidase; mAb: monoclonal antibody; pAb: polyclonal antibody.

2.8. Statistical analysis

Categorical clinical data is presented as absolute frequencies. Fisher's exact test was applied to detect differences between both groups (cRR and iRR). Continuous demographical and molecular expression data are presented as mean ± standard deviation. The normality of the distribution was tested by the D'Agostino & Pearson omnibus method. Detection of sample outliers in immunoblot analysis was performed with the ROUT method, with the most stringent cutoff (0.1% FDR, "Q"). The differences between groups were tested with the unpaired two-tailed t-test, if the variables were normally distributed, or with the Mann-Whitney test, if otherwise. Correlation between clinical parameters and the relative expression of the proteins was evaluated with Pearson's test if data presented a normal distribution and with Spearman's test, if otherwise. All statistical tests were done with GraphPad Prism 6 and, in any case, p <0.05 was considered significant.

3. Results

As in the case of ***Chapter II***, all subjects included in this study presented moderate-to-severe AS, according to ESC's and AHA's guidelines [25]. In all cases, AVAi was below 0.60 cm^2/m^2, except one subject with an AVAi of 0.61 cm^2/m^2, and the peak Ao was over 4 m/s, except two subjects, one with a peak Ao of 3.81 m/s and other with 3.87 m/s. The mean aortic transvalvular pressure gradient ranged between 36 and 80 mmHg, without significant differences between cRR and iRR regarding the severity of the stenosis. The patients with cRR and iRR were also not significantly different with concern to potential risk factors, such as age, gender, obesity, hypertension, diabetes mellitus, CAD, smoking history or co-existing extra-aortic valve disorders. Beyond the demographics, the patients were quite homogeneous concerning myocardial remodeling and systolic function. In the discovery proteomics cohort, iRR showed a slightly less concentric remodeling that was quite close to the threshold (mean preoperative RWT = 0.41, threshold = 0.42). Still, these and all the remaining patients displayed preserved systolic function. Therefore, in the following sections, the differences in the PF proteome reflect the higher or lower proclivity to post-AVR LVM regression.

3.1. The pericardial fluid proteome profile in aortic stenosis patients with complete and incomplete reverse remodeling

By applying a NPs@EDTA-based fractionation approach, 761 proteins could be identified in human PF. Since CAD is the most prevalent heart disease [31], and it is unethical to collect PF from healthy patients, the proteome of CAD patients was used to control the experiment, providing an added degree of specificity in what concerns the identification of potential molecular markers of iRR. As shown in the Venn diagrams (**Figure 1A**) almost 10% of the proteins (74) were exclusively identified in controls. From the remaining 687 proteins, 4.1% (28 proteins) were only associated with AS patients showing cRR and 24.4% (168 proteins) to iRR patients. The first comparison between controls and AS patients elicited 22 dysregulated proteins in AS (**Figure 1B**, top, **Table 3**). Then, the proteome of AS patients with cRR and iRR was compared, showing that seven proteins are significantly altered between these two groups (**Figure 1B**, bottom, **Table 4**). A significant increase in the apolipoproteins C-III and A-IV, protein AMBP and the phosphatidylinositol-glycan-specific phospholipase D (GPLD1) levels and a significant decrease in complement C8 (α, β and γ chains) levels was found in patients with iRR. All these seven proteins showed a large effect-size, as shown by a Cohen's d >0.8. Except for GPLD1, all the above proteins were identified in all AS patients. Furthermore, all the remaining six proteins showed a strong (≥1.5-fold) and consistent variation (see **Supplementary Figure S8, Appendix** displaying Cohen's d 95% confidence interval) and presented specificity to AS, as these proteins did not vary significantly when comparing to controls. Hence, the apolipoproteins C-III, A-IV, protein AMBP and complement C8 emerge as candidate prognostic markers of iRR.

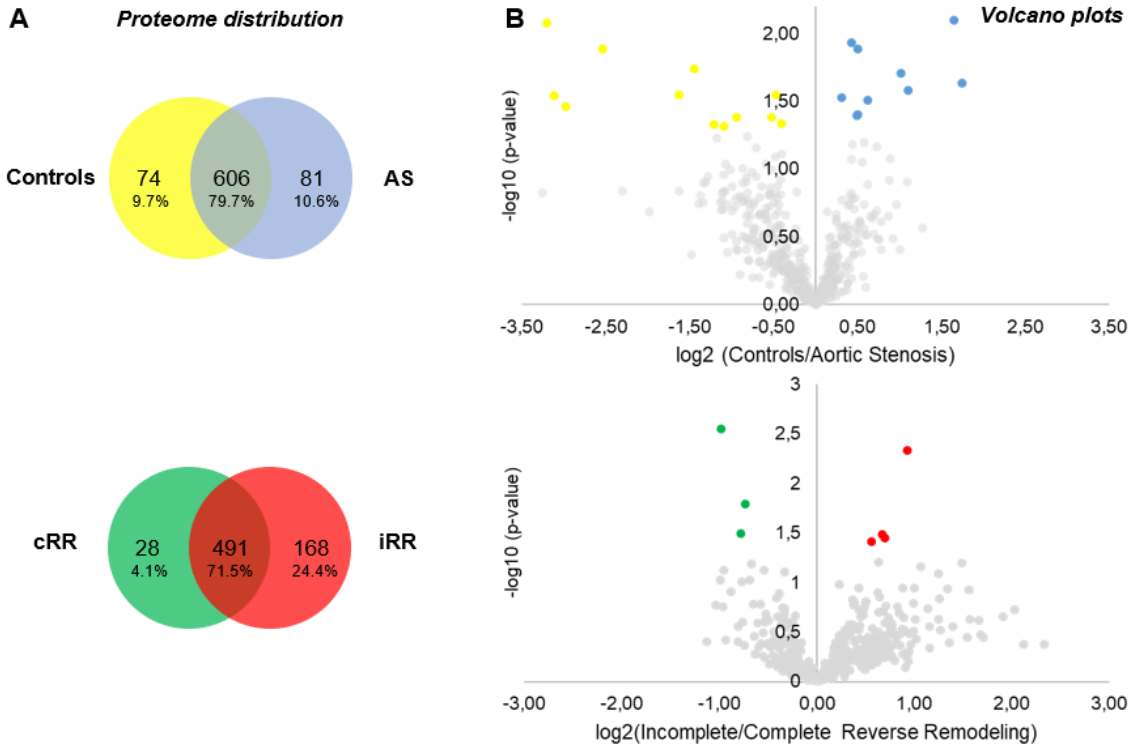

Figure 1. Characterization of the pericardial fluid proteome in aortic stenosis patients with complete and incomplete reverse remodeling. **A.** Venn charts showing the distribution of the proteins identified in aortic stenosis (blue) and in controls (yellow) as well as in patients with complete (green) and incomplete (red) reverse remodeling. **B.** Volcano plots representing dysregulated proteins in aortic stenosis (top) as well as in incomplete versus complete reverse remodeling (bottom). Gray dots represent proteins with no significant differences between both groups.

Table 3. Pericardial fluid proteins significantly changed between aortic stenosis (AS) and controls (coronary artery disease, CAD) patients. Proteins are sorted in descending order of the fold-change.

UniProt ID	Gene Name	Full name	# Pep.	Seq. Cov. (%)	n (AS)	n (CAD)	FC	Cohen's d	*p*
P02792	FTL	Ferritin light chain	2	17.7	2	3	3.4	3.86	0.023
P0DP01	IGHV1-8	Immunoglobulin heavy variable 1-8	2	22.2	3	4	3.1	3.32	0.008
P11597	CETP	Cholesteryl ester transfer protein	3	7.7	8	4	2.1	1.79	0.026
Q9UBP4	DKK3	Dickkopf-related protein 3	5	22.6	10	5	2.0	1.56	0.020
P05154	SERPINA5	Plasma serine protease inhibitor	17	37.9	12	6	1.5	1.20	0.031
P03952	KLKB1	Plasma kallikrein	44	69.3	12	6	1.4	1.36	0.013
P00748	F12	Coagulation factor XII	32	54.6	12	6	1.4	1.08	0.040
P49908	SELENOP	Selenoprotein P	9	17.3	12	6	1.4	1.07	0.041
P12111	COL6A3	Collagen α-3(VI) chain	32	13.3	12	6	1.3	1.34	0.012
P01042	KNG1	Kininogen-1	42	45.7	12	6	1.2	1.23	0.030
A1L4H1	SSC5D	Soluble scavenger receptor cysteine-rich domain-containing protein SSC5D	8	9.9	7	4	1.3	1.54	0.046
P05090	APOD	Apolipoprotein D	12	41.3	12	6	1.4	1.34	0.028
P02452	COL1A1	Collagen α-1(I) chain	8	7	9	4	1.4	1.34	0.041
Q14152	EIF3A	Eukaryotic translation initiation factor 3 sub. A	5	4.8	4	3	1.9	2.12	0.041
A0A075B6I0	IGLV8-61	Immunoglobulin λ variable 8-61	2	20.5	3	3	2.1	2.29	0.048
P11021	HSPA5	Endoplasmic reticulum chaperone BiP	13	27.5	11	6	2.3	1.08	0.047
P00488	F13A1	Coagulation factor XIII A chain	12	19.9	12	6	2.7	1.38	0.018
P07355	ANXA2	Annexin A2	21	63.7	12	6	3.1	1.21	0.028
P35579	MYH9	Myosin-9	61	37	12	6	5.8	1.56	0.013
P69905	HBA1/HBA2	Hemoglobin sub. α	15	95.1	12	6	7.8	1.15	0.034
P68871	HBB	Hemoglobin sub. β	26	95.2	12	6	8.7	1.20	0.029
P02730	SLC4A1	Band 3 anion transport protein	9	14.7	5	4	9.2	2.43	0.008

Abbreviations: FC: fold-change; Pep.: peptides; Seq. Cov.: sequence coverage.

Table 4. Pericardial fluid proteins significantly changed between patients with complete (cRR) and incomplete reverse remodeling (iRR). Proteins are sorted in descending order of the fold-change.

UniProt ID	Gene Name	Full name	# Pep.	Seq. Cov. (%)	n (cRR)	n (iRR)	FC	Cohen's d	*p*	AUC (95% I)
P02656	APOC3	Apolipoprotein C-III	6	43.4	5	7	1.9	2.09	0.003	0.97 (0.77-1)
P02760	AMBP	Protein AMBP	14	35.5	5	7	1.6	1.52	0.035	0.91 (0.66-1)
P80108	GPLD1	Phosphatidylinositol-glycan-specific phospholipase D	4	6.2	4	5	1.6	1.80	0.033	[a]
P06727	APOA4	Apolipoprotein A-IV	46	74.7	5	7	1.5	1.32	0.039	0.83 (0.49-1)
P07358	C8B	Complement component C8 β chain	34	62.8	5	7	1.7	1.66	0.016	0.89 (0.60-1)
P07357	C8A	Complement component C8 α chain	26	44	5	7	1.7	1.48	0.032	0.89 (0.57-1)
P07360	C8G	Complement component C8 γ chain	13	65.8	5	7	2.0	2.44	0.003	1 (1-1)

a) AUC was not calculated because the protein was not identified in all samples.

Abbreviations: AUC (95% I): Area under the curve and the respective 95% confidence interval; FC: fold-change; Pep.: peptides; Seq. Cov.: sequence coverage.

In order to test the performance of the six proteins as prognostic markers of iRR, ROC analysis was performed based on LFQ data (**Figure 2**). All six proteins presented an AUC >0.80, being all good classifiers. Particularly, apolipoprotein C-III and the protein AMBP were found to be very good classifiers of iRR, with an AUC >0.90. Remarkably, semi-quantification of complement C8 γ chain levels in PF through proteomics demonstrates an excellent separation (AUC = 1) of cRR and iRR, with 100% sensitivity and 100% specificity.

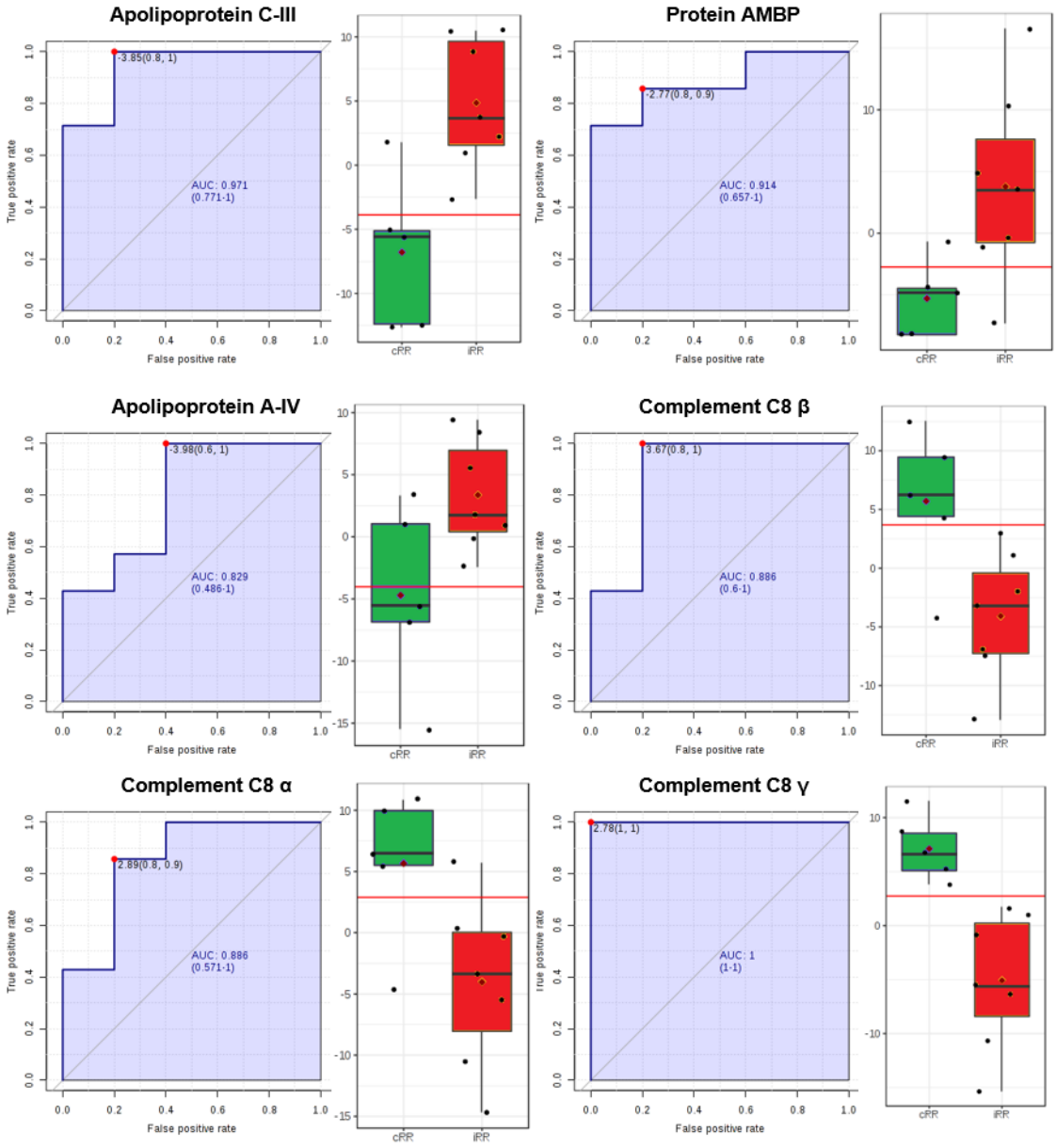

Figure 2. Receiver operating characteristic (ROC) curve and respective boxplot of each dysregulated protein identified in the pericardial fluid of all aortic stenosis patients. Sensitivity and specificity are respectively represented in the vertical and horizontal axes. The area under the curve is shown in blue. In each boxplot, a horizontal line indicates the optimal cutoff.

To get a glimpse over the dysregulated biological processes and pathways that can be monitored in PF, as well as the molecular functions and the origin of the proteins contained therein, GOEA was performed with FunRich (**Figure 3**). In all cases, the percentage of proteins covering each of the FunRich terms in each group is given, in addition to the *p*-value for the enrichment in relation to the whole proteome. In general terms, GOEA shows an increase in the PF levels of proteins related to general metabolism (+7.3%), nucleic acid metabolism (+11.4%) and protein metabolism (+3.8%, p <0.01) in iRR. Curiously, an apparent decrease in the PF levels of proteins associated with immune response (-9.5%) and with transport (-5.6%) is observed in iRR. Concerning the biological pathways, it is notorious an overrepresentation of proteins associated with gene expression, both at transcriptional (e.g. mRNA metabolism, +7.6%, p <0.01) and translational levels (e.g. translation initiation, +5%, p <0.01). As expected by the results of dysregulated proteins analysis, showing the decrease in three complement C8 chains in the PF of iRR patients, a strong representation of the term complement activity (+9.4%, p <0.01) was found in cRR. Also worth mentioning the higher association of catalytic activity (+4.1%) and peroxidase activity (+2.7%) wit cRR. Finally, with regard to the origin of proteins found in PF, it is evident a higher contribution of intracellular contents in the case of iRR, as shown by higher representation of the terms cytoplasm (+22.7%, p <0.01), nucleus (+15.5%, p <0.05) and mitochondrion (+14.4%, p <0.01). Aiming to take a more in-depth analysis of the dysregulated biological processes associated with the PF proteome, a second GOEA with ClueGO was performed. **Figure 4** shows a network representing all dysregulated biological processes in RR, for a GO range between 3 and 8. Probably due to the much higher number of exclusive proteins identified in the PF of AS patients with iRR (6 times more), the mapped GO terms corresponded only to upregulated biological processes in iRR. This analysis further corroborated the strong activity of the immune system in iRR, as shown by the coverage of terms such as humoral immune response mediated by circulating immunoglobulins, antigen processing and presentation of peptide antigen via MHC class I and type I IFN production. In addition, there is evidence of negative regulation of the pro-survival erbB pathway in patients with iRR.

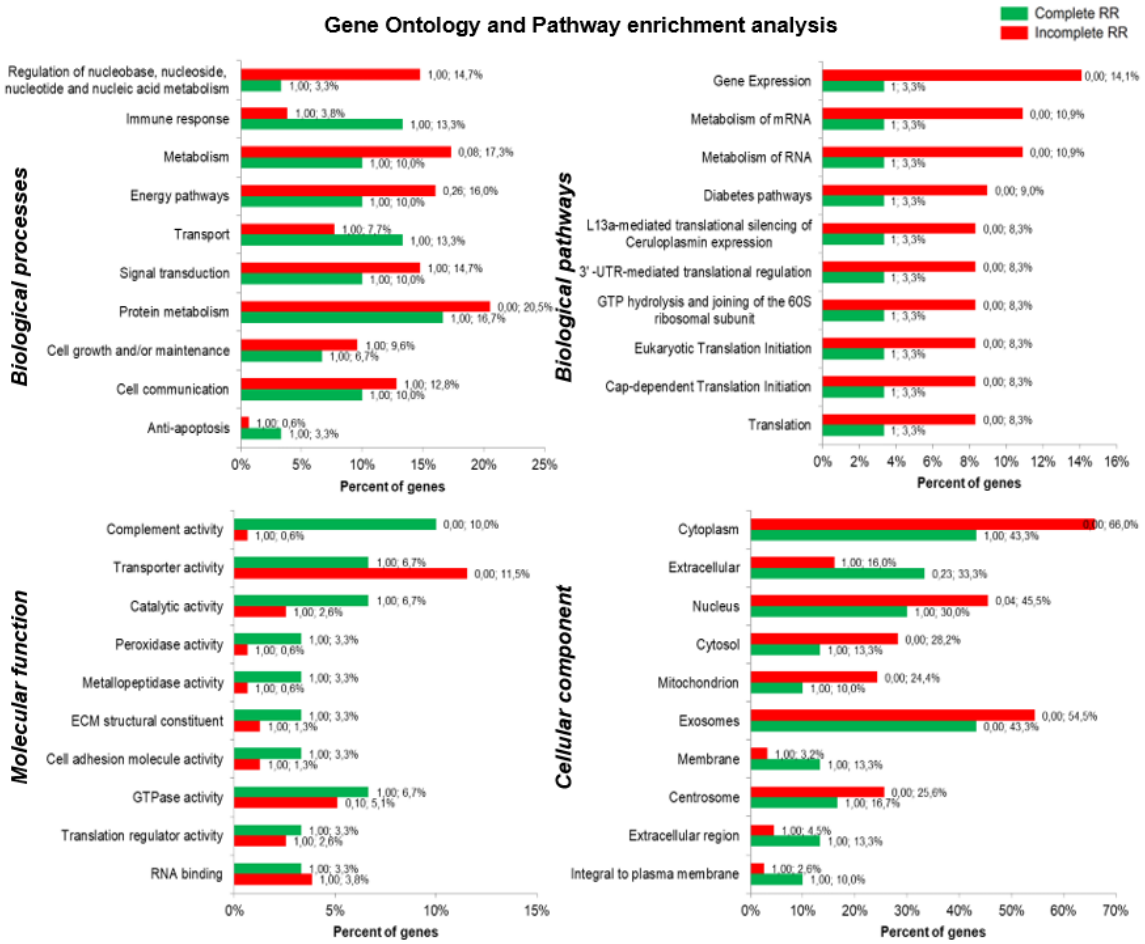

Figure 3. FunRich enrichment analysis of gene ontology terms (biological processes, molecular function and cellular component) and biological pathways. The percentage of proteins (associated genes) covering each term and the Bonferroni-corrected *p*-value for the enrichment with respect to the whole proteome are indicated ahead of each bar.

Similarly to the case of myocardial proteomics, a multivariate analysis (PLS-DA) was undertaken with PF proteome to identify protein groups that, by regulating the same biological process, may explain the phenotypical divergence in patients with cRR and iRR. However, a first comparison was made between AS and controls (**Supplementary Figure S9, Appendix**). This is important to separate proteins that respond specifically to pressure overload from proteins that come into play, regardless of the cause of homeostasis perturbation, in this case, pressure overload versus ischemia. Then, a second PLS-DA was undertaken between cRR and iRR. **Figure 5A** shows the complete separation of the two study groups through PLS-DA. Although, herein only 18% of data variability could be explained in the two first components, perhaps due to the lower number of proteins that could be quantified in this biological matrix, but also due to the nature of the sample (PF, with systemic contributions from plasma, versus the myocardium in ***Chapter II***).

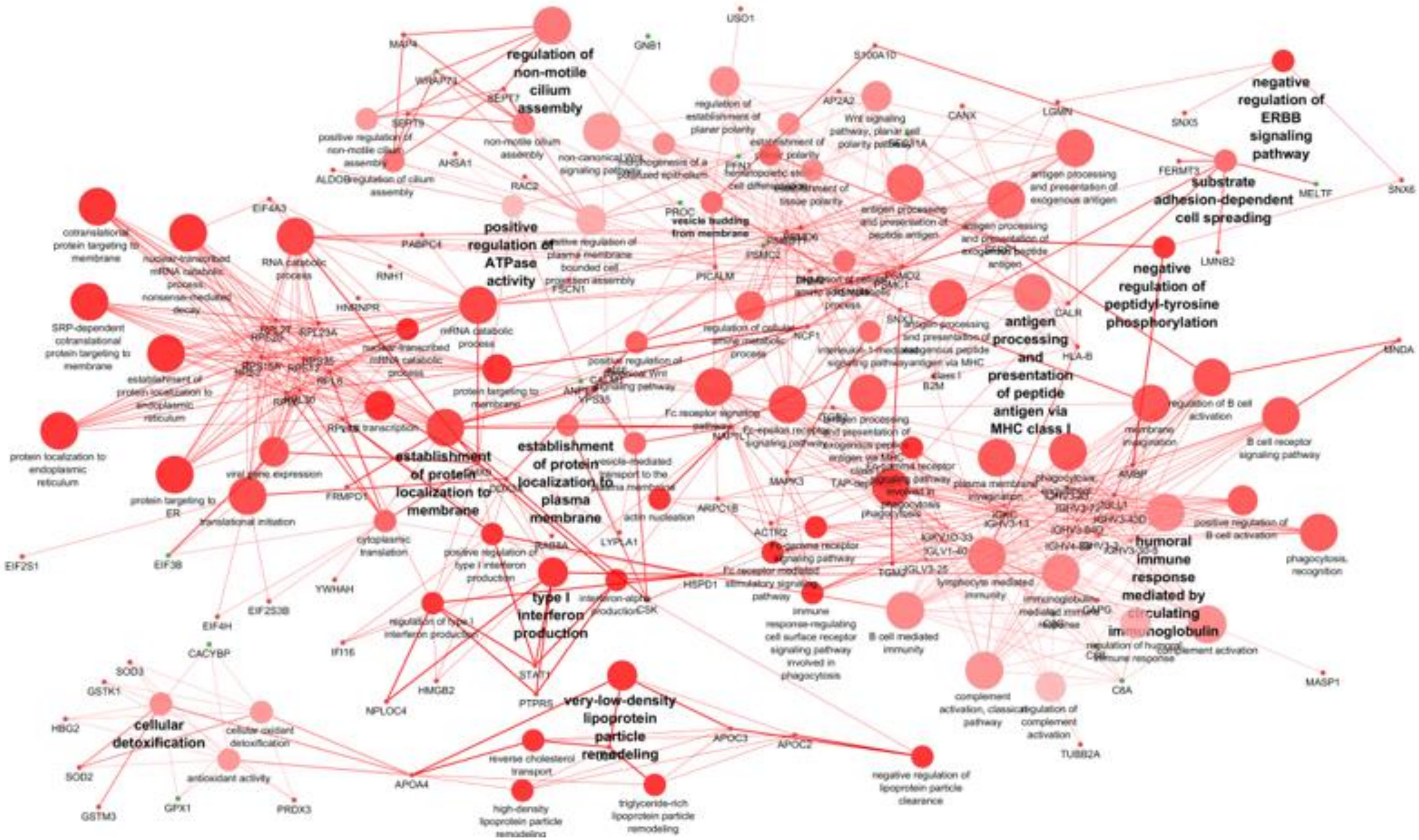

Figure 4. Network representing the dysregulated biological processes in incomplete reverse remodeling, according to ClueGO+CluePedia enrichment analysis. Green nodes represent upregulation in complete reverse remodeling, while red nodes represent upregulation in incomplete reverse remodeling. GO range was set between 3 and 8 as to provide detailed biological information. Proteins are identified through the respective gene name.

In fact, VIP score analysis (**Figure 5B**), showed that three proteins (marked in yellow) were common in the Top 10 most important variables in separating CAD vs AS and cRR from iRR. Anyhow, apart from those, it was found that proteins with chemotactic properties (α2-antiplasmin, retinoic acid receptor responder protein 2 and neuropilin-1), involved in leukocyte adhesion (moesin) or that are part of the complement system (factor D and C8α) shape the phenotypical divergence of AS patients after the AVR procedure.

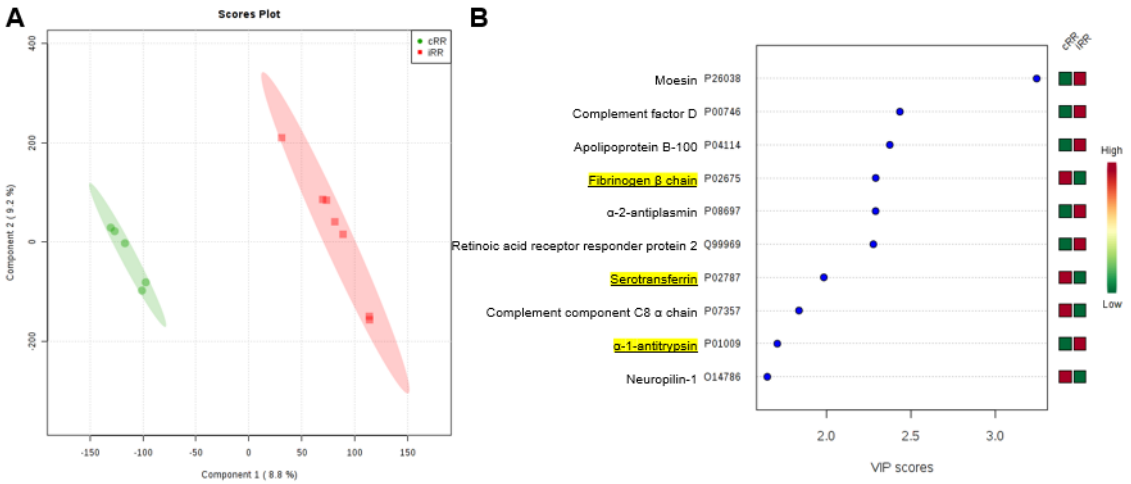

Figure 5. A. PLS-DA plot showing the separation of patients with complete (green) and incomplete (red) reverse remodeling. **B.** Top 10 proteins with the highest VIP (variable importance in projection) score. Proteins marked in yellow are also important to separate aortic stenosis from the control condition (see Appendix, Supplementary Figure S9) and should be disregarded for the sake of reverse remodeling.

3.2. Immunoblot validation of potential markers of incomplete reverse remodeling and correlation analysis

In order to find potential prognostic markers of iRR in the PF, some proteins were selected for slot blot analysis (**Figure 6**). In all cases, a first comparison was made between control patients and AS patients, as to judge the specificity of the protein. Then, the association between the PF levels of such proteins and the LVM regression was tested. Since complement dysregulation was also clear through PF proteomics, the complement C3 was quantified through western blot (**Figure 7**). In this experiment, all new AS patients were collected blindly with relation to the extent of LVM regression, spanning from -32.1% to +45.6%. Additional correlations with other clinical parameters were also tested.

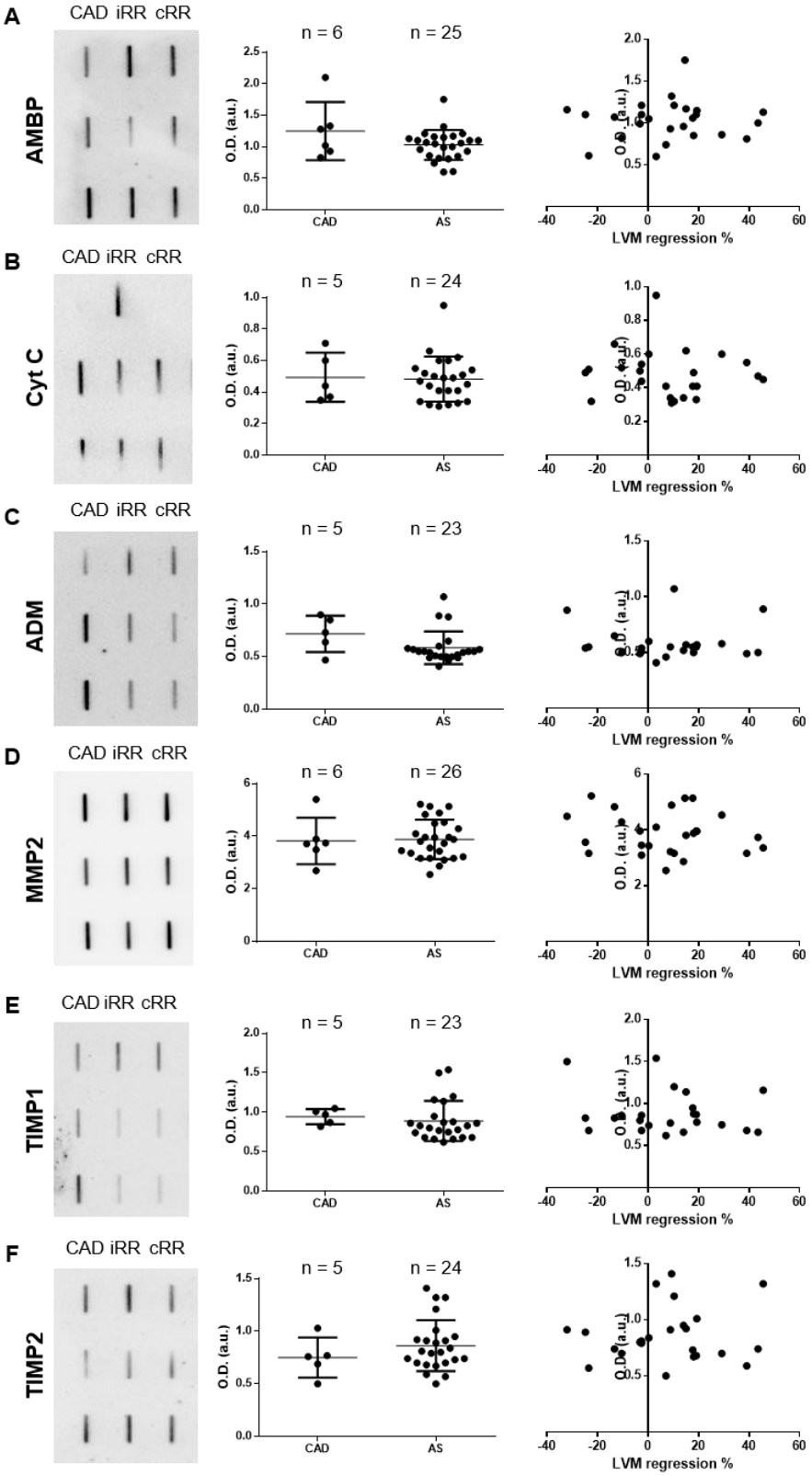

Figure 6. Slot blot quantification of **A.** protein AMBP **B.** cytochrome C (Cyt C), **C.** adrenomedullin (ADM), **D.** matrix metalloproteinase 2 (MMP2), **E.** tissue inhibitor of metalloproteinase 1 (TIMP1) and **F.** 2 (TIMP2) in aortic stenosis patients with different degrees of reverse remodeling. A representative section of each blot is shown on the left. For each protein, a first comparison (middle graph) was made between controls (coronary artery disease) and cases (aortic stenosis) to inquire specificity. Then, the association between the levels of these proteins and left ventricle mass regression was tested (right graph).

Among the four proteins found significantly increased in the PF of iRR patients, the protein AMBP was selected for validation (**Figure 6A**). GPLD1 was excluded because it was not identified in all individuals. The apolipoprotein A-IV presented the lowest AUC. The apolipoprotein C-III, in turn, despite having better biomarker performance than AMBP (AUC 0.97 vs 0.91), has already been associated with over 100 conditions, showing much lower specificity according to DisGeNET (a database of gene-disease associations [32]). Although no significant differences were found between AS patients and controls, in agreement with the proteome analysis, no correlation between AMBP and LVM regression was observed, showing that this protein may not serve as a marker for iRR. Still, a significant opposite association to preoperative Peak Ao and the maximum aortic transvalvular pressure gradient was found (in both cases, r = -0.43, p = 0.03).

From the analysis of the PF proteome, it was again evident the relevance of complement in shaping the phenotype of AS patients undergoing AVR, as shown by a reduction of the complement C8 in patients with iRR. One hypothesis to explain this decrease is the accumulation of complement C8 in membrane attack complexes (composed by C5b to C9) on susceptible cardiomyocytes, causing consumption of the PF complement. In the previous ***Chapter II***, the β chain of complement C3, was found tendentiously higher in the myocardium of iRR patients. Therefore, it was hypothesized that similarly to C8, the levels of C3, the central element of the three complement cascades (classical, lectin and alternative pathways) [33], would be lower in the PF or iRR patients, as a result of complement depletion [34]. To test this hypothesis, the complement C3 was also assessed in the PF through western blot (**Figure 7**). OD analysis showed that despite the fact C3 β chain was, on average, 0.7-fold lower in the PF of iRR patients, this was not significant.

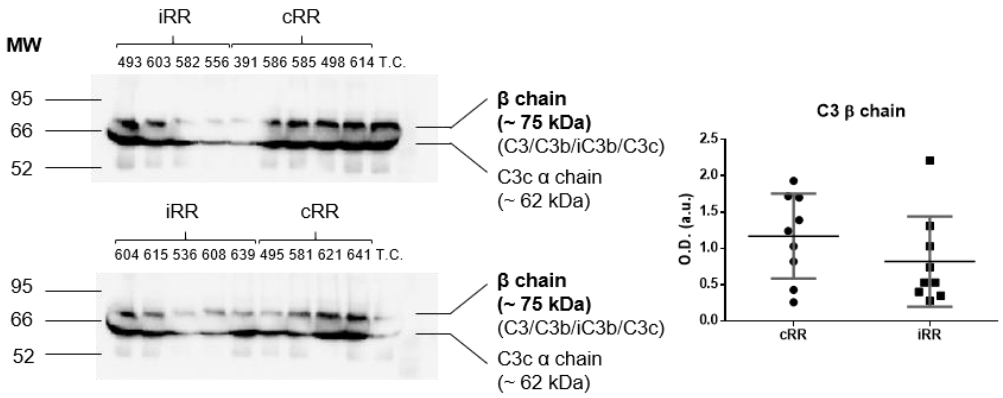

Figure 7. Western blot quantification of complement C3 in the pericardial fluid of patients with complete (cRR) or incomplete (iRR) reverse remodeling. T.C. designates a technical control. Optical density quantification of complement C3 β chain is shown on the right. This chain is conserved in all fragments that are originated after C3 activation (C3b, iC3b and C3c).

Given the overrepresentation of proteins with mitochondrial origin in the PF of iRR patients, suggesting the loss of intracellular contents due to cell death, the PF levels of cytochrome C were quantified through slot blot (**Figure 6B**). Nevertheless, no association between this apoptosis marker and LVM regression or any other clinical parameter was found. Apart from AMBP, complement C3 and cytochrome C, other proteins were also analyzed through slot blot analysis, because in a previous systematic review [16], important correlations were observed between the PF levels and common parameters of myocardial structure and function (**Table 3**, ***Chapter I***), anticipating a potential prognostic role in AS as well. For instance, the vasodilator peptide ADM was quantified in the PF (**Figure 6C**) due to the reported positive association to LV mass and negative association to LVEF. Nevertheless, no significant correlations were found between ADM PF levels and any of the clinical parameters tested. Next, the MMP2, and its inhibitors, TIMP1 and TIMP2, were quantified in the PF due to previously reported correlations between MMP2 and LV diastolic/systolic volumes (positive) and systolic function (LVEF, negative). As shown in **Figures 6D to 6F**, none of these proteins has shown a significant correlation to LVM regression. Of note, though, a significant association between TIMP1 and preoperative LVEF ($r = 0.45$, $p = 0.04$) was found, in agreement with its MMP2 inhibitory activity.

4. Discussion

Nowadays, physicians resort to imaging techniques, such as echocardiography, cardiac magnetic resonance or computed tomography to diagnose AS, to stratify the risk of patients before being elected to AVR or when there is a need to obtain prognostic information. The BNP is currently the only molecular marker recommended by ESC to screen in the sera of patients with asymptomatic AS in order to define the optimal time for intervention [35]. This is because serum (and also PF) BNP correlates strongly with LVEF, a major index of systolic function [36], and predicts patients survival [37]. However, as shown in ***Chapter I***, many other molecular markers in PF show important associations with diverse parameters of cardiac structure (e.g. LV systolic and diastolic dimensions, volumes and mass) and function (e.g. LVEF, LV systolic and diastolic pressures), such as ADM, insulin-like growth factor-1, MMP2 and asymmetric dimethylarginine. In order to get an unbiased look at

potential new surrogate markers of iRR and to complement the understanding of RR pathobiology, the PF proteome was profiled in AS patients undergoing AVR.

A first look at the dysregulated biological processes associated to iRR, tracked through PF proteomics, was made through GOEA. In agreement with the myocardial proteome (***Chapter II***), there is evidence of high transcriptional and translational rates in patients with iRR, which may explain the permanent sarcomere buildup and hypertrophy, even after afterload relief. In apparent contrast to the findings of myocardial proteomics, though, the PF proteome of iRR presents a larger percentage of proteins associated to energy pathways and to metabolism (such as protein metabolism). However, by looking at the distribution of proteins according to their origin, one can clearly witness the enrichment of cytoplasmic, nuclear and mitochondrial proteins in the PF of iRR patients. In contrast, cRR patients show two times higher percentage of extracellular proteins. Taken together, this suggests a higher loss of cellular contents in patients with iRR, most probably due to cell death. In support of this idea, the enzyme glutathione peroxidase 1 was the only mitochondrial protein exclusively identified in the PF of cRR patients. In turn, many mitochondrial proteins were exclusively identified in the PF of iRR patients, such as the Krebs cycle enzyme citrate synthase, the β-oxidation trifunctional enzyme, the complex V proteins ATP synthase subunits α and β, the antioxidant proteins, superoxide dismutase (Mn) and peroxiredoxin III, the mitochondrial chaperonin heat shock protein 60 and the elongation factor Tu, required for mitochondrial translation. Furthermore, from these eight proteins, only peroxiredoxin III and the elongation factor III are predicted to be non-classically secreted, according to the SecretomeP 2.0 algorithm [38], and none show a predicted signal peptide for secretion (according to the SignalP 5.0 algorithm [39]). This reinforces the idea of a higher mitochondria loss due to cell death in iRR patients. Since the circulating level of cytochrome C, a marker of apoptosis, has been previously proposed as a myocardial infarction marker [40], this protein was also assessed through slot blot. Notwithstanding, no association to LVM regression was found. Thus, no potential prognostic value is anticipated for cytochrome C in the setting of AS. In the previous ***Chapter II***, the TRAIL signaling pathway, responsible for the activation of the death receptor-mediated extrinsic apoptotic pathway [41], was more prominent in iRR. Since the cytochrome C release is a marker of the intrinsic (mitochondrial) pathway, and it was not dysregulated in the AS setting, it is probable that extrinsic cues are the main drivers of cell death in iRR. In the future, the terminal deoxynucleotidyl transferase dUTP nick end labeling (TUNEL) staining assay (or equivalent) and the immunodetection of TRAIL receptors are required to shed light into the main mechanisms of cardiomyocyte death under AS-induced pressure

overload. Furthermore, the potential prognostic role of the aforementioned mitochondrial proteins should be ruled out, as these may mark loss of cardiomyocyte integrity. Of note, the lower protection against cell death in iRR patients may be explained by, among other factors, the downregulation of the pro-survival erbB signaling pathway, as deemed by ClueGO analysis (**Figure 4**), which is in agreement with the pathway analysis to the myocardial phosphoproteome (**Figure 4**, ***Chapter II***).

The release of the intracellular content, in particular, mitochondria material, from dying cardiomyocytes may instigate an immune-inflammatory response [42]. Today, it is recognized that the release of mitochondrial danger-associated molecular patterns (DAMPs), such as mitochondrial DNA, RNA and protein (e.g. mitochondrial transcription factor A, TFAM) activate macrophages, dendritic cells or neutrophils [42]. Somewhat intriguing, FunRich analysis showed a higher proportion of proteins involved in the immune response in cRR, although not significantly enriched when compared to the reference human proteome. This is explained by a much more diverse set of proteins identified in iRR. In fact, according to FunRich, four proteins (out of 30 annotated) were mapped to immune response in cRR, as opposed to six (out of 152 annotated) in iRR Actually, PLS-DA shows that the chemotactic protein retinoic acid receptor responder protein 2, as well as moesin, involved in leukocyte adhesion, are important to separate patients with iRR from patients with cRR. Moreover, by doing a cluster-based analysis with ClueGO, it was clear that, despite some proteins associated to cRR (such as complement C8 chains represented as small green nodes), the activity of the immune system is obviously pronounced in AS patients developing iRR. For instance, consistent with the pathway analysis to the myocardial phosphoproteome (**Figure 4**, ***Chapter II***), the PF proteome supports higher production of INF γ in iRR patients that, although protective against hypertrophy [43,44], is associated to chronic heart failure [45]. Interestingly, the IFN pathway is commonly activated upon the release of mitochondrial DAMPs [42]. Hence, in the future, the screening of mitochondrial proteins in the PF should be done in a larger scale and the association to apoptotic/necrotic cardiomyocytes should be tested, as new surrogate prognostic markers of iRR may arise from this approach.

Interestingly, it has also been demonstrated that mitochondria membranes isolated from human heart can activate, *in vitro*, the components C1, C2, C3 and C4, resulting in their consumption from human sera [46]. The decrease in the soluble levels of complement C8, as determined by PF proteomics, might as well be explained by myocardial deposition. Indeed, the complement C8 is the first component to penetrate into the plasma membrane

to coordinate the interaction between the preassembled membrane attack complex precursor C5b-7 and the pore-forming component C9, orchestrating the formation of the membrane attack complex [47]. This is corroborated by the observation of increased myocardial deposition of the C5b-C9 components in the myocardium of failing human hearts (regardless of an ischemic or non-ischemic origin), normalized after LVAD implantation [48]. To confirm this hypothesis, in the future, the assessment of soluble membrane attack complex in the PF and of the C8 accumulation in the myocardium of patients with cRR and iRR is imperative. Herein, attention was given to C3 because, in the previous ***Chapter II***, an upward trend in complement C3 β chain myocardial levels in iRR was observed, suggesting myocardial complement consumption. Moreover, complement C3 is the point of convergence of all three complement activation pathways [33], and its depletion has been previously demonstrated in the sera of patients suffering an acute myocardial infarction, leading to extensive myocardial necrosis [46]. Consistent with this view of myocardial complement C3 consumption, a lower mean level of C3 β chain in the PF of patients with iRR was observed, although this was not statistically significant. Therefore, although important, complement activation should not be the only factor limiting a complete response after AVR.

One of the consequences of cardiomyocytes loss during AS-induced myocardial remodeling is the phenomenon of replacement fibrosis [49,50]. This is characterized by increased synthesis of ECM proteins, such as collagen, and decreased degradation by MMPs, whose activity is regulated by TIMPs [51]. Since the balance between MMPs and TIMPs determines the organization and the increase/decrease of ECM volume, and fibrosis is associated with myocardial dysfunction [52], the determination of the PF levels of these ECM regulators may have important prognostic impact. Even though none of these proteins were found dysregulated through PF proteomics, the MMP2, in addition to its inhibitors TIMP1 and TIMP2, were assessed through slot blot, as the PF levels of this metalloproteinase have been associated with LV remodeling in patients undergoing CABG [23]. If the MMP2 was found negatively correlated to LVEF in the setting of CAD [23], herein a positive association was found between TIMP1 PF levels and LVEF, in agreement with its inhibitory role. This observation strengthens the idea that, although etiologically distinct, the LV maladaptive remodeling in the setting of CAD and the incomplete RR, in the setting of AS, share some common ground, regarding the development of systolic dysfunction due to extensive fibrosis. It is, thus, possible, that the development of targeted therapies for iRR, may also be useful in other heart diseases not causing pressure overload.

The work herein presented is the first attempt to characterize the PF proteome in AS patients showing different degrees of RR, after AVR. However, there are important limitations that should be reminded, some of which result from the utilization of human samples. Hence, some are shared with the myocardial (phospho)proteomics approach. Despite the access to a large biobank of human samples, most implicated patients are older patients with multiple comorbidities and from whom substantial clinical data was collected, allowing to identify patients with other significant heart diseases (e.g. CAD, dilated or hypertrophic cardiomyopathy). Thus, a first limitation was the relatively low number of subjects enrolled (12 AS cases and 6 controls) due to the inherent difficulty in retrieving patients with isolated AS. For biomarker validation, 14 additional patients were included, but this number should be increased in the future. Second, the assessment of myocardial structure and function relied on echocardiographic evaluations taken post-AVR in different time-points. Since data was collected retrospectively, it spanned from four months up to two years and three months (median was 10 months), and some heterogeneity in the assessment LVM regression should not be excluded. Nevertheless, it has been established that most regression occurs during the first six months after AVR [4,53]. Third, although samples were fractionated with NPs@EDTA to largely reduce the amount of albumin (and some immunoglobulins as well), it is possible that other abundant proteins (of plasmatic origin) such as apolipoproteins, fibrinogen, haptoglobin or the complement component themselves are masking other relevant dysregulated proteins [54]. Thus, multi-dimension PF proteome separation will certainly help extend the number of potential markers of iRR.

5. Conclusions

Despite the proximity between PF and the heart, little attention has been devoted to PF's diagnostic/prognostic potential in the setting of heart diseases. This is the first study characterizing the PF proteome in AS patients with complete and incomplete RR. Even though no definitive prognostic markers of iRR could be detected, the circulating or the myocardial levels of C8 (as part of the membrane attack complex) require further investigation in this regard. In addition, the comprehensive characterization of the PF proteome opened new questions concerning the pathological mechanisms driving to an incomplete response. For instance, is the extrinsic apoptotic pathway determinant for

cardiomyocyte loss during myocardium remodeling under pressure overload? Are the mitochondrial contents released from dying cells responsible for complement activation? Or, instead, is the lytic activity of the membrane attack complex responsible for the release of mitochondria? In any case, targeting both avenues of cell death (death receptor-mediated and complement-mediated cell lysis) may be important therapies to pursue in patients undergoing AVR, as to avoid the irreversible deposition of fibrotic tissue.

The present work was presented at the European Bioinformatics (EuBIC) Winter School, organized by the European Proteomics Association (EPA) that took place on January 15th-18th (2019) in Zakopane, Poland, under the title "Bioinformatics pipeline for the analysis of proteome data: uncovering surrogate markers of incomplete myocardial reverse remodeling through pericardial fluid proteomics" (poster session).

6. References

[1] C. Gavina, I. Falcão-Pires, P. Pinho, M.-C. Manso, A. Gonçalves, F. Rocha-Gonçalves, A. Leite-Moreira, Relevance of residual left ventricular hypertrophy after surgery for isolated aortic stenosis, Eur. J. Cardio-Thoracic Surg. 49 (2015) 952–959. doi:10.1093/ejcts/ezv240.

[2] J.M. Beach, T. Mihaljevic, J. Rajeswaran, T. Marwick, S.T. Edwards, E.R. Nowicki, J. Thomas, L.G. Svensson, B. Griffin, A.M. Gillinov, E.H. Blackstone, Ventricular hypertrophy and left atrial dilatation persist and are associated with reduced survival after valve replacement for aortic stenosis, J. Thorac. Cardiovasc. Surg. 147 (2014) 362–369. doi:10.1016/j.jtcvs.2012.12.016.

[3] T. Hatani, T. Kitai, R. Murai, K. Kim, N. Ehara, A. Kobori, M. Kinoshita, S. Kaji, T. Tani, Y. Sasaki, T. Yamane, T. Koyama, M. Nasu, Y. Okada, Y. Furukawa, Associations of residual left ventricular and left atrial remodeling with clinical outcomes in patients after aortic valve replacement for severe aortic stenosis, J. Cardiol. 68 (2016) 241–247. doi:10.1016/j.jjcc.2015.09.017.

[4] R.W.W. Biederman, J.A. Magovern, S.B. Grant, R.B. Williams, J.A. Yamrozik, D.A. Vido, V.K. Rathi, G. Rayarao, K. Caruppannan, M. Doyle, LV reverse remodeling imparted by aortic valve replacement for severe aortic stenosis; is it durable? A cardiovascular MRI study sponsored by the American Heart Association, J Cardiothorac Surg. 6 (2011) 1–8. doi:10.1186/1749-8090-6-53.

[5] N. Hanayama, G.T. Christakis, H.R. Mallidi, V. Rao, G. Cohen, B.S. Goldman, S.E. Fremes, C.D. Morgan, C.D. Joyner, Determinants of Incomplete Left Ventricular Mass Regression Following Aortic Valve Replacement for Aortic Stenosis, J. Card. Surg. 20 (2005) 307–313. doi:10.1111/j.1540-8191.2005.200485.x.

[6] K. Vogiatzidis, S.G. Zarogiannis, I. Aidonidis, E.I. Solenov, P.-A. Molyvdas, K.I. Gourgoulianis, C. Hatzoglou, Physiology of pericardial fluid production and drainage, Front. Physiol. 6 (2015) 1–6. doi:10.3389/fphys.2015.00062.

[7] J.-J. Santiago, L.J. McNaughton, N. Koleini, X. Ma, B. Bestvater, B.E. Nickel, R.R. Fandrich, J.T. Wigle, D.H. Freed, R.C. Arora, E. Kardami, High Molecular Weight Fibroblast Growth

Factor-2 in the Human Heart Is a Potential Target for Prevention of Cardiac Remodeling, PLoS One. 9 (2014) e97281. doi:10.1371/journal.pone.0097281.
[8] J.-Y. Liou, P.-L. Kuan, K.-G. Shyu, M.-J. Lu, H.-H. Chao, B.-W. Wang, Pericardial Fluid and Serum Levels of Vascular Endothelial Growth Factor and Endostatin in Patients With or Without Coronary Artery Disease, J. Formos. Med. Assoc. 105 (2006) 377–383. doi:10.1016/S0929-6646(09)60133-9.
[9] M. Fujita, M. Ikemoto, M. Kishishita, H. Otani, R. Nohara, T. Tanaka, S. Tamaki, A. Yamazato, S. Sasayama, Elevated Basic Fibroblast Growth Factor in Pericardial Fluid of Patients With Unstable Angina, Circulation. 94 (1996) 610–613. doi:10.1161/01.CIR.94.4.610.
[10] T. Miyazaki, H.P. Pride, D.P. Zipes, Prostaglandins in the pericardial fluid modulate neural regulation of cardiac electrophysiological properties., Circ. Res. 66 (1990) 163–175. doi:10.1161/01.RES.66.1.163.
[11] T. Ege, S. Canbaz, V. Yuksel, E. Duran, Effect of pericardial fluid pro-inflammatory cytokines on hemodynamic parameters, Cytokine. 23 (2003) 47–51. doi:10.1016/S1043-4666(03)00180-7.
[12] A.D. Ristić, S. Pankuweit, R. Maksimović, R. Moosdorf, B. Maisch, Pericardial cytokines in neoplastic, autoreactive, and viral pericarditis, Heart Fail. Rev. 18 (2013) 345–353. doi:10.1007/s10741-012-9334-y.
[13] I. Kiris, S. Kapan, H. Okutan, C. Narin, M. Ozaydin, M.C. Cure, R. Sutcu, Relationship between site of myocardial infarction, left ventricular function and cytokine levels in patients undergoing coronary artery surgery, Cardiovasc. J. Afr. 27 (2016) 299–306. doi:10.5830/CVJA-2016-027.
[14] R.W. Troughton, C.R. Asher, A.L. Klein, Pericarditis, Lancet. 363 (2004) 717–727. doi:10.1016/S0140-6736(04)15648-1.
[15] B. Boulanger, Z. Yuan, M. Flessner, J. Hay, M. Johnston, Pericardial Fluid Absorption into Lymphatic Vessels in Sheep, Microvasc. Res. 57 (1999) 174–186. doi:10.1006/mvre.1998.2127.
[16] F. Trindade, R. Vitorino, A. Leite-Moreira, I. Falcão-Pires, Pericardial fluid: an underrated molecular library of heart conditions and a potential vehicle for cardiac therapy, Basic Res. Cardiol. 114 (2019) 10. doi:10.1007/s00395-019-0716-3.
[17] Y. Adler, P. Charron, M. Imazio, L. Badano, G. Barón-Esquivias, J. Bogaert, A. Brucato, P. Gueret, K. Klingel, C. Lionis, B. Maisch, B. Mayosi, A. Pavie, A.D. Ristić, M. Sabaté Tenas, P. Seferovic, K. Swedberg, W. Tomkowski, 2015 ESC Guidelines for the diagnosis and management of pericardial diseases: The Task Force for the Diagnosis and Management of Pericardial Diseases of the European Society of Cardiology (ESC)Endorsed by: The European Association for Cardio-Thoracic Surg, Eur. Heart J. 36 (2015) 2921–2964. doi:10.1093/eurheartj/ehv318.
[18] Z. Nemeth, A. Cziraki, S. Szabados, B. Biri, S. Keki, A. Koller, Elevated Levels of Asymmetric Dimethylarginine (ADMA) in the Pericardial Fluid of Cardiac Patients Correlate with Cardiac Hypertrophy, PLoS One. 10 (2015) e0135498. doi:10.1371/journal.pone.0135498.
[19] B. Sax, B. Merkely, K. Túri, A. Nagy, A. Ahres, I. Hartyánszky, T. Hüttl, Z. Szabolcs, K. Cseh, V. Kékesi, Characterization of pericardial and plasma ghrelin levels in patients with ischemic and non-ischemic heart disease, Regul. Pept. 186 (2013) 131–136. doi:10.1016/j.regpep.2013.08.003.
[20] A.G. Driver, C.A. Kukoly, P.A. Spence, W.R. Chitwood, S.J. Mustafa, Pericardial Fluid Adenosine in Ischemic and Valvular Heart Disease, Chest. 107 (1995) 346–351. doi:10.1378/chest.107.2.346.
[21] L. Selmeci, M. Antal, F. Horkay, B. Merkely, I. Szokodi, L. Bíró, M. Székely, J. Jobbágy, J. Szépvölgyi, M. Tóth, Enhanced accumulation of pericardial fluid ferritin in patients with coronary artery disease, Coron. Artery Dis. 11 (2000) 53–56. doi:10.1097/00019501-200002000-00010.
[22] T. Nishikimi, H. Asakawa, H. Iida, Y. Matsushita, I. Shibasaki, K. Tadokoro, Y. Mori, H. Mori, Y. Mochizuki, Y. Okamura, S. Miyoshi, K. Kangawa, H. Matsuoka, Different secretion patterns of two molecular forms of cardiac adrenomedullin in pressure- and volume-overloaded human heart failure, J. Card. Fail. 10 (2004) 321–327. doi:10.1016/j.cardfail.2003.12.002.
[23] S. Miyamoto, N. Nagaya, M. Ikemoto, K. Tambara, Y. Kihara, Y. Onozawa, K. Hasegawa, A. Yamazato, M. Fujita, Elevation of matrix metalloproteinase-2 level in pericardial fluid is closely associated with left ventricular remodeling, Am. J. Cardiol. 89 (2002) 102–105.

doi:10.1016/S0002-9149(01)02179-8.
[24] R.M. Lang, L.P. Badano, V. Mor-Avi, J. Afilalo, A. Armstrong, L. Ernande, F.A. Flachskampf, E. Foster, S.A. Goldstein, T. Kuznetsova, P. Lancellotti, D. Muraru, M.H. Picard, E.R. Rietzschel, L. Rudski, K.T. Spencer, W. Tsang, J.-U. Voigt, Recommendations for Cardiac Chamber Quantification by Echocardiography in Adults: An Update from the American Society of Echocardiography and the European Association of Cardiovascular Imaging, Eur. Hear. J. - Cardiovasc. Imaging. 16 (2015) 233–271. doi:10.1093/ehjci/jev014.
[25] H. Baumgartner, J. Hung, J. Bermejo, J.B. Chambers, A. Evangelista, B.P. Griffin, B. Iung, C.M. Otto, P.A. Pellikka, M. Quiñones, Echocardiographic Assessment of Valve Stenosis: EAE/ASE Recommendations for Clinical Practice, J. Am. Soc. Echocardiogr. 22 (2009) 1–23. doi:10.1016/j.echo.2008.11.029.
[26] F. Trindade, P. Bastos, A. Leite-Moreira, B. Manadas, R. Ferreira, S.F. Soares, A.L. Daniel-da-Silva, I. Falcão-Pires, R. Vitorino, A fractionation approach applying chelating magnetic nanoparticles to characterize pericardial fluid's proteome, Arch. Biochem. Biophys. 634 (2017) 1–10. doi:10.1016/j.abb.2017.09.016.
[27] Y. Perez-Riverol, A. Csordas, J. Bai, M. Bernal-Llinares, S. Hewapathirana, D.J. Kundu, A. Inuganti, J. Griss, G. Mayer, M. Eisenacher, E. Pérez, J. Uszkoreit, J. Pfeuffer, T. Sachsenberg, S. Yilmaz, S. Tiwary, J. Cox, E. Audain, M. Walzer, A.F. Jarnuczak, T. Ternent, A. Brazma, J.A. Vizcaíno, The PRIDE database and related tools and resources in 2019: improving support for quantification data, Nucleic Acids Res. 47 (2019) D442–D450. doi:10.1093/nar/gky1106.
[28] J. Cox, M.Y. Hein, C.A. Luber, I. Paron, N. Nagaraj, M. Mann, Accurate Proteome-wide Label-free Quantification by Delayed Normalization and Maximal Peptide Ratio Extraction, Termed MaxLFQ, Mol. Cell. Proteomics. 13 (2014) 2513–2526. doi:10.1074/mcp.M113.031591.
[29] M. Pathan, S. Keerthikumar, C.-S. Ang, L. Gangoda, C.Y.J. Quek, N.A. Williamson, D. Mouradov, O.M. Sieber, R.J. Simpson, A. Salim, A. Bacic, A.F. Hill, D.A. Stroud, M.T. Ryan, J.I. Agbinya, J.M. Mariadason, A.W. Burgess, S. Mathivanan, FunRich: An open access standalone functional enrichment and interaction network analysis tool, Proteomics. 15 (2015) 2597–2601. doi:10.1002/pmic.201400515.
[30] G. Bindea, B. Mlecnik, H. Hackl, P. Charoentong, M. Tosolini, A. Kirilovsky, W.-H. Fridman, F. Pagès, Z. Trajanoski, J. Galon, ClueGO: a Cytoscape plug-in to decipher functionally grouped gene ontology and pathway annotation networks., Bioinformatics. 25 (2009) 1091–1093. doi:10.1093/bioinformatics/btp101.
[31] B.E. J., M. Paul, A. Alvaro, B.M. S., C.C. W., C.A. P., C.A. M., C.A. R., C. Susan, D.S. R., D.F. N., D. Luc, E.M. S.V., F.J. F., F. Myriam, J.L. Chaffin, K.S. S., K.B. M., K.K. L., K.T. W., L.D. T., L.T. T., L.J. H., L.C. T., L.M. Shane, L.P. L., M.S. S., M. Kunihiro, M.A. E., M.M. E., O. Martin, P. Ambarish, P.A. M., R.W. D., R.G. A., S.U. K.A., S.G. M., S.E. B., S.S. H., S.N. L., S. Andrew, T.D. L., T.C. W., T.M. P., V.L. B., W.J. T., W.S. S., V.S. S., null null, Heart Disease and Stroke Statistics—2019 Update: A Report From the American Heart Association, Circulation. 139 (2019) e56–e528. doi:10.1161/CIR.0000000000000659.
[32] J. Piñero, N. Queralt-Rosinach, À. Bravo, J. Deu-Pons, A. Bauer-Mehren, M. Baron, F. Sanz, L.I. Furlong, DisGeNET: a discovery platform for the dynamical exploration of human diseases and their genes, Database . 2015 (2015). doi:10.1093/database/bav028.
[33] K.T. Lappegård, P. Garred, L. Jonasson, T. Espevik, P. Aukrust, A. Yndestad, T.E. Mollnes, A. Hovland, A vital role for complement in heart disease, Mol. Immunol. 61 (2014) 126–134. doi:10.1016/j.molimm.2014.06.036.
[34] T. Chakraborti, A. Mandal, M. Mandal, S. Das, S. Chakraborti, Complement activation in heart diseases: Role of oxidants, Cell. Signal. 12 (2000) 607–617. doi:10.1016/S0898-6568(00)00111-X.
[35] V. Falk, H. Baumgartner, J.J. Bax, M. De Bonis, C. Hamm, P.J. Holm, B. Iung, P. Lancellotti, E. Lansac, D.R. Muñoz, R. Rosenhek, J. Sjögren, P. Tornos Mas, A. Vahanian, T. Walther, O. Wendler, S. Windecker, J.L. Zamorano, 2017 ESC/EACTS Guidelines for the management of valvular heart disease, Eur. J. Cardio-Thoracic Surg. 52 (2017) 616–664. doi:10.1093/ejcts/ezx324.
[36] S. Amjad, S.A. Sami, M.N. Basir, K. Hameed, M. Fujita, H.R. Ahmad, Pericardial fluid and serum biomarkers equally predict ventricular dysfunction, Asian Cardiovasc. Thorac. Ann. 21 (2013) 160–165. doi:10.1177/0218492312450292.
[37] B.-K. Jutta, K. Ursula, H. Maria, R. Raphael, M. Gerald, G. Harald, B. Thomas, P. Richard,

M. Gerald, B. Helmut, Natriuretic Peptides Predict Symptom-Free Survival and Postoperative Outcome in Severe Aortic Stenosis, Circulation. 109 (2004) 2302–2308. doi:10.1161/01.CIR.0000126825.50903.18.
[38] J.D. Bendtsen, L.J. Jensen, N. Blom, G. von Heijne, S. Brunak, Feature-based prediction of non-classical and leaderless protein secretion, Protein Eng. Des. Sel. 17 (2004) 349–356. doi:10.1093/protein/gzh037.
[39] J.J. Almagro Armenteros, K.D. Tsirigos, C.K. Sønderby, T.N. Petersen, O. Winther, S. Brunak, G. von Heijne, H. Nielsen, SignalP 5.0 improves signal peptide predictions using deep neural networks, Nat. Biotechnol. 37 (2019) 420–423. doi:10.1038/s41587-019-0036-z.
[40] T. Alleyne, J. Joseph, V. Sampson, Cytochrome-c detection: a diagnostic marker for myocardial infarction, Appl. Biochem. Biotechnol. 90 (2001) 97–105. doi:10.1385/ABAB:90:2:97.
[41] A. Thorburn, Tumor Necrosis Factor-Related Apoptosis-Inducing Ligand (TRAIL) Pathway Signaling, J. Thorac. Oncol. 2 (2007) 461–465. doi:10.1097/JTO.0b013e31805fea64.
[42] S. Grazioli, J. Pugin, Mitochondrial Damage-Associated Molecular Patterns: From Inflammatory Signaling to Human Diseases, Front. Immunol. 9 (2018) 832. doi:10.3389/fimmu.2018.00832.
[43] H. Jin, W. Li, R. Yang, A. Ogasawara, H. Lu, N.F. Paoni, Inhibitory effects of interferon-γ on myocardial hypertrophy, Cytokine. 31 (2005) 405–414. doi:10.1016/j.cyto.2005.06.013.
[44] K. Akihiko, I. Yuko, F. Machi, N. Mizuho, K. Yumi, T. Akira, M. Naofumi, K. Toshikazu, Protective Roles of Interferon-γ in Cardiac Hypertrophy Induced by Sustained Pressure Overload, J. Am. Heart Assoc. 7 (2019) e008145. doi:10.1161/JAHA.117.008145.
[45] R. Iskandar, S. Liu, F. Xiang, W. Chen, L. Li, W. Qin, F. Huang, X. Chen, Expression of pericardial fluid T-cells and related inflammatory cytokines in patients with chronic heart failure, Exp. Ther. Med. 13 (2017) 1850–1858. doi:10.3892/etm.2017.4202.
[46] R.N. Pinckard, M.S. Olson, P.C. Giclas, R. Terry, J.T. Boyer, R.A. O'Rourke, Consumption of classical complement components by heart subcellular membranes in vitro and in patients after acute myocardial infarction, J. Clin. Invest. 56 (1975) 740–750. doi:10.1172/JCI108145.
[47] D. Bubeck, P. Roversi, R. Donev, B.P. Morgan, O. Llorca, S.M. Lea, Structure of Human Complement C8, a Precursor to Membrane Attack, J. Mol. Biol. 405 (2011) 325–330. doi:10.1016/j.jmb.2010.10.031.
[48] G.H.M. Oliveira, C.N. Brann, K. Becker, V. Thohan, M.M. Koerner, M. Loebe, G.P. Noon, G. Torre-Amione, Dynamic Expression of the Membrane Attack Complex (MAC) of the Complement System in Failing Human Myocardium, Am. J. Cardiol. 97 (2006) 1626–1629. doi:10.1016/j.amjcard.2005.12.056.
[49] B.R. Lindman, M.-A. Clavel, P. Mathieu, B. Iung, P. Lancellotti, C.M. Otto, P. Pibarot, Calcific aortic stenosis, Nat. Rev. Dis. Prim. 2 (2016) 16006. doi:10.1038/nrdp.2016.6.
[50] M.R. Dweck, N.A. Boon, D.E. Newby, Calcific Aortic Stenosis: A Disease of the Valve and the Myocardium, J. Am. Coll. Cardiol. 60 (2012) 1854–1863. doi:10.1016/j.jacc.2012.02.093.
[51] C. Gavina, I. Falcão-Pires, F. Rocha-Goncalves, A. Leite-Moreira, Left Ventricular Hypertrophy in Isolated Aortic Stenosis: Primetime for the Ventricle, Curr. Pharm. Biotechnol. 13 (2012) 2503–2514. doi:10.2174/1389201011208062503.
[52] A.N. Rassi, P. Pibarot, S. Elmariah, Left Ventricular Remodelling in Aortic Stenosis, Can. J. Cardiol. 30 (2014) 1004–1011. doi:10.1016/j.cjca.2014.04.026.
[53] U.C. Sharma, P. Barenburg, S. Pokharel, W.R.M. Dassen, Y.M. Pinto, J.G. Maessen, Systematic review of the outcome of aortic valve replacement in patients with aortic stenosis, Ann Thorac Surg. 78 (2004) 90–95. doi:10.1016/j.athoracsur.2004.02.020.
[54] E. Gianazza, I. Miller, L. Palazzolo, C. Parravicini, I. Eberini, With or without you — Proteomics with or without major plasma/serum proteins, J. Proteomics. 140 (2016) 62–80. doi:10.1016/j.jprot.2016.04.002.

Chapter VII

General Discussion and Final Remarks

In increasingly ageing societies, VHD and, particularly, AS are burdening the healthcare services, as reflected in the growing number of AVR procedures performed every year [1]. The fact that AVR is not a definitive solution for many patients, who show incomplete myocardial RR, aggravates this scenario. Despite the identification of many potential risk factors, a patient's response to valve replacement is still currently unpredictable. Furthermore, the full comprehension of the biological mechanisms explaining an incomplete response is far, and co-adjuvant therapies to boost complete RR are missing. To address these issues, in this thesis, a (phospho)proteomics approach was followed to characterize, for the first time, the human myocardium and PF in AS patients showing a complete to incomplete RR.

As an adaptive response to pressure afterload, the myocardium undergoes a multitude of molecular, structural and functional adaptations to cope with increased wall stress [2–4]. For this reason, the myocardium was first object of (phospho)proteomic characterization, aiming primarily at identifying dysregulated biological processes and pathways in the origin of an incomplete response, but also potential prognostic markers. Then, considering the specific features of PF, namely the proximity to the heart, storing many heart-derived factors, but still reflecting systemic responses, this biofluid followed as the matrix for the interrogation of proteomic changes associated to an incomplete phenotype. With PF proteomics, the main goal was to identify potentially trackable and more easily translatable biomarkers of such a poor outcome. In any case, though, potential targets of therapy were browsed, whether on more general biological phenomena or, specifically, one relevant proteins/kinases. Either for myocardium or PF, an initial screen of dysregulated proteins was undertaken, showing that over 80 myocardial proteins and seven PF proteins differed significantly between AS patients with complete or incomplete RR. In line with the expectations of a plasma-like biofluid, with an inherent high dynamic range of proteins [5], a lower number of dysregulated proteins was quantified in PF in comparison to myocardium. In the future, pre-fractionation approaches, such as the one used with NPs@EDTA, will have to be conjugated with more complex separation techniques, such as isoelectric focusing or strong cation/anion exchange chromatography methods, if one aims to get deeper coverage of the low abundance PF proteome. Nonetheless, judging by GOEA and pathway analysis, a congruent picture of the dysregulated biological processes on the source of an incomplete RR was obtained with the two biological materials. For instance, the pro-anabolic state in iRR, with increased transcription rates (myocardial proteomics), mRNA metabolism and translation (PF proteomics) and the activation of the immune system (myocardial and PF proteomics) were suggested by these analyses. Furthermore, although

no causal relationships could be drawn from this cross-sectional study, several hypotheses emerge to explain the observed post-AVR phenotypical divergence of AS patients, through the analysis of the (phospho)proteome, kinase prediction, immunoblots and clinical correlations. These hypotheses, based on the evidences collected from ***Chapters II*** to ***VI***, and supported by the literature and gene annotation were fitted together in a model, depicted in **Figure 1**, and discussed henceforth.

In AS, the obstruction of the aortic valve is responsible for a pressure overload state, and this form of mechanical stress is the main driver of myocardial remodeling [2,3,6,7]. The angiotensin II receptor (AT2R) type 1 is among the myocardial players involved in mechanosensing (others include integrins, or stretch-activated channels), and, remarkably, AT2R can be directly activated through mechanical forces (stretch), without angiotensin II binding [8]. The activation of the AT2R is a well-known driver of cardiac hypertrophy and fibrosis and, for this reason, this should be highlighted as a key signaling pathway in AS patients with complete or incomplete RR. The AT2R is a G protein-coupled receptor, and its stimulation leads to G protein activation: G_q in cardiomyocytes and G_i in cardiac fibroblasts. In the latter, the subsequent activation of the Ras-Raf-MAPK (mitogen-activated protein kinase) pathway triggers fibroblast proliferation and fibrosis, while in the former the activation of PLC promotes cardiomyocyte growth [9]. This is due to the generation of inositol triphosphate (IP_3) and diacylglycerol (DAG), second messengers that unfold a myriad of responses. These include, for instance, calcium release from sarcoplasmic reticulum through binding of IP_3 to its receptor (IP_3R). The rise in cytosolic calcium levels is responsible for the activation of calcium-dependent proteins, such as calmodulin (CaM) and calcineurin (CaN). CaN pro-hypertrophic role relies on its phosphatase activity, which is responsible for the dephosphorylation and consequent activation of the NFAT, which is shuttled to the nucleus to initiate a pro-hypertrophic gene program [10]. In turn, DAG's pro-hypertrophic effect is attributed to the activation of PKC [11]. Despite the activation of this central pathway, during myocardial remodeling, the results of this thesis suggest that specific biological phenomena and pathways tailor the response of AS patients towards a more complete or incomplete RR:

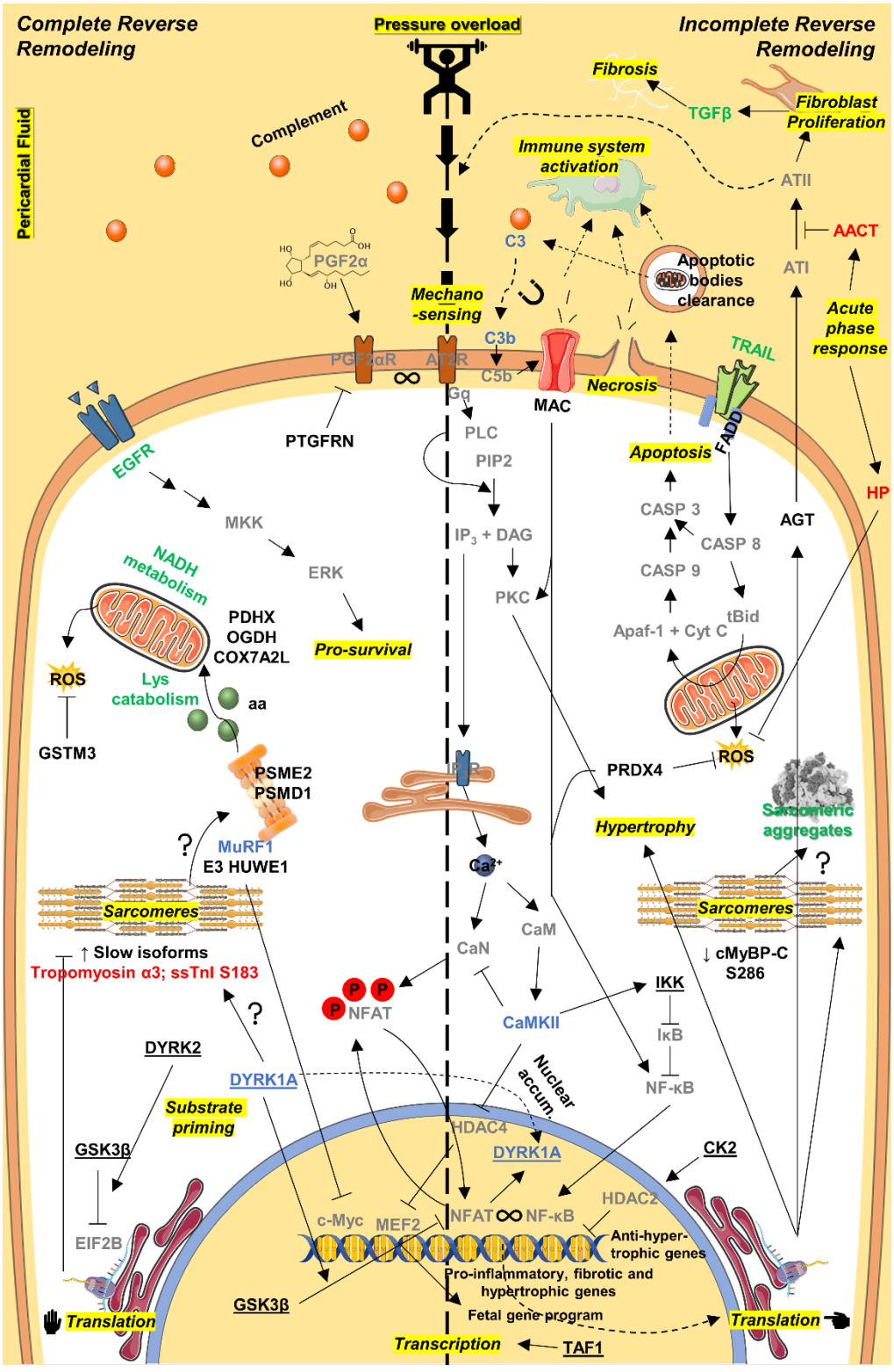

Figure 1. Proposed model to explain the phenotypical divergence during reverse remodeling. A common pathway involved in pressure overload-induced mechanosensing is shown in the middle. Biological mechanisms and pathways as well as the specific protein players associated to a complete response are depicted on the left, and those associated to an incomplete response are depicted on the right. See text for explanations and abbreviations. Proteins identified are in black, proteins validated by immunoblot in blue, predicted kinases are underlined, proteins associated to discriminant analysis are in red and in green are evidences collected from GOEA. Solid arrows represent activation; dashed arrows represent movement and T-shaped lines mean inhibition. Symbols: ∞ - synergy; ✋ - stop; ☜ - stimulus.

Modulation of the hypertrophic and pro-fibrotic signaling pathways. One of the consequences of pressure overload is the release of prostaglandin F2-α (at least partly, due to PKC activation) [12]. This bioactive compound binds to a transmembrane receptor (PGF2αR) which can dimerize and synergize (symbolized by ∞) with AT2R, further exacerbating the hypertrophic phenotype [11]. Thus, one potential protective mechanism favoring a complete RR might be related to the higher expression of the negative regulator of the prostaglandin F2-α receptor (PTGFRN), as determined by myocardial proteomics, leading to a reduction in PGF2αR number. Apart from prostaglandin F2-α, other humoral factors, such as angiotensin II itself, may further exacerbate the pro-hypertrophic and pro-fibrotic phenotype. In fact, during pressure overload, angiotensin II can be released autocrinally or paracrinally [8,9], but such an angiotensin II overload should be present in patients showing an incomplete response. This is supported by a 4-fold elevation in the expression of its precursor, angiotensinogen, in patients with iRR, as deemed by myocardial proteomics. The high humoral load of angiotensin II in iRR patients describes a positive feedback loop by feeding the AT2R pathway and, ergo, leading to enhanced sarcoplasmic reticulum calcium leak in cardiomyocytes. The activated calcium-dependent proteins CaN and CaM should be implicated in dramatizing the hypertrophic phenotype: the former through NFAT activation, and the latter through CAMK2 activation [10]. Indeed, the myocardial phosphoproteome shows a high level of phosphorylation (Ser 330, Ser 333 and Thr 337) in iRR patients, anticipating that the (dys)regulation of this kinase is of importance for this phenotype. However, the biological meaning of such modifications remains elusive and will require more attention. Probably, despite an initial regulation of CaN, the persistent activation of CAMK2 might favor an incomplete regression. For instance, CAMK2-mediated phosphorylation-inhibition of HDAC4 activates the basally repressed MEF2, resulting in fetal gene program reactivation [10]. In turn, angiotensin II-mediated activation of the AT2R pathway in cardiac fibroblasts should favor fibrosis, in a process mediated by TGF-β, at least, considering the GOEA to myocardial dysregulated proteins.

Regulation of transcription and protein synthesis. GOEA and pathway analysis with either myocardial or PF proteome data also suggests a higher rate of transcription (particularly gene expression) as well as translation in iRR patients. Kinase prediction further supports this idea. For instance, TAF1 presented as the kinase with the second highest predicted activity in iRR, and this kinase lies in the core of the transcription factor TFIID, an essential factor for RNA polymerase II-mediated transcription [13]. In turn, the kinase family IKK, which is activated by CAMK2 itself, blocks the inhibition of NF-κB by IκB, hence promoting the nuclear import of this transcription factor [14]. The NF-κB, in turn, is

responsible for the expression of pro-inflammatory and pro-fibrotic genes, in addition to pro-hypertrophic genes, by synergizing with NFAT [15]. Despite the relatively higher transcriptional activity in iRR, it should be noted that mechanisms repressing gene expression should also be implicated in modulating the phenotype of iRR patients. For instance, one of the many substrates of CK2 (the kinase with the highest predicted activity in iRR) is HDAC2 that, when activated, prevents the expression of anti-hypertrophic genes [16]. In this regard, patients with cRR should be protected by three kinases, DYRK1A, DYRK2 and GSK3, which were predicted from myocardial phosphoproteome analysis. For instance, DYRK1A expression is induced by NFAT and this kinase then primes NFAT for GSK3-mediated inhibition, hence describing a negative feedback loop [17–19]. In turn, DYRK2 promotes GSK3-mediated inhibition of the eukaryotic translation initiation factor 2B, repressing cardiac hypertrophy by blocking protein synthesis [20]. Of note, despite the association of DYRK1A activity to patients with cRR, a higher expression of DYRK1A was confirmed in iRR patients, by western blot, and a negative correlation with LVM regression was also observed. These seemingly contradictory findings may actually be explained by a pathological cytosolic loss-of-function/nuclear gain-of-function, provided that DYRK1A is constitutively active [17]. In fact, previous studies have shown that in basal conditions, most DYRK1A is found in the cytoskeleton and, when overexpressed, this kinase concentrates in the nucleus [21,22]. Hence, a hypothesis emerges whereby, shuttling to the nucleus, DYRK1A reduces its cytosolic and cytoskeleton activity due to the loss of contact with the usual interacting proteins.

UPS, metabolic adaptations and oxidative stress. Sarcomere recycling through the UPS may also be another hypertrophy-limiting factor during RR. The results of this thesis suggest that cRR patients may be protected by higher activity of the UPS. In fact, myocardial proteomics shows increased expression of the ubiquitin ligase HUWE1. This enzyme controls hypertrophy by catalyzing the polyubiquitination (and, thereby, degradation) of the pro-hypertrophic transcription factor c-Myc [23]. In addition, an increase in proteasome subunits (PSME2 and PSMD1) anticipate a rise in the proteolytic flux through the proteasome. This will require confirmation since PSMD1 western blot was inconclusive. In addition, proteasome activity assays will be necessary to draw definitive conclusions. Still, by now, the negative correlation observed between MuRF1 and a postoperative hypertrophy marker (IVST), in a larger cohort, foresees a relevant role of E3 ubiquitin ligases in shaping the RR phenotype. Patients with iRR, on the contrary, are expected to present a higher degree of protein aggregation, in line with reported observations in a mouse model

of angiotensin II-induced hypertension/pressure overload [24], and supported by the mapping of the term “amyloid-beta metabolic processing” in this subset of patients.

Cardiac metabolic abnormalities and energetic imbalance due to mitochondrial dysfunction were lately shown to play an important role in cardiac remodeling [25]. Therefore, these factors should also be key in RR. In this regard, there might be a potential advantage of cRR patients, in particular due to amino acid degradation. These metabolites are rendered by proteasome activity and, despite not being the preferred source of ATP in healthy myocardium (fatty acids are the first choice [26]), these may contribute positively to favorable bioenergetics. This idea is corroborated by ClueGO analysis showing a significant association of Lys (ketogenic amino acid) catabolism and concomitant NADH metabolism to cRR patients. FunRich analysis also shows a preponderance of energy and metabolic pathways, particularly of amino acids and their derivatives in cRR. Amino acids have already been acknowledged as important energetic substrates during cardiac ischemia [27], which is itself a hallmark of pressure overload-induced myocardium remodeling [4]. Furthermore, the myocardial proteome in cRR patients demonstrated a higher expression of proteins associated with the pyruvate dehydrogenase complex (PDHX), Krebs cycle (OGDH) and electron transport chain (COX7A2L). This suggests higher mitochondrial biogenesis and/or higher metabolic flux through this organelle in patients with cRR. Apart from the utilization of amino acids, this picture is also compatible with a more efficient glucose oxidation, because a greater activity of the pyruvate dehydrogenase prevents the anaplerotic loss of pyruvate [28]. Curiously, an increased expression of the ssTnI, as found in cRR patients, has been associated with higher pyruvate dehydrogenase activity (and, thus higher production of ATP from pyruvate) and to confer protection against hypertrophy in ssTnI transgenic mice submitted to pressure overload [28]. The downside of higher mitochondrial activity is the unavoidable generation of reactive oxygen species (ROS), requiring matched protection by antioxidant proteins. DEP analysis showed a higher expression of glutathione S-transferase (GSTM3) in patients with cRR. This enzyme promotes the conjugation of glutathione to hydrophobic electrophiles in order to neutralize ROS. In turn, a higher expression of peroxiredoxin-4 was associated to patients with iRR. Nevertheless, in spite of neutralizing hydrogen peroxide, peroxiredoxin-4 may also lead to NF-κB activation, through the regulation of IκB phosphorylation (according to UniProt), thus conferring limited protection.

Complement system activity and cell death. Multiple pieces of evidence (DEP analysis, discriminant analysis and western blot) collected through myocardial and PF analysis

anticipate a major role of complement system during RR. For instance, a trend for an increase of the complement C3 in the myocardium was observed, likely at the expense of circulating complement in the PF (e.g. PF's complement C8 was found in lower amounts in patients with iRR). What drives this accumulation is yet to unravel in post-AVR myocardial remodeling, but previous studies have suggested that mitochondrial proteins released during ischemic injury may trigger complement deposition [29]. Curiously, FunRich analysis disclosed a significant enrichment of proteins with mitochondrial origin in the PF of iRR patients. The accumulation of complement proteins in the membrane of cardiomyocytes, and later formation of a membrane attack complex, may unfold multiple responses. At sublytic concentrations, this complex might feed the activation of hypertrophic (via PKC) as well as pro-inflammatory pathways (via NF-κB). Although, when the lytic concentration threshold is exceeded, it might lead to cell lysis and death [29]. Beyond the activity of the mebrane attack complex, cardiomyocyte loss in iRR may be a consequence of TRAIL pathway activation, as suggested by GOEA. In this case, the activated death receptors recruit and activate caspase (CASP) 8, which may initiate the mitochondrial apoptotic pathway (through Bid cleavage that stimulates the release of proapoptotic proteins from mitochondria) or may directly activate the effector caspase 3 [30]. Still, the hypothesis of complement system activation being a response to cells already committed to death cannot be excluded. Either way, the timeline of the events will require more investigation as will the hypothesis of both complement activation and cell death being concurring events. In the case of cRR patients, protection against cell death may arise from the activation of pro-survival pathways, such as the EGFR pathway [31], as suggested by GOEA and pathway analysis in both myocardium and PF.

Immune-inflammatory response. A common finding after DEP, multivariate analysis and GOEA of the myocardial and PF proteome was the activation of the acute-phase response and of the immune system, markedly on patients with an incomplete LVM regression. One hypothesis to explain this observation is the secretion of pro-inflammatory cytokines due to higher NF-κB activity and the release of danger signals from dying cells. Particularly in what concerns the acute-phase response, the association of haptoglobin (HP) and of α1-antichymotrypsin to iRR patients may be viewed as a compensatory mechanism. Haptoglobin exerts antioxidant effects, according to UniProt, and, thus, it may limit the oxidative burden associated with inflammation. In turn, α1-antichymotrypsin (AACT) is a chymase inhibitor, considered to be the main responsible of heart *in situ* conversion of angiotensinogen to angiotensin II [11,32]. Given the phenotype of iRR patients, it is likely that α1-antichymotrypsin, on its own, does not provide enough cardioprotection. However,

in a recent clinical trial it was found that the chymase inhibitor fulacimstat is safe and well-tolerated by stable acute myocardial infarction patients with LV dysfunction. Besides, the drug did not change blood pressure nor heart rate as compared to placebo, which is consistent with a local, rather than systemic, targeting of angiotensin II production [33]. Hence, this trial corroborates the pharmacological inhibition of chymase as a potential therapy for AS patients undergoing AVR.

Contractile properties. Finally, and despite all patients enrolled in the study presented with preserved systolic function at the time of surgery, some proteomic changes observed between patients with complete and incomplete RR suggest some mechanical differences in cardiomyocytes, which may have later functional consequences. Concerning cRR, the higher expression of ssTnI and of the tropomyosin's slower isoform (α3) deserve further attention because these may confer functional protection. For instance, cardiomyocytes from mutant mice expressing the former TnI isoform have shown higher myofilamentary calcium sensitivity [34]. Regarding iRR, a dramatic decrease in cMyBP-C Ser 286 phosphorylation was observed. This residue belongs to the cMyBP-C regulatory domain (M domain) and its phosphorylation reduces interaction with F-actin, likely regulating cross-bridge kinetics [35]. Therefore, this lack of regulation may prompt cardiac dysfunction in iRR patients. This is supported by the observation of reduced levels of cMyBP-C Ser 284, Ser 286 and Thr 290 phosphorylation in patients with heart failure [36]. Thus, the functional consequences of Ser 286 dephosphorylation will require clarification as it may become a target of therapeutic modulation during RR. Lastly, according to the functional studies performed with mutant cardiomyocytes (Dyrk1a$^{+/-}$), showing a different response to stretch and a decreased force development capacity, DYRK1A dysregulation may promote increased sarcomere stiffness and favor diastolic dysfunction. Thus, it is hypothesized that patients with increased expression of DYRK1A, and subsequent nuclear accumulation, are at higher risk for diastolic dysfunction. Albeit, it remains to demonstrate ssTnI phosphorylation on Ser 183 by DYRK1A and to understand its functional relevance. Altogether, though, these data suggest that it should be an important adaptation to pressure overload, being relevant for myocardial relaxation.

In conclusion, the combined characterization of the myocardial (phospho)proteome and PF proteome in AS patients with different degrees of RR, supported by clinical correlates, immunoblot and functional studies:

i) Disclosed a myriad of biological factors that may be on the root of a post-AVR incomplete response, such as the overactivation of pro-hypertrophic pathways (e.g. NFAT and NF-κB), increased transcription and translation rates, reduced UPS activity, metabolic inefficiency, mitochondria loss, complement activation and cell death;
ii) Established new potential prognostic markers of incomplete RR, such as MuRF1, complement C3 (β chain) and DYRK1A;
iii) Identified many relevant avenues of therapy, namely the modulation of the kinases CK2, IKK and GSK3 and/or their substrates to mitigate hypertrophy and/or the inhibition of extrinsic cues of cell death (lytic complements and/or TRAIL).
iv) Demonstrated the influence of DYRK1A expression in cardiomyocyte contractile properties, showing that the modulation of this kinase may be an important avenue to fight diastolic dysfunction, which adds to its known anti-hypertrophic activity.

The results obtained in this thesis provided a comprehensive picture of the dysregulated biological processes condemning AS patients to an incomplete myocardial RR, and many questions arise that should be object of research in the future. From the many mechanisms that favor a pro-hypertrophic state, the inhibitory role of GSK3β in protein synthesis, for example, should be confirmed on patients with cRR, and the levels of Ser 9 phosphorylation in GSK3β should be assessed, because, despite the same levels of expression, a higher predicted activity of GSK3 on cRR suggests GSK3β inhibition in iRR patients. Since the proteasome influx also controls cell hypertrophy, the activity of these organelles should be determined in myocardial samples, as to confirm the higher degree of protein recycling in patients with cRR. Animal models of aortic banding-induced pressure overload may also be helpful to understand whether a ketogenic or protein-rich diet can favor a cRR phenotype. Attention should also be given to the mechanisms of cell death, in order to understand which is the main route of cardiomyocyte loss during myocardial remodeling, i.e. are the extrinsic pathways more important than the intrinsic death signals? To that end, evaluation of apoptosis (e.g. TUNEL), immunohistochemical detection of death receptors (e.g. TRAIL receptor) and of the membrane attack complex may give important insights. Furthermore, the characterization of the immune system cell subpopulations present in the PF will also be key to disclose their role in RR. Animal models of aortic banding-debanding shall also be of great usefulness to test the therapeutic power of PTGFRN and membrane attack complex hindrance; CK2, CAMK2 and IKK inhibition or even MuRF1, DYRK1A and GSK3β agonism. Particularly, regarding DYRK1A, coimmunoprecipitation studies may shed light

into the cytoskeletal and cytosolic interacting partners during pressure overload. Functional studies with skinned or intact cardiomyocytes, obtained from patients with iRR and/or with diastolic dysfunction, and incubated with recombinant DYRK1A will clarify the beneficial role of this kinase. Finally, in the future, the PF prognostic and functional properties should be further explored. Considering the large amounts of protein available in PF, proteome characterization might be deepened through the conjugation of multiple fractionation strategies and/or by increasing the quantification power through DIA or SWATH-MS approaches. In turn, targeted detection (e.g. multiple reaction monitoring) of specific markers (e.g. mitochondria markers, complement components, soluble membrane attack complex) may also provide useful prognostic tools. Finally, the incubation of cardiomyocytes with PF collected from patients with iRR or with cRR might also be important to identify protein species capable of modulating cardiomyocyte function.

References

[1] S.D. Culler, D.J. Cohen, P.P. Brown, A.D. Kugelmass, M.R. Reynolds, K. Ambrose, M.L. Schlosser, A.W. Simon, M.R. Katz, Trends in Aortic Valve Replacement Procedures Between 2009 and 2015: Has Transcatheter Aortic Valve Replacement Made a Difference?, Ann. Thorac. Surg. 105 (2018) 1137–1143. doi:10.1016/j.athoracsur.2017.10.057.

[2] I. Falcão-Pires, C. Gavina, A.F. Leite-Moreira, Understanding the molecular and cellular changes behind aortic valve stenosis, Curr. Pharm. Biotechnol. 13 (2012) 2485–2496. doi:10.2174/138920112804583050.

[3] M.R. Dweck, N.A. Boon, D.E. Newby, Calcific Aortic Stenosis: A Disease of the Valve and the Myocardium, J. Am. Coll. Cardiol. 60 (2012) 1854–1863. doi:10.1016/j.jacc.2012.02.093.

[4] B.R. Lindman, M.-A. Clavel, P. Mathieu, B. Iung, P. Lancellotti, C.M. Otto, P. Pibarot, Calcific aortic stenosis, Nat. Rev. Dis. Prim. 2 (2016) 16006. doi:10.1038/nrdp.2016.6.

[5] E. Gianazza, I. Miller, L. Palazzolo, C. Parravicini, I. Eberini, With or without you — Proteomics with or without major plasma/serum proteins, J. Proteomics. 140 (2016) 62–80. doi:10.1016/j.jprot.2016.04.002.

[6] C. Gavina, I. Falcão-Pires, F. Rocha-Goncalves, A. Leite-Moreira, Left Ventricular Hypertrophy in Isolated Aortic Stenosis: Primetime for the Ventricle, Curr. Pharm. Biotechnol. 13 (2012) 2503–2514. doi:10.2174/1389201011208062503.

[7] G.L. Perrucci, M. Zanobini, P. Gripari, P. Songia, B. Alshaikh, E. Tremoli, P. Poggio, Pathophysiology of Aortic Stenosis and Mitral Regurgitation, Compr. Physiol. 7 (2017) 799–818. doi:doi:10.1002/cphy.c160020.

[8] Z. Daniela, S. Junichi, Solving the Cardiac Hypertrophy Riddle: The Angiotensin II–Mechanical Stress Connection, Circ. Res. 113 (2013) 1192–1195. doi:10.1161/CIRCRESAHA.113.302501.

[9] T. Yamazaki, Y. Yazaki, Role of tissue angiotensin II in myocardial remodelling induced by mechanical stress, J. Hum. Hypertens. 13 (1999) S43–S48. doi:10.1038/sj.jhh.1000747.

[10] D. Matthias, von der L. Albert, K.H. A., B. Johannes, Calcium Signaling and Transcriptional Regulation in Cardiomyocytes, Circ. Res. 121 (2017) 1000–1020. doi:10.1161/CIRCRESAHA.117.310355.

[11] S.J. Forrester, G.W. Booz, C.D. Sigmund, T.M. Coffman, T. Kawai, V. Rizzo, R. Scalia, S. Eguchi, Angiotensin II Signal Transduction: An Update on Mechanisms of Physiology and Pathophysiology, Physiol. Rev. 98 (2018) 1627–1738. doi:10.1152/physrev.00038.2017.
[12] G.K. Oriji, Angiotensin II stimulates hypertrophic growth of cultured neonatal rat ventricular myocytes: roles of PCK and PGF2alpha, Prostaglandins, Leukot. Essent. Fat. Acids. 62 (2000) 233–237. doi:10.1054/plef.2000.0148.
[13] R.K. Louder, Y. He, J.R. López-Blanco, J. Fang, P. Chacón, E. Nogales, Structure of promoter-bound TFIID and model of human pre-initiation complex assembly, Nature. 531 (2016) 604. doi:10.1038/nature17394.
[14] J. Beckendorf, M.M.G. van den Hoogenhof, J. Backs, Physiological and unappreciated roles of CaMKII in the heart, Basic Res. Cardiol. 113 (2018) 29. doi:10.1007/s00395-018-0688-8.
[15] L. Qinghang, C. Yi, A.-M. Mannix, M.J. D., Interaction Between NFκB and NFAT Coordinates Cardiac Hypertrophy and Pathological Remodeling, Circ. Res. 110 (2012) 1077–1086. doi:10.1161/CIRCRESAHA.111.260729.
[16] E.G. Hyeon, C.Y. Kuk, K. Jeong-Hyeon, S. Sera, C. Nakwon, K. Yoojung, J. Hosouk, K. Hyung-Seok, N. Kwang-Il, K.H. Jin, K. Hyun, Casein Kinase-2α1 Induces Hypertrophic Response by Phosphorylation of Histone Deacetylase 2 S394 and its Activation in the Heart, Circulation. 123 (2011) 2392–2403. doi:10.1161/CIRCULATIONAHA.110.003665.
[17] W. Becker, W. Sippl, Activation, regulation, and inhibition of DYRK1A, FEBS J. 278 (2011) 246–256. doi:10.1111/j.1742-4658.2010.07956.x.
[18] C. Kuhn, D. Frank, R. Will, C. Jaschinski, R. Frauen, H.A. Katus, N. Frey, DYRK1A Is a Novel Negative Regulator of Cardiomyocyte Hypertrophy, J. Biol. Chem. . 284 (2009) 17320–17327. doi:10.1074/jbc.M109.006759.
[19] Y. Gwack, S. Sharma, J. Nardone, B. Tanasa, A. Iuga, S. Srikanth, H. Okamura, D. Bolton, S. Feske, P.G. Hogan, A. Rao, A genome-wide Drosophila RNAi screen identifies DYRK-family kinases as regulators of NFAT, Nature. 441 (2006) 646–650. doi:10.1038/nature04631.
[20] C.S. Weiss, M.M. Ochs, M. Hagenmueller, M.R. Streit, P. Malekar, J.H. Riffel, S.J. Buss, K.H. Weiss, J. Sadoshima, H.A. Katus, S.E. Hardt, DYRK2 Negatively Regulates Cardiomyocyte Growth by Mediating Repressor Function of GSK-3β on eIF2Bε, PLoS One. 8 (2013) e70848. doi:10.1371/journal.pone.0070848.
[21] J. Roewenstrunk, C. Di Vona, J. Chen, E. Borras, C. Dong, K. Arató, E. Sabidó, M.S.Y. Huen, S. de la Luna, A comprehensive proteomics-based interaction screen that links DYRK1A to RNF169 and to the DNA damage response, Sci. Rep. 9 (2019) 6014. doi:10.1038/s41598-019-42445-x.
[22] W. Kaczmarski, M. Barua, B. Mazur-Kolecka, J. Frackowiak, W. Dowjat, P. Mehta, D. Bolton, Y.-W. Hwang, A. Rabe, G. Albertini, J. Wegiel, Intracellular distribution of differentially phosphorylated dual-specificity tyrosine phosphorylation-regulated kinase 1A (DYRK1A), J. Neurosci. Res. 92 (2014) 162–173. doi:10.1002/jnr.23279.
[23] K. Dadson, L. Hauck, Z. Hao, D. Grothe, V. Rao, T.W. Mak, F. Billia, The E3 ligase Mule protects the heart against oxidative stress and mitochondrial dysfunction through Myc-dependent inactivation of Pgc-1α and Pink1, Sci. Rep. 7 (2017) 41490. doi:10.1038/srep41490.
[24] S. Ayyadevara, F. Mercanti, X. Wang, S.G. Mackintosh, A.J. Tackett, S.V.S. Prayaga, F. Romeo, R.J. Shmookler Reis, J.L. Mehta, Age- and Hypertension-Associated Protein Aggregates in Mouse Heart Have Similar Proteomic Profiles., Hypertension. 67 (2016) 1006–1013. doi:10.1161/HYPERTENSIONAHA.115.06849.
[25] G.D. Lopaschuk, Metabolic Modulators in Heart Disease: Past, Present, and Future, Can. J. Cardiol. 33 (2017) 838–849. doi:10.1016/j.cjca.2016.12.013.
[26] I. Shimizu, T. Minamino, Physiological and pathological cardiac hypertrophy, J. Mol. Cell. Cardiol. 97 (2016) 245–262. doi:10.1016/j.yjmcc.2016.06.001.
[27] K.J. Drake, V.Y. Sidorov, O.P. Mcguinness, D.H. Wasserman, J.P. Wikswo, Amino acids as metabolic substrates during cardiac ischemia, Exp. Biol. Med. 237 (2012) 1369–1378. doi:10.1258/ebm.2012.012025.
[28] C.A. N., T.D. M., B. Jian, S.R. John, L.E. Douglas, Metabolic Efficiency Promotes Protection From Pressure Overload in Hearts Expressing Slow Skeletal Troponin I, Circ. Hear. Fail. 8 (2015) 119–127. doi:10.1161/CIRCHEARTFAILURE.114.001496.
[29] T. Chakraborti, A. Mandal, M. Mandal, S. Das, S. Chakraborti, Complement activation in heart diseases: Role of oxidants, Cell. Signal. 12 (2000) 607–617. doi:10.1016/S0898-

6568(00)00111-X.
[30] A. Thorburn, Tumor Necrosis Factor-Related Apoptosis-Inducing Ligand (TRAIL) Pathway Signaling, J. Thorac. Oncol. 2 (2007) 461–465. doi:10.1097/JTO.0b013e31805fea64.
[31] S.J. Fuller, K. Sivarajah, P.H. Sugden, ErbB receptors, their ligands, and the consequences of their activation and inhibition in the myocardium, J. Mol. Cell. Cardiol. 44 (2008) 831–854. doi:10.1016/j.yjmcc.2008.02.278.
[32] M. Shimizu, R. Tanaka, T. Fukuyama, R. Aaoki, K. Orito, Y. Yamane, Cardiac Remodeling and Angiotensin II-Forming Enzyme Activity of the Left Ventricle in Hamsters with Chronic Pressure Overload Induced by Ascending Aortic Stenosis, J. Vet. Med. Sci. 68 (2006) 271–276. doi:10.1292/jvms.68.271.
[33] H.-D. Düngen, L. Kober, S. Nodari, M. Schou, C. Otto, M. Becka, F. Kanefendt, B.R. Winkelmann, G. Gislason, F. Richard, O.W. Nielsen, M. Gheorghiade, M. Senni, Safety and Tolerability of the Chymase Inhibitor Fulacimstat in Patients With Left Ventricular Dysfunction After Myocardial Infarction—Results of the CHIARA MIA 1 Trial, Clin. Pharmacol. Drug Dev. 0 (2018) 1–10. doi:10.1002/cpdd.633.
[34] R.C. Fentzke, S.H. Buck, J.R. Patel, H. Lin, B.M. Wolska, M.O. Stojanovic, A.F. Martin, R.J. Solaro, R.L. Moss, J.M. Leiden, Impaired cardiomyocyte relaxation and diastolic function in transgenic mice expressing slow skeletal troponin I in the heart, J. Physiol. 517 (1999) 143–157. doi:10.1111/j.1469-7793.1999.0143z.x.
[35] J.F. Shaffer, R.W. Kensler, S.P. Harris, The Myosin-binding Protein C Motif Binds to F-actin in a Phosphorylation-sensitive Manner, J. Biol. Chem. . 284 (2009) 12318–12327. doi:10.1074/jbc.M808850200.
[36] V. Kooij, R.J. Holewinski, A.M. Murphy, J.E. Van Eyk, Characterization of the cardiac myosin binding protein-C phosphoproteome in healthy and failing human hearts, J. Mol. Cell. Cardiol. 60 (2013) 116–120. doi:10.1016/j.yjmcc.2013.04.012.

Appendix

Contents

1. Supplementary material of *Chapter II*

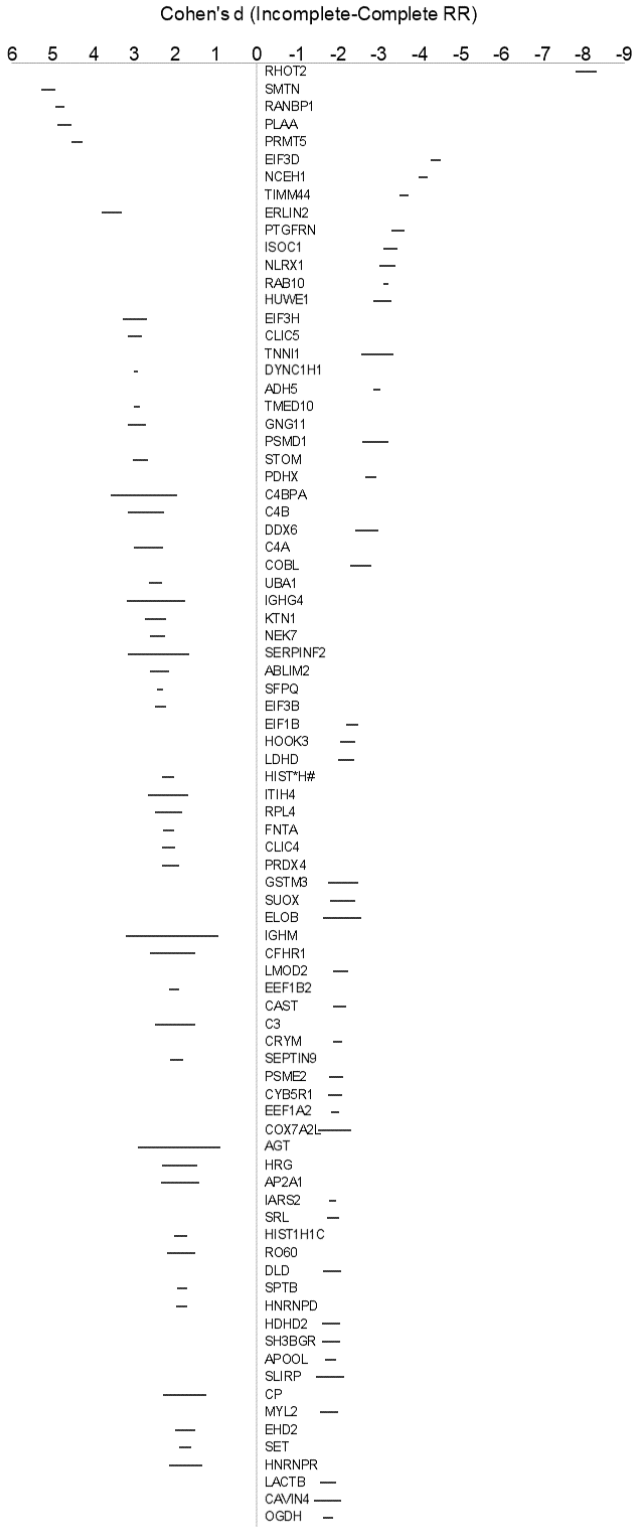

Figure S1. 95% confidence interval of the Cohen's d, for each of the differentially expressed proteins in the myocardium of patients with complete and incomplete reverse remodeling. Proteins are identified with the respective gene name. Proteins are also identified in **Table 3**, ***Chapter II***.

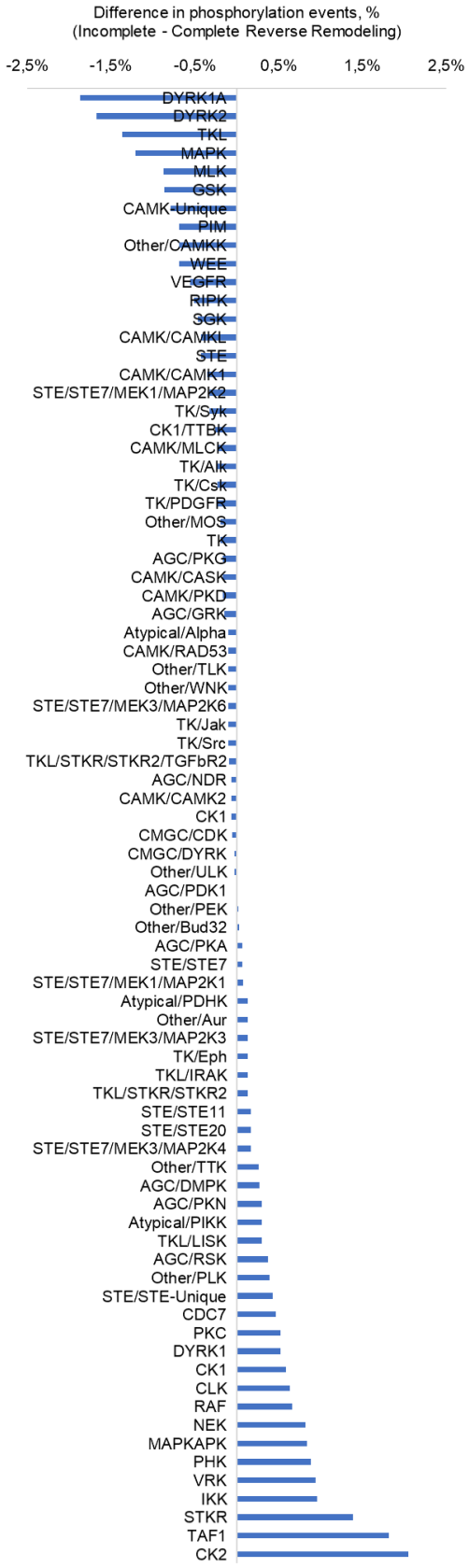

Figure S2. Kinase rank. Kinases were predicted with GPS 3.0 and sorted according to the percentage of associated phosphorylation events. Kinases (or families) associated with complete reverse remodeling are on the left side of the axis and those associated with incomplete reverse remodeling are on the right side.

Supplementary Table S1. Complete Kinase Rank, containing all predicted kinases and kinase families and the respective percentage of phosphorylation events in complete and incomplete reverse remodeling.

Predicted Kinase/Family	Family	Kinase/Kinase Group	% Phosphorylation events		
			cRR	iRR	Δ
CMGC/DYRK/DYRK1/ DYRK1A	CMGC	Dual specificity tyrosine-phosphorylation-regulated kinase 1A	2.5%	0.7%	-1.9%
CMGC/DYRK/DYRK2	CMGC	Dual specificity tyrosine-phosphorylation-regulated kinase 2	2.1%	0.4%	-1.7%
TKL	TKL	-	3.2%	1.8%	-1.4%
CMGC/MAPK	CMGC	Mitogen-Activated Protein Kinase	2.5%	1.3%	-1.2%
TKL/MLK	TKL	Mixed Lineage Kinases	3.0%	2.1%	-0.9%
CMGC/GSK	CMGC	Glycogen Synthase Kinase	4.8%	4.0%	-0.9%
CAMK/CAMK-Unique	CAMK	Unique	0.9%	0.1%	-0.8%
CAMK/PIM	CAMK	Pim	0.7%	0.0%	-0.7%
Other/CAMKK	Other	CAM kinase kinase	0.7%	0.0%	-0.7%
Other/WEE	Other	Wee	0.7%	0.0%	-0.7%
TK/VEGFR	TK	Vascular Endothelial Growth Factor Receptor	0.7%	0.1%	-0.6%
TKL/RIPK	TKL	Receptor Interacting Protein Kinases	2.8%	2.2%	-0.5%
AGC/SGK	AGC	Serum and Glucocorticoid induced Kinases	0.5%	0.0%	-0.5%
CAMK/CAMKL	CAMK	CAM kinase-like	0.7%	0.3%	-0.4%
STE	STE	-	0.7%	0.3%	-0.4%
CAMK/CAMK1	CAMK	Calcium/calmodulin-dependent protein kinase type 1	1.1%	0.8%	-0.4%
STE/STE7/MEK1/MAP 2K2	STE	Dual specificity mitogen-activated protein kinase kinase 2	0.5%	0.1%	-0.3%
TK/Syk	TK	Spleen tyrosine kinase	0.5%	0.1%	-0.3%
CK1/TTBK	CK1	Tau-Tubulin Kinase	0.9%	0.7%	-0.3%
CAMK/MLCK	CAMK	Myosin Light Chain Kinase	0.2%	0.0%	-0.2%
TK/Alk	TK	Anaplastic Lymphoma Kinase	0.2%	0.0%	-0.2%
TK/Csk	TK	C-terminal Src kinases	0.2%	0.0%	-0.2%
TK/PDGFR	TK	Platelet-Derived Growth Factor Receptor	0.2%	0.0%	-0.2%
Other/MOS	Other	Mos	0.5%	0.3%	-0.2%
TK	TK	-	0.5%	0.3%	-0.2%
AGC/PKG	AGC	Protein Kinase G	0.7%	0.5%	-0.2%
CAMK/CASK	CAMK	Calcium/calmodulin-dependent serine protein kinase	0.7%	0.5%	-0.2%
CAMK/PKD	CAMK	Protein Kinase D	0.7%	0.5%	-0.2%
AGC/GRK	AGC	G-protein-coupled receptor kinases	2.5%	2.4%	-0.1%
Atypical/Alpha	Atypical	Alpha	0.2%	0.1%	-0.1%
CAMK/RAD53	CAMK	Checkpoint kinase 2	0.2%	0.1%	-0.1%
Other/TLK	Other	Tousled-Like Kinase	0.2%	0.1%	-0.1%

Other/WNK	Other	"With no K (Lysine)" kinase	0.2%	0.1%	-0.1%
STE/STE7/MEK3/MAP2K6	STE	Dual specificity mitogen-activated protein kinase kinase 6	0.2%	0.1%	-0.1%
TK/Jak	TK	Janus Kinases	0.2%	0.1%	-0.1%
TK/Src	TK	Src family	0.2%	0.1%	-0.1%
TKL/STKR/STKR2/TGFbR2	TKL	Transforming growth factor-beta receptor type 2	1.1%	1.1%	-0.1%
AGC/NDR	AGC	NDR family	0.5%	0.4%	-0.1%
CAMK/CAMK2	CAMK	Calcium/calmodulin-dependent protein kinase type 2	0.5%	0.4%	-0.1%
CK1	CK1	-	0.5%	0.4%	-0.1%
CMGC/CDK	CMGC	Cyclin Dependent Kinases	1.4%	1.3%	-0.1%
CMGC/DYRK	CMGC	Dual specificity Tyrosine Regulated Kinase	0.7%	0.7%	0.0%
Other/ULK	Other	Unc-51 like kinase	0.7%	0.7%	0.0%
AGC/PDK1	AGC	3-phosphoinositide-dependent protein kinase 1	5.3%	5.3%	0.0%
Other/PEK	Other	PEK family	2.8%	2.8%	0.0%
Other/Bud32	Other	Bud32 family	0.2%	0.3%	0.0%
AGC/PKA	AGC	Protein Kinase A	0.5%	0.5%	0.1%
STE/STE7	STE	STE7	0.5%	0.5%	0.1%
STE/STE7/MEK1/MAP2K1	STE	Dual specificity mitogen-activated protein kinase kinase 1	2.3%	2.4%	0.1%
Atypical/PDHK	Atypical	Pyruvate Dehydrogenase Kinases	0.0%	0.1%	0.1%
Other/Aur	Other	Aurora family	0.0%	0.1%	0.1%
STE/STE7/MEK3/MAP2K3	STE	Dual specificity mitogen-activated protein kinase kinase 3	0.0%	0.1%	0.1%
TK/Eph	TK	Ephrin receptors	0.0%	0.1%	0.1%
TKL/IRAK	TKL	Interleukin 1 Receptor Associated Kinase	0.0%	0.1%	0.1%
TKL/STKR/STKR2	TKL	Serine Threonine Kinase Receptors Type 2	0.0%	0.1%	0.1%
STE/STE11	STE	STE11	0.2%	0.4%	0.2%
STE/STE20	STE	STE20	0.2%	0.4%	0.2%
STE/STE7/MEK3/MAP2K4	STE	Dual specificity mitogen-activated protein kinase kinase 4	0.2%	0.4%	0.2%
Other/TTK	Other	Tau Tubulin Kinase	0.0%	0.3%	0.3%
AGC/DMPK	AGC	Myotonic Dystrophy Protein Kinase	1.8%	2.1%	0.3%
AGC/PKN	AGC	Protein Kinase N	0.2%	0.5%	0.3%
Atypical/PIKK	Atypical	Phosphatidyl inositol 3’ kinase-related kinases	0.2%	0.5%	0.3%
TKL/LISK	TKL	LISK family	0.2%	0.5%	0.3%
AGC/RSK	AGC	Ribosomal protein S6 Kinases	1.6%	2.0%	0.4%
Other/PLK	Other	Polo-Like Kinases	5.3%	5.7%	0.4%
STE/STE-Unique	STE	Unique	0.2%	0.7%	0.4%

Other/CDC7	Other	Cell division cycle 7-related protein kinase	0.5%	0.9%	0.5%
AGC/PKC	AGC	Protein Kinase C	9.6%	10.2%	0.5%
CMGC/DYRK/DYRK1	CMGC	Dual specificity tyrosine-phosphorylation-regulated kinase 1A	0.0%	0.5%	0.5%
CK1/CK1	CK1	Casein Kinase 1 Family	9.2%	9.8%	0.6%
CMGC/CLK	CMGC	CDC-like kinase 1 family	0.7%	1.3%	0.6%
TKL/RAF	TKL	Raf family	0.9%	1.6%	0.7%
Other/NEK	Other	Nek family	0.2%	1.1%	0.8%
CAMK/MAPKAPK	CAMK	MAPK-Activated Protein Kinase	3.0%	3.8%	0.8%
CAMK/PHK	CAMK	Phosphorylase Kinase	5.0%	5.9%	0.9%
CK1/VRK	CK1	Vaccinia Related Kinase	2.8%	3.7%	0.9%
Other/IKK	Other	I-kappa kinase	1.1%	2.1%	1.0%
TKL/STKR	TKL	Serine Threonine Kinase Receptors	0.5%	1.8%	1.4%
Atypical/TAF1	Atypical	Transcription initiation factor TFIID subunit 1	0.7%	2.5%	1.8%
CMGC/CK2	CMGC	Casein Kinase 2	1.4%	3.4%	2.1%

Kinase Families	
AGC	Named after the Protein Kinase A, G, and C families (PKA, PKG, PKC)
Atypical	Set of diverse kinases with no structural similarity with the remaining eukaryotic protein kinases
CAMK	Calcium/calmodulin regulated kinases
CMGC	Named after the CDK, MAPK, GSK3 and CLK families
CK1	Casein Kinase 1/Cell Kinase 1 family
Other	Set of unique kinases that do not belong to the remaining categories
PKL	Protein Kinase-Like family
RGC	Receptor Guanylate Cyclases
STE	Homologs of the yeast STE7, STE11, and STE20 genes, which form the MAPK cascade
TK	Tyrosine Kinase family, which targets Tyr residues
TKL	Tyrosine kinase-like family, similar to TK, but targeting Ser/Thr

2. Supplementary material of *Chapter III*

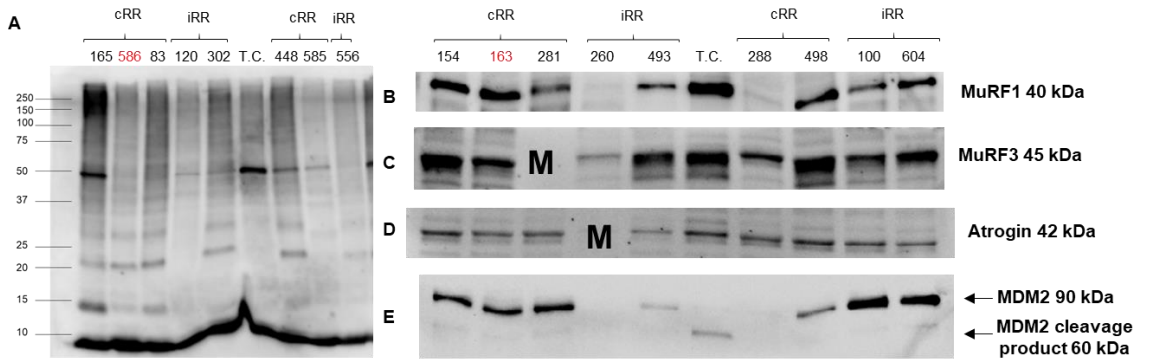

Figure S11. Ubiquitination profile and expression of ubiquitin ligases in the human myocardium collected from patients with complete (cRR) or incomplete (iRR) reverse remodeling. Representative western blot scans are depicted for ubiquitin-tagged proteins (A) and for the E3 ubiquitin ligases Muscle Ring Finger (MuRF) 1 (B), MuRF3 (C), atrogin-1 (D) and Murine Double Minute 2 (MDM2) (E). In the latter, two bands are identified with arrows, referring to intact MDM2 (upper arrow) and its cleavage product (lower arrow), as reported in the datasheet. Quantification was based on the intact band only. The respective optical density-based semi-quantification is shown **Figure 1F-J**, ***Chapter III***. T.C. designates the technical control. "M" means missing. Samples 163 and 586 are marked in red because these were excluded from the study a posteriori (aortic insufficiency was found to be more or as severe as aortic stenosis).

3. Supplementary Material of *Chapter V*

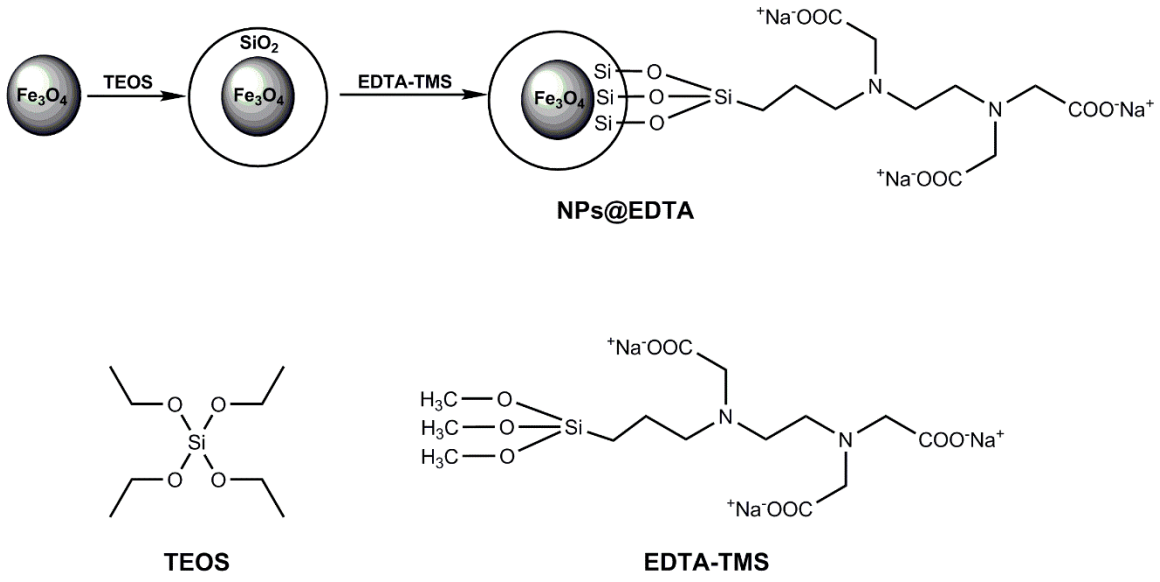

Figure S12. Scheme of the chemical strategy followed for preparing the magnetic nanoprobes comprising the synthesis of the magnetic core, silica encapsulation using tetraethyl ortho-silicate (TEOS) and the surface functionalization with the chelating agent EDTA-TMS. The chemical structure of TEOS and EDTA-TMS precursors is shown at the bottom.

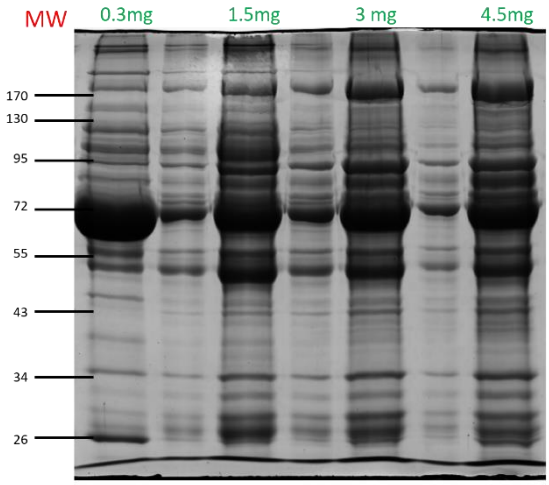

Figure S5. SDS-PAGE profile of the adsorbed protein fractions retrieved after the processing of 0.3 mg, 1.5 mg, 3 mg and 4.5 mg of PF protein from sample PF1.

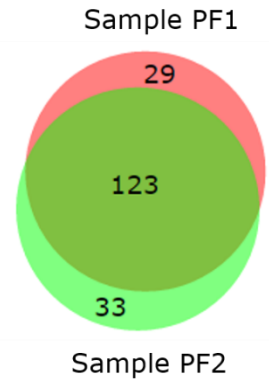

Figure S6. Venn's graphical representation of the identified PF proteins in the two individuals, in the saturation assay.

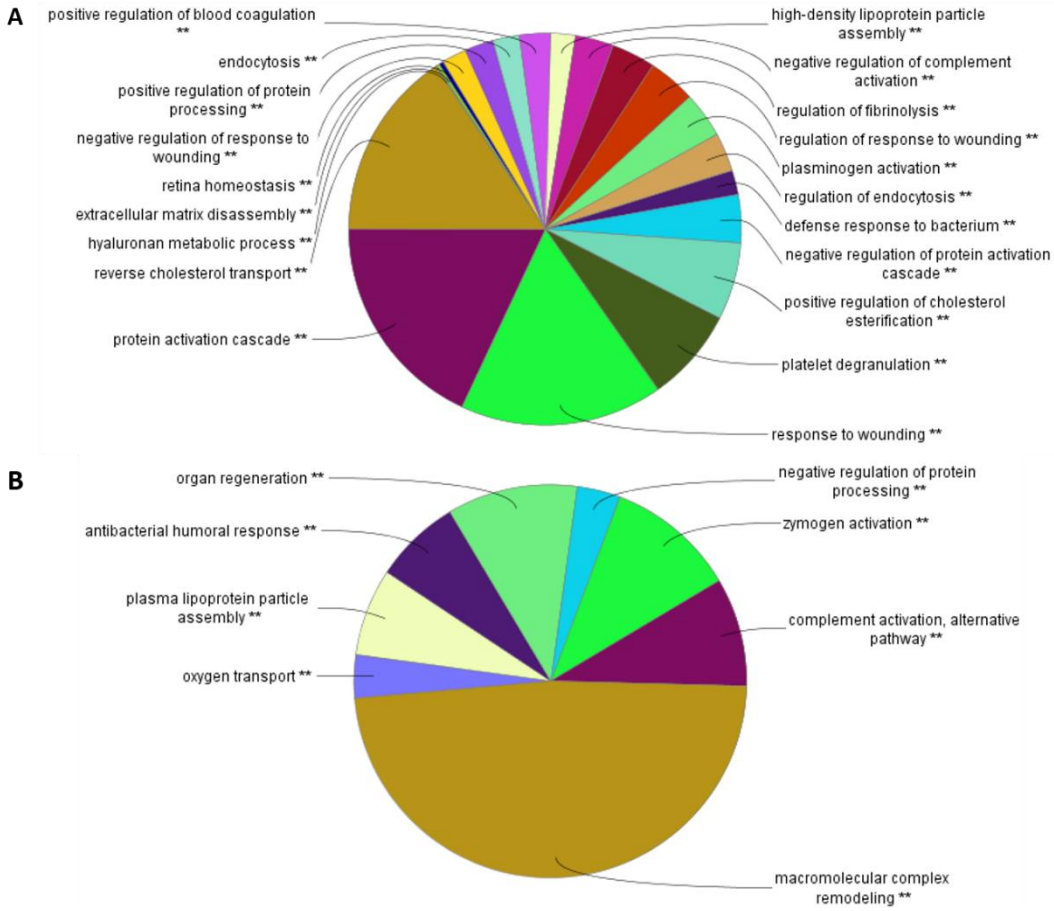

Figure S7. Significant annotated biological processes associated to both approaches (**A**) and unspecific biological processes (**B**).

Supplementary Table S2. Top 10 "Cellular Component" GO terms as retrieved by STRING webtool, associated to the proteins identified through the commercial kit and with the NPs@EDTA-based fractionation method.

Method 1: Depletion of HSA and IgG	FDR	Method 2: Enrichment with NPs@EDTA	FDR
Blood microparticle	5.61×10^{-105}	Extracellular space	4.45×10^{-120}
Extracellular space	1.4×10^{-85}	Blood microparticle	5.64×10^{-110}
Extracellular exosome	6.5×10^{-57}	Extracellular region part	4.67×10^{-81}
Extracellular region part	3.56×10^{-55}	Extracellular exosome	1.92×10^{-77}
Membrane-bounded vesicle	5.96×10^{-52}	Extracellular region	7.35×10^{-72}
Extracellular region	2.47×10^{-49}	Membrane-bounded vesicle	6.84×10^{-70}
Cytoplasmic membrane-bounded vesicle lumen	2.02×10^{-30}	Vesicle	8.37×10^{-70}
Secretory granule lumen	6.77×10^{-21}	Cytoplasmic membrane-bounded vesicle lumen	2.88×10^{-32}
Platelet alpha granule lumen	8.45×10^{-19}	Secretory granule lumen	1.20×10^{-20}
Platelet alpha granule	2.03×10^{-17}	Platelet alpha granule	2.61×10^{-19}

4. Supplementary Material of *Chapter VI*

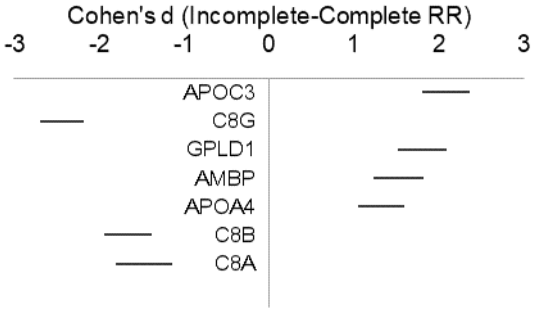

Figure S8. 95% confidence interval of the Cohen's d, for each of the proteins significantly different in the pericardial fluid of patients with complete and incomplete reverse remodeling. Proteins are identified with the respective gene name. Proteins are also identified in **Table 4**, ***Chapter VI***.

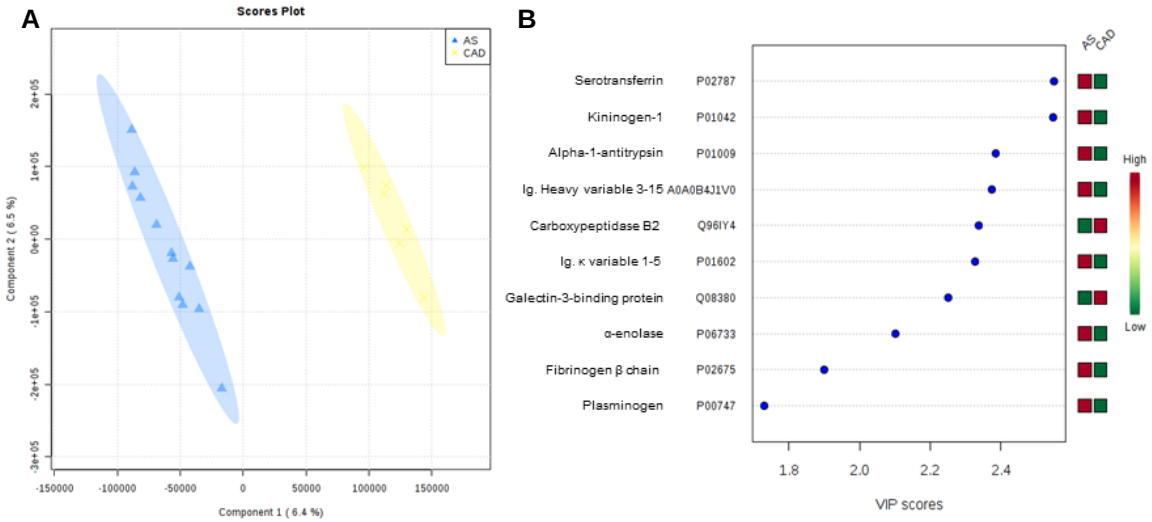

Figure S9. A. PLS-DA plot showing the separation of patients with coronary artery disease (yellow) and aortic stenosis (blue). **B.** Top 10 proteins with the highest VIP (variable importance in projection) score.